

RECONSTRUCTING PALEOENVIRONMENTS USING
A MASS-ENERGY FLUX FRAMEWORK

by

Anthony Njuguna Macharia

A dissertation submitted to the faculty of
The University of Utah
in partial fulfillment of the requirements for the degree of

Doctor of Philosophy

Department of Geography

The University of Utah

December 2012

Copyright © Anthony Njuguna Macharia 2012

All Rights Reserved

ABSTRACT

Spatial patterns in $^{13}\text{C}/^{12}\text{C}$ ratios of soil and sedimentary organic carbon are related to the woody cover distribution in a landscape and can aid in reconstructing environments. Woody cover is, in turn, controlled by climate, hydrology, and disturbance regime within an ecosystem. Geomorphology, disturbance, hydrology, and climate are the major factors that drive material fluxes and biogeochemical transformation in landscapes and should be accounted for when reconstructing past environments from soils and sediments.

Disturbance, mainly from fire and other anthropogenic activities such as tree harvesting, offset climatic driven moisture availability by creating open woodlands and grasslands within a landscape. On the other hand, geomorphology and hydrology exert strong effects on floodplains with meandering river systems supporting higher woody cover than straight channels. In lakes, the water inflow and outflow dynamics, bathymetry, and watershed geomorphology influence the water balance, material fluxes, and consequently, the biogeochemical characteristics in the water column and sediments. We evaluate how we may reconstruct historic and prehistoric environments through geochemical proxies including stable isotopes and mineralogy, and biological proxies such as diatoms, charcoal, and palynology.

TABLE OF CONTENTS

ABSTRACT.....	iii
LIST OF TABLES.....	viii
PREFACE	ix
CHAPTER	
1. BACKGROUND AND RESEARCH QUESTIONS	1
1.1 Introduction.....	1
1.2 Mass-energy flux framework.....	3
1.3 Local and regional controls of water balance.....	3
1.4 Interactive effects of solar radiation and woody cover on herbaceous cover in the tropics.....	5
1.5 Biological and geochemical indicators of disturbance in soils and lake sediments.....	7
1.6 Stable isotope indicators of disturbance, moisture fluxes, and woody cover ...	9
1.6.1 Stable isotope indicators of disturbance	11
1.6.2 Stable isotope indicators of energy flux in lakes	12
1.6.3 Stable isotope indicators of woody cover in the tropics	14
1.7 Research design and methodology.....	17
1.8 Relevance of research.....	20
1.9 References.....	20
2. IMPLICATIONS OF SPATIAL VARIATIONS IN SOIL ORGANIC MATTER $\delta^{13}\text{C}$ VALUES ON RECONSTRUCTING PALEOENVIRONMENTS IN EASTERN AFRICA.....	24
2.1 Introduction.....	24
2.2 Methods and materials.....	28
2.2.1 Study area.....	28
2.2.2 Soil sampling and preparation	28
2.2.3 Stable isotope analysis of soil organic matter (SOM)	28
2.2.4 Image classification and F_{WC} analysis.....	30
2.2.5 Patch-scale image analysis.....	30

2.2.6	Landscape-scale image analysis	33
2.2.7	$\delta^{13}\text{C}_{\text{SOC}}$ modeling.....	33
2.2.8	Relationship between woody cover and water deficit	34
2.3	Results.....	37
2.3.1	Woody cover classification.....	37
2.3.2	Relationship between woody cover and water deficit	38
2.3.3	The relationship between net aboveground primary productivity patterns and F_{WC}	45
2.4	Discussion.....	46
2.4.1	Variations of F_{WC} and $\delta^{13}\text{C}_{\text{SOC}}$ patterns with water deficit.....	46
2.4.2	Variations of $\delta^{13}\text{C}_{\text{SOC}}$ patterns with hydrology.....	47
2.4.3	Relevance of $\delta^{13}\text{C}_{\text{SOC}}$ patterns in paleoenvironmental reconstruction in Eastern Africa	48
2.5	Conclusion.....	49
2.6	Acknowledgements.....	50
2.7	References.....	50
3.	CHANGES IN NUTRIENT AND CARBON INFLUXES IN FOY LAKE, MONTANA BEFORE AND AFTER EUROPEAN SETTLEMENTS IN FLATHEAD VALLEY.....	56
3.1	Background.....	56
3.2	Study area.....	58
3.3	Material and methods.....	58
3.3.1	Isotopic analysis.....	60
3.3.1.1	Stable isotope analysis of organic matter (OM)	60
3.3.1.2	$\delta^{18}\text{O}$ and $\delta^{13}\text{C}$ stable isotope analysis of sedimentary carbonates.....	61
3.3.1.3	$\delta^{18}\text{O}$ and δD stable isotope analysis of water samples	62
3.3.2	Age chronology.....	62
3.3.3	Estimation of percent land cover / land use in watershed.....	62
3.3.4	Pollen processing.....	65
3.3.5	Charcoal analysis.....	66
3.3.6	Diatom processing	66
3.4	Results.....	66
3.4.1	Particulate matter fluxes in Foy Lake	66
3.4.2	Pollen data.....	68
3.4.3	Charcoal records	68
3.4.4	Diatom records.....	68
3.4.5	Stable isotope records of the sediment core.....	73
3.5	Discussion.....	73
3.5.1	Effects of lake water balance on $\delta^{13}\text{C}_{\text{CaCO}_3}$ and $\delta^{18}\text{O}_{\text{CaCO}_3}$	76
3.5.2	Organic matter $\delta^{15}\text{N}_{\text{BOM}}$, $\delta^{13}\text{C}_{\text{BOM}}$, and C:N ratios evidence of material fluxes in Foy Lake	79

3.5.3	The charcoal influx and fire history	83
3.5.4	The impact of cultural eutrophication of carbon cycling.....	83
3.6	Conclusion.....	84
3.7	Acknowledgements.....	85
3.8	References.....	85
4.	DISTURBANCE AND HYDROLOGICAL HISTORY OF UTAH LAKE, UT: ISOTOPIC, POLLEN, AND CHARCOAL RECORDS OF MATERIAL FLUXES AND WATER BALANCE.....	89
4.1	Introduction.....	89
4.2	Study area.....	90
4.3	Methods.....	92
4.3.1	Isotope analysis.....	92
4.3.1.1	Stable isotope analysis of OM	93
4.3.1.2	Stable isotope analysis of sedimentary carbonate.....	94
4.3.1.3	Stable isotope analysis of water samples	94
4.3.2	²¹⁰ Pb dating of sediments.....	94
4.3.3	Loss on ignition (LOI) analysis.....	95
4.3.4	Estimation of percent land cover / land use in watershed.....	95
4.3.5	Pollen processing.....	96
4.3.6	Charcoal analysis.....	97
4.4	Results.....	97
4.4.1	²¹⁰ Pb _{ex} activity profile, magnetic susceptibility, loss on ignition, charcoal counts with sediment depth	97
4.4.2	δ ¹³ C _{SOM} and C:N ratios records with depth	99
4.4.3	Pollen records.....	99
4.4.4	Stable isotope records	103
4.5	Discussion.....	103
4.5.1	²¹⁰ Pb radiometric profile	103
4.5.2	δ ¹⁵ N _{SOM} evidence of agricultural and urban development.....	108
4.5.3	Feedback mechanisms maintaining Utah Lake in eutrophic and turbid state.....	109
4.5.4	δ ¹³ C _{SOM} and C:N ratios as evidence of eutrophication	109
4.5.5	Pollen evidence of land use change in Utah Lake	110
4.5.6	Carbonate accumulation as evidence of enhanced algal photosynthesis.....	112
4.5.7	δ ¹⁸ O _{CaCO3} , δD and δ ¹⁸ O _{H2O} evidence of authigenic carbonate in Utah Lake.....	112
4.6	Conclusion.....	114
4.7	Acknowledgements.....	114
4.8	References.....	115
5.	A SYNTHETIC REVIEW OF TERRESTRIAL AND LACUSTRINE INDICATORS OF CLIMATE AND DISTURBANCE FROM RECORDS IN	

UTAH LAKE, UT, FOY LAKE, MT, AND SOIL ORGANIC .. MATTER, EAST AFRICA 119

5.1 Introduction..... 119
5.2 Woody cover patterns in watersheds 121
5.3 Woody cover reconstruction in East Africa..... 123
5.4 The influence of woody cover on material fluxes in lakes 125
5.5 The influence of topography, hydrology, and bathymetry on material and energy fluxes in lakes..... 126
5.6 The role of fire on material fluxes in lakes 129
5.7 $\delta^{15}\text{N}_{\text{BOM}}$ enrichments as indicator of nitrogen sources 129
5.8 $\delta^{15}\text{N}_{\text{BOM}}$ enrichments as indicator of fire episodes 130
5.9 Conclusion..... 131
5.10 Acknowledgements..... 132
5.11 References..... 132

APPENDIX

A. SUPPLEMENTAL INFORMATION FOR CHAPTER 1 137
B. SUPPLEMENTAL INFORMATION FOR CHAPTER 2 138
C. SUPPLEMENTAL INFORMATION FOR CHAPTER 3 157
D. SUPPLEMENTAL INFORMATION FOR CHAPTER 4 168

LIST OF TABLES

Table

1.	High spatial resolution imagery from different sensors used in woody cover estimation.....	30
2.	Climate data and woody cover of selected study sites.....	43
3.	The age model for Foy Lake freeze core based on ^{210}Pb activity, varve counts, and ^{14}C dates of woody material.....	66
4.	A summary of equations used to model that past water temperature from $\delta^{18}\text{O}_{\text{H}_2\text{O}}$, $\delta\text{D}_{\text{H}_2\text{O}}$, and $\delta^{18}\text{O}_{\text{CaCO}_3}$ values.....	137
5.	A summary of the $\delta^{13}\text{C}$ values from each of the sites collected including canopy gaps, within forests.	138
6.	Temperature reconstruction of Utah Lake from $\delta^{18}\text{O}_{\text{calcite}}$ (‰) VPDB and $\delta^{18}\text{O}_{\text{water}}$ (‰) VSMOW	169

PREFACE

This study seeks to identify and account for ecosystem processes that drive changes in element cycling and community structure in modern terrestrial and lacustrine ecosystems in order to reconstruct past environments. In the first chapter, I describe the mass-energy flux conceptual model and outline geochemical and optical methods used to account for material fluxes into soil and lake environments. Land cover and land use history are incorporated in evaluating changes in ecosystem processes resulting from disturbance, in addition to solar energy and precipitation.

In the second chapter, I present my research findings of a study evaluating the relationship between soil organic carbon-13 composition ($\delta^{13}\text{C}_{\text{SOC}}$) and woody cover in East Africa. The study employs remote-sensing techniques in developing spatially explicit $\delta^{13}\text{C}_{\text{SOC}}$ models. High spatial resolution orthoimages are used to develop woody cover grids whereupon woody cover is computed for statistically evaluating $\delta^{13}\text{C}_{\text{SOC}}$ against water deficit (WD) and precipitation patterns (magnitude and frequency of storm events). The results of this analysis are discussed in the context of the efficacy of $\delta^{13}\text{C}_{\text{SOC}}$ as a proxy for woody cover in distribution in the tropics and its significance to paleoenvironmental reconstructions.

In the third chapter, I present and discuss my research findings from analysis of Foy Lake (Montana) sedimentary profiles. I evaluate the $\delta^{13}\text{C}$ composition of bulk

organic matter in sediments ($\delta^{13}\text{C}_{\text{BOM}}$) in relation to current and historic land cover changes. Pollen, algae, including diatoms, and ^{15}N composition of bulk organic matter in sediments ($\delta^{15}\text{N}_{\text{BOM}}$), carbon to nitrogen ratio (C/N), and ^{13}C and ^{18}O composition of bulk carbonates in sediments ($\delta^{13}\text{C}_{\text{CaCO}_3}$ and $\delta^{18}\text{O}_{\text{CaCO}_3}$, respectively) are used as indicators of ecosystem responses following woody cover changes in the watershed. The changes in sediment geochemistry are discussed in the context of historical land use and climatic events in the watershed.

In the fourth chapter, I present and discuss palynological and geochemical records of Utah Lake integrated in a 43 cm deep sediment core covering historical land cover and land use change in the watershed. Variations in stable isotope records of organic matter and carbonates, pollen, and charcoal content in sediments are evaluated in relation to nutrient cycling and water budget under disturbance and nondisturbance conditions.

In the fifth chapter, I provide a synthesis on the relationship between woody cover and $^{13}\text{C}/^{12}\text{C}$ ratios of soil organic carbon in East Africa, organic matter fluxes into lakes, and changes in material fluxes and element cycling resulting from anthropogenic disturbance and woody cover change in lakes in the northwestern USA. I compare and contrast the geochemical and palynomorphologic records of Utah Lake and Foy Lake in relation to geomorphological, hydrological, land cover, and land use differences and discuss the implications of these differences on selection of lakes for reconstructing past environments. I summarize by discussing how geomorphology, hydrology, disturbance, and climate may confound interpretation of soil and sedimentary records through interacting and independent effects.

CHAPTER 1

BACKGROUND AND RESEARCH QUESTIONS

1.1 Introduction

This study uses modern ecosystems as analogues for reconstructing environments in the past. To achieve this objective, woody cover, climate, disturbance, and geomorphology are considered within terrestrial and lacustrine contexts. Soil organic carbon is used as a proxy for reconstructing woody cover within terrestrial environments in the tropics. Pollen influx, charcoal influx, diatom abundance, and stable isotopes composition of sediments and lake water are used as proxies for accounting for material fluxes in lakes.

The Achilles' heel of interpreting climate records within soils and sediments is the poor understanding of the independent and interactive effects of climate, disturbance, and geomorphology. Climate and humans are the main drivers of recent geochemical processes and shifts in ecosystem structure in recent decades. Evidence of these drivers may be discerned from soils, lake water, and sediments through biological and geochemical proxies. Stable isotopes can be used to infer transformation processes attributable to human activities and climate based on observed trends in modern environments. Understanding the interaction between energy and material fluxes from a local or patch scale (≤ 10 ha area), how such interactions scale-up to regional and global

scale, and how such processes are recorded in soil and sediments is necessary for accurate reconstruction of past environments. In order to shed more light on these factors, three testable hypotheses are posited:

1. The $^{13}\text{C}/^{12}\text{C}$ ratios of soil organic matter in the tropics reflect the contribution of C_3 and C_4 plants, whose distribution is, in turn, related to woody cover distribution in Eastern Africa whereas $^{13}\text{C}/^{12}\text{C}$ ratios and C:N ratios of sedimentary organic matter relate to woody cover around lakes in temperate lakes.
2. Hydrology, geomorphology, climate, and disturbance influence woody cover distribution at patch-scale and landscape-scale levels that create a diversity of vegetation physiognomies in tropical and temperate environments.
3. Disturbance complicates the interpretation of climate-driven moisture deficit that results in the coexistence of open grasslands and forests within an area of similar climatic characteristics in the tropics, and masks climate signals integrated in lake sediments through increased influx of dissolved and particulate materials from inside and outside the lake.

To improve our understanding of the influence of climate, disturbance, hydrology, and geomorphology on the biological and geochemical characteristics of soils and sediments, spatial and temporal trends in stable isotopes are explored by using the mass-energy flux model proposed by Leavitt et al. (2009). Within this conceptual framework, the sources of materials and the pathways of their translocation into soils and sediments are considered for disturbed and undisturbed states. The mass-energy flux conceptual framework is used to evaluate the influences of woody cover, hydrology, and geomorphology on the material influx and geochemical fluxes in soils and sediments.

1.2 Mass-energy flux framework

Two components of a mass-energy flux conceptual framework are recognized: mass and energy (Leavitt et al., 2009). The interaction of these two components determines ecosystem structure as well as geochemical and biological processes characterizing that ecosystem. For instance, solar radiation accounts for 99.8 % of earth's energy and powers micrometeorological processes, soil heat flux, soil temperature, sensible heat flux, surface and air temperatures, wind and turbulent transport, evapotranspiration, growth, and activity of plants and animals (Kumar et al., 1997). Woody cover distribution patterns, in turn, determine the herbaceous cover distribution patterns within and between tree canopies. The interactive effects between solar radiation and moisture availability are manifested in the distribution of woody cover and the water balance of lake systems (Figure 1). In this study, solar radiation influence on water balance in soils and lakes is explored with regard to woody cover distribution patterns and isotopic indicators (^{18}O and D abundance) of lake water evaporation, respectively.

1.3 Local and regional controls of water balance

Solar energy is the principal driver of atmospheric circulation, and it influences precipitation patterns, including the location and strength of jet streams, frontal boundaries, the monsoon systems, El Niño Southern Oscillation (ENSO) events, the Pacific Decadal Oscillation that varies on a 20–30 year cycle (McCabe et al., 2003; Loik et al., 2004; Chesson et al., 2004), and the Atlantic Multidecadal Oscillation (AMO) that varies on a 65–80 year cycle (McCabe et al., 2003). Water is the primary factor that

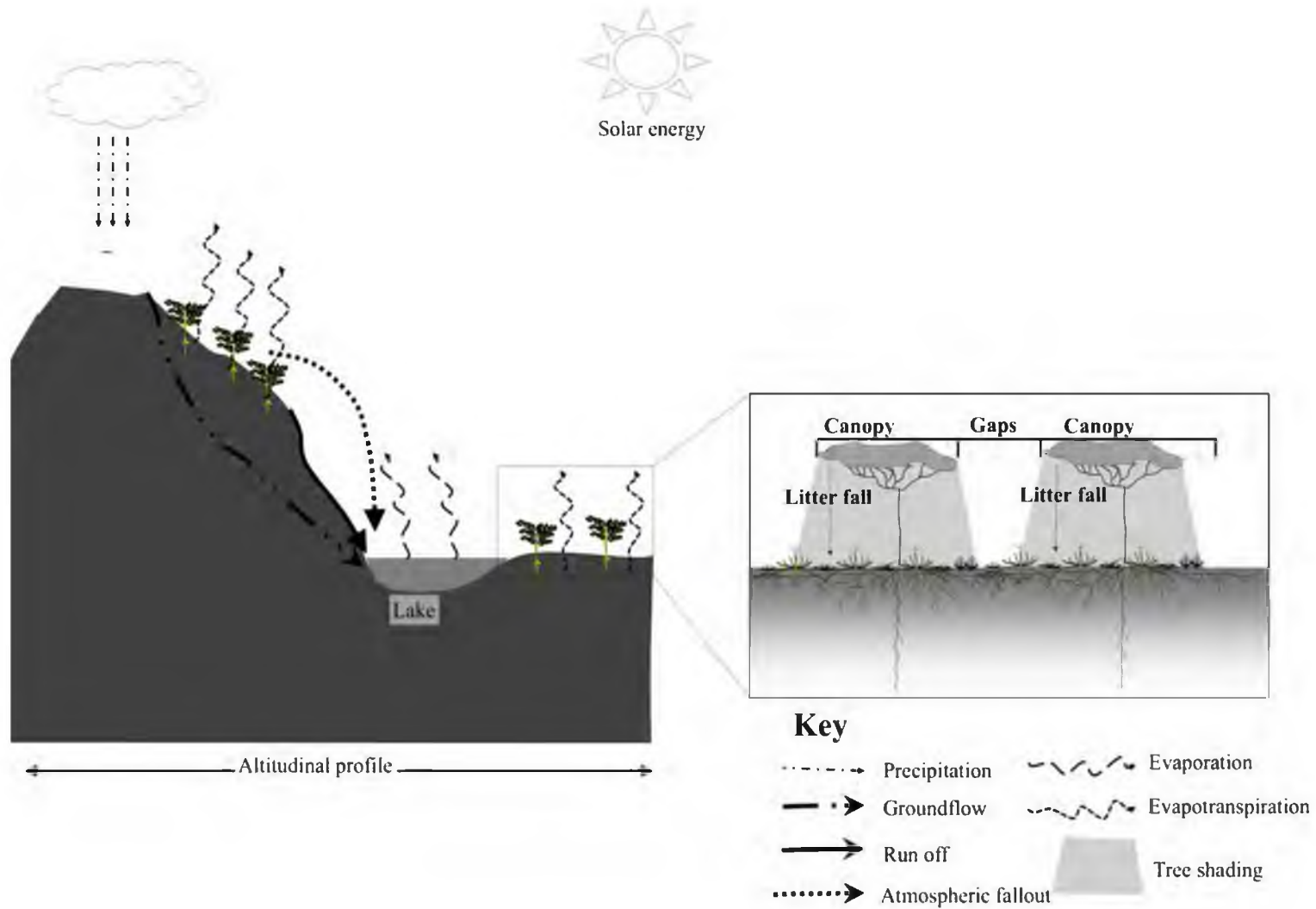


Figure 1. An illustration of the impact of solar radiation on evaporation and evapotranspiration in lakes and on land, respectively, and the influence of woody cover on ground shading.

limits plant growth and moisture pulses bring nutrient resources that drive net primary production (Schwinning & Sala, 2004) and influence species dynamics through recruitment (Ostfeld & Keesing, 2000; Lundholm & Larson, 2004). It is therefore expected that water is the primary factor driving shifts in ecosystem structure temporally and spatially.

Solar radiation affects lake water budget through interactive effects of lake bathymetry, hydrology, atmospheric temperatures, and humidity. Incoming solar radiation that is predominantly of short wavelength is absorbed by water molecules, generating heat at the lake surface (Figure 2). The kinetic energy gained by water molecules near the surface helps break intermolecular bonds, resulting in the escape of water into the vapor phase. Some heat energy is lost from the water surface as sensible heat flux. Beneath the lake surface is a layer of heat exchange with the atmosphere where heat energy is transmitted from the surface through conduction and convection currents. The heat exchange gradient layer has a relatively constant temperature. Beneath the heat exchange layer is a layer of rapid decrease in temperature (thermocline) that separates surface waters from cold deep waters. The thermocline may either be permanent in very deep lakes, seasonally transient in moderately deep lakes, or non-existent in very shallow lakes. Overall, heat and light derived from solar radiation influence organic matter synthesis and carbonate precipitation in lakes.

1.4 Interactive effects of solar radiation and woody cover on herbaceous cover in the tropics

Woody cover shading lowers evapotranspiration in the understory. At a patch scale, vegetation alters the microclimate through absorption, reflection, and scattering of

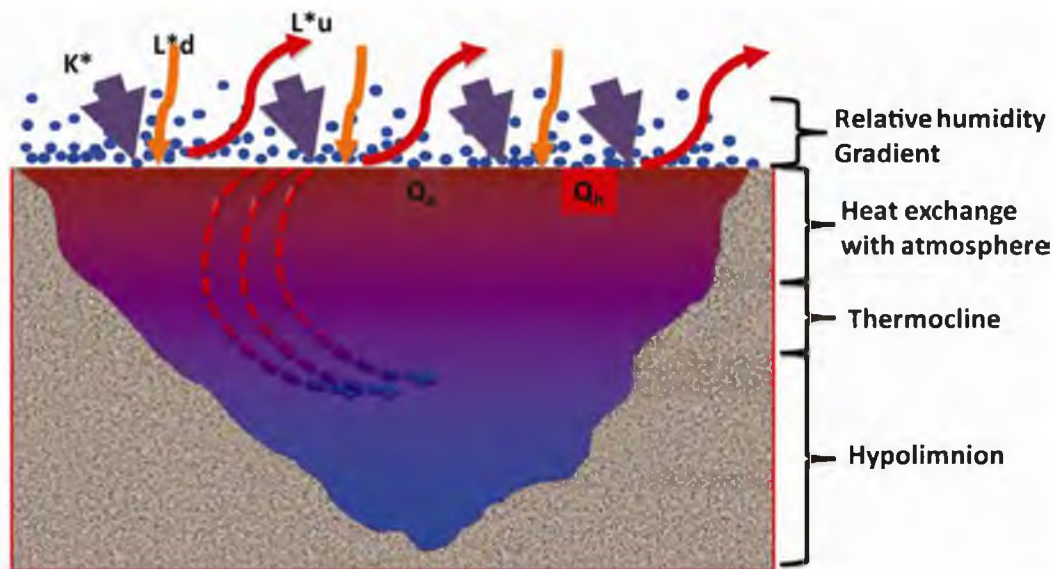


Figure 2. Solar radiation effects on the water and energy budget at the surface layer boundary of a lake. K_d is the incoming global shortwave radiation (Wm^{-2}), A_s is the shortwave albedo of the lake surface, L^*d is the incoming longwave radiation, L^*u is the outgoing longwave radiation, Q_e is the heat of vaporization (Mj kg^{-1}), and Q_h is the sensible heat flux. Solar radiation driven thermal stratification determines physical-chemical gradients in the water column, including those in dissolved O_2 and CO_2 .

radiation by the canopy (Figure 3). From an individual tree standpoint, the amount of transmitted light reaching Earth's surface through the tree canopy is attenuated in accordance to Beers Law (Figure 3). Consequently, canopy shading is denser immediately underneath the trees, and becomes lighter between canopies. At a patch scale, the degree of shading depends on the fraction of woody cover in that patch (F_{WC}) that impacts the abundance and composition of herbaceous plant community in the understory. Herbaceous species are generally shallow-rooted and hence more sensitive to moisture deficit than woody plants. Consequently, the abundance of herbaceous community is strongly influenced by moisture abundance in the surface horizons of the soil. Woody species create refugia for herbaceous species by lowering the soil surface temperature through shading and reducing the evapotranspiration.

1.5 Biological and geochemical indicators of disturbance in soils and lake sediments

Climate and humans have become the main drivers of geochemical processes and shifts in ecosystem structure in recent decades and their effects may be discerned in soils, lake water, and biological and geochemical proxies in sediments. The mass-energy flux model identifies disturbance as “an information filter” (*sensu* Leavitt et al., 2009) because materials transformed and translocated into lakes through disturbance do not necessarily reflect the primary original climatic signal created by solar radiation and precipitation. Further, hysteresis in woody plants' response to climatic changes is asynchronous relative to that of phytoplankton community which respond rapidly to climatic variations (Leavitt et al., 2009). Consequently, understanding the independent and interactive effects of

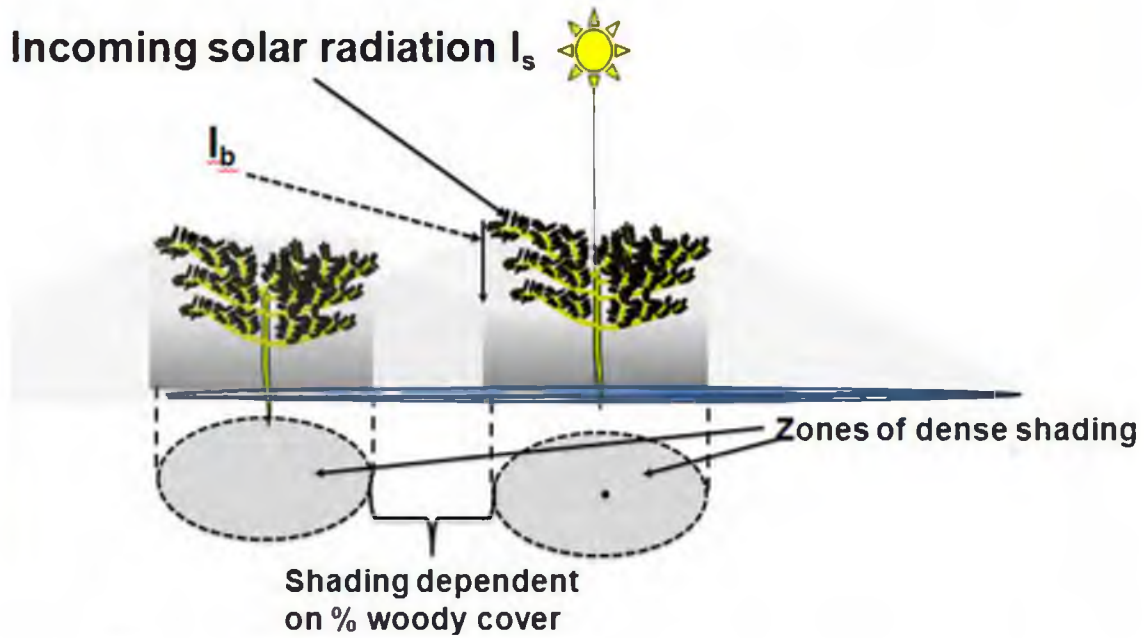


Figure 3. An illustration of the effect of woody cover on the extinction of incoming solar radiation (I_s) due to absorption, reflection, and scatter of radiation, hence reducing the levels of transmitted light (I_b) through the canopy in accordance to Beers Law.

moisture drivers and disturbance is critical in decoupling the climatic and disturbance history in the past environments. A multiproxy approach may therefore provide data necessary for accounting for material sources and ecosystem processes arising from disturbance or climate forcing within spatial and temporal domains. Changes in fossil and subfossil charcoal, pollen, and diatom abundance as recorded in lake sediments through time may be used to indicate changes in ecosystem structure within lakes and their watersheds that allow a link between vegetation structure in watershed and lake processes to be established. Palynomorphologic and geochemical proxies may therefore be used independently to infer origin of particulate and dissolved substances accumulating in lake sediments as well as to identify transformation processes accompanying their influx (Figure 4).

1.6 Stable isotope indicators of disturbance, moisture fluxes, and woody cover

Isotope values are calculated as shown in Equation 1.

$$\delta X (\text{‰}) = 1000 * (R_{\text{sample}} / R_{\text{standard}} - 1) \quad \text{Equation 1}$$

where 'X' is either ^{15}N , ^{18}O , or ^{13}C , R is $^{15}\text{N} / ^{14}\text{N}$, $^{18}\text{O} / ^{16}\text{O}$, or $^{13}\text{C} / ^{12}\text{C}$, respectively, and δX is expressed in permil (‰) relative to internationally agreed standards: V-PDB for both carbon and oxygen, and atmosphere (AIR) for nitrogen $\delta^{15}\text{N}$, respectively. The process that results in isotopic enrichment is referred to as isotopic fractionation. The

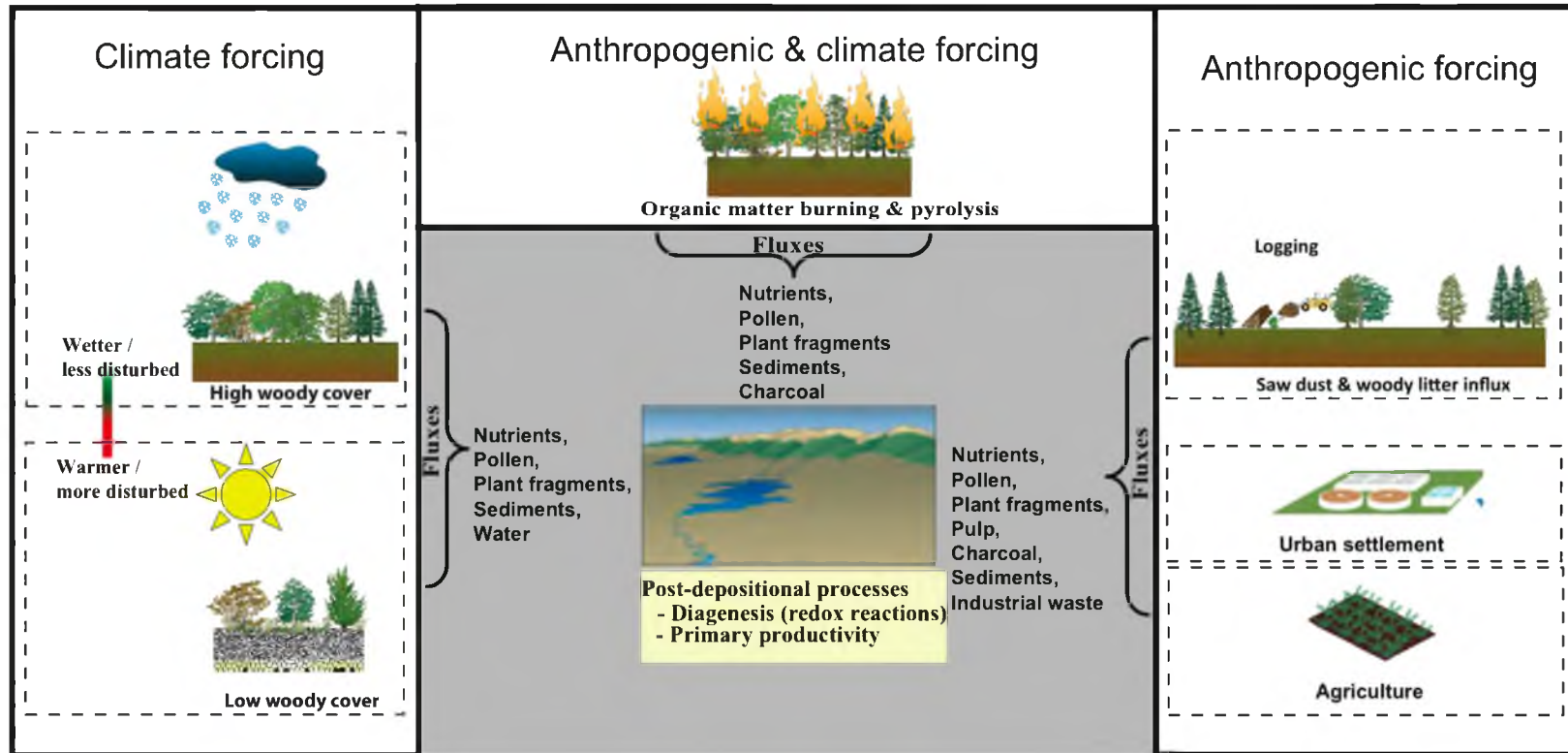


Figure 4. A conceptual model of material fluxes elicited by climate and anthropogenic disturbance. The graphics used to develop this conceptual model are derived from Integration and Application Network (IAN) graphics library (ian.umces.edu/symbols/).

isotope fractionation factor relates to substances A and B. In equilibrium reactions, there is no “substrate” or “product”; isotope fractionation describes isotope equilibrium reactions, a related term is “discrimination” as in a nonreversible reaction involving substrate and production (e.g., photosynthesis).

$$\alpha_{A-B} = \frac{1000 + \delta_A}{1000 + \delta_B} \quad \text{Equation 2}$$

1.6.1 Stable isotope indicators of disturbance

The transport of materials arising from disturbances in the watershed is modulated by hydrology and geomorphology. Nutrient influxes in lakes from riverine transport (Mayer et al., 2002) or atmospheric deposition (Nannus et al., 2003; Saros et al., 2003) can potentially alter lake nutrient budgets and can trigger changes in lake productivity and plankton community composition. Studies on isotopic imprints of patch-scale (e.g., Macharia et al., 2012) and watershed-scale (Mayer et al., 2002) disturbance can provide conceptual understanding of how such disturbances may influence the stable isotope composition of soils and sediments and thus aid in interpreting the history of disturbances. For instance, $\delta^{15}\text{N}$ of nitrates for watersheds in eastern USA with limited land use range from 3.5 to 5.5‰ and watersheds with greater than 15% agricultural or urban land use range from 6 to 9‰ (Mayer et al., 2002). In reconstructing past and predicting future changes in climate and disturbance regimes, watershed-scale changes in nutrient budgets associated with urban development and agriculture must be factored in.

1.6.2 Stable isotope indicators of energy flux in lakes

The influence of solar radiation on lake evaporation is manifested through ^{18}O and ^2H (D) enrichments of lake water relative to meteoric water sources (e.g., Henderson & Shuman, 2009). Deuterium (D) and ^{18}O fractionate together, typically in 8:1 ratio in the sea-atmosphere boundary layer where the vapor and liquid phase are at equilibrium (Craig, 1961). Clouds form at a relative humidity of 85% at sea level and subsequent precipitation shows a deuterium excess of +10‰, a relationship illustrated by the global meteoric waterline (GMWL) (Craig, 1961). Lake waters that are isotopically the same as precipitation plot on or close to the GMWL, whereas evaporated lake waters plot off the GMWL on a local evaporation line (LEL) (Leng et al., 2004; Figure 5). For instance, lakes in northern New Mexico and southern Colorado receive significant moisture inputs during the summer monsoon and have an isotopic composition of meteoric water skewed towards summer precipitation (Henderson & Shuman, 2009).

When $\delta^{18}\text{O}_{\text{CaCO}_3}$ is used to estimate changes in lake water balance in the past, carbonate sources (detrital or autochthonous) must be considered. In temperate environments, the amount and forms of carbonates deposited in sediments vary with summer photosynthesis (e.g., McConnaughey et al., 1994; Drummond et al., 1995). Calcite precipitation mainly occurs in the epilimnion where photosynthesis and heat exchange between the lake and atmosphere occurs (e.g., McConnaughey et al., 1994; Drummond et al., 1995; Sharpley, 2010). However, calcite derived from algal photosynthesis may dissolve as it is translocated to the hypolimnion of groundwater-fed lakes where CO_2 fugacity is high because of the influx of CO_2 derived from soil

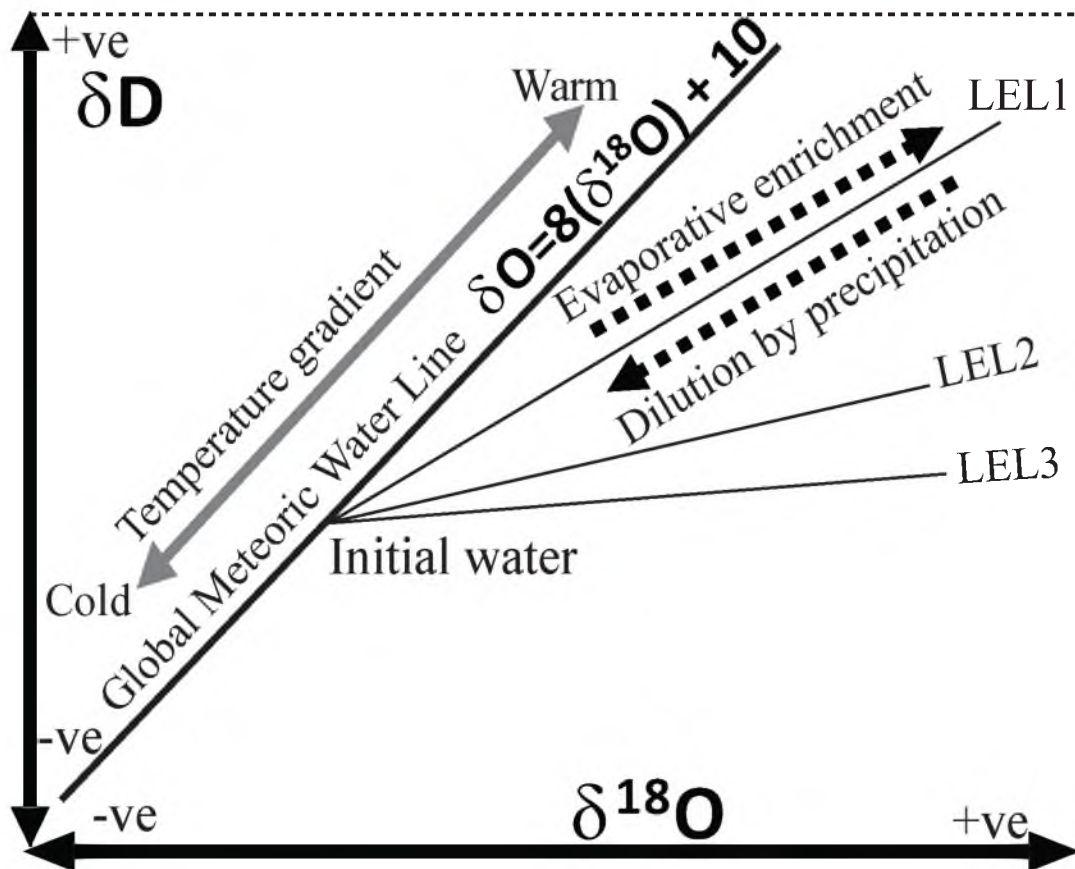


Figure 5. Processes influencing $\delta^{18}O$ and δD of lake water (modified after Leng et al., 2004). LEL1, 2, and 3 represent lake evaporation lines having the same initial water source but different atmospheric conditions which causes lakes in region 1 to be more evaporated than those of regions 2 and 3, respectively.

respiration delivered through groundwater transport (Sharpley, 2010). Further, high magnesium ion concentration ($[Mg^{2+}]$) in groundwater-fed lakes may interfere with nucleation of calcium carbonate and hence result in magnesium calcite formation (McConnaughey et al., 1994; Drummond et al., 1995). Other processes that include sedimentation, organic matter oxidation, and evaporation must be considered when interpreting isotopic signals imprinted in sedimentary carbonates because they influence the $\delta^{13}C_{CaCO_3}$ and $\delta^{18}O_{CaCO_3}$ values (Figure 6). Reconstruction of water balance history of lakes from stable isotope of carbonates is achieved through palaeo-temperature equations developed from calibration experiments in laboratories and field sediment trap experiments that assume an equilibrium temperature of carbonate precipitation. Whilst $\delta^{18}O$ of carbonate ($\delta^{18}O_{CaCO_3}$) is reported relative to PDB, $\delta^{18}O$ and δD of water ($\delta^{18}O_{H_2O}$ and δD_{H_2O} , respectively) are typically reported relative to SMOW. Various equations have been developed to relate $\delta^{18}O_{H_2O}$ and δD_{H_2O} to $\delta^{18}O_{CaCO_3}$ (Appendix A).

1.6.3 Stable isotope indicators of woody cover in the tropics

Soil organic carbon reflects how open the vegetation is in a particular environment. More open environments receive higher levels of solar insolation and therefore experience higher temperature and greater evapotranspiration than closed canopy forest. C_4 plants are more adapted to environments that experience water stress since they have evolved a CO_2 concentrating mechanism that allows more efficient photosynthetic pathways at high temperatures and under water stressed conditions. C_3 plants are more sensitive to water stress than C_4 plants and lack the CO_2 concentrating mechanism.

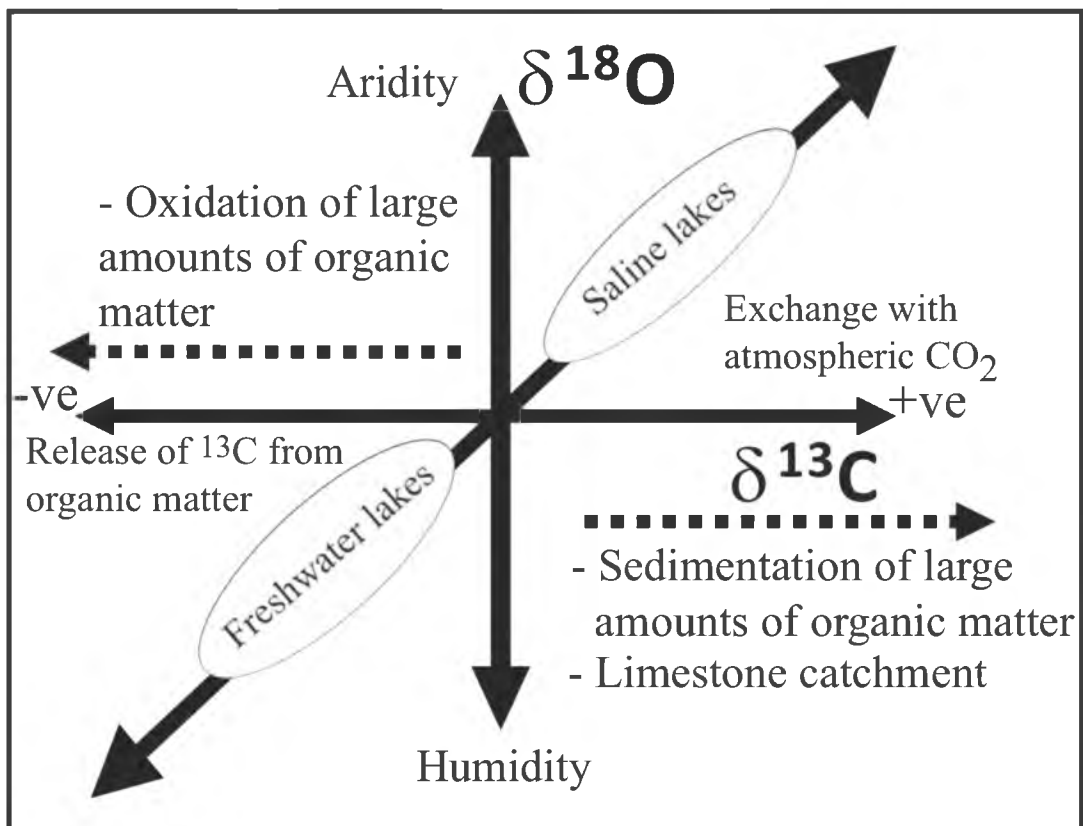


Figure 6. A schematic diagram showing possible $\delta^{18}\text{O}$ and $\delta^{13}\text{C}$ trajectories of lake carbonates based on lake water evaporative enrichments, sedimentation, and oxidation of organic matter (Modified after Leng et al., 2004).

When $\delta^{13}\text{C}$ values of soil organic carbon ($\delta^{13}\text{C}_{\text{SOC}}$) are used to reconstruct the vegetation structure in the tropical systems, the role of disturbance on the distribution patterns of woody cover at local and regional moisture gradients must be considered. Studies show that woody cover distribution influences the distribution of C_3 and C_4 vegetation in the tropics that is predictable from $\delta^{13}\text{C}_{\text{SOC}}$ (e.g., Cerling et al., 2011). This study evaluates the relationship between solar radiation and woody cover distribution, and the influence of local and regional controls on water and nutrient budgets as woody cover, by accounting for materials fluxes from disturbance and solar radiation.

In the tropics, high soil surface temperatures subjects soils to high evaporations that results in low water potential (high moisture deficit), favoring plants that use the C_4 photosynthetic pathway more than the C_3 plants. Woody cover in the tropics controls the distribution of C_3 and C_4 by providing shade that attenuates the impact of solar radiation on light intensity and moisture deficit. Reduced soil insolation from shading by woody species results in lower soil temperatures and evapotranspiration in shaded compared to unshaded areas (Figure 4). The F_{WC} therefore determines the $\delta^{13}\text{C}_{\text{SOC}}$ through the fractional woody cover (F_{WC}) influence on the abundance of C_3 relative to C_4 plant species in the tropics. In contrast, the influence of F_{WC} on the $\delta^{13}\text{C}_{\text{SOC}}$ of temperate environments is hard to model because herbaceous plants including many grasses and woody species are predominantly C_3 . The density of woody cover in a given patch influences the proportion of herbaceous plants that use the C_3 relative to the C_4 carbon fixation pathway. The contribution of organic matter by woody species and C_3 herbs to soils is greater as woody cover increases, which results in a more negative $\delta^{13}\text{C}_{\text{SOC}}$ than in grasslands or wooded grasslands. Canopy shading lowers the soil temperatures and

light intensity in the understory, favoring C₃ herbs in patches with a higher F_{WC} while C₄ herbs become more competitive in open grassland and woodland environment (low F_{WC}) (Figure 7).

The abundance of C₄ plants in temperate ecosystems varies seasonally, becoming more abundant towards the summer and less abundant towards the winter. As a consequence, C₃ plants dominate the herbaceous communities in temperate environments with C₄ plants exerting less influence on $\delta^{13}\text{C}_{\text{SOC}}$ than in tropical environments. It is worth noting that much of the American Midwest (e.g., Iowa) is considered temperate but has a lot of C₄ grasses.

1.7 Research design and methodology

In this study, we evaluate the geospatial relationship between percent woody cover and $\delta^{13}\text{C}_{\text{SOC}}$ models, potential evapotranspiration, and land use in landscapes for imprints of climate and disturbance (Figure 8). We utilize high-resolution satellite imagery to evaluate the relationship between percentage woody cover and $\delta^{13}\text{C}_{\text{SOC}}$ values in East Africa. This study provides an analogue for interpreting paleoenvironments in East Africa, an important region in understanding mammalian (including hominid) evolution.

This research tests the following hypotheses:

1. Water is the primary factor driving shifts in ecosystem structure temporally and spatially.

Wooded grassland

Grassland

Open woodland



Figure 7. An illustration of the relationship between tree clustering patterns and herbaceous cover distribution patterns. The C_3 plants (mainly dicots) are more abundant in shaded than unshaded environments, while C_4 plants (mainly monocots) are more abundant in unshaded than in shaded areas.

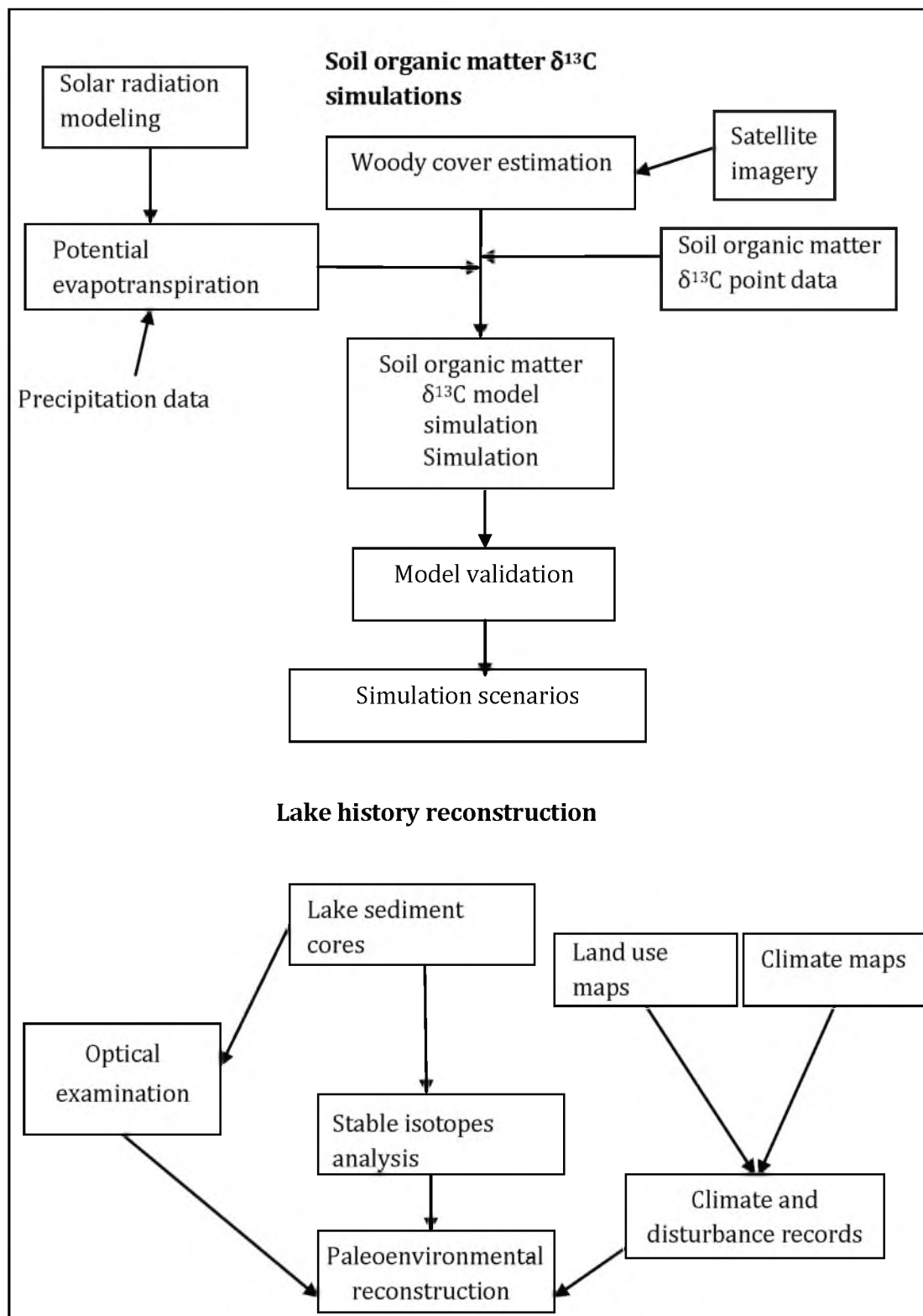


Figure 8. An illustration of the methodology employed in this study to evaluate the influence of climate, land use, and geomorphology on soils and sediments.

2. Disturbance masks isotopic signals in soils and sediments set by lake moisture drivers.
3. Geomorphology influences hydrology and moisture distribution patterns within landscapes and also determines the rates of terrigenous material influx into lakes.

1.8 Relevance of research

This study contributes to the development of methodologies and conceptual understanding on the impact of climatic, geomorphic, and ecosystem disturbances to the geochemical and biological composition of lake sediments. These efforts are geared to improving the interpretation of the biogeochemical signature imprinted in soils and sediments relative to geomorphic, anthropogenic disturbances, and climatic factors that caused them. Accurate reconstruction of historic and paleohistoric records are important in fostering the understanding of the interaction between climate change, effects of land-use change, ecosystem monitoring and restoration projects, and providing contexts for interpreting the fossil record. Further, for recognition of the influence of global climate change, and degradation of land and water quality, such studies are critical in future management of land and water resources.

1.9 References

Anderson, T. F., & Arthur, M. A. (1983). Stable isotopes of oxygen and carbon and their application to sedimentological and palaeoenvironmental problems. In: Arthur, M. A. Anderson, T. F. Kaplan, I. R. Veizer, J., Land, L. S., (Eds.), *Stable Isotopes in Sedimentary Geochemistry: Society of Economic Palaeontologists and Mineralogists Short Course, 10*, 1–151.

- Austin, A. T., Yadhjian, L., Stark, J. M., Belnap, J., Porporato, A., Norton, U., Ravetta, D. A., & Scheffer, S. M. (2004). Water pulses and biogeochemical cycles in arid and semi-arid ecosystems. *Oecologia*, *141*, 221–235.
- Böhm, F., Joachimski, M. M., Dullo, W., Eisenhauer, A., Lehnert, H., Reitner, J., & Wörheide, G. (2000). Oxygen isotope fractionation in marine aragonite of coralline sponges. *Geochimica et Cosmochimica Acta*, *64*(10), 1695–1703.
- Cerling, T. E., Andanje, S. A., Bird, M. I., Korir, D. K., Levin, N. E., Mace, W., Macharia, A. N., Remein C. H., & Wynn J. G. (2011). Woody cover and hominin environments in the past 6 million years. *Nature*, *476*, 51–56, doi:10.1038/nature10306.
- Chesson, P., Gebauer, R. L. E., Schwinning, S., Huntly, N., Wiegand, N., Ernest, M. S. K., Sher, A., Novoplansky, A., & Weltzn, J. F. (2004). Resource pulses, species interactions, and diversity maintenance in arid and semi-arid environments. *Oecologia*, *141*, 236–253.
- Coplen, T. B., Kendall, C., & Hopple, J. (1983). Comparison of stable isotope reference samples. *Nature*, *302*, 236–238.
- Craig, H. (1961). Isotopic variations in meteoric waters. *Science*, *133*, 1702–1703.
- Craig, H. (1965). The measurement of oxygen isotope palaeotemperatures. In: Tongiorgi E. (ed.), *Stable Isotopes in Oceanographic Studies and Palaeotemperatures* (pp. 161–182). Pisa, Consiglio Nazionale delle Ricerche Laboratorio di Geologia Nucleare.
- Drummond, C. N., Patterson, W. P., & Walker, J. G. G. (1995). Climatic forcing of carbon-oxygen isotopic covariance in temperate-region marl lakes. *Geology*, *23*(11), 1031–1034, doi: 10.1130/0091-7613(1995)023<1031:CFOCOI>2.3.CO;2.
- Epstein, S., Buchsbaum, R., Lowenstam, H. A., & Urey, H. C. (1953). Revised carbonate water isotopic temperature scale. *Geological Society of America Bulletin*, *64*, 1315–1326.
- Friedman, I., & O'Neil, J. R. (1977). Compilation of stable isotope fractionation factors of geochemical interest. In: Fleischer M. (ed.), *Data of Geochemistry* (pp. 1–40). Sixth edition. Geological Survey Professional Paper 440-KK, US Government Printing Office, Washington.
- Grogan, P., Bruns, T. D., & Chapin III, F. S. (2000). Fire effects on ecosystem nitrogen cycling in a Californian bishop pine forest. *Oecologia*, *122*, 537–544.
- Grossman, E.L., & Ku, T-L. (1986). Oxygen and carbon isotope fractionation in biogenic aragonite: Temperature effects. *Chemical Geology (Isotope Geoscience Section)*, *59*, 59–74

- Henderson, A. K., & Shuman, B. N. (2009). Hydrogen and oxygen isotopic compositions of lake water in the western United States. *Geological Society of America Bulletin*, *121*, 1179–1189, doi: 10.1130/B26441.1.
- Kim, S.T., & O'Neil, J. R. (1997). Equilibrium and nonequilibrium oxygen isotope effects in synthetic carbonates. *Geochimica et Cosmochimica Acta*, *61*, 3461–3475.
- Kim, S., O'Neil, J. R., Hillaire-Marcel, C., & Muccia, A. (2007). Oxygen isotope fractionation between synthetic aragonite and water: Influence of temperature and Mg²⁺ concentration. *Geochimica et Cosmochimica Acta*, *71*, 4704–4715.
- Kumar, L., Skidmore, A. K., & Knowles, E. (1997). Modeling topographic variation in solar radiation in a GIS environment. *International Journal of Geographical Information Science*, *11*(5), 475–497, doi:10.1080/136588197242266.
- Leavitt, P. R., Fritz, S. C., Anderson, N. J., Baker, P. A., Blenckner, T., Bunting, L., Catalan, J., Conley, D. J., Hobbs, W. O., Jeppesen, E., Korhola, A., McGowan, S., Rühland, K., Rusak, J. A., Simpson, G. L., Solovieva, N., & Werne, J. (2009). Paleolimnological evidence of the effects on lakes of energy and mass transfer from climate and humans. *Limnology & Oceanography*, *54*(6, part 2), 2330–2348.
- Leng, M. J., & Marshall, J. D. (2004). Palaeoclimate interpretation of stable isotope data from lake sediment archives. *Quaternary Science Reviews*, *23*, 811–831.
- Loik, M. E., Breshears, D. D., Lauenroth, W. K., & Belnap, J. (2004). Multiscale perspective of water pulses in dry-land ecosystems: Climatology and ecohydrology of the western USA. *Oecologia*, *141*, 269–281.
- Lundholm, J. T., & Larson, D. W. (2004). Experimental separation of resource quantity from temporal variability: seedling responses to water pulses. *Oecologia*, *141*, 346–352.
- Macharia, A. N., Uno, K. T., Cerling, T. E., & Brown, F. H. (2012). Isotopically distinct modern carbonates in abandoned livestock corrals in northern Kenya. *Journal of Archaeological Science*, *39*, 2198–2205, doi:10.1016/j.jas.2012.02.005.
- Mayer, B., Boyer, E. W., Goodale, C., Jaworski, N. A., Van Breemen, N., Howarth, R. W., Seitzinger, S., Billen, G., Lajtha, L. J., Nosal, M., & Paustian, K. (2002). Sources of nitrate in rivers draining sixteen watersheds in the Northeastern U.S.: Isotopic constraints. *Biogeochemistry*, *57*, 171–197.
- McCabe, G. J., Palecki, M. A., & Betancourt, J. L. (2003). Pacific and Atlantic Ocean influences on multidecadal drought frequency in the United States. *Proceedings of the National Academy of Sciences USA*, *101*, 4136–4141.

- McConnaughey, T. A., LaBaugh, J. W., Rosenberry, D. O., Striegl, R. G., Reddy, M. M., Schuster, P. F., & Carter, V. (1994). Carbon budget for a groundwater-fed lake: calcification supports summer photosynthesis. *Limnology and Oceanography* 39(6), 1319–1332.
- Meyers, P. A., & Lallier-Verges, E. (1999). Lacustrine sedimentary organic matter records of Late Quaternary paleoclimates. *Journal of Paleolimnology*, 21, 345–372.
- Nanus, L., Campbell, D. H., Ingersoll, G. P., Clow, D. W., & Mast, M. A. (2003). Atmospheric deposition maps for the Rocky Mountains. *Atmospheric Environment*, 37, 4881–4892.
- Ostfeld, R. S., & Keesing, F. (2000). Pulsed resources and community dynamics of consumers in terrestrial ecosystems. *Tree*, 15(6), 232–237.
- Patterson, W. P., Smith, G. R., & Lohmann, K. C. (1993). Continental paleothermometry and seasonality using the isotopic composition of aragonitic otoliths of freshwater fishes. In *Climate Change in Continental Isotopic Records* (ed. P. K. Swart et al.) (Vol. 78, pp.191–202). Geophysical Monograph Series.
- Power, M. J., Whitlock, C., Bartlein, P. J., & Stevens, L. (2006). Fire and vegetation history during the last 3800 years in northwestern Montana. *Geomorphology*, 75, 420–436.
- Reynolds, J. F., Kemp, P. R., Ogle, K., & Fernandez, R. J. (2004). Modifying the “pulse-reserve” paradigm for deserts of North America: precipitation pulses, soil water, and plant responses. *Oecologia*, 141, 194–210.
- Saros, J. E., Clow, D. W., Blett, T., & Wolfe, A. P. (2003). Critical nitrogen deposition loads in high-elevation lakes of the Western US inferred from paleolimnological records. *Water Air Soil Pollution*, 216, 193–202, doi: 10.1007/s11270-010-0526-6.
- Schwinning, S., & Sala, O. E. (2004). Hierarchy of responses to resource pulses in arid and semi-arid ecosystems. *Oecologia*, 141, 211–220.
- Thorrold, S. R., Campana, S. E., Jones, C. M., & Swartz, P. K. (1997). Factors determining $\delta^{13}\text{C}$ and $\delta^{18}\text{O}$ fractionation in aragonitic otoliths of marine fish. *Geochimica et Cosmochimica Acta*, 61(14), 2909–2919.
- White, R. M. P., Dennis, P. F., & Atkinson, T. C. (1999). Experimental calibration and field investigation of the oxygen isotopic fractionation between biogenic aragonite and water. *Rapid Communication in Mass Spectrometry*, 13, 1242–1247.
- Zhou, G. & Zheng, Y. (2003). An experimental study of oxygen isotope fractionation between inorganically precipitated aragonite and water at low temperatures. *Geochimica et Cosmochimica Acta*, 67(3), 387–399.

CHAPTER 2

IMPLICATIONS OF SPATIAL VARIATIONS IN SOIL ORGANIC MATTER $\delta^{13}\text{C}$ VALUES ON RECONSTRUCTING PALEOENVIRONMENTS IN EASTERN AFRICA

2.1 Introduction

Tropical plants principally use two photosynthetic pathways: the "C₃- and "C₄- photosynthetic pathways." Almost all dicots, including many herbaceous plants, use the C₃ pathway, whereas most tropical grasses and sedges (monocots) are C₄ plants. Isotopic differences arise from the two primary photosynthetic pathways of the Calvin cycle (C₃) and the Hatch–Slack cycle (C₄) (O'Leary, 1981, 1988) that differ in leaf-level ¹³C discrimination during carboxylation reactions (Farquhar et al., 1982). Consequently, the C₃ and C₄ vegetation are distinct in foliar ¹³C ($\delta^{13}\text{C}_{\text{FC}}$) values, with C₃ plants averaging ~ -27.5‰ while C₄ average -12.0‰ (Smith & Epstein, 1971). Isotope values are calculated as shown in equation 3.

$$\delta X (\text{‰}) = 1000 * (R_{\text{sample}} / R_{\text{standard}} - 1)$$

Equation 3

where ‘ X ’ is either ^{15}N , ^{18}O , or ^{13}C , R is $^{15}\text{N}/^{14}\text{N}$, $^{18}\text{O}/^{16}\text{O}$, or $^{13}\text{C}/^{12}\text{C}$, respectively, and δX is expressed in permil (‰) relative to internationally agreed standards: V-PDB for both carbon and oxygen, and atmosphere (AIR) for nitrogen $\delta^{15}\text{N}$, respectively.

The East African rift system contains hominin-bearing deposits that are important archives for reconstructing paleovegetation in the Neogene (Feibel et al., 1991). In East Africa, tectonic uplift has played a significant role in drastic reorganization of atmospheric circulation, leading to more arid and open “savannas” over the last 8 million years (Sepulchre et al., 2006). Between 10 and 6 Ma, ungulate mammals shifted from C_3 -dominated diets in the earlier middle to late Miocene to C_4 (grass-dominated) diets (Leakey et al., 1996; Uno et al., 2011). The tectonics movements also caused geomorphic changes, altering the flow patterns of major rivers (including Omo) in the East African Rift system throughout the Pleistocene (Brown & Feibel, 1991; Bruhn et al., 2011; Levin et al., 2011).

The $\delta^{13}\text{C}$ values of soil carbonates indicate that vegetation cover in the Omo-Turkana basin was open (less than 40% woody cover) over the last ~6 million years (Cerling et al., 2011) with temperature comparable to that of the modern day (mean annual temperature ~ 29 °C) (Passey et al., 2010). As a consequence, riparian corridors were preferred habitats of hominins (WoldeGabriel et al., 1994) as most hominin sites occur around riparian habitats (e.g., Johanson et al., 1982; Leakey et al., 1995; Asfaw et al., 1999). Modern riparian corridors contain a mosaic of grasslands, open bushlands, and gallery forest that are hotspots of biodiversity (e.g., Measey & Tolley, 2011) and influence the areal distribution of ungulates in this region (Feibel et al., 1991). The range of land cover types associated with riparian corridors are thought to have presented a

range of biomes that *Homo erectus* may have exploited during dispersal out of Africa (Huffman, 1999, 2001; Bettis et al., 2009).

To accurately assess the impact of climate change in this region, spatially explicit criteria for reconstructing environments that reduce ambiguity must be developed to link paleoecology to patterns and processes of early hominid evolution (Kingston, 2007). Such criteria would enhance conceptualization, modeling, and interpretation of environmental data at a given spatial or temporal resolution (Monger et al., 2010). For instance, the leaf level ^{13}C fractionation varies with moisture availability, photon flux density, relative humidity, and temperature (Farquhar et al., 1989) that scale-up from leaf-scale, to patch-scale, all the way to regional- and global-scale (Still et al., 2003). Consequently, different combinations of these ecological factors influence the $\delta^{13}\text{C}_{\text{fc}}$ of C_3 and C_4 plants variously.

The $\delta^{13}\text{C}$ values of soil organic carbon (hereafter $\delta^{13}\text{C}_{\text{SOC}}$) from a variety of sites ranging from forest to desert are related to woody cover of the landscape (e.g., Cerling et al., 2011, 2010; Wynn & Bird, 2010). Two end member mixing models are often used when reconstructing paleovegetation from $\delta^{13}\text{C}_{\text{SOC}}$ (Equations 4–5: Wang et al., 2008).

$$\text{C}_3 \% = (\delta^{13}\text{C}_{\text{SOM}} - \delta^{13}\text{C}_{\text{C}_4}) / (\delta^{13}\text{C}_{\text{C}_3} - \delta^{13}\text{C}_{\text{C}_4}) \times 100 \quad \text{Equation 4}$$

$$\text{C}_4 \% = 100 - \text{C}_3 (\%) \quad \text{Equation 5}$$

However, fractional woody cover (F_{WC}) is nonlinearly related to total $\delta^{13}\text{C}_{\text{SOC}}$ (Magnusson et al., 2002; Wynn et al., 2006; Wynn & Bird, 2008; Wang et al., 2009; Cerling et al., 2010; Cerling et al., 2011). Because of the presence of C_3 forbs and herbs,

the contribution of C₃ woody cover to total vegetation is not a simple linear mixing relationship between C₃ and C₄ end members, as is implied by Equations 4 and 5 (Cerling et al., 2010; Cerling et al., 2011). Understanding the relationship between F_{WC} and $\delta^{13}\text{C}_{\text{SOC}}$ is therefore key to reconstructing vegetation cover from paleosols.

Fine spatial resolution (below 1 m) images are required for mapping individual trees and shrubs (Moran et al., 1997) and for determining the F_{WC} for modeling $\delta^{13}\text{C}_{\text{SOC}}$ (Goetz et al., 2003). This is because low-resolution imagery may miss strips and patches of vegetation smaller than the dimensions of individual pixels and may be assigned extraneous land cover classes during classification (Foschi & Smith, 1997). High spatial resolution orthoimagery, including IKONOS (Goetz et al., 2003), Quickbird (Mueller & Pierce, 2003; Wang et al., 2009), and aerial photographs (Bai et al., 2009) yield high quality estimates of woody cover for determining soil properties. However, generating accurate $\delta^{13}\text{C}_{\text{SOC}}$ models is often a challenge because C₄ grasses commonly dominate the understory and thus influence the $\delta^{13}\text{C}_{\text{SOC}}$ values as F_{WC} changes.

In the current study, we test the hypothesis that soil $\delta^{13}\text{C}_{\text{SOC}}$ values indicate woody cover distribution patterns that are influenced by tree local disturbance and moisture availability at patch-scale (≤ 10 ha) and water deficit at landscape-scale. We establish the spatial relationship between F_{WC} and $\delta^{13}\text{C}_{\text{SOC}}$ within East Africa at patch-scale and landscape-scale in order to reconstruct probable past vegetation structure from $\delta^{13}\text{C}_{\text{SOC}}$. We use spectral parameters of high-resolution orthoimagery to estimate F_{WC} at selected sites in eastern Africa, and to generate spatially predictive models for $\delta^{13}\text{C}_{\text{SOC}}$ values. We evaluate the models generated against the regional moisture deficit to determine the role of climate on $\delta^{13}\text{C}_{\text{SOC}}$ values.

2.2 Methods and materials

2.2.1 Study area

The study sites include closed canopy forests, closed woodlands, open woodlands, bushland/thickets, and grasslands in Kenya and Ethiopia (Figure 9) and encompass nearly the entire range of habitat types described by United Nations Scientific and Cultural Organization (UNESCO) (White, 1983).

2.2.2 Soil sampling and preparation

From each site, soils samples (0 to 10 cm depth) were collected in canopy gaps and under the canopies of woody vegetation, sieved through a 140 mesh sieve to remove litter and other plant fragments, and dried at 60 °C for 48 hrs. Subsamples for analysis of soil organic matter were treated with excess 0.1N HCl to remove soil carbonates, and left to react for 48 hrs. The samples were then transferred into 1.7 ml centrifuge vials, placed into a centrifuge, and spun at 4000 rpm for five minutes, following which the supernatant was decanted. Remaining acid was rinsed from the soils by adding distilled water, centrifuging, and decanting the supernatant. Rinsing was repeated with distilled water until the pH became neutral ($\text{pH} \approx 7.0$). The soils were then dried in an oven at 60 °C for 48 hrs.

2.2.3 Stable isotope analysis of soil organic matter (SOM)

Treated soils for analysis of $\delta^{15}\text{N}_{\text{SOM}}$ and $\delta^{13}\text{C}_{\text{SOM}}$ were combusted in a Costech 4010 Elemental Analyzer at 1650 °C and inlet to a Finnigan® MAT 252 Isotope Ratio

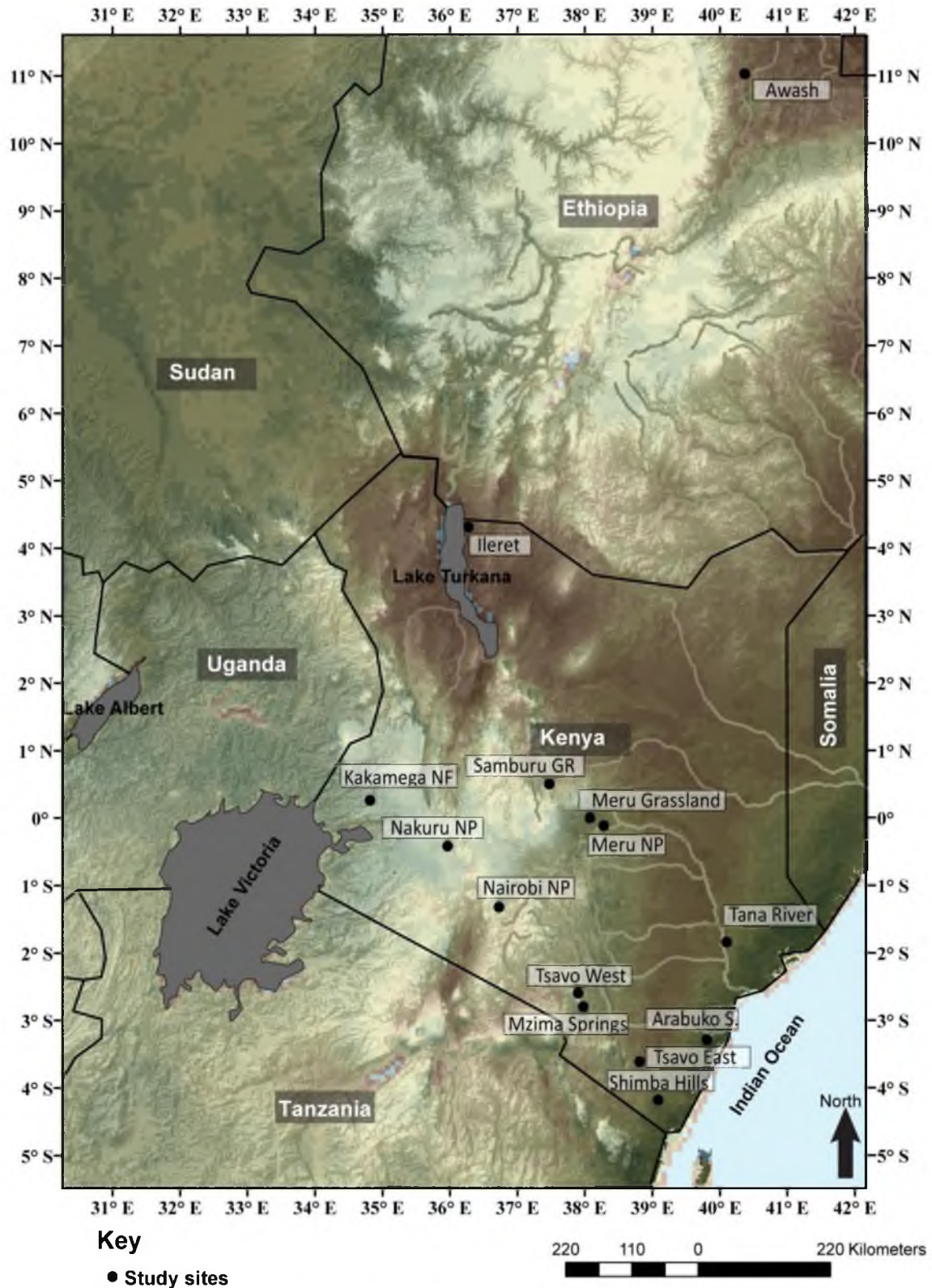


Figure 9. Map of study sites. Of the 15 sites, 14 are located in Kenya while 1 site (Awash) is in Ethiopia. These sites vary in woody cover as influenced by climate and

Mass Spectrometer (IRMS) in continuous flow mode. Isotope values were calculated as shown in Equation 3. Carbon and nitrogen yields were determined from the preliminary samples, optimum sample sizes established, and samples run in duplicate with newly determined masses. The analytical precision of isotopic analysis of $\delta^{15}\text{N}_{\text{SOM}}$ and $\delta^{13}\text{C}_{\text{SOM}}$ are 0.1‰ and 0.2‰, respectively.

2.2.4 Image classification and F_{WC} analysis

Radiometrically and geometrically corrected high-resolution orthoimagery was acquired from EMAP Inc. (e.g., IKONOS, Quickbird, Geoeye1, and WV1). The images were selected such that the study sites were cloud free and the entire image had less than 15% cloud cover (Table 1). There were insufficient ground control points to perform further geometrical corrections.

2.2.5 Patch-scale image analysis

1–10 hectare areas centered on the soil sample sites were clipped from the orthoimagery and classified. All image classification was performed in ENVI 4.7 (ITT VIS Inc.). Various supervised classification algorithms, including spectral angle mapper, Mahalanobis distance, minimum distance, maximum likelihood, and parallelepiped classifiers were used on the red-blue-green (RGB – also called true-color) imagery (IKONOS and Quickbird). An error matrix was generated from independent training sets and classification accuracy assessed with the Kappa statistic (Equation 6).

Table 1. High spatial resolution imagery from different sensors used in woody cover estimation. Riparian corridors, grasslands maintained by burning (Shimba Hills), and agricultural areas are included in woody cover calculations. The images vary in spectral and spatial resolution but generally have pixel sizes less than a meter.

Location	Latitude Degrees (°)	Longitude Degrees (°)	Sun Angle Azimuth Degrees (°)	Sun Elev. Degrees (°)	Av. Sat. Elev. Degrees (°)	Tot Area km ²	Adj. Area km ²	Sensor	Acquisition date
Arabuko Sokoke	-3.30	39.91	126.3	57.6	80.5	25.1	15.6	WV01	14-Jan-2008
Awash Ileret	11.09	40.54	125.9	71.2	72.9	25.3	21.5	QB02	23-Sep-2008
Bushland	4.29	36.26	146.3	59.4	60.8	25.2	25.2	WV01	26-Nov- 2008
Ileret Riparian	4.32	36.27	73.3	66.3	87.0	25.2	21.5	QB02	23-Sep-2008
Kakamega	0.37	34.87	97.3	68.0	84.2	25.0	15.9	QB02	25-Aug- 2004
Meru forest	-0.07	38.42	103.4	61.8	ND	48.9	48.9	GeoEye-1	4-Mar-2009
Meru open Mzima Springs	0.20 -2.96	38.23 38.04	101.9 127.3	70.5 64.9	80.5 64.2	25.5 25.2	18.3 18.9	WV01	2-Oct-2008 30-Jan-2010
Nairobi N P	-1.34	36.79	128.0	61.3	50.5	28.7	24.5	WV02	27-Jan-2010
Nakuru Forest	-0.40	36.11	125.7	55.3	81.8	26.7	24.2	QB02	22-Jan-2004
Nakuru Bushland	-0.32	36.04	144.5	63.5	59.4	25.9	25.3	WV01	30-Nov- 2008
Nakuru Grassland	-0.44	38.42	144.6	63.4	60.1	25.6	18.5	WV01	30-Nov- 2008
Samburu	0.59	37.53	142.9	60.7	58.4	26.1	26.1	QB02	7-Jan-2008
Shimba Hills	-4.24	39.41	126.4	59.3	ND	49.1	31.6	IKONOS- 2	13-Jan-2008
Tana River	-1.88	40.14	114.2	62.5	ND	49.0	28.6	IKONOS- 2	15-Feb-2007
Tsavo West	-2.74	38.13	100.5	70.6	76.0	17.4	11.7	WV02	27-Jan-2010

ND signifies a field for which no data are available.

Adj. Area refers to the actual area used to compute woody cover after clouds, riparian corridors, and areas impacted by humans (i.e., agricultural and urban areas) are masked out. In some images, the adjusted area is equal to the total area (Tot. Area) encompassed by the orthoimagery

Ave. Sat. Elev. stands for the average satellite elevation angle from the ground (Nadir) when the photo was taken.

Table 1. continued

Spectral Res.	Spatial Res. m	Orthorectification		Cloud cover	F _{wc}	Accuracy	Kappa
		Bias error (m)	Random error (m)	%	%	%	Coefficient
PAN	0.5	9.7	0.1	0.0	ND	ND	ND
RGB	0.60	19.09	0.12	9.99	12.70	90.52	0.86
PAN	0.5	20.8	0.1	0.3	ND	ND	ND
PAN	0.6	20.22	0.12	0.00	22.81	95.13	0.90
RGB	0.60	30.55	0.12	7.10	77.04	98.12	0.96
RGB	0.50	20.50	0.25	0.00	64.84	98.95	0.98
PAN	0.5	16.00	14.08	0.10	ND	ND	ND
PAN	0.5	16.9	0.1	0.0	ND	ND	ND
RGB	0.50	3.49	0.10	0.00	30.86	96.99	0.89
RGB	0.6	4.43	0.40	10.0	41.49	95.96	0.92
PAN	0.5	19.6	0.1	0.0	ND	ND	ND
PAN	0.5	18.4	0.1	0.0	ND	ND	ND
RGB	0.60	26.45	0.12	0.00	19.79	96.90	0.96
RGB	0.8	20.8	0.1	14.00	64.59	95.92	0.93
RGB	0.80	4.39	0.40	1.00	28.1	92.20	0.89
RGB	0.5	18.2	0.1	0.0	38.3	96.4	0.95

$$K = \frac{P(a) - P(e)}{1 - P(e)} \quad \text{Equation 6}$$

$P(a)$ is the proportion of ground-truth pixels observed to agree with those of the classified image, and $P(e)$ is the hypothetical probability that ground-truth pixels agree with those of the classified image by chance alone (Cohen, 1968). The maximum likelihood approach yielded the best classification result and was adopted in subsequent classification of RGB imagery.

Decision tree image classification methods combining texture filtering and density slicing were employed on panchromatic imagery (WV1, WV2, and GeoEye). The density slicing classification was done by visual inspection of classified outputs under various grayscale value cut-offs. Generating an error matrix and using it to compute the Kappa statistic helped assess the classification accuracy.

2.2.6 Landscape-scale image analysis

Supervised image classification of each whole image (landscape-wide) using maximum likelihood was performed as outlined in Section 2.4.1, but this time, the classification was done for RGB imagery. The details on the classification accuracy are shown in Table 1 with the various land cover and land-use elements across the classified imagery.

2.2.7 $\delta^{13}\text{C}_{\text{SOC}}$ modeling

From each thematic land cover grid that included woody vegetation, grasslands, base, water, and man-made features, water bodies and manmade features were masked

out; woody cover binary grids were derived by lumping the woody and shrubs pixels into a woody category (DN value = 1) and all other pixels as nonwoody (DN value = 0) (Equation 5).

$$Pixels_{output} = \begin{cases} 1woody \\ 0nonwoody \end{cases} \quad \text{Equation 7}$$

The fractional woody cover grids were computed using a Gaussian filter (PSF Gaussian) developed by Frank Varossi (NASA/GFSC; http://idlastro.gsfc.nasa.gov/ftp/pro/image/psf_gaussian.pro [June 2nd 2011]) that resamples pixel values under a weighted scheme (Figure 10). A regression of woody cover against $\delta^{13}C_{SOM}$ (Equation 8; $R^2 = 0.83$):

$$\delta^{13}C_{SOC} = -9.9725 * (\arcsin[\sqrt{[\% Woody Cover]}]) - 14.128 \quad \text{Equation 8}$$

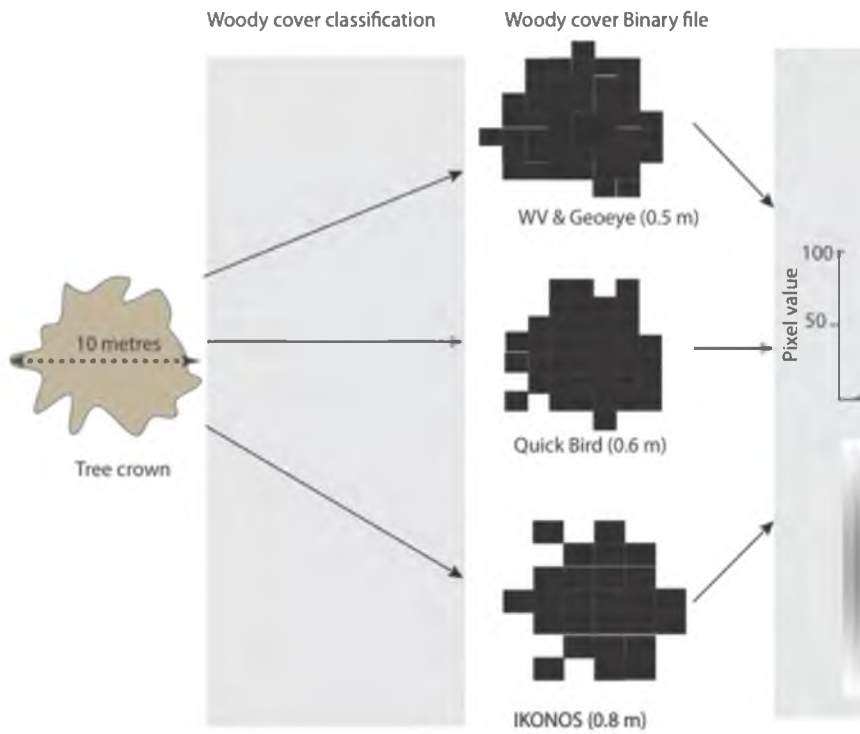
was used to generate $\delta^{13}C_{SOC}$ prediction grids for study sites that include patch-scale (1–10 hectare areas) and landscape-scale (>10 hectare area) and their corresponding histograms and cumulative frequency curves were computed.

37

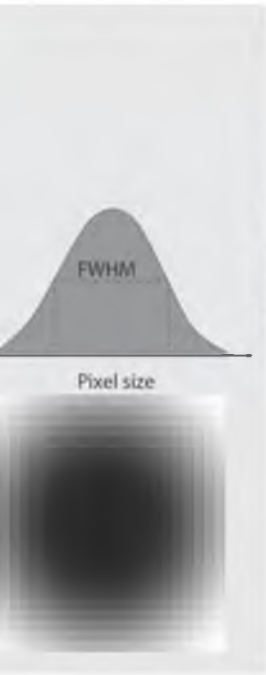
2.2.8 Relationship between woody cover and water deficit

In relating climate-influenced water deficit on the woody cover at landscape levels, excluding the riparian corridors was necessary to control for the influence of water derived from rivers on the immediate floodplain. Developed areas (urban and

Figure 10. An illustrated procedure for transforming woody cover grids of various spatial resolutions into equally weighted output grids for $\delta^{13}\text{C}_{\text{SOC}}$ modeling. Fine resolution imagery yields classification results that bear closer resemblance to the original crown outline than coarse resolution imagery. The Gaussian filter resamples woody cover pixels such that the higher resolution pixels are weighted more heavily than coarse resolution pixels. The least common multiple (LCM) of the spatial resolutions of the input imagery becomes the standardizing function that determines how many pixels of the input grids are used in developing images with a common spatial resolution. The desired Full-Width Half-Max (FWHM) is specified as an array of pixels in the x and y dimensions of the image that act as normalizing centers of the Gaussian filter. The pixel values of the resulting output grid are normalized, hence allowing for more accurate modeling of $\delta^{13}\text{C}_{\text{SOC}}$ and subsequent comparisons among study areas.



Gaussian filter



Woody cover model

Output resolution = LCM (12m)



agricultural areas), grasslands maintained by burning, and tree shadows were also masked out. Water deficit (the difference between precipitation and the amount of moisture that would be lost to evapotranspiration under unlimited moisture supply (Levin et al., 2006; Wynn et al., 2006) was compared with woody cover (Wynn et al., 2006). Water deficit was modeled through Thornthwaite's equation for potential evapotranspiration (Thornthwaite, 1948) because climate data in East Africa are limited:

$$ET_o = C(10 * t_{med} / I)^a \quad \text{Equation 9}$$

$$I = \sum i \quad \text{Equation 10}$$

$$i = (t_{med}/5)^{1.514} \quad \text{Equation 11}$$

$$a = 0.49239 + 1792 \times 10^{-5} I - 771 \times 10^{-7} I^2 + 675 \times 10^{-9} I^3 \quad \text{Equation 12}$$

where ET_o is the potential evapotranspiration (mm d^{-1}); I is the annual heat index (the sum of 12 monthly index values i); i is the monthly heat index; and t_{med} is the mean daily temperature ($^{\circ}\text{C}$). a = coefficient, which varies with the heat index. The values are then corrected for day length and computed from the Julian date and latitude using equations of Forsythe et al. (1995) and number of days in a month. The rainfall dataset was derived from data in the 1975 report of the East African Meteorological Department (EAMD) and from other published weather data for places where EAMD data were not available.

2.3 Results

2.3.1 Woody cover classification

The results of woody cover classification reveal variations in woody cover at landscape-scales ($\sim 25 \text{ km}^2$) where hydrology (e.g., Awash, Samburu, and Tana River),

anthropogenic disturbance (e.g., Kakamega forest and Shimba Hills Game Reserve), and topography (e.g., Nakuru) have a significant influence (Figure 11).

The relationship between $\delta^{13}\text{C}_{\text{SOM}}$ and FWC for East African sites analyzed in this study is nonlinear and using the variance stabilizing arcsin squareroot transformation (i.e., $\arcsin[\sqrt{\% \text{ Woody Cover}}]$) gives the best fit line to relate the dependent variable that was a fraction cover to $\delta^{13}\text{C}_{\text{SOM}}$ (Figure 12). There is a greater variation at 40% FWC whereby one site (Nakuru Bush) has woody cover 40% and $\delta^{13}\text{C}_{\text{SOM}}$ value of -15.8‰ while another site (Turkwel) with a similar woody cover (41%) has $\delta^{13}\text{C}_{\text{SOM}}$ (-24.4‰). These disparate values are a manifestation of the relative contribution of grass cover on soil organic matter that may be influenced by edaphic factors at patch-scale (<10 ha) as manifested in wide-ranging values in $\delta^{13}\text{C}_{\text{SOM}}$ values (Figure 13) and also at landscape-scale (Figure 14).

2.3.2 Relationship between woody cover and water deficit

The water deficit varies significantly among sites, with Ileret having the greatest water deficit (1604 mm/year) while Kakamega Forest has the least (245 mm/year) (see Table 2). However, Arabuko Sokoke has the greatest woody cover (97%) while Tsavo West has the lowest woody cover (~9%).

The relationship between moisture deficit and woody cover of upland (nonriparian) sites is linear (Figure 15) but weakly correlated ($R^2 = 0.31$). The $p < \alpha$ values (df 1,8; $\alpha 0.05$) indicate there is a relationship between water deficit and woody cover. However, the woody cover and water deficit are poorly correlated.

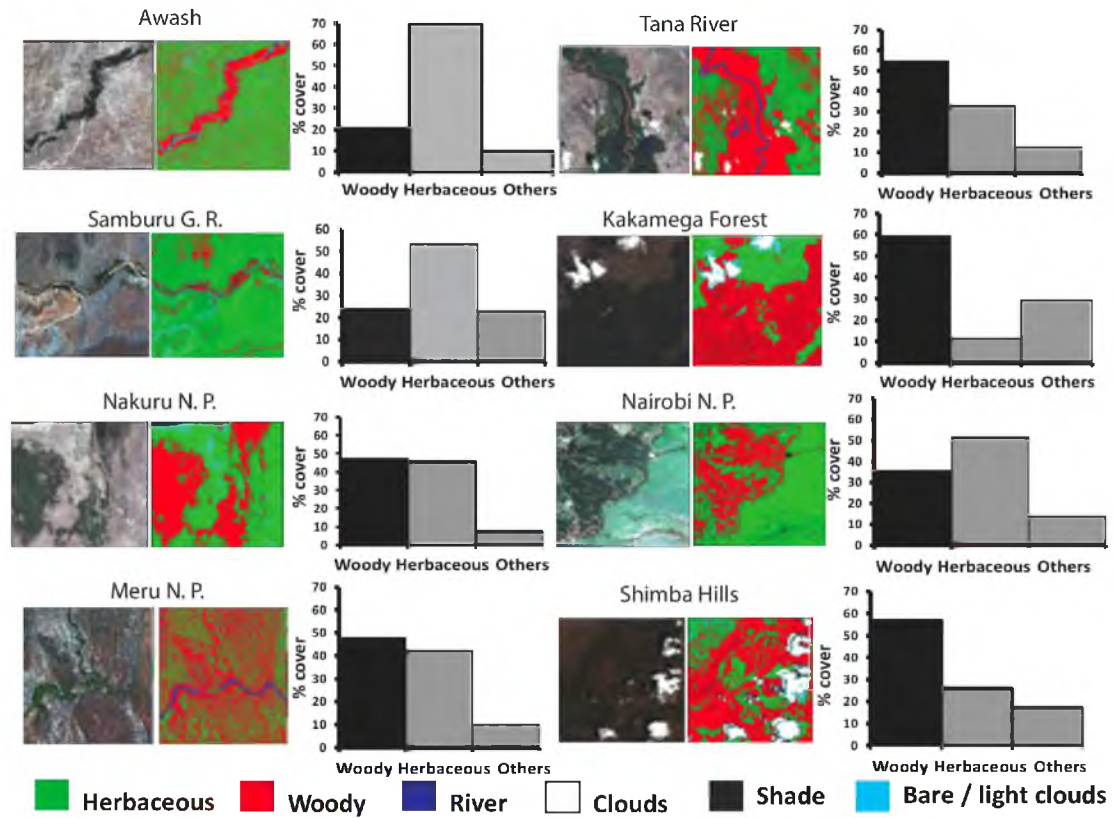


Figure 11. Results of woody cover classification of selected sites. Cloudy areas are excluded in the analysis.

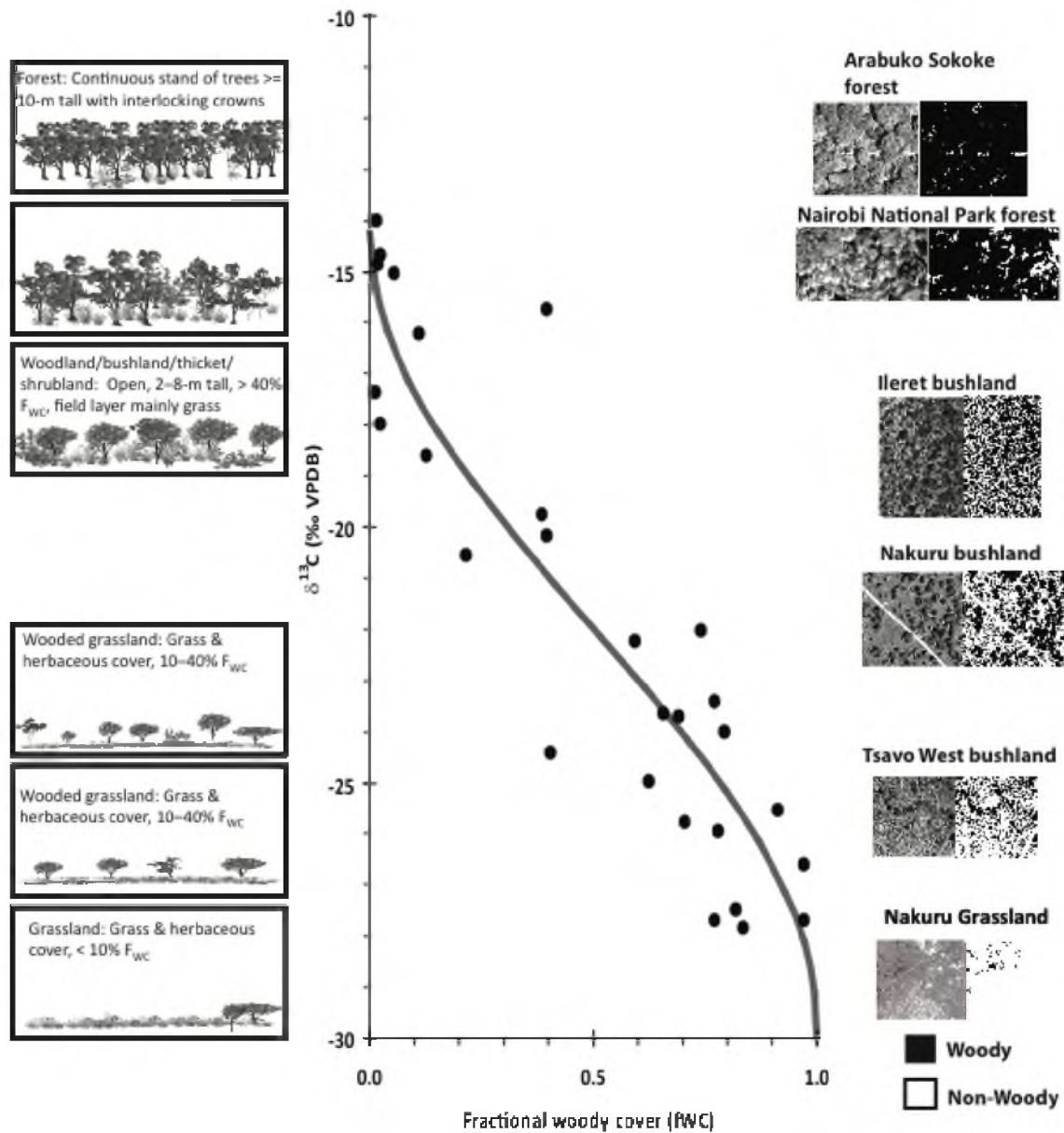


Figure 12. Woody cover versus measured $\delta^{13}\text{C}_{\text{SOC}}$ (Cerling et al., 2011) with a generalized vegetation structure on the left and some examples of the woody cover grids (~ 1 ha) on the right. The model integrates the soil samples obtained within the canopy and canopy gaps, so that the $\delta^{13}\text{C}_{\text{SOC}}$ variance within site is captured (see data in the Appendix A). Nonlinear regression is performed using arcsine and square-root transformation of woody cover to achieve the best fit of the data.

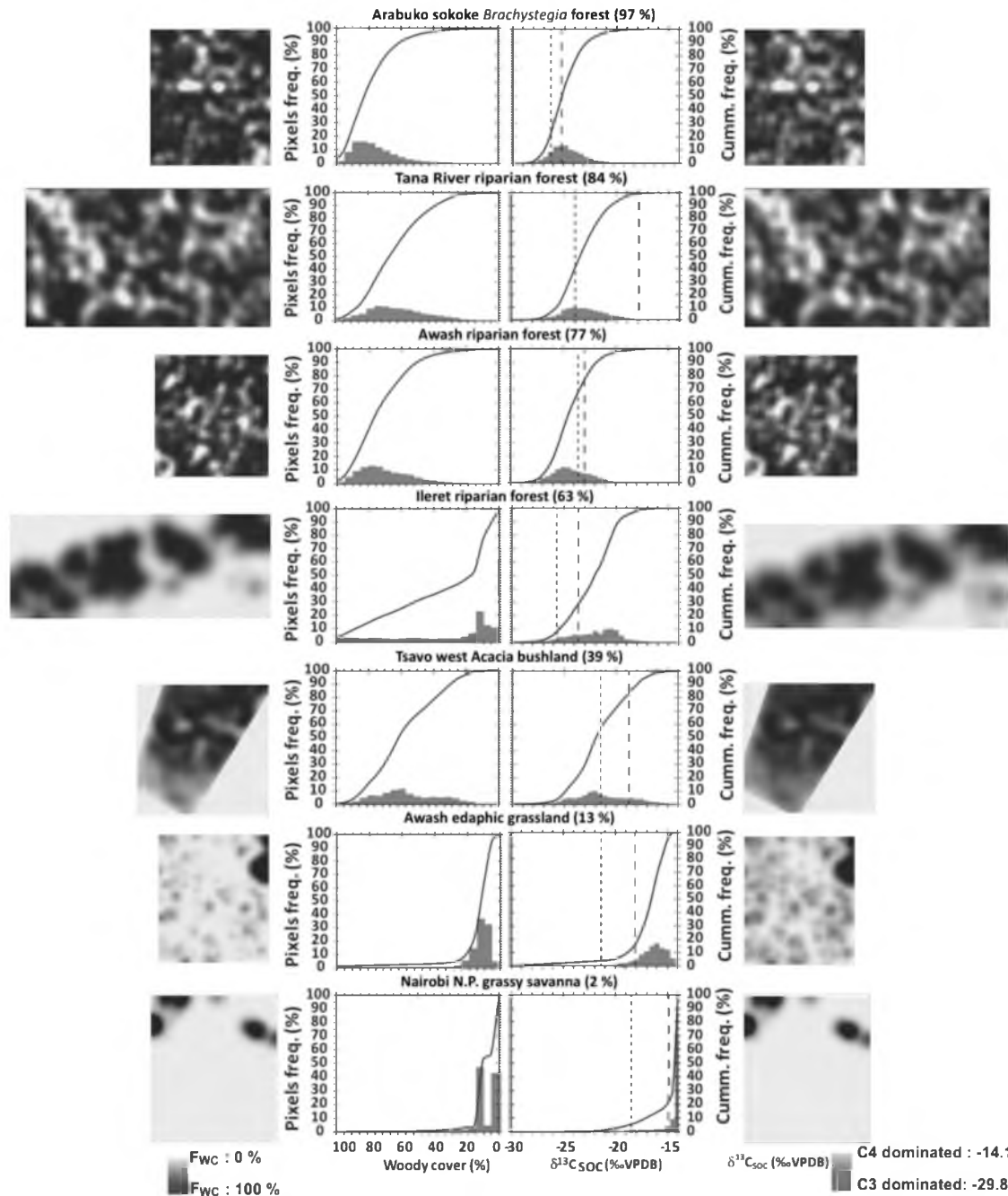


Figure 13. Histograms, cumulative frequency curves, and prediction grids of $\delta^{13}\text{C}_{\text{SOC}}$ for 7 study sites ranging from 1 to 10 hectare in size and whose woody cover is indicated in parentheses. These grids represent areas where the soil samples used to develop the regression model were obtained (i.e., subsections of landscape grids in Figure 10). The lines (---) and (---) indicate the average $\delta^{13}\text{C}_{\text{SOC}}$ values of the soil samples collected under canopy and in canopy gaps, respectively. These $\delta^{13}\text{C}_{\text{SOC}}$ trends are expected if the sites were to be randomly sampled.

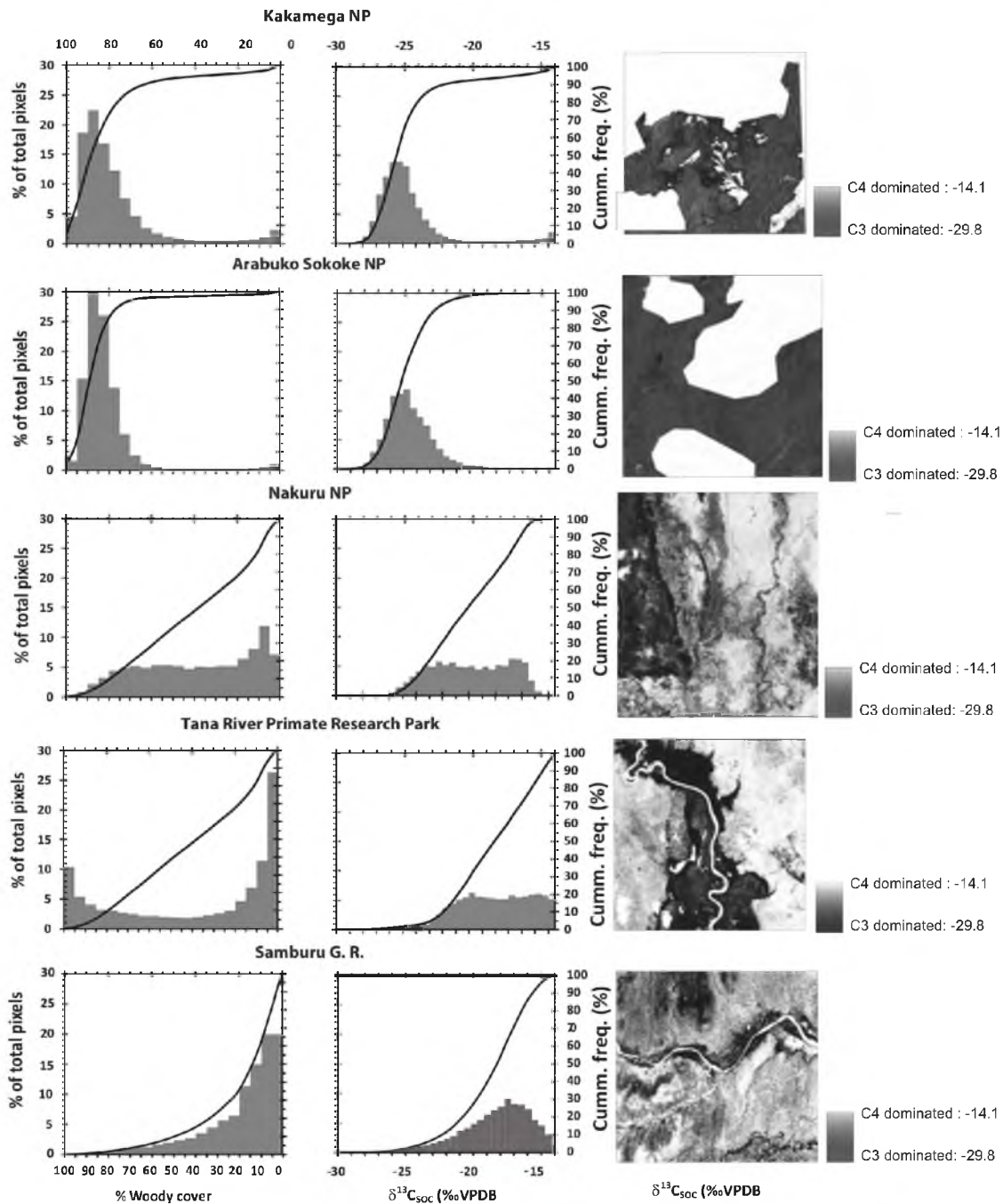


Figure 14. Histograms, cumulative frequency curves, and prediction grids of $\delta^{13}\text{C}_{\text{SOC}}$ for 5 study sites. These models show the expected $\delta^{13}\text{C}_{\text{SOC}}$ trends if the sites were to be randomly sampled. There is a significant influence of hydrology on $\delta^{13}\text{C}_{\text{SOC}}$ values at the landscape-scale evaluated.

Table 2. Climate data and woody cover of selected study sites. The climate summaries were calculated from the East African Meteorological Department report (1970) and from Barboni et al. (1999) for Awash study site. Water deficit (WD) calculations are discussed in the Methods section. The initials NP, GR, and PR refer to National Park, Game Reserve, and Primate Research. The areas excluded in woody cover calculations are indicated and explanation provided in the footnotes.

Study Location	Climate Station	Latitude	Longitude	Altitude m	MAT °C	MAP mm	RH %	WD mm/yr	WC %
Arabuko Sokoke NP	Malindi Airport	-3.23	40.01	20	26.1	1096	80	540	97
§Awash	Barboni <i>et al.</i> , 1999	11.07	40.54	515	30.0	500	ND	1320	13
*Kakamega NP	Kitale Met. Station	-0.17	35.00	1919	18.2	1191	81	245	77
Ileret	Lodwar	3.12	35.62	506	29.2	178	57	1604	23
†Nairobi NP	Nairobi, Wilson Air.	-0.30	36.75	1792	17.6	909	81	540	33
†Nakuru NP	Nakuru	-0.27	36.07	1871	17.4	957	77	451	41
Samburu GR	Isiolo	0.35	37.58	1104	23.5	648	62	927	20
§Tana River PR	Hola, Tana River	-0.48	40.02	44	27.5	475	76	1241	6
‡Tsavo West NP	Voi	-3.40	38.57	560	24.9	549	73	1059	38
Meru NP	Garissa Met. Sta.	-0.47	34.12	147	28.5	321	45	1254	65

† Urban areas excluded as well as grasslands falling in a different climate regime from the forest

* Agricultural areas and managed grasslands excluded

§ Riparian corridors excluded because they do not reflect the climate of the site

‡ Area where woody cover classification was confounded poor spectral resolution excluded

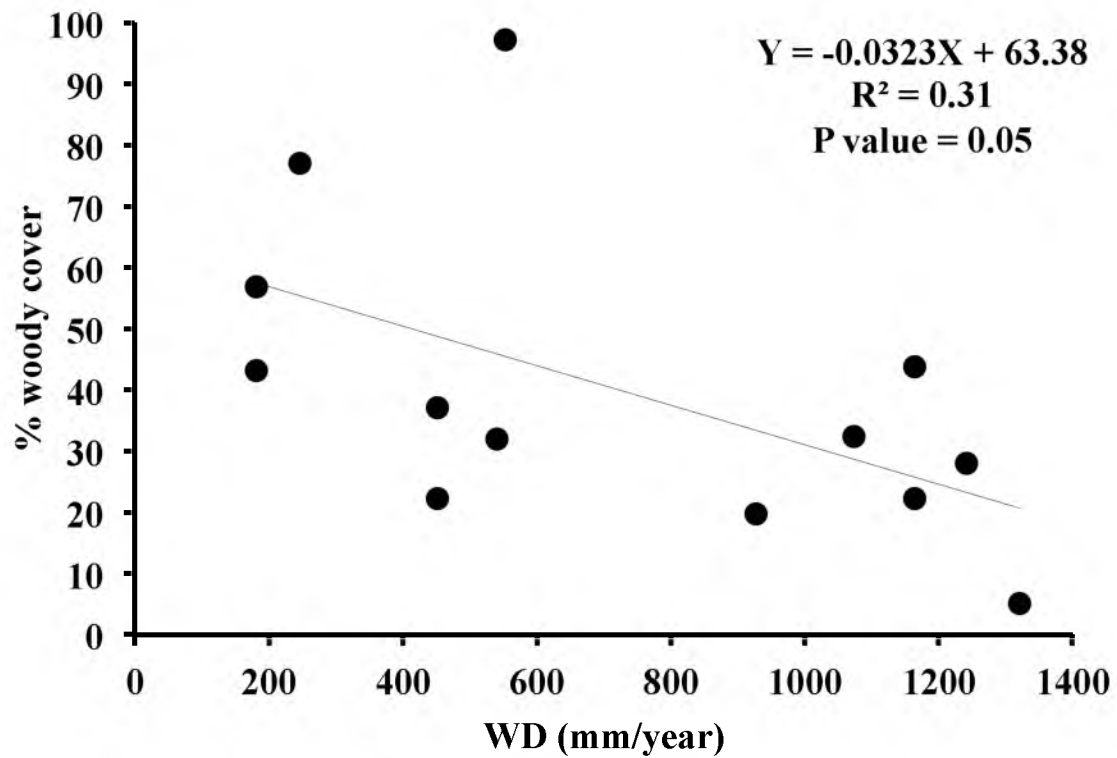


Figure 15. The relationship between water deficit (WD) and woody cover for selected sites with relatively accurate woody cover classification. There is a linear relationship, suggesting that WD can account for woody cover distribution in the East African Region. Sites (Arabuko Sokoke and Shimba Hills) proximal to the Indian Ocean have high woody cover due to high relative humidity in addition to high precipitation.

2.3.3 The relationship between net aboveground primary productivity patterns and F_{WC}

We used the normalized difference vegetation index (NDVI) from the SPOT VGT 10S series as an indicator of change in the aboveground net primary productivity (AG-NPP) in response to precipitation pulses. AG-NPP is strongly correlated to woody cover (Paruelo et al., 1997) and reflects how effective moisture pulses are in driving photosynthesis. A 10-day 1 km normalized difference vegetation index (NDVI) from SPOT VGT 10S series imagery covering the period between April 1998 and November 2009 were downloaded (<http://free.vgt.vito.be/>) and used to statistically evaluate changes in AG-NPP. The NDVI images were layer-stacked chronologically, and used to calculate the long-term average and standard deviation of NDVI values per pixel.

A spatial correspondence between herbaceous cover and NDVI variations is evident by comparing the NDVI response patterns represented by 12-year standard deviation of SPOT NDVI series and the MODIS VCF product that models woody and herbaceous cover distribution patterns at the subpixel level (Appendix B).

2.4 Discussion

The hypothesis that soil $\delta^{13}C_{SOC}$ values indicate woody cover distribution patterns that are influenced by tree local disturbance and moisture availability at patch-scale (≤ 10 ha) are well supported by the data in this analysis. However, the relationship between woody cover and water deficit at landscape-scale is weak and insignificant. The study shows that the savanna biome contains enormous diversity in physiognomy and spatial structure of the vegetation. Variations in $\delta^{13}C_{SOC}$ are sufficiently characterized and modeled using fine-resolution orthoimagery through spatial analysis of clustering

and dispersion patterns of individual trees and shrubs. Since F_{WC} is related to percent abundance of C_3 plants in the tropics (Goetz et al., 2003; Wang et al., 2009; Bai et al., 2009) in contrast to regions where C_3 vegetation also dominates non-ligneous vegetation (Magnusson et al., 2002; Still et al., 2003), characterizing the woody cover at landscape-scale will aid in establishing factors that cause patch-scale variations in woody cover and also in determining how they scale-up. Knowledge of factors that determine woody cover is essential in characterizing historical changes in $\delta^{13}C_{SOC}$ from climate and disturbance (Bai et al., 2009), and also in providing a context for interpreting paleoenvironments (Cerling et al., 2011).

2.4.1 Variations of F_{WC} and $\delta^{13}C_{SOC}$ patterns with water deficit

The broad distribution in woody cover and $\delta^{13}C_{SOC}$ in areas with less than 80% woody cover (Figure 13–14) and the poor correlation between woody cover and water deficit (Figure 15) indicates that several biomes (forest, savanna, and treeless (barren or grassy)) co-exist within each landscape (Appendix B). In Kakamega NP and Shimba Hills GR, clear patches of grassland amid closed-canopy forests represent bimodal states promoted by frequent burns. Fire acts as a positive feedback that maintains open canopies in stable states (Keeley & Rundel, 2005; Hirota et al., 2011; Staver et al., 2011) and results in discontinuous woody cover with intermediate rainfall (1000 to 2500 millimeters) (Hirota et al., 2011; Staver et al., 2011). Edaphic factors may also contribute to the observed variations in F_{WC} within landscapes. For instance, Wynn et al. (2006) observed that mean vapor pressure deficit and annual flux of water available to plants

exert a strong influence on woody cover and soil organic carbon $\delta^{13}\text{C}$ values in addition to soil texture.

It has been argued that fire played a crucial role in the global expansion of savanna and C_4 grasslands in the Miocene, a period characterized by increased aridity and rainfall seasonality (Keeley & Rundel, 2005). According to NDVI response patterns, areas with high standard deviations of SPOT NDVI also have greater proportion of herbaceous cover areas as per MODIS VCF estimates (Appendix A). This suggests that herbaceous plants account for the most significant changes in aboveground primary productivity. C_4 vegetation that dominates the herbaceous community in Eastern Africa (Tieszen et al., 1997) may influence the $\delta^{13}\text{C}_{\text{SOC}}$ in the Eastern African region according to how open the woody cover is.

2.4.2 Variations of $\delta^{13}\text{C}_{\text{SOC}}$ patterns with hydrology

Hydrology, moderated by landscape geomorphology, influences the woody cover within a riparian corridor in proportion to the volume of water flowing through the river and the shape of the river channel (straight or meandering). Meandering river systems have particularly strong influence on woody cover, as is evident along the Awash, Tana, and Samburu rivers (Figure 10) from percolation of water from the river into the hyporrheic zone, an effect that may be further enhanced by "hydraulic lift" (Ludwig et al., 2003). For instance, the riparian corridor along the Tana River is situated on a relatively flat floodplain and has a nearly closed-canopy woody cover (74 %), which corresponds to a mean $\delta^{13}\text{C}_{\text{SOC}}$ value of $\sim -24.5\%$. The distribution patterns of $\delta^{13}\text{C}_{\text{SOC}}$ values for a hectare-scale section of Tana River riparian forest with a woody cover of $\sim 84\%$ is

similar to that of Kakamega Forest (Figure 14) and borders a nonriparian area with a woody cover of $\sim 28\%$ that has a mean $\delta^{13}\text{C}_{\text{SOC}}$ value of $\sim -16.6\text{‰}$. Therefore, riparian zones have higher woody cover than nonriparian zones and may skew the distribution of F_{WC} and $\delta^{13}\text{C}_{\text{SOM}}$ values towards a riparian zone microclimate rather than reflecting a landscape-wide climate regime.

Landscape-scale histograms of $\delta^{13}\text{C}_{\text{SOC}}$ prediction grids indicate that dry sites with low woody cover adjacent to a riparian corridor (with high woody cover) are skewed towards the C_4 end member (Figure 15; e.g., Tana River and Awash). As woody cover increases outside the riparian zone, the $\delta^{13}\text{C}_{\text{SOC}}$ distribution becomes bimodal and the skew in $\delta^{13}\text{C}_{\text{SOC}}$ distribution shifts from C_4 end member (-14‰) toward C_3 end member (-30‰) (e.g., Ileret and Nakuru). As the woody cover approaches closed canopy, the $\delta^{13}\text{C}_{\text{SOC}}$ becomes skewed towards the C_3 end member (-30‰) (e.g., Kakamega Forest, Arabuko Sokoke, and Shimba Hills).

2.4.3 Relevance of $\delta^{13}\text{C}_{\text{SOC}}$ patterns in paleoenvironmental reconstruction in Eastern Africa

The distribution patterns of $\delta^{13}\text{C}_{\text{SOC}}$ values provide a way to reconstruct vegetation patterns at patch-scale and landscape-scales (Figures 13–14). In this regard, skew of the landscape-scale distribution of $\delta^{13}\text{C}_{\text{SOC}}$ values towards the C_3 end member is interpreted as resulting from an environment with high woody cover that is closely clustered (e.g., Arabuko Sokoke and Kakamega forests) because of climatic effects (Figure 14). The histograms of $\delta^{13}\text{C}_{\text{SOC}}$ values with bimodal peaks close to the center of the C_3 and C_4 end members represent open woodland with sparsely distributed trees and

shrubs (e.g., Ileret). A strong unimodal distribution of $\delta^{13}\text{C}_{\text{SOC}}$ values towards a C_4 end member represents open grassland (e.g., Athi River). Further, the histograms of $\delta^{13}\text{C}_{\text{SOC}}$ values indicate that variations in physiognomy caused by other nonclimatic factors have little influence on the structure of $\delta^{13}\text{C}_{\text{SOC}}$ values histograms. Climate is the dominant factor determining the F_{WC} at landscape-scale.

At patch-scale (~1–10 hectare size), skew of $\delta^{13}\text{C}_{\text{SOC}}$ values towards the C_3 end member may occur, as is evident within the riparian corridor along the Tana River in a region that is otherwise xeric with a woody cover < 10% (Figure 13). These riparian areas are thought to have been important to the early hominins for shade, food, and shelter. On geological timescales, river systems meander across the entire floodplain, even though a unique riparian corridor may comprise only a small fraction of the floodplain area.

2.5 Conclusion

We show through models of $\delta^{13}\text{C}_{\text{SOC}}$ in different vegetation cover types in the East African region that fractional woody cover determines the $\delta^{13}\text{C}_{\text{SOC}}$ values and is scale-dependent distribution pattern. In this regard, skew of the distribution of $\delta^{13}\text{C}_{\text{SOC}}$ values towards the C_3 end member is interpreted as an environment with high woody cover while a unimodal distribution of $\delta^{13}\text{C}_{\text{SOC}}$ values towards a C_4 end member represents open grasslands. Existence of multiple biomes within a landscape results in multiple $\delta^{13}\text{C}_{\text{SOC}}$ peaks spanning the transition between C_3 and C_4 end members and is the reason that the water deficit is uncorrelated with F_{WC} . Riparian environments have high woody cover associated with river systems, and these can occur in otherwise open

environments such as grasslands or wooded grasslands. Our models indicate that interpreting paleoenvironments from soil organic matter of paleosols in the East African region should be done with reference to both local and regional climate and disturbance. The distribution patterns of $\delta^{13}\text{C}_{\text{SOC}}$ values provide an independent way to reconstruct vegetation patterns at landscape scales.

2.6 Acknowledgements

We are very thankful to Dr. Francis H. Brown for his insights, advice, and support throughout this project, including scrutiny of the manuscript. We also thank Kevin Uno and Kendra Chritz for their help with isotope analysis of soil samples and the staff of KWS for their help in collecting the soil samples. This research was funded by the National Science Foundation (BCS06-21543).

2.7 References

- Asfaw, B., White, T., Lovejoy, O., Latimer, B., Simpson, S., & Suwa, G. (1999). *Australopithecus garhi*: a new species of early hominid from Ethiopia. *Science*, *284*, 629–635.
- Bai, E., Boutton, T. W., Wu, X. B., Liu, F., & Archer, S. R. (2009) Landscape-scale vegetation dynamics inferred from spatial patterns of soil $\delta^{13}\text{C}$ in a subtropical savanna parkland. *Journal of Geophysical Research*, *114*, G01019 1–10, doi:10.1029/2008JG000839.
- Bettis III, E. A., Milius, A. K., Carpenter, S. J., Larick, R., Zaim, Y., Rizal, Y., Ciochon, R. L., Tassier-Surine, S. A., Murray, D., Suminto, & Bronto, S. (2009). Way out of Africa: Early Pleistocene paleoenvironments inhabited by *Homo erectus* in Sangiran, Java. *Journal of Human Evolution*, *56*, 11–24.
- Bond, W. J., Woodward, F. I., & Midgley, G. F. (2005). The global distribution of ecosystems in a world without fire. *New Phytologist*, *165*, 525–538.

Brown, F. H., & Feibel, C. S. (1991). Stratigraphy, depositional environments, and palaeogeography of the Koobi Fora Formation. In: Harris, J.M. (Ed.), Koobi Fora Research Project (Vol. 3. pp. 130). : The Fossil Ungulates: Geology, Fossil Artiodactyls, and Palaeoenvironments, Clarendon Press, Oxford,.

Bruhn, R. L., Brown, F. H., Gathogo, P. N., & Haileab, B. (2011). Pliocene volcano-tectonics and paleogeography of the Turkana Basin, Kenya and Ethiopia. *Journal of African Earth Sciences*, 59, 295–312.

Buchmann, N., Brooks, J. R., Rapp, K. D., & Ehleringer, J. R. (1994). Carbon isotope composition of C₄ grasses is influenced by light and water supply. *Plant Cell and Environment*, 19(4), 392–404.

Cerling, T. E., Harris, J. M., MacFadden, B. J., Leakey, M. G., Quade, J., Eisenmann V., & Ehleringer, J. R. (1997) Global vegetation change through the Miocene/Pliocene boundary. *Nature*, 389, 153–158.

Cerling, T. E., Levin, N. E., Quade, J., Wynn, J. G., Fox, D. L., Kingston, J. D., Klein, R. G., & Brown, F. H. (2010). Comment on the Paleoenvironment of *Ardipithecus ramidus*. *Science*, 328, 1105-d DOI: 10.1126/science.1185274

Cerling, T. E., Wynn, J. G., Andanje, S. A., Bird, M. I., Korir, D. K., Levin, N. E., Mace, W., Macharia, A. N., Quade, J., & Remien, C.H. (2011). Woody cover and hominin environments in the past 6 million years. *Nature*, doi:10.1038/nature10306

Cohen, J. (1968). "Weighed kappa: Nominal scale agreement with provision for scaled disagreement or partial credit". *Psychological Bulletin*, 70(4), 213–220. doi:10.1037/h0026256. PMID 19673146.

Ehleringer, J. R., & Pearcy, R. W. (1983). Variation in quantum yield for CO₂ uptake among C₃ and C₄ plants. *Plant Physiology*, 73, 555–559.

Farquhar, G. D., O'Leary, M. H., & Berry, J. A. (1982). On the relationship between carbon isotope discrimination and the intercellular carbon dioxide concentration in leaves. *Australian Journal of Plant Physiology*, 9, 139–154.

Farquhar, G. D. (1983). On the nature of carbon isotope discrimination in C₄ species. *Australian Journal Plant Physiology*, 9(1), 121–137.

Farquhar, G. D., Ehleringer, J. R., & Hubic, K. T. (1989) Carbon isotope discrimination and photosynthesis. *Annual Reviews in Plant Physiology and Plant Molecular Biology*, 40, 503–37.

- Fernandez, I., Mahieu, N., & Cadisch, G. (2003) Carbon isotopic fractionation during decomposition of plant materials of different quality. *Global Biogeochemical Cycles*, *17*(3), 1075, doi:10.1029/2001GB001834.
- Fiebel, C. S., Harris, J. M., & Brown, F. H. (1991). Palaeoenvironmental context for the Late Neogene of the Turkana Basin J.M. Harris (Ed.), Koobi Fora Research Project, Volume 3. The fossil ungulates: Geology, Fossil Artiodactyls, and Palaeoenvironments, Clarendon, Oxford, 321–346.
- Foschi, P. G., & Smith, D. K. (1997). Detecting subpixel woody vegetation in digital imagery using two artificial intelligence approaches. *Photogrammetric Engineering & Remote Sensing*, *63*(5), 493–500.
- Forsythe, W. C., Rykiel Jr., E. J., Stahl, R. S., Wu, H., & Schoolfield, R. M. (1995). A model comparison for daylength as a function of latitude and day of year. *Ecological Modelling*, *80*(1), 87–95, doi:10.1016/0304-3800(94)00034-F
- Goetz, S. J., Wright, R. K., Smith, A. J., Zinecker, E., & Schaub, E. (2003). IKONOS imagery for resource management: Tree cover, impervious surfaces, and riparian buffer analyses in the mid-Atlantic region. *Remote Sensing of Environment*, *88*, 195 – 208.
- Hill, M. J., Román, M. O., Schaaf, C. B., Hutley, L., Brannstrom, C., Etter, A., & Hanan, N. P. (2011). Characterizing vegetation cover in global savannas with an annual foliage clumping index derived from the MODIS BRDF product. *Remote Sensing of Environment*, *115*, 2008–2024.
- Hirota, M., Holmgren, M., Van Nes, E. H., & Scheffer, M. (2011). Global resilience of tropical forest and savanna to critical transitions. *Science*, *334*, 232–235, doi: 10.1126/science.1210657.
- Huffman, O. F. (1999) Variety in the paleoenvironment of early *Homo erectus* of Java, Indonesia. *Journal of Human Evolution*, *36*, A8–A9.
- Huffman, O. F. (2001). Geologic context and age of the Perring/Mojokerto *Homo erectus*, East Java. *Journal of Human Evolution*, *40*, 353–362.
- Johanson, D. C., Taieb, M., & Coppens, Y. (1982). Pliocene hominids from the Hadar Formation, Ethiopia (1973–1977): Stratigraphic, chronologic and paleoenvironmental contexts, with notes on Hominid morphology and systematics. *American Journal of Physical Anthropology*, *57*, 373–402.
- Keeley, J., & Rundel, P. (2005). Fire and the Miocene expansion of C₄ grasslands. *Ecological letters*, *8*, 683–690, doi: 10.1111/j.1461-0248.2005.00767.x.

- Kingston, J. D. (2007). Shifting adaptive landscapes: Progress and challenges in reconstructing early hominid environments. *Year book of Physically Anthropology*, 50, 20–58, 2007.
- Leakey, M. G., Feibel, C. S., McDougall, I., & Walker, A. (1995). New four-million-year old hominid species from Kanapoi and Allia Bay, Kenya. *Nature*, 376, 565–571.
- Levin, N. E., Cerling, T. E., Passey, B. H., Harris, J. M., & Ehleringer, J. R. (2006). A stable isotope aridity index for terrestrial environments. *PNAS*, 103(30), 11201–11205.
- Levin, N. E., Brown, F. H., Behrensmeyer, A. K., Bobe, R., & Cerling, T. E. (2011). Paleosol carbonates from the Omo Group: Isotopic records of local and regional environmental change in East Africa. *Palaeogeography, Palaeoclimatology, Palaeoecology*, 307, 75–89.
- Liu, W., Feng, X. H., Ning, Y., Zhang, Q., Cao, Y., & Sheng, A. Z. (2005). $\delta^{13}\text{C}$ variation of C_3 and C_4 plants across an Asian monsoon rainfall gradient in arid northwestern China. *Global Change Biology*, 11, 1094–1100, doi: 10.1111/j.1365-2486.2005.00969.x.
- Lu, H., Raupach, M. R., McVicar, T. R., & Barrett, D. J. (2003). Decomposition of vegetation cover into woody and herbaceous components using AVHRR NDVI time series. *Remote Sensing of Environment*, 86, 1–18, doi:10.1016/S0034-4257(03)00054-3.
- Ludwig, F., Dawson, T. E., de Kroon, H., Berendse, F., & Prins, H. H. T. (2003). Hydraulic lift in *Acacia tortilis* trees on an East African savanna. *Oecologia*, 134(3), 293–300, doi: 10.1007/s00442-002-1119-x.
- Magnusson, W.E., Sanaiotti, T.M., Lima, A.P., Martinelli, L.A., Victoria, R.L., de Araujo, M.C., & Albernaz, A.L. (2002). A comparison of $\delta^{13}\text{C}$ ratios of surface soils in savannas and forests in Amazonia. *Journal of Biogeography*, 29, 857–863.
- Measey, G. J., & Tolley, K. A. (2011). Sequential fragmentation of Pleistocene forests in an East Africa biodiversity hotspot: chamleons as a Model to Track Forest History. *PLoS ONE*, 6 (10), 1–9.
- Leakey, M. G., Feibel, C. S., Bernor, R. L., Harris, J. M., Cerling, T. E., Stewart K. M., Storrs G. W., Walker, A., Werdelin L., & Winkler A. J. (1996) Lothagam: a record of faunal change in the late Miocene of East Africa. *Journal of Vertebrate Paleontology*, 16(3), 556–570.
- Monger, H. C., Cole, D. R., Buck, B. J., & Gallegos, R. A. (2009) Scale and the isotopic record of C_4 plants in pedogenic carbonate: from the biome to the rhizosphere. *Ecology*, 90(6), 1498–1511.

- Mueller, T., & Pierce, F. (2003). Soil carbon maps: enhancing spatial estimates with simple terrain attributes at multiple scales. *Soil Science Society of America Journal*, *67*, 258–267.
- Moran, M. S., Humes, K. S., & Pinter Jr., P. J. (1997). The scaling characteristics of remotely-sensed variables for sparsely-vegetated heterogeneous landscapes. *Journal of Hydrology*, *190*, 337–362.
- O’Leary, M. H. (1981). Carbon isotopic fractionation in plants. *Phytochemistry*, *20*, 553–567.
- O’Leary, M. H. (1988). Carbon isotopes in photosynthesis. *BioScience*, *38*, 328–336.
- Passey, B. H., Levin, N. E., Cerling T. E., Brown F. H., & Eiler J. M. (2010). High-temperature environments of human evolution in East Africa based on bond ordering in paleosol carbonates. *PNAS*, *107*(25), 11245–11249.
- Schulze, E. D., Ellis, R., Schulze, W., Trimborn, P., & Ziegler, H. (1996). Diversity of metabolic types and $\delta^{13}\text{C}$ carbon isotope ratios in the grass flora of Namibia in relation to growth form, precipitation and habitat conditions. *Oecologia*, *106*(3), 352–369.
- Sepulchre, P., Ramstein, G., Fluteau, F., Schuster, M., Tiercelin, J., & Brunet, M. (2006). Tectonic Uplift and Eastern Africa Aridification. *Science*, *313*, 1419–1423, doi: 10.1126/science.1129158.
- Smith, B. N., & Epstein, S. (1971). Two categories of $^{13}\text{C}/^{12}\text{C}$ ratios for higher plants. *Plant Physiology*, *47*, 380–384.
- Staver, A. C., Archibald, S., & Levin, S. A. (2011). The global extent and determinants of savanna and forest as alternative biome states. *Science*, *334*, 230–232; doi: 10.1126/science.1210465.
- Still, C. J., Berry, J. A., Collatz, G. J., & DeFrie, R. S. (2003). Global distribution of C_3 and C_4 vegetation: Carbon cycle implications. *Global Biogeochemical Cycles*, *17*(1), 6-1–6-13.
- Thornthwaite, C. W. (1948). An approach toward a rational classification of climate: *Geographical Review*, *38*, 55–94.
- Tieszen, L. L., Reed, B. C., Bliss, N. B., Wylie, B. K., & DeJong, D. D. (1997). NDVI, C_3 and C_4 production, and distributions in Great Plains grassland land cover classes. *Journal of Ecological Applications*, *7*, 59–78.

- Tieszen, L. L., Senyimba, M. M., Imbamba, S. K., & Troughton, J. H. (1979). The distribution of C₃ and C₄ grasses along an altitudinal and moisture gradient in Kenya. *Oecologia*, *37*, 337–350.
- Wang, G., Feng, X., Han, J., Zhou, L., Tan, W., & Su, F. (2008) Paleovegetation reconstruction using $\delta^{13}\text{C}$ of soil organic matter. *Biogeosciences*, *5*, 1325–1337.
- Wang, L., Okin, G. S., & Macko, S. A. (2009). Satellite prediction of soil $\delta^{13}\text{C}$ distributions in a southern African savanna. *Journal of Geochemical Exploration*, *102*(3), 137–141.
- Wang, G., Han, J., Zhou, L., Xiong, X., & Wu, Z. (2005). Carbon isotope ratios of plants and occurrences of C₄ species under different soil moisture regimes in arid region of Northwest China. *Physiologia Plantarum*, *125*, 74–81.
- White, F. (1983). The vegetation of Africa. Natural Resources Research, Vol. 20. (United Nations Scientific and Cultural Organization, Paris).
- WoldeGabriel, G., White, T., Suwa, G., Renne, P., de Heinzelin, J., Hart, W. K., & Heiken, G. (1994). Ecological and temporal placement of early Pliocene hominids at Aramis, Ethiopia. *Nature*, *371*, 330–333.
- Wynn, J. G. (2000). Paleosols, stable carbon isotopes, and paleoenvironmental interpretation of Kanapoi, Northern Kenya. *Journal of Human Evolution*, *39*, 411–432.
- Wynn, J. G. (2004). Influence of Plio-Pleistocene aridification on human evolution: Evidence from paleosols of the Turkana Basin, Kenya. *American journal of Physical Anthropology*, *123*, 106–118.
- Wynn, J. G., Bird, M. I., Vellen, L., Grand-Clement, E., Carter, J., & Berry, S. L., (2006). Continental-scale measurement of the soil organic carbon pool with climatic, edaphic, and biotic controls. *Global Biogeochemical Cycles*, *20*, GB1007, doi:10.1029/2005GB002576.
- Wynn, J. G., & Bird, M. I. (2010). Environmental controls on the stable carbon isotopic composition of soil organic carbon: implications for modelling the distribution of C₃ and C₄ plants, Australia. *Tellus B*, *60*(4), 604–621, doi: 10.1111/j.1600-0889.2008.00361.x.
- Xiao, J., & Moody, A. (2005). A comparison of methods for estimating fractional green vegetation cover within a desert-to-upland transition zone in central New Mexico, USA. *Remote Sensing of Environment*, *98*(2-3), 237–250.

CHAPTER 3

CHANGES IN NUTRIENT AND CARBON INFLUXES IN FOY LAKE, MONTANA BEFORE AND AFTER EUROPEAN SETTLEMENTS IN FLATHEAD VALLEY

3.1 Background

Materials originating from the watershed linked to either climatic processes such as snowmelt (Piatek et al., 2005; Widory et al., 2005; Elliot & Brush, 2006) and fire episodes (e.g., Power et al., 2006; Power et al., 2011) or non-climatic process such as human activities (e.g., Mayer et al., 2002) may significantly alter biogeochemical processes that occur within lakes. For instance, nutrient transported into lakes via rivers (Mayer et al., 2002; Gravelle et al., 2009) or atmospheric deposition (Nannus et al., 2003; Saros et al., 2003) may potentially alter lake nutrient budgets and trigger changes in lake productivity and plankton community composition. Thus, distinguishing the sources of materials and their impact on lake ecosystem processes is important in accurately reconstructing past environments from sedimentary archives. The use of multiproxy approaches advocated by Leavitt et al. (2009) provides a means to account for processes linked to climatic and nonclimatic processes in sedimentary archives, thus enabling a reconstruction of past environments. Within that framework, influence of ionic balance

(Shapley, 2010), evaporation (Henderson & Shuman, 2009), and particulate fluxes with lake bathymetry (e.g., Stone & Fritz, 2004; Stevens et al., 2006; Stone et al., 2005; Shuman et al., 2009;) may be integrated in reconstructing climate and disturbance within the lake and its watershed in the past.

In reconstructing water balance in groundwater-fed lakes, changes in the magnitude and timing of runoff in the mountains are important because climate change alters the timing and magnitude of snow pack melt (e.g., Owen et al., 2009). The stable isotope composition of lake water (^{18}O and D) reflects the isotopic composition of the melt water as do climatic factors including precipitation, relative humidity, and temperature (Henderson & Shuman, 2009). When the ^{18}O abundance in lake carbonates are used to infer past changes in lake water balance, the influence of photosynthesis within the lake, detrital carbonates, and variability in isotopic composition among carbonate minerals must be considered (see Leng et al., 2004). Studies show that carbonates deposited in sediments of groundwater-fed lakes increases during summer photosynthesis (McConnaughey et al., 1994; Drummond et al., 1995) and therefore, changes in the photosynthetic activity in the water column are expected to increase carbonate precipitation.

The objective of this study is to evaluate the hypothesis that forest clearing elicits an influx of nutrients and terrigenous materials that alter carbon cycling in lacustrine environments compared to the period before Euro-American settlement (pre-A.D. 1880). To evaluate this hypothesis, we use stable isotope and optical methods (charcoal, pollen, and diatom counts) to account for nutrient fluxes and particulate matter fluxes in sediments of Foy Lake, which is recharged primarily through groundwater. Watershed

geomorphology, modern land cover/ land use, and lake bathymetry are all considered.

3.2 Study area

Foy Lake, MT, (Figure 16) occupies the edge of the forest-steppe border of the Flathead Valley of Northwestern Montana at an altitude of 1006 m surrounded by open grassy woodlands comprised of *Peudotsuga menziesii*, *Pinus ponderosa*, and *Larix occidentalis*, with *Pinus contorta* scattered throughout (Power et al., 2006). The lake is a groundwater outcrop with minimal stream inputs, has a maximum water depth of about 39.9 m, and a surface area of 110 ha. Sediments in Foy Lake are laminated (Power et al., 2006; Stevens et al., 2006), making it possible to visualize the variation in sediment characteristics through time.

3.3 Material and methods

A 55 cm-long frozen sediment core was obtained in 2006 from the deepest portion of the lake and water samples were collected during the summer of 2010. A 2-cm wide 55 cm-long section of the Foy Lake core was cut from the freeze core. The remainder of the sequence has been archived at the Natural History Museum of Utah. Sediment sequences ranging from 5 to 8 cm in length were cut with a razor blade and placed on Petri dishes. High-resolution photographs were captured from the cut segments of the freeze core whereupon identifiable varves were cut with a razor blade from the core starting from the top (sediment-water interface) and placed in a freezer at 4 °C to allow ice crystals to sublimate and reveal the laminations (see Appendix C). High-

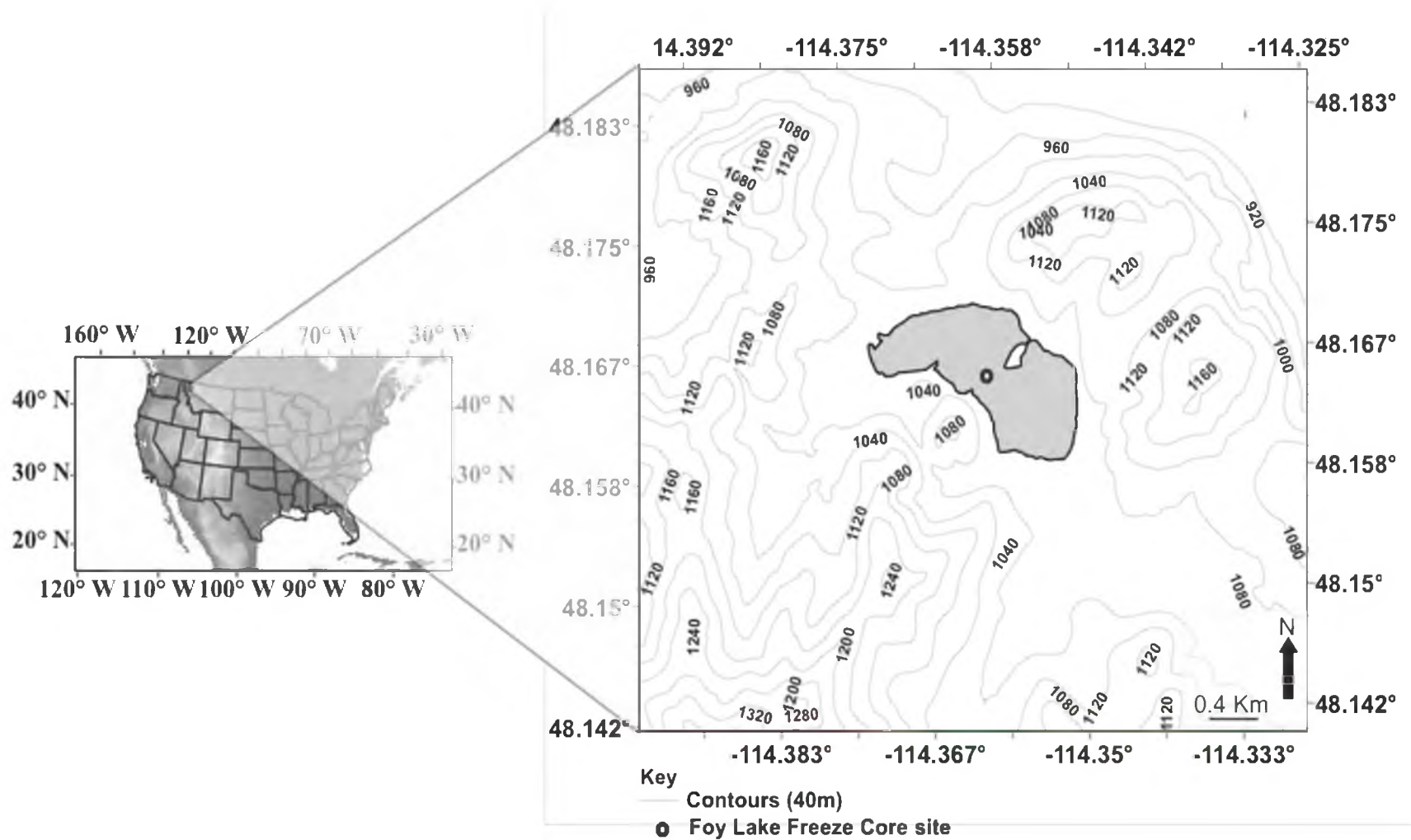


Figure 16. Location of Foy Lake. Foy Lake is situated in the Rocky Mountains adjacent to the Flathead Valley. The lake has no surface inlets or outlets.

resolution photos were used to determine the optimum sampling protocols for the sediments. From each section, samples were obtained by cutting sections of the cores at equal intervals along the varves and placed in pre-labeled centrifuge tubes.

3.3.1 Isotopic analysis

The stable isotope analysis was carried out in stable isotope laboratories of the Biology Department at the University of Utah. An aliquot of about 600–700 mg was obtained from sample tubes, transferred into new centrifuge vials, and dried at 60 °C for at least 48 hrs. Two aliquots of about 300 mg each were obtained for each sample after oven-drying and transferred to new pre-labeled centrifuge vials. One of these aliquots was treated with dilute hydrochloric acid to remove carbonates and rinsed with distilled water. The other 300 mg sample, destined for carbonate analysis, was left untreated.

3.3.1.1 Stable isotope analysis of organic matter (OM)

The acid-treated aliquots were dried at 60 °C for at least 24 hrs. About 10 to 20 mg of the samples were weighed and analyzed for carbon-13 and nitrogen-15 abundance in the Geochemistry Laboratory of the Biology Department at the University of Utah. Yeast of known isotopic composition was used as an internal standard for these analyses. The samples were combusted in a Costech 4010 Elemental Analyzer at 1650 °C and inlet to a Finnigan® MAT 252 Isotope Ratio Mass Spectrometer (IRMS) in continuous flow mode. Isotope values were calculated as shown in Equation 13.

$$\delta X (\text{‰}) = 1000 * (R_{\text{sample}} / R_{\text{standard}} - 1) \quad \text{Equation 13}$$

where ‘ X ’ is either ^{15}N , ^{13}C , ^{18}O , or D , while R is $^{15}\text{N}/^{14}\text{N}$, $^{13}\text{C}/^{12}\text{C}$, $^{18}\text{O}/^{16}\text{O}$, or D/H , respectively, and δX is expressed in per mil (‰) relative to internationally agreed standards: V-PDB for both organic and carbonate carbon and oxygen, VSMOW for oxygen and deuterium in water, and atmosphere (AIR) for nitrogen $\delta^{15}\text{N}$, respectively. Water oxygen and deuterium values are reported relative to the VSMOW standard. Carbon and nitrogen yields were determined from the preliminary samples, optimum sample sizes established, and samples run in duplicate with newly determined masses. The analytical precision of isotopic analysis of $\delta^{15}\text{N}_{\text{SOM}}$, and $\delta^{13}\text{C}_{\text{SOM}}$ are 0.1‰ and 0.2‰, respectively.

3.3.1.2 $\delta^{18}\text{O}$ and $\delta^{13}\text{C}$ stable isotope analysis of sedimentary carbonates

The analysis was limited only to the top 5 cm section of the core to increase the sample size of isotopic data for comparison with isotopic data of the presettlement period (Stevens et al., 2006). The untreated aliquots were sieved through a 140 μm sieve to remove coarse debris and analyzed for $\delta^{18}\text{O}$ and $\delta^{13}\text{C}$ via continuous flow with a GasBench (ThermoScientific Inc.) coupled to a Finnigan MAT 252 IRMS. UU Carrara (carbonate) of grain size $< 140 \mu\text{m}$ was used as an internal standard for all analyses. About 5 mg of each sediment sample was weighed into 25 ml screw-top vials with septa, purged with helium to remove atmospheric gases in the headspace, injected with phosphoric acid to evolve carbon dioxide, and left to react overnight at 72 °C. UU Carrara (carbonate) was used as an internal standard. The standard deviations (1σ) of isotope measurements of $\delta^{13}\text{C}$ and $\delta^{18}\text{O}$ were ≤ 0.07 and ≤ 0.02 ‰, respectively. The new dataset was collated with data on the oxygen and carbon-isotopes of the carbonates

(see Stevens et al., 2006).

3.3.1.3 $\delta^{18}\text{O}$ and δD stable isotope analysis of water samples

Water isotope analysis was done in a thermo combustion elemental Analyzer (TCEA) linked to a Delta-plus IRMS in the SIRFER Lab, University of Utah. The samples were run together with internal standards (PLRM-1, PLRM-2, and SLRM) calibrated to VSMOW water. The $\delta^{18}\text{O}_{\text{H}_2\text{O}}$ and $\delta\text{D}_{\text{H}_2\text{O}}$ were calculated as shown in Equation 13.

3.3.2 Age chronology

The chronology of the analyzed 55-cm deep Foy Lake core covering the last 350 years was developed from varves and a series of ^{210}Pb dates (Stevens et al., 2006) (Figure 17). The chronology was based on a 2nd-order polynomial age model (Table 3).

3.3.3 Estimation of percent land cover / land use in watershed

GAP analysis maps were used to estimate the relative proportions of land around the Foy Lake watershed under different land cover types and land uses by reclassifying 90 m² land cover pixels (Gap Analysis Project, University of Idaho - <http://gap.uidaho.edu/index.php/landcover/>) downloaded in June 2010. Developed, open space, low, medium, and high intensity, pasture/Hay were considered developed, while the North American arid west emergent marsh, Rocky Mountain alpine-montane wet meadow, lower montane riparian woodland and shrubland; harvested forest-tree regeneration, forest-shrub regeneration, forest-grass regeneration; and Northern Rocky

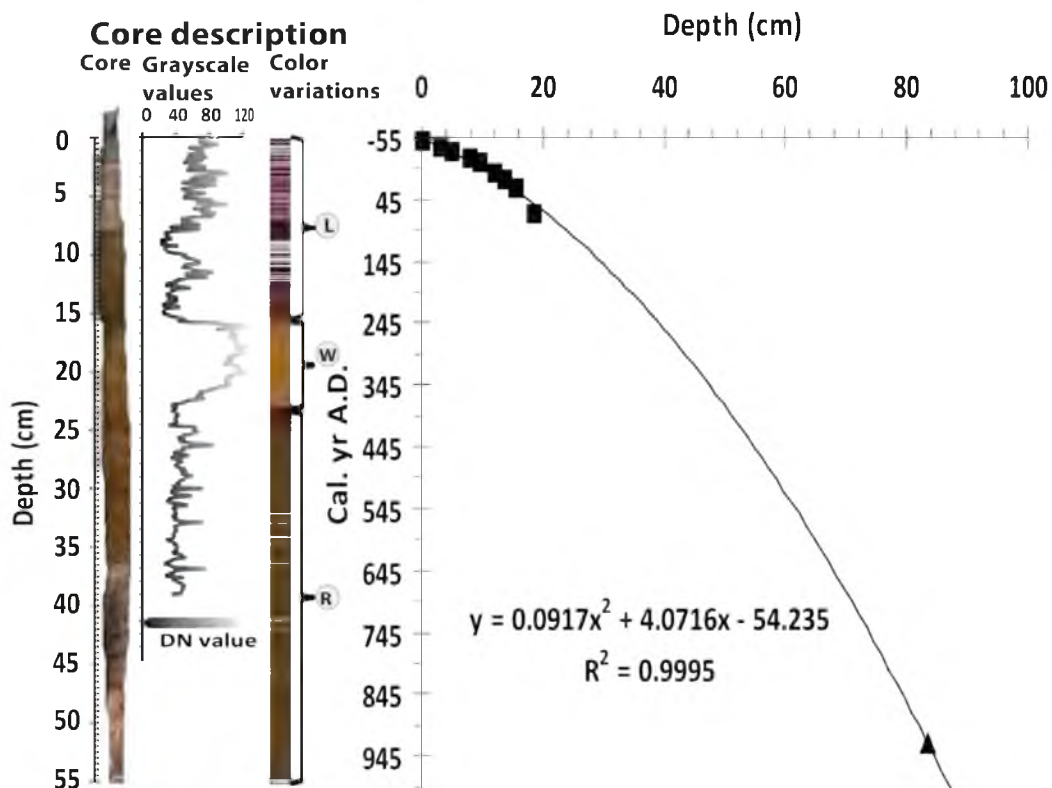


Figure 17. Age model for Foy Lake, Montana, generated by 2nd-order polynomial regression between the modern lake surface (top of mud-water interface) and the ²¹⁰Pb dates taken from terrestrial wood fragments. The sections labeled L, W, and R signify finely laminated, nonlaminated, and poorly laminated sediments. The grayscale analysis was performed on the original core using image J software (<http://rsbweb.nih.gov/>) and shows that the unlaminated section is much lighter in color than the laminated sections.

Table 3. The age model for Foy Lake freeze core based on ^{210}Pb activity, varve counts, and ^{14}C dates of woody material. ^{210}Pb ages were provided by Daniel Engstrom, St. Croix Watershed Research Station.

Depth interval (cm)	Age (AD) ^a	Error of age (years) +/- 1 SD	Median depth
	<u>Base of interval</u>		
0-0.5	1998	3.88 ^a	0.25
3-3.5	1987	4.63 ^a	3.25
5-5.5	1980	4.91 ^a	5.25
8-8.5	1969	4.65 ^a	8.25
9.5-10	1962	5.31 ^a	9.75
12-12.5	1945	7.96 ^a	12.25
13.5-14	1935	9.96 ^a	13.75
15.5-16	1922	14.74 ^a	15.75
18.5-19	1880	54.30 ^a	18.75
		925+/-35 ^b	83.50

a ^{210}Pb ages provided by Daniel Engstrom, St. Croix Watershed Research Station.

b ^{14}C dates from a woody material (Lab ID. No. NSRL-1197) used to constrain bottom age of the freeze core age model used to construct using a 2nd-order polynomial. The age range 744-926 Cal. B. P. (2d) was calibrated with CALIB 5 using the Stuiver et al. (1998) data set.

Mountain montane-foothill deciduous shrubland; subalpine deciduous shrubland, ponderosa pine woodland and savanna, subalpine-montane mesic meadow, subalpine deciduous shrubland, dry-mesic montane mixed conifer forest were categorized as undeveloped. Open water was excluded from the analysis. The watersheds were digitized from 10 m USGS digital elevation models (DEMs). Sections of the land use maps outside the regions of interests (watersheds) were masked out using the digitized watershed in ENVI 4.7 (ITT VIS Inc.). The percentage land cover / land use was calculated as shown in Equation 14:

$$\% \text{ Land use per cover class} = \frac{\text{Pixels per land cover class}}{\sum_{i=1}^n \text{Pixels per land cover class}} \quad \text{Equation 14}$$

where ‘n’ represents the number of land cover classes in the watershed.

3.3.4 Pollen processing

Sediment samples (1cc each) were obtained at 1 cm intervals (~ 6 – 7 yr intervals) and processed following the methods of Faegri et al. (1989). A *Lycopodium* tablet was added to each sample as an exotic tracer. At least 300 terrestrial grains were counted for each sample processed, counts were converted to percentages of the total terrestrial grains, and pollen influx rates (grains cm⁻² yr⁻¹) were calculated for each pollen taxon over the course of the record.

3.3.5 Charcoal analysis

Macroscopic charcoal (particles $>125\ \mu\text{m}$) were used to reconstruct the fire history. One cubic centimeter sediment samples were obtained from the frozen core at contiguous one-centimeter depth intervals. The samples were disaggregated with potassium hydroxide, washed through a $125\ \mu\text{m}$ sieve, identified, and counted at 36X with a dissecting microscope. Fire events were statistically determined by Char Analysis© software whereby peaks of charcoal counts above a background level constitute fire events. Other identifiable macroscopic plant or animal remains were also recorded.

3.3.6 Diatom processing

Diatom samples were cleaned of organic debris and mounted for light microscope observations following the techniques outlined in Battarbee (1986). This processing approach uses 10% HCl to remove carbonates and cold 30% hydrogen peroxide to oxidize organic matter. When possible, 300 to 500 diatom valves were identified and counted from each sediment sample.

3.4 Results

3.4.1 Particulate matter fluxes in Foy Lake

The pollen and charcoal influx in Foy Lake indicates an unprecedented influx of pollen that triggered changes in phytoplankton composition, increasing the relative abundance in benthic and tycho plankton at the expense of true plankton (Figure 18).

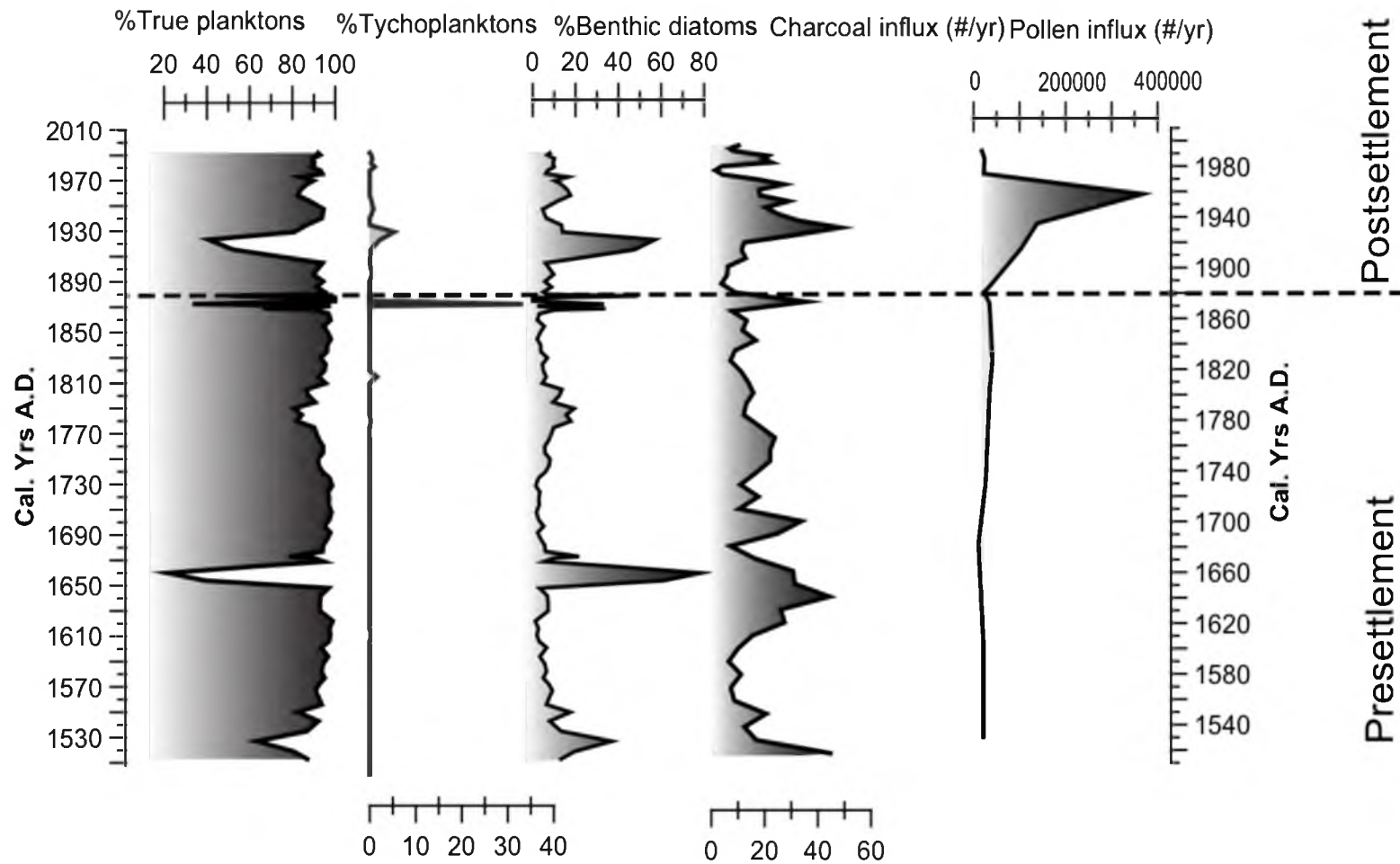


Figure 18. Temporal variations in abundance of plankton (true plankton, tychoplankton, and benthic diatoms), charcoal, and pollen in Foy Lake.

3.4.2 Pollen data

The pollen influx record of Foy Lake reveals a period of heightened pollen influx between 1880–1980 (Figure 19). The pollen influx before 1880 was ~15,617 grains per year and ~ 89,391 grains per year after 1880 A. D. The dominant pollen in the lake is *Pinus* sp. that accounts for 61% of the pollen influx before 1880 A. D. and ~ 45% after 1880.

3.4.3 Charcoal records

The charcoal influx data indicate episodic influxes of charcoal in Foy Lake (Figure 20). Nine fire episodes were detected, yielding a fire return interval of 25 to 45 years. Average charcoal accumulation rates (particles $\text{cm}^{-2} \text{yr}^{-1}$) are ~20 for the presettlement period, and 152 for the postsettlement period.

3.4.4 Diatom records

The diatom record shows that *Cyclotella bodanica* var. *lemnaica* is the dominant diatom with a relative abundance of >95% (Figure 21). *Cyclotella bodanica* var. *lemnaica* is the most common of the true plankton, while *Fragillaria*, *anamoensis*, *Craticula* sp., *Navicula* sp., *Gomphonema* sp., and *Nitzschia palea* constitute the major benthic diatoms. The influx of benthic diatoms shows an inverse relationship to the influx of true diatoms.

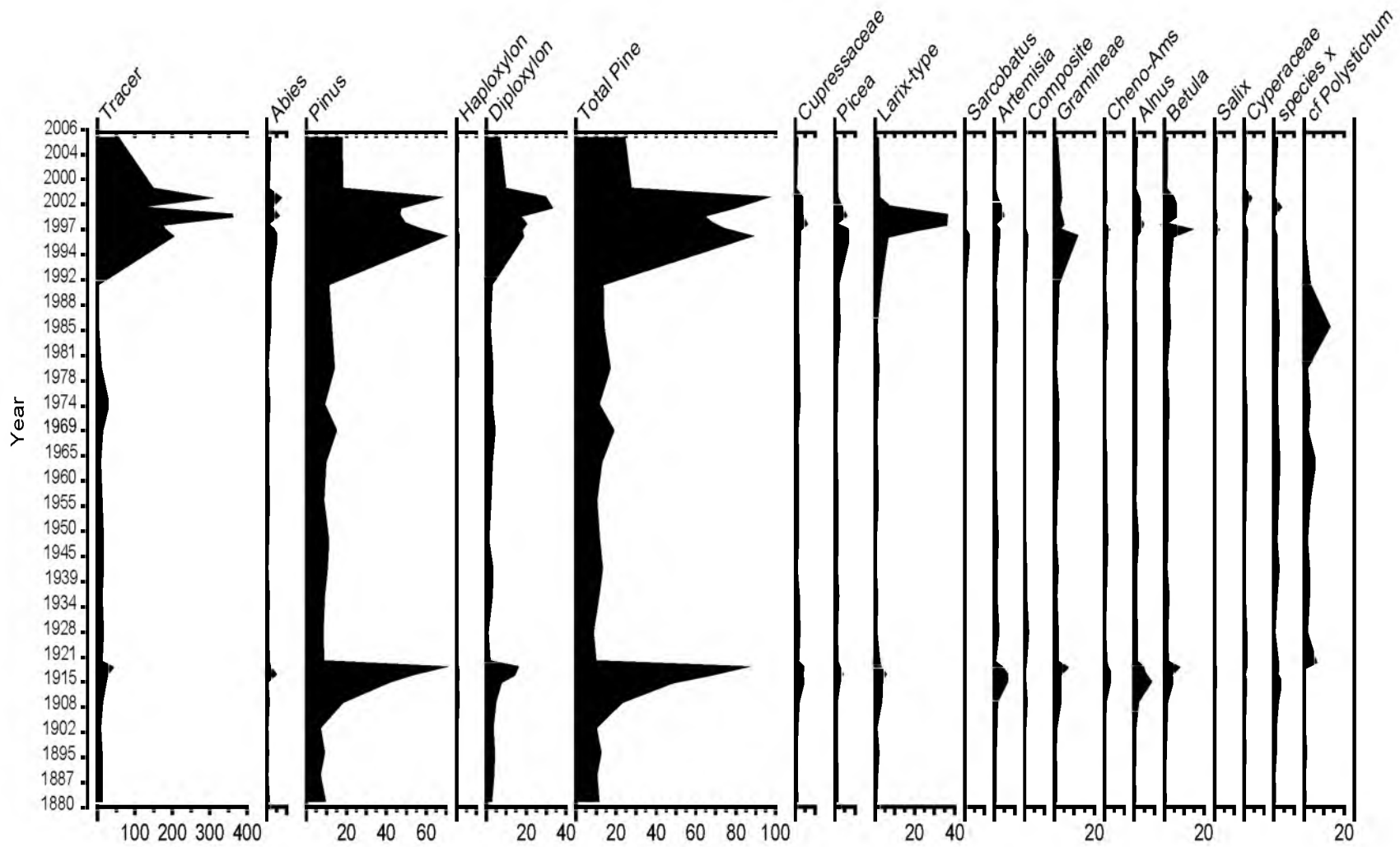


Figure 19. The pollen influx record of Foy Lake. The pollen influx shows that two episodes of accelerated influxes (1900-1921 and 1992-2000) coincide with tree harvesting in Foy Lake watershed. Cheno-Ams stands for Chenopodiaceae and Amaranthaceae.

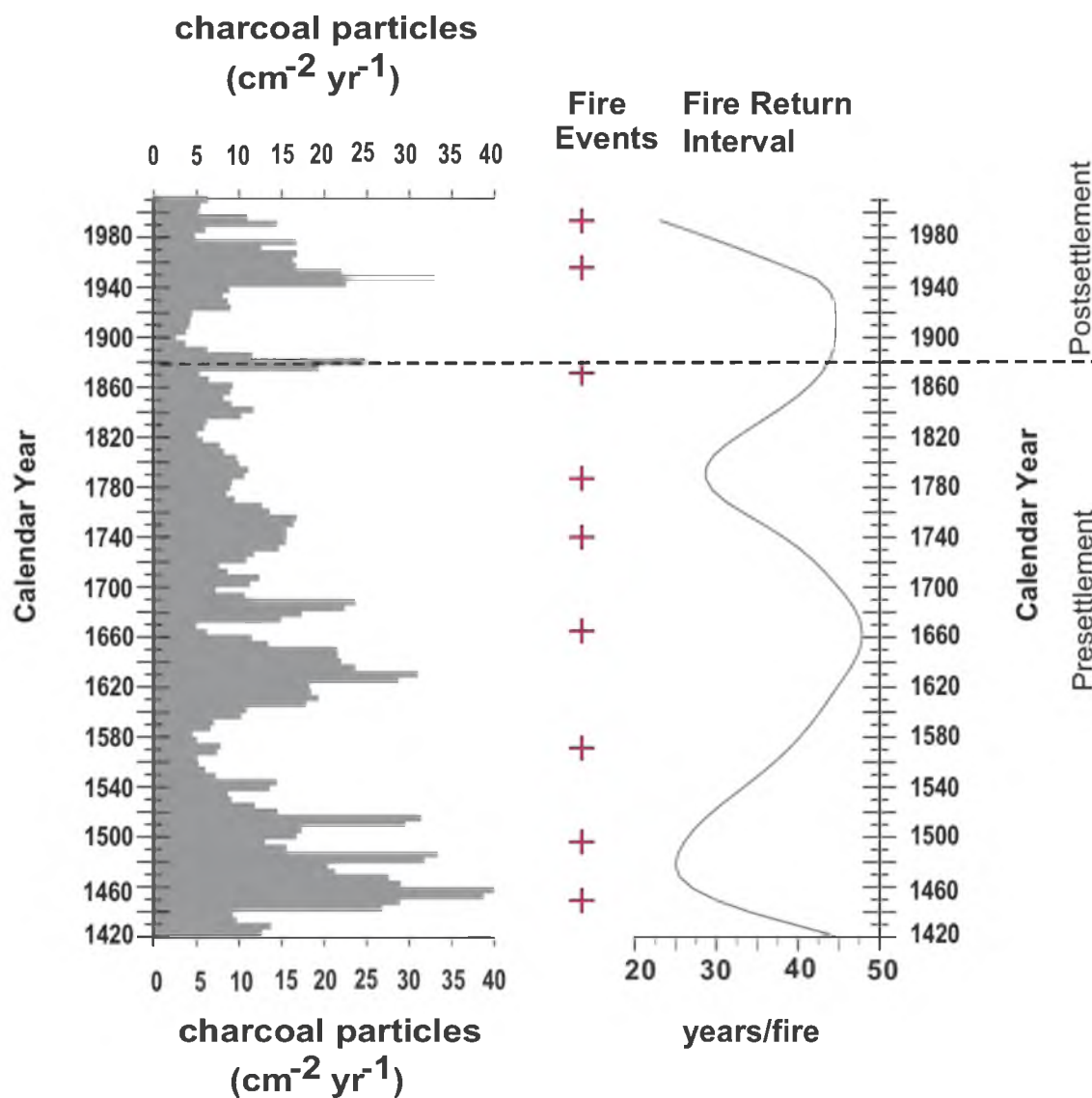


Figure 20. Plot of Foy Lake charcoal records. The char analysis detects 9 fire episodes over the past 580 years and a fire return interval in Foy Lake is between 25 to 45 years.

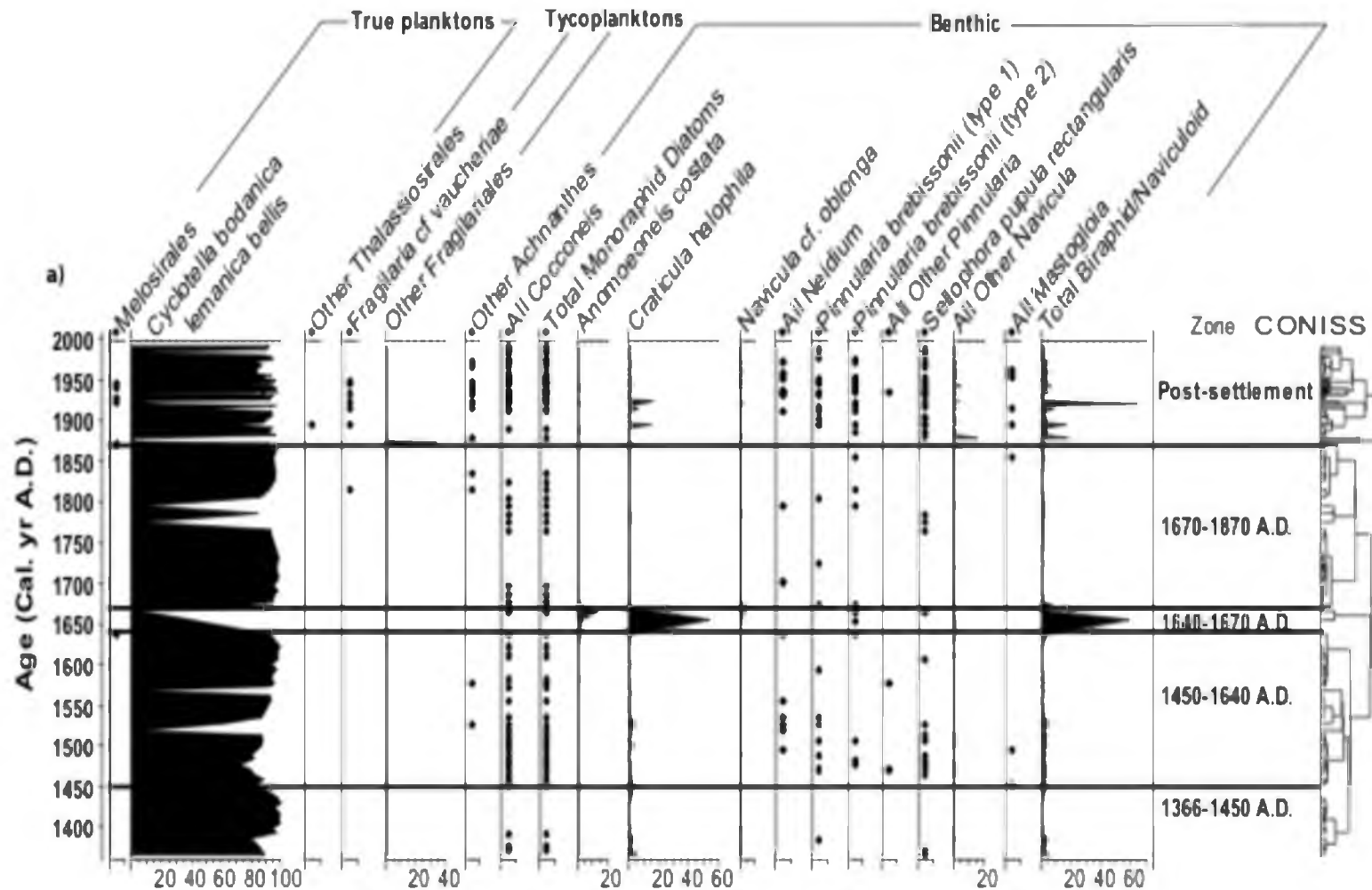


Figure 21. Tilia plots of the major diatoms in Foy Lake sediment records. *Cyclotella bodanica* var. *lemnica* is the most abundant among the true plankton, while *Fragillaria*, *anamoensis*, *Craticula* sp., *Navicula* sp., *Gomphonema* sp., and *Nitzschia palea* constitute the major benthic diatoms. The influx of benthic diatoms shows an inverse relationship to the influx of true diatoms.

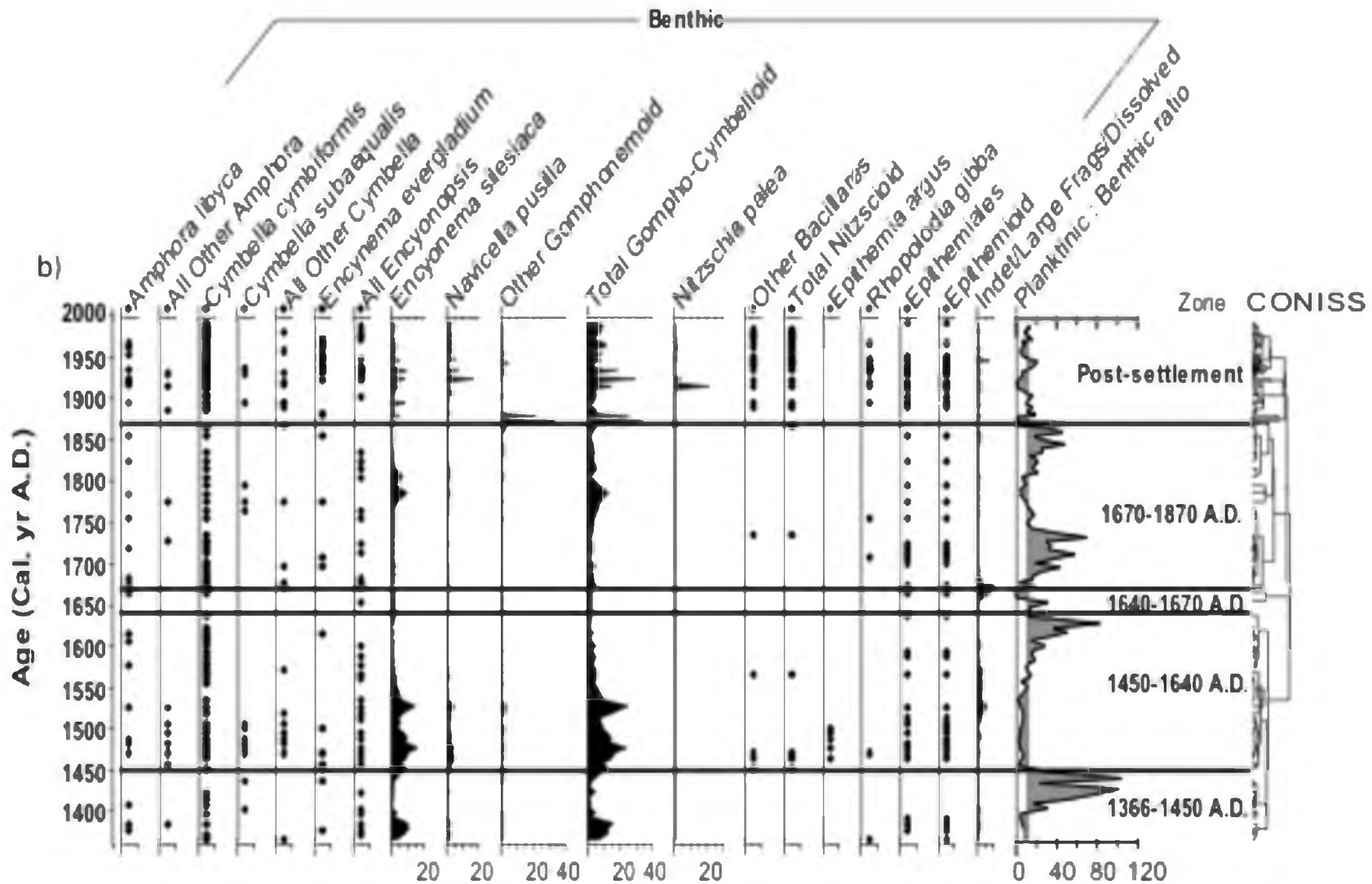


Figure 21 continued.

3.4.5 Stable isotope records of the sediment core

The $\delta^{15}\text{N}_{\text{BOM}}$ values in Foy Lake range from 0.5‰ to ~8.0‰ (Figure 22). In the presettlement period (1380 to 1880), the $\delta^{15}\text{N}_{\text{BOM}}$ values vary from 0.5‰ to 3.5‰. A positive excursion in $\delta^{15}\text{N}_{\text{BOM}}$ values of about 2‰ associated with establishment of Foy Mill (Power et al., 2006) marks the period of European settlement in the Flathead Valley. Positive excursions in $\delta^{15}\text{N}_{\text{BOM}}$ coincide with negative shifts in $\delta^{13}\text{C}_{\text{BOM}}$ values with the most significant change occurring in 1870 (from -25‰ to -28‰) at the time when Foy Mill was established. A positive shift in C:N ratios from 10.5 to ~ 17 also occurs at the same time. From ~ 1900, a negative shift in $\delta^{15}\text{N}_{\text{BOM}}$ values and a decrease in C:N ratios occurs with one notable exception in 1935, when a large excursion in $\delta^{15}\text{N}_{\text{BOM}}$ values (from ~3‰ to ~8‰) occurs that coincides with a decrease in C:N ratios from 10.5 to 8. There is a strong relationship between $\delta^{13}\text{C}_{\text{CaCO}_3}$ and $\delta^{18}\text{O}_{\text{CaCO}_3}$ between the top section of Foy Lake and the bottom section of the lake (Figure 23).

3.5 Discussion

Historical timber harvesting has had a significant impact on both sediment and nutrient influx into Foy Lake. The $\delta^{13}\text{C}$ and $\delta^{15}\text{N}$ values of bulk organic matter (hereafter $\delta^{13}\text{C}_{\text{BOM}}$ and $\delta^{15}\text{N}_{\text{BOM}}$, respectively), C:N ratios, and pollen and charcoal influxes provide clues on the source of materials getting into Foy Lake while diatom records indicate the impact of those materials on phytoplankton community dynamics and other ecosystem processes. The lake carbonates $\delta^{13}\text{C}$ and $\delta^{18}\text{O}$ values (hereafter $\delta^{13}\text{C}_{\text{CaCO}_3}$ and $\delta^{18}\text{O}_{\text{CaCO}_3}$, respectively) provide clues about lake water balance, and provide an understanding of the

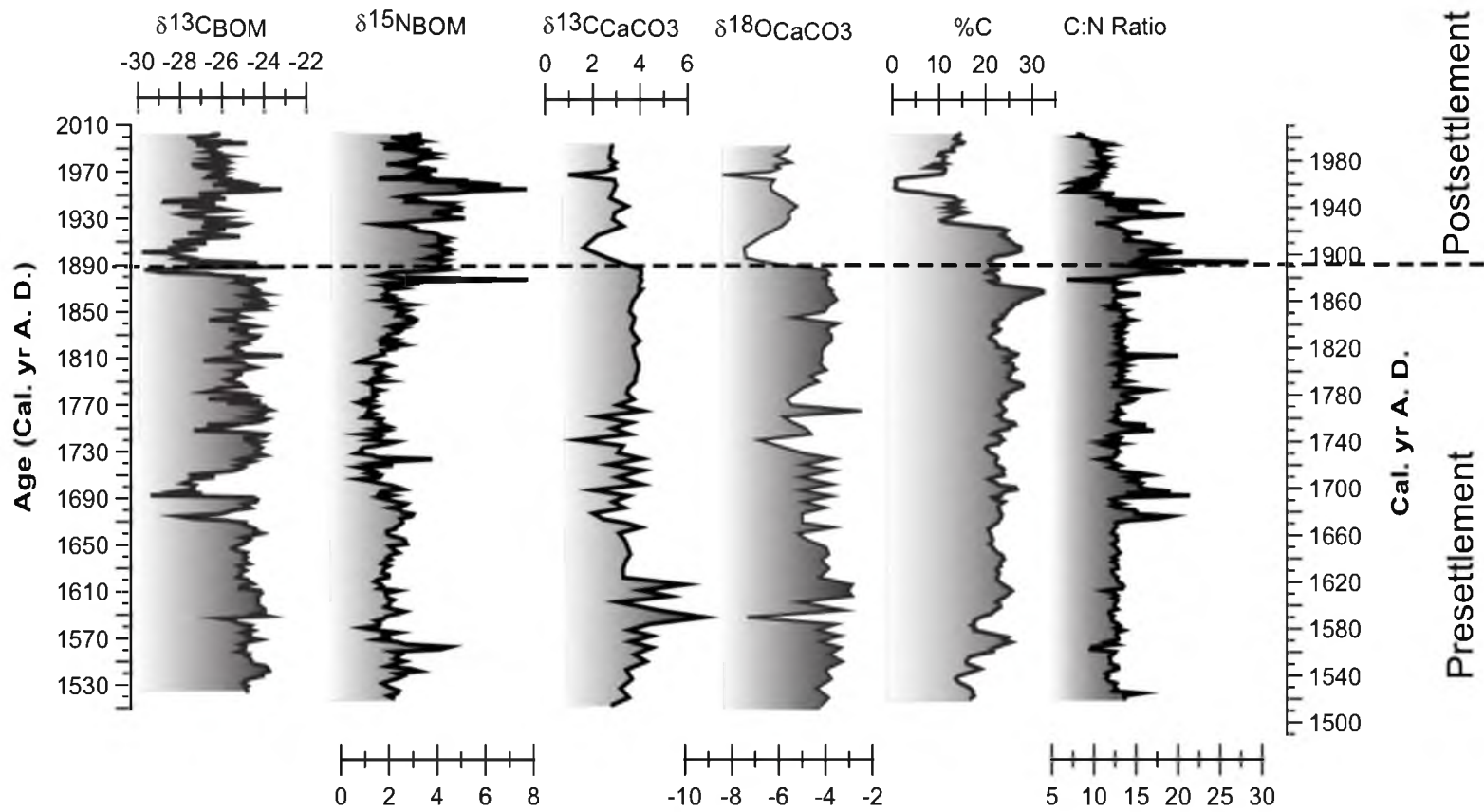


Figure 22. The $\delta^{13}C_{BOM}$, $\delta^{15}N_{BOM}$, $\delta^{13}C_{CaCO_3}$, and $\delta^{18}O_{CaCO_3}$, C:N ratio, and organic carbon content (% C) profiles in Foy Lake.

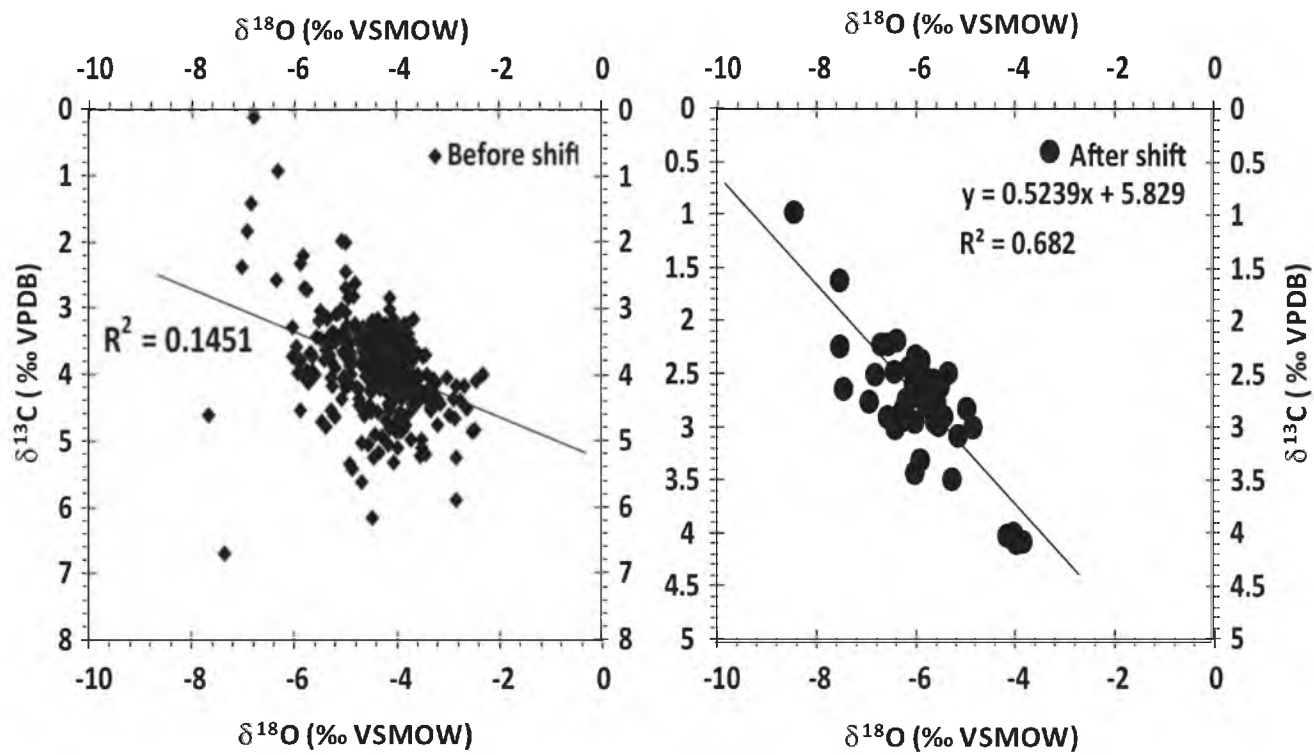


Figure 23. A scatter plot of the $\delta^{13}\text{C}_{\text{CaCO}_3}$ and $\delta^{18}\text{O}_{\text{CaCO}_3}$ before (left) and after (right) the major isotopic shift.

shifts in carbon cycling through water and nutrient budgets in Foy Lake before and after European settlement.

3.5.1 Effects of lake water balance on $\delta^{13}\text{C}_{\text{CaCO}_3}$ and $\delta^{18}\text{O}_{\text{CaCO}_3}$

Inferring past water balance from oxygen and carbon stable isotopes values based exclusively on the analysis of carbonates in lake sediments may lead to erroneous interpretations because there are numerous factors that cause $\delta^{18}\text{O}_{\text{CaCO}_3}$ and $\delta^{13}\text{C}_{\text{CaCO}_3}$ to vary within one lake. The study demonstrates that a multiproxy approach provides a holistic method for reconstructing past hydrological variations where nutrient and particulate material fluxes into the lake are accounted for. The historical precipitation records around Foy Lake indicate a significant decline in precipitation ~ 1980 A.D. (Appendix C) although the shift in $\delta^{13}\text{C}_{\text{CaCO}_3}$ and $\delta^{18}\text{O}_{\text{CaCO}_3}$ composition occurred ~ 1890 A. D. (Figure 22). The nutrients washed down from the watershed as well as resuspended sediments from the shallow sections of the lake may provide clues on the coeval processes associated with shifts in $\delta^{13}\text{C}_{\text{CaCO}_3}$ and $\delta^{18}\text{O}_{\text{CaCO}_3}$.

Original analysis of the $\delta^{18}\text{O}_{\text{CaCO}_3}$ (Stevens et al., 2006) in Foy Lake attributed the depletion in ^{18}O to change in water residence time after a shallow outlet on the northern end of the lake that operates intermittently during spring runoff, and was believed to have been modified in the late 1800s to power the Foy lumber mill. The shift in $\delta^{18}\text{O}_{\text{CaCO}_3}$ of $\sim 2\text{‰}$ around 1890 A.D. is attributed to changes in water residence time (Stevens et al., 2006) in Foy lake. These observations are consistent with numerical simulations by Shapely et al. (2008) based on mass-balance models that show that under the same

precipitation and evaporation scenario, $\delta^{18}\text{O}_{\text{CaCO}_3}$ values may vary significantly because of the contribution of groundwater from aquifers relative to precipitation. Under high groundwater fluxes and/or low lake volume, low lake fluid residence time dampens the amplitude of $\delta^{18}\text{O}_{\text{CaCO}_3}$ variation from climatic variability (Shapley et al., 2008).

Consequently, lake $\delta^{18}\text{O}_{\text{CaCO}_3}$ values reflect changes in precipitation, evaporation, as well as groundwater contribution to the lake water balance. The $\delta^{18}\text{O}_{\text{CaCO}_3}$ changes expected from climate forcing may be therefore hard to predict because of variations in groundwater-lake exchange and associated changes in lake residence time, and $\delta^{18}\text{O}_{\text{H}_2\text{O}}$ values of inflowing water and evaporative ^{18}O enrichment.

While the shift in $\delta^{18}\text{O}_{\text{CaCO}_3}$ of $\sim 2\text{‰}$ around 1890 A.D. is attributed to changes in water residence time (Stevens et al., 2006) in the lake, the shifts in $\delta^{13}\text{C}_{\text{CaCO}_3}$ are more complicated to interpret. For instance, Myrbo and Shapley (2006) demonstrate that $\delta^{13}\text{C}$ values of dissolved inorganic carbon ($\delta^{13}\text{C}_{\text{DIC}}$) in six carbonate-precipitating temperate lakes in Montana and Minnesota vary between epilimnetic waters and hypolimnetic waters. There are idiosyncrasies in $\delta^{13}\text{C}_{\text{DIC}}$ trends with dissolved inorganic carbon (DIC) content in individual lake water columns that may not be readily explained in terms of lake stratification, algal productivity, hydraulic residence time, or water chemistry (Myrbo & Shapley, 2006). Relating the magnitude of distinct DIC pools to carbonate mineral equilibria, microbial activity, lake residence time, and material fluxes in stratified lakes provide more predictable $\delta^{13}\text{C}_{\text{DIC}}$ behavior. Myrbo and Shapley (2006) identify three relationships of $\delta^{13}\text{C}_{\text{DIC}}$ values between DIC concentration ([DIC]) that exist in groundwater-fed lakes; (1) $\delta^{13}\text{C}_{\text{DIC}}$ values decreasing with increasing [DIC], (2) $\delta^{13}\text{C}_{\text{DIC}}$

values increasing with increasing [DIC], and (3) $\delta^{13}\text{C}_{\text{DIC}}$ values decreasing with increasing [DIC] but increasing again at the highest [DIC]. The variations in $\delta^{13}\text{C}_{\text{CaCO}_3}$ are therefore variously attributed to the magnitude of carbonate fluxes from the epilimnion to hypolimnion, carbonate dissolution kinetics in the water column, and microbial-mediated carbon cycling in the hypolimnion (e.g., Acetotrophic methanogenesis) (Myrbo & Shapley, 2006). The $\delta^{13}\text{C}_{\text{CaCO}_3}$ variations are therefore a function of physical-chemical gradients and microbial processes within the lake, while the $\delta^{18}\text{O}_{\text{CaCO}_3}$ values reflect changes in water residence.

Bicarbonates (HCO_3^-) and magnesium ions (Mg^{2+}) have a significant influence on magnesium to calcium ratios in groundwater-fed Lakes like Foy Lake (Shapley et al., 2010). Several groundwater springs suggests that the aquifers around the lake are rich in HCO_3^- and Mg^{2+} (LaFave, 2000). Therefore, the water derived from Foy Lake is rich in magnesium ions, as is evident from the presence of low magnesium calcite in the lake (Appendix C). The magnesium ions inhibit calcium carbonate nucleation with the crystal formation of calcium carbonate forming pure calcium carbonate (e.g., Meister et al., 2011). The presence of low magnesium calcite in the sediments is an indication of a high magnesium ion concentration in the lake water whose precipitation conforms to the summer calcification mediated by phytoplankton communities (Appendix C). As such, Foy Lake fits the description of a marl lake, characterized as having almost pure (90%–95%) low magnesium calcite, with no significant fluvial inflow-outflow system (*sensu* Drummond et al., 1995).

The influence of material fluxes on carbonate precipitation is best illustrated by the differences in correlation between $\delta^{13}\text{C}_{\text{CaCO}_3}$ and $\delta^{18}\text{O}_{\text{CaCO}_3}$ before and after the

European settlement of the Foy Lake watershed (Figure 23). Within the postsettlement section, 1880 through present, there is a strong positive correlation in $\delta^{13}\text{C}_{\text{CaCO}_3}$ and $\delta^{18}\text{O}_{\text{CaCO}_3}$ values ($R^2=0.7$) while the bottom section shows no correlation ($R^2=0.1$). Such positive correlations have been observed in small lakes where the contribution of autochthonous carbonates, especially during periods of high sedimentation rates, is significant (Horvatini et al., 2008). The relatively small surface area to volume ratio of Foy Lake (~ 0.03) makes the lake's $\delta^{13}\text{C}_{\text{CaCO}_3}$ and $\delta^{18}\text{O}_{\text{CaCO}_3}$ particularly sensitive to the influence of autochthonous carbonates.

3.5.2 Organic matter $\delta^{15}\text{N}_{\text{BOM}}$, $\delta^{13}\text{C}_{\text{BOM}}$, and C:N ratios evidence of material fluxes in Foy Lake

Groundwater-fed lakes like Foy Lake that primarily receive most of their water from spring snowmelt are likely to receive nutrients mainly leached from the watersheds (e.g., Campbell et al., 2002; McHale et al., 2002). However, nitrates washed in from runoff from watersheds having agricultural and urban settlements are generally more enriched in ^{15}N than nutrients arising from mineralization of organic nitrogen (Burns & Kendall, 2002; Mayer et al., 2002). Although our estimates based on GAP analysis maps shows only $\sim 7.6\%$ of the watershed has been developed (Appendix C), the reduced woody cover and increase in other forms of anthropogenic disturbance around Foy Lake led to the development of its eutrophic status, as is evident in C:N ratios and $\delta^{15}\text{N}_{\text{BOM}}$ values.

During the presettlement period, pulses of leached nitrates flushed from soils in the watershed may have gotten into the lake via basal flow during the spring snowmelt or surface runoff. Forest clearing during the late 19th and early 20th centuries resulted in an

influx of nutrients through surface water runoff, an observation that has been made from other watersheds in northern Idaho (Gravelle et al., 2009). Along with enhanced nutrient fluxes into lakes, particulate matter (e.g., pollen and diatoms) fluxes also increase during and after the tree logging.

The influx of woody pulp following the establishment of Foy Mill in Foy Lake watershed is evident in $\delta^{13}\text{C}_{\text{BOM}}$ values and C:N ratios. During the presettlement period, the C:N ratios average ~ 12.5 (Figure 22) while $\delta^{13}\text{C}_{\text{BOM}}$ values average $\sim -25\text{‰}$ with modest variations. However, tree logging operations led to an influx of woody material that increased the C:N ratios by as much as 29 with concomitant negative excursions in $\delta^{13}\text{C}_{\text{BOM}}$ values to as low as $\sim -30\text{‰}$. The postsettlement period exhibits a shift in C:N ratios and $\delta^{13}\text{C}_{\text{BOM}}$ values of greater than 1 and 0.5‰ , respectively (Figure 22).

The influx of woody debris from fire episodes causes slight enrichments in $\delta^{15}\text{N}_{\text{BOM}}$ values ($< 3\text{‰}$) (Figure 22). During the presettlement period, the $\delta^{15}\text{N}_{\text{BOM}}$ values generally show a more delayed response to material fluxes, suggesting the system was resilient to variability in material fluxes prior to European settlement. For instance, after an influx of materials (based on charcoal records) in 1420 A. D., the $\delta^{15}\text{N}_{\text{BOM}}$ values increase slowly, reaching a peak in ~ 1520 , and then decreases thereafter. However, timber harvesting elicits large and more rapid response in material fluxes, as is evident from large positive excursions in $\delta^{15}\text{N}_{\text{BOM}}$ values (Figure 22). The presettlement $\delta^{15}\text{N}_{\text{BOM}}$ values in Foy Lake vary between ~ 1 to $\sim 3.5\text{‰}$ but an isotopic enrichment of $\sim 3\text{‰}$ occurs following the logging operation in 1880s A.D. The poor correlation between $\%N$ and $\delta^{15}\text{N}_{\text{BOM}}$ in Foy Lake and the $\delta^{15}\text{N}_{\text{BOM}}$ trends through time indicate intermittent nitrogen influxes into Foy Lake (Appendix C).

Bivariate scatterplots of C:N ratios and $\delta^{13}\text{C}_{\text{BOM}}$ indicate that Foy Lake organic matter is derived from both algal and C_3 plants based on Meyers and Lallier-Verges' (1999) model (Appendix C). Prior to deforestation of Foy Lake watershed, conifer species, including *Pinus ponderosa*, *Larix occidentalis*, and *Pseudotsuga menziesii*, known for their prolific production of aerielly transported pollen, were major contributors of terrigenous organic matter input into the lake (Figure 19). The decline in woody cover after Euro-American settlement reduced their contribution to sedimentary organic matter, resulting in the observed decrease in C:N ratios (Figure 22). In addition, enhanced influx of fine particulates, including silts and clay, into Foy Lake during erosion events triggered by disturbances caused resuspension of sediments from shallow sections of the lake and redeposition of the same into deep sections of the lake (Stone & Fritz, 2004). The postlogging period is also marked by enhanced accumulation of quartz in sediments (Stevens et al., 2006). Therefore, the observed negative shift in C:N ratios (~ 2.5) and $\delta^{13}\text{C}_{\text{BOM}}$ values ($\sim 1.5\text{‰}$) was a consequence of reduced influx of woody materials as well as the enhanced influx of tycho plankton and benthic diatoms into lake sediments (Figure 18–22).

Within the last ~ 500 years, the diatom community in Foy Lake reflect material influx from the shallow sections of the lake to deeper sections of the lake consistent with the planktic:benthic ratios model of Stone and Fritz (2004). However, geochemical data suggest that the relationship between the changes in planktic:benthic ratios and water depth may be not just a function of changes in lake water level but also disturbance. For instance, the increase in planktic:benthic ratio between 1580 to 1640 A.D. coincide with negative shifts in organic carbon content ($\%C$) and a significant positive excursion in

$\delta^{15}\text{N}_{\text{BOM}}$ values (Figure 21–22) and positive shifts in $\delta^{13}\text{C}_{\text{CaCO}_3}$ values. In contrast, the increase in benthic:planktonic ratio values between 1670 and 1710 A. D. (Figure 21) coincides with a significant negative shift in $\delta^{13}\text{C}_{\text{BOM}}$, a positive shift in C:N ratio, and a less significant shift in $\delta^{15}\text{N}_{\text{BOM}}$ values (Figure 22). These data suggest that organic material fluxes from the watershed (terrigenous) and benthic environments (autochthonous) vary in magnitude throughout the study periods and these materials differ in C:N ratios, $\delta^{15}\text{N}_{\text{BOM}}$, and $\delta^{13}\text{C}_{\text{BOM}}$ values (Figure 22).

During the postsettlement period (after 1890 A.D.), the significant negative excursion in $\delta^{13}\text{C}_{\text{BOM}}$ values that coincides with an equally significant positive excursion in $\delta^{15}\text{N}_{\text{BOM}}$ values and C:N ratios (Figure 22) is also marked by an increased influx of certain species of benthic plankton, particularly members of the genera *Gomphonema*, *Nitzschia*, *Navicula*, and *Craticula* sp. (Figure 21). In addition, the significant increase in relative abundance of tychoplankton in 1890 A.D. (Figure 18) signifies the onset of disturbance within Foy Lake. Tychoplanktons have their true habitat in the benthos but can be found resuspended in the water column and are especially common in lakes where benthic diatoms are especially abundant and easily detached and resuspended into the water column (Smol et al., 2001). Therefore, the postsettlement influx of the benthic and tychoplanktons is largely a consequence of disturbance in the watershed and stirring up of sediments in the upper section of the lake, as opposed to modification of the outlet in the northern section of the lake as was earlier thought (Stevens et al., 2006). The significant positive correlation between $\delta^{13}\text{C}_{\text{CaCO}_3}$ and $\delta^{18}\text{O}_{\text{CaCO}_3}$ in the postsettlement period is therefore a consequence of a mixture between authigenic and detrital carbonates in the Lake (Figure 23).

3.5.3 The charcoal influx and fire history

The large positive shift in C:N ratios of ~ 10 observed between 1610 and 1650 is accompanied by an increase in the charcoal influx by ~ 5 particles $\text{cm}^{-2} \text{yr}^{-1}$. Similarly, the large positive shifts in C:N ratios at the beginning of tree logging is accompanied by an increase in charcoal influx of ~ 5 particles $\text{cm}^{-2} \text{yr}^{-1}$. Changes in charcoal influx suggest that positive excursions in C:N ratios arise from an influx of terrigenous organic matter. However, charcoal influx does not exclusively account for the positive shifts in C:N ratios, since the high peaks in C:N ratios (e.g., between 1750-1800) are not always accompanied by significant charcoal influxes (Figure 20, 22). During the predisturbance period, the C:N ratios are constant during certain periods and variable in other periods, suggesting that material influxes into Foy Lake are intermittent. The trends in $\delta^{15}\text{N}_{\text{BOM}}$ values also suggest that nutrient fluxes in Foy Lake occur in pulses.

3.5.4 The impact of cultural eutrophication of carbon cycling

Stevens et al. (2006) report that beginning in 1890 A.D., there is an increase in quartz, calcite, total inorganic carbon (TIC), a decrease in total organic carbon, and an increase followed by a decrease in C:N ratios of organic matter. Results of organic matter analysis in this study corroborate these findings (Figure 22). The increase in $\delta^{15}\text{N}_{\text{BOM}}$ values at the beginning of the tree logging operation (1880 A.D.) suggests an influx of terrigenous materials. The decrease in organic carbon (% C) after cessation of timber harvesting also indicates an increase in influx of inorganic materials in Foy Lake. The shift from high to low C:N ratios of the organic matter (this study) and a corresponding increase in calcite content following deforestation (Stone et al., 2005;

Stevens et al., 2006) is an indication of an increase in productivity from heightened nutrients influx and an increase in algal-derived organic matter of low C:N ratio mainly from benthic origin. This study illustrates the need to account for nutrient and particulate matter fluxes within and around the lake when reconstructing past environments from lake sediment records (Appendix C).

3.6 Conclusion

This study evaluated the hypothesis that forest clearing elicits an unprecedented influx of nutrients and terrigenous materials that alter carbon cycling in lake environments compared to the period before Euro-American settlement (pre-A.D. 1880). The stable isotope and palynomorphic data (charcoal, pollen, and diatom counts) indicate an unprecedented influx of nutrients and particulate matter in lake sediments. Watershed geomorphology, tree harvesting, and lake bathymetry all contribute to the changes in influx of materials into the lake. Changes in woody cover following tree harvesting altered the material fluxes into the lake and are manifested as shifts in elemental stoichiometry (C:N ratios), inorganic materials (e.g., carbonates), and organic materials (e.g., diatoms, pollen). Shifts in $\delta^{13}\text{C}_{\text{CaCO}_3}$ and $\delta^{18}\text{O}_{\text{CaCO}_3}$ values are most likely driven by enhanced algal productivity and influx of resuspended sediments from terrigenous sources and sediment focusing within the lake, as illustrated by a material flux conceptual model (Appendix C). Consequently, the sources of materials should be documented when reconstructing paleoenvironments.

3.7 Acknowledgements

The stable isotope analysis of the sediments was funded and facilitated through Dr. Thure Cerling's lab (University of Utah). We thank Dr. Cerling, Kevin Uno, and Kendra Chritz for the invaluable advice and suggestions they gave us during the analysis of Foy Lake sediments and preparation of this manuscript.

3.8 References

- Battarbee, R. W. (1986). Diatom analysis. In B. E. Berglund [ed.], *Handbook of Holocene palaeoecology and palaeohydrology* (pp. 527–570). Wiley.
- Burns, D. A., & Kendall, C. (2002) Analysis of $\delta^{15}\text{N}$ and $\delta^{18}\text{O}$ to differentiate NO_3^- sources in runoff at two watersheds in the Catskill Mountains of New York. *Water Resource Research*, 38(5), 1–12.
- Campbell, D. H., Kendall, C., Chang, C. C. Y., Silva, S. R., & Tonnessen, K. A. (2002). Pathways for nitrate release from alpine watershed: Determination using $\delta^{15}\text{N}$ and $\delta^{18}\text{O}$. *Water resources research*, 38(5), 1–9.
- Coplen, T.B., & Kendall, C. (2000). Stable hydrogen and oxygen isotope ratios for selected sites of the U.S. Geological Survey's NASQAN and benchmark surface-water networks. U.S. Geological Survey, Open-File Report 00–160: 409 pp.
- Craig, H. (1961). Isotopic variations in meteoric waters. *Science*, 133, 1702–1703.
- Drummond, C. N., Patterson, W. P., & Walker, J. G. G., (1995). Climatic forcing of carbon-oxygen isotopic covariance in temperate-region marl lakes. *Geology*, 23(11), 1031–1034, doi: 10.1130/0091-7613(1995)023<1031:CFOCOI>2.3.CO;2.
- Elliot, E. M. & Brush, G. S. (2006). Sedimented organic nitrogen isotopes in freshwater wetlands record long-term changes in watershed nitrogen source and land use. *Environment Science & Technology*, 40: 2910–2916.
- Gravelle, J. A., Ice, G., Link, T. E., & Cook, D. L. (2009). Nutrient concentration dynamics in an inland Pacific Northwest watershed before and after timber harvest. *Forest Ecology & Management*, 257, 1663–1675, doi:10.1016/j.foreco.2009.01.017.

- Grossman, E. L., & Ku, T. L. (1986). Oxygen and carbon isotope fractionation in biogenic aragonite—temperature effects. *Chemical Geology*, *59*, 59–74.
- Henderson, A. K., & Shuman, B. N. (2009). Hydrogen and oxygen isotopic compositions of lake water in the western United States. *Geological Society of America Bulletin*, *121*, 1179–1189, doi: 10.1130/B26441.1
- Horvatini, N., Barešić, J., Babinka, S., Obeli, B., Broni, I. K., Vreca, P., & Suckow, A. (2008). Towards a deeper understanding of how carbonate isotopes (^{14}C , ^{13}C , ^{18}O) reflect environmental changes: a case study with recent ^{210}Pb dated sediments of the Plitvice Lakes, Croatia. *Radiocarbon*, *50*(2), 233–253.
- Leng, M. J., Jones, M. D., Frogley, M. R., Eastwood, W. J., Kendrick, C. P., & Roberts, C. N. (2010). Detrital carbonate influences on bulk oxygen and carbon isotope composition of lacustrine sediments from the Mediterranean. *Global & Planetary Change*, *71*, 175–182.
- Leavitt, P. R., Fritz, S. C., Anderson, N. J., Baker, P. A., Blenckner, T., Bunting, L., Catalan, J., Conley, D. J., Hobbs, W. O., Jeppesen, E., Korhola, A., McGowan, S., Rühland, K., Rusak, J.A., Simpson, G. L., Solovieva, N., & Werne, J. (2009). Paleolimnological evidence of the effects on lakes of energy and mass transfer from climate and humans. *Limnology & Oceanography*, *54*(6, part 2), 2330–2348.
- LaFave, J. I. (2000). Dissolved constituents map of the deep aquifer, Kalispell valley, Flathead County, Montana (open file version): Montana Bureau of Mines and Geology Ground Water Assessment Atlas 02B-3.
- Mayer, B., Boyer, E. W., Goodale, C., Jaworski, N. A., Van Breemen, N., Howarth, R. W., Seitzinger, S., Billen, G., Lajtha, L. J., Nosal, M., & Paustian, K. (2002) Sources of nitrate in rivers draining sixteen watersheds in the Northeastern U.S.: Isotopic constraints. *Biogeochemistry*, *57*, 171–197.
- McConnaughey, T. A., LaBaugh, J. W., Rosenberry, D. O., Striegl, R. G., Reddy, M. M., Schuster, P. F., & Carter, V. (1994) Carbon budget for a groundwater-fed lake: calcification supports summer photosynthesis. *Limnology and Oceanography*, *39*(6), 1319–1332.
- Meister, P., Johnson, O., Corsetti, F., & Nealson, K. H. (2011). Magnesium inhibition controls spherical carbonate precipitation in ultrabasic springwater (Cedars, California) and culture experiments. *Advances in Stromatolite Geobiology Lecture Notes in Earth Sciences*, Volume 131/2011, 101–121, doi: 10.1007/978-3-642-10415-2_6.

- Meyers, P. A., & Lallier-Verges, E (1999). Lacustrine sedimentary organic matter records of Late Quaternary paleoclimates. *Journal of Paleolimnology*, 21, 345–372.
- McHale, M. R., McDonnell, J. J., Mitchel, M. J., & Cirimo, C. P. (2002). A field based study of soil water and ground water nitrate release, in an Adirondack forested watershed. *Water Resources Research*, 38(4), 1031–1046.
- Nanus, L., Campbell, D. H., Ingersoll, G. P., Clow, D. W., & Mast, A. M. (2003). Atmospheric deposition maps for the Rocky Mountains. *Atmospheric Environment*, 37, 4881–4892.
- Owen, L. A., Thackray, G., Anderson, R. S., Briner, J., Kaufman, D., Roe, G., Pfeffer, W., & Chaolu, Y. C. (2009). Integrated research on mountain glaciers: Current status, priorities and future prospects. *Geomorphology*, 103: 158–171.
- Piatek, K. B., Mitchel, M. J., Silva, S. R., & Kendall, C. (2005). Sources of nitrate in snowmelt discharge: Evidence from water chemistry and stable isotopes of nitrate. *Water, Air and Soil Pollution*, 165, 13–35.
- Power, M. J., Whitlock, C., Bartlein, P. J., & Stevens, L. (2006). Fire and vegetation history during the last 3800 years in northwestern Montana. *Geomorphology*, 75, 420–436.
- Power, M. J., Whitlock, C., & Bartlein, P. J. (2011). Postglacial fire, vegetation, and climate history across an elevational gradient in the Northern Rocky Mountains, USA. *Quaternary Science Reviews*, 30(19–20): 2520–2533.
- Saros, J. E., Clow, D. W., Blett, T., & Wolfe, A. P. (2010). Critical nitrogen deposition loads in high-elevation lakes of the Western US inferred from paleolimnological records. *Water Air Soil Pollution*, doi 10.1007/s11270-010-0526-6.
- Shapley, M. D., Ito, E., & Forester, R. M. (2010). Negative correlations between Mg:Ca and total dissolved solids in lakes: False aridity signals and decoupling mechanism for paleohydrologic proxies. *Geology*, 38(5), 427–430, doi: 10.1130/G30718.1; 5.
- Shuman, B., Henderson, A., Colman, S. M., Stone, J. R., Fritz, S. C., Stevens, L. R., Power, M. J., & Whitlock, C. (2009). Holocene lake-level trends in the Rocky Mountains, U.S.A. *Quaternary Science Reviews*, 28(19-20), 1861–1879.
- Smol, J. P., Birks, H. J. B., & Last, W. M. (eds.), (2001). Tracking Environmental Change Using Lake Sediments, Volume 3. Terrestrial, Algal, and Siliceous Indicators. Kluwer Academic Publishers, Dordrecht, The Netherlands.

Stevens, L. R., Stone, J. R., Campbell, J., Fritz, S. C. (2006). A 2200-yr record of hydrologic variability from Foy Lake, Montana, USA, inferred from diatom and geochemical data. *Quaternary Research*, 65, 264–274.

Stone, J. R., & Fritz, S. C. (2004). Three-dimensional modeling of lacustrine diatom habitat areas: Improving paleolimnological interpretation of planktic:benthic ratios. *Limnology and Oceanography*, 49, 1540–1548.

Stone, F. R. (2005). A high-resolution record of Holocene drought variability and the diatoms stratigraphy of Foy Lake, Montana. PhD Dissertation. University of Nebraska, Lincoln, Nebraska.

Widory, D., Petelet-Giraud, E., Negrel, P., Ladouche, B. (2005). Tracking the sources of nitrate in groundwater using coupled nitrogen and boron isotopes: A Synthesis. *Environment Science & Technology*, 39, 539–548.

CHAPTER 4

DISTURBANCE AND HYDROLOGICAL HISTORY OF UTAH

LAKE, UT: ISOTOPIC, POLLEN, AND CHARCOAL

RECORDS OF MATERIAL FLUXES

AND WATER BALANCE

4.1 Introduction

Anthropogenic disturbances can impact lake biogeochemical processes significantly and may mask climatic signals embedded in lake sediment records (e.g., Rosén et al., 2000). Such ecological disturbances have been referred to as “information filters” (*sensu* Leavitt et al., 2009) since they complicate the interpretation of the climatic signals. Leavitt et al. (2009) propose a process-oriented approach where energy and material fluxes are accounted for. In accounting for biogeochemical processes imprinted in lake sediments from disturbance and climate, integrating several paleoecological methods may yield more accurate results.

Isotopic information gleaned from lake sediments is invaluable in accounting for biogeochemical processes induced by natural and anthropogenic activities. For instance, ^{15}N abundance is a reliable indicator of disturbance that can be used to estimate influence of agricultural and urban disturbance in watersheds (Elliot & Brush 2006; Mayer et al., 2009). Corroborating such isotopic imprints with palynomorphic records (e.g., spores

and pollen) and charcoal may constrain the interpretation of sedimentary records and hence provide analogues for interpreting past climate and land use change within watersheds.

In this study, we combine palynomorphic (charcoal, pollen, and macrofossil), elemental, isotopic analysis, and loss on ignition analysis of bulk sediments to decipher the influence of anthropogenic activities in and around Utah Lake, UT. The size and geomorphology of the lake, hydrology, and land use history of its watershed are considered. This study is not only important for understanding factors that have altered the lake ecosystem in the past, but it also provides background information for restoring the lake and its threatened native biodiversity (e.g., Kaperman et al., 2010).

4.2 Study area

Utah Lake, UT, is surrounded by farmlands and urban centers and is bordered by the Wasatch Range to the east, the Traverse Range to the north, and the Lake Mountains to the west (Figure 24). The lake is fed by both spring and stream water with Provo, Spanish Fork, American Fork, and Hobbie Creek constituting the main rivers. The dominant land cover types include invasive perennial grasslands (14.3%), crop fields (14.4%), intermountain basin sagebrush steppe (10.7%), Gambel oak mixed montane shrubland (21%), and other plant communities (see Appendix D). The lake is 35.4 km long, 16.1 km wide, and extremely shallow, having an average depth of 2.4 m and a maximum of 4 m.

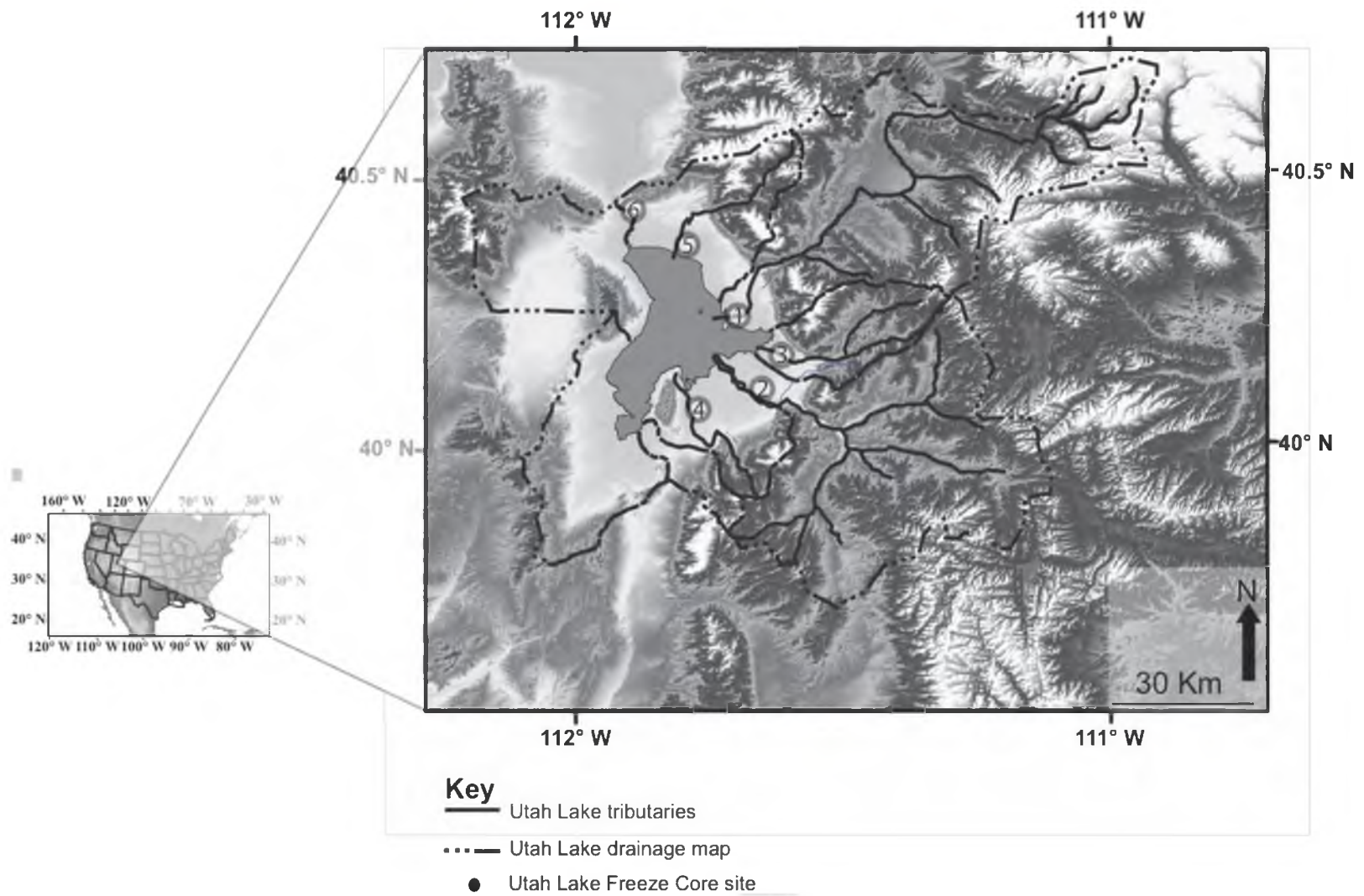


Figure 24. Map of Utah Lake and its watershed. The lake is fed by Provo River (1), Spanish Fork (2), Hobbie Creek (3), Spring Creek (4), and American Fork (5). Jordan River (6) as the only outlet.

4.3 Methods

A 43 cm freeze core was recovered from sediments in the center of Utah Lake in September 2009. The upper 23 cm of the core are medium to dark-gray silty clay that is poorly compacted, and high in water content. Below 23 cm, the sediment grades into more compact light to medium to gray clay that extends to a depth of 43 cm. The core was kept frozen and transported back to a laboratory in the Natural History Museum of Utah for analysis. High-resolution photos were taken to determine the optimum sampling protocols for the sediments whereupon subsamples were obtained for isotope, loss on ignition, pollen, and charcoal analyses at 0.5 cm intervals from the bottom. The samples were placed in pre-labeled centrifuge tubes.

Water samples were collected in June 2010 from three locations in the lake at about 1 meter deep. The screw top of the sample bottle was reinforced with parafilm to prevent water loss due to evaporation. The samples were placed in a cooler, transported to the lab, and kept below 4 °C until analyzed.

4.3.1 Isotope analysis

The stable isotope analysis was carried out in stable isotope laboratories of the Biology Department at the University of Utah. Forty-three sediment samples at centimeter spacing were obtained for the analysis. An aliquot of about 600–700 mg was transferred into new centrifuge vials, and put into an oven to dry for at least 48 hrs at 60 °C. Two subsamples of about 300 mg each were obtained from the oven-dried samples and transferred to new pre-labeled centrifuge vials. The other 300 mg sample, destined for carbonate analysis, was left untreated.

4.3.1.1 Stable isotope analysis of OM

Sediment samples were treated with dilute hydrochloric acid to remove carbonates, rinsed with distilled water, and then oven-dried at 60 °C for at least 24 hrs. 10 to 20 milligrams of the samples were weighed into 4 mm x 6 mm compressed tin capsules (Costech Inc.), and analyzed for stable isotopes of carbon (^{13}C) organic and nitrogen (^{15}N) in stable isotope laboratories in the Biology Department, University of Utah. Yeast of known isotopic composition was used as an internal standard for these analyses. The samples were combusted in a Costech 4010 Elemental Analyzer at 1650 °C and inlet to a Finnigan® MAT 252 Isotope Ratio Mass Spectrometer (IRMS) in continuous flow mode. Isotope values were calculated as shown in Equation 13.

$$\delta X (\text{‰}) = 1000 * (R_{\text{sample}} / R_{\text{standard}} - 1) \quad \text{Equation 15}$$

where ‘ X ’ is either ^{15}N or ^{13}C , R is $^{15}\text{N} / ^{14}\text{N}$, or $^{13}\text{C} / ^{12}\text{C}$, respectively, and δX is expressed in permil (‰) relative to internationally agreed standards: V-PDB for both carbon and oxygen, and atmosphere (AIR) for nitrogen $\delta^{15}\text{N}$, respectively. Water oxygen and deuterium values are reported relative to VSMOW standard. Carbon and nitrogen yields were determined from preliminary, optimum sample sizes established, and run in duplicate.

4.3.1.2 Stable isotope analysis of sedimentary carbonate

The untreated aliquots were sieved through a 140 μm sieve to remove coarse debris and were analyzed for $\delta^{18}\text{O}$ and $\delta^{13}\text{C}$ via continuous flow with a GasBench (ThermoScientific Inc.) coupled to a Finnigan MAT 252 IRMS. UU Carrara (carbonate) of grain size $< 140 \mu\text{m}$ was used as an internal standard for all analyses. About 5 mg of each sediment sample was weighed into 25 ml screw-top vials with septa, purged with helium to remove atmospheric gases in the headspace, injected with phosphoric acid to evolve carbon dioxide, and left to react overnight at 72 $^{\circ}\text{C}$. UU Carrara (carbonate) was used as an internal standard. The standard deviations (1σ) of isotope measurements of $\delta^{13}\text{C}$ and $\delta^{18}\text{O}$ were ≤ 0.07 and ≤ 0.02 ‰, respectively. All isotope values were calculated as shown in Equation 13.

4.3.1.3 Stable isotope analysis of water samples

Water isotope analysis was done in a high temperature combustion elemental analyzer (TCEA) in the Stable Isotope Research Facility for Environmental Research (SIRFER) Lab, University of Utah. The samples were run together with internal standards (PLRM-1, PLRM-2, and SLRM) calibrated to VSMOW water. $\delta^{18}\text{O}_{\text{H}_2\text{O}}$ and δD were calculated as shown in Equation 13.

4.3.2 ^{210}Pb dating of sediments

^{210}Pb -based dating was considered appropriate for dating the Utah Lake sediment core spanning the last 130–150 years (Last & Smol, 2001) based on the assumption that unsupported ^{210}Pb activity diminishes continuously and after 6–8 half lives (half-life

~22.3 yrs), the activity is comparable to background. Samples were counted for ^{210}Pb activity at Brigham Young University (BYU) by alpha spectrometry of ^{210}Po assumed to be in secular equilibrium with ^{210}Pb . In brief, samples were decalcified with weak HCl, dried, and spiked with ^{210}Po . Samples were then digested in Teflon beakers on a hot plate with aqua regia at temperatures $<90\text{ }^\circ\text{C}$. After drying, samples were taken up in 0.1M HCl and filtered. Po-bearing solutions were treated with hydroxylamine to chelate Po, and sodium citrate and ascorbic acid to keep the iron in the ferrous state. Silver discs were added to the solution where Po spontaneously implants into the silver disc.

4.3.3 Loss on ignition (LOI) analysis

Sediment samples were collected at each centimeter interval starting at the top of the freeze core and a gram weighed into porcelain vials and placed in an oven at $70\text{ }^\circ\text{C}$ for 48 hrs to remove water. Following this, the samples were reweighed, placed in a muffle furnace heated to $550\text{ }^\circ\text{C}$ for two hours, after which the samples were reweighed to determine the organic content. The samples were then returned to the muffle furnace at $950\text{ }^\circ\text{C}$ for two hours and again reweighed to determine the carbonate content.

4.3.4 Estimation of percent land cover / land use in watershed

A GAP analysis map for southwestern US (Lowry et al., 2007) generated from landsat imagery collected between 1999 and 2001 was used to estimate the proportion of land under different land cover and land use within the Utah Lake Watershed. The Rocky Mountain subalpine dry and mesic meadow, aspen forest and woodland, montane mesic mixed conifer and woodland, alpine bedrock and scree, lodgepole pine forest;

Colorado Plateau pinyon juniper woodland; Great Basin pinyon juniper woodland; and Intermountain big sagebrush shrubland, montane big sagebrush steppe, invasive annual grassland, and basin playa were categorized as undeveloped. The developed areas included the developed open space - low and high intensity (categorized as urban), and agricultural land. Water category was excluded in the analysis. The watersheds were digitized from 10 m USGS digital elevation models (DEMs). Sections of the land use maps outside the regions of interests (watersheds) were masked out using the digitized watershed in ENVI 4.7 (ITT VIS Inc.). The percentage land cover / land use was calculated as shown in Equation 16:

$$\% \text{ Land use per cover class} = \frac{\text{Pixels per land cover class}}{\sum_{i=1}^n \text{Pixels per land cover class}} \quad \text{Equation 16}$$

where ‘n’ represents the number of land cover classes in the watershed.

4.3.5 Pollen processing

Sediment samples (1cc each) were obtained at 1 cm intervals (~ 6–7 yr intervals) and processed following the methods of Faegri et al. (1989). A *Lycopodium* tablet was added to each sample as an exotic tracer. At least 300 terrestrial grains were counted for each sample processed. Counts were converted to percentages of the total terrestrial grains, and pollen influx rates (grains/cm²/ yr) were calculated for each pollen taxon over the course of the record.

4.3.6 Charcoal analysis

Macroscopic charcoal was used to reconstruct fire history and fire frequency. A cubic centimeter sediment sample was obtained from the freeze core at one-centimeter sediment depth intervals. The samples were disaggregated with potassium hydroxide, washed through a 150 μm sieve, identified, and counted with a dissecting microscope. Charcoal values were converted to concentration (particles cm^{-2}) and used to estimate sediment influx from historical brush burning in the watershed.

4.4 Results

4.4.1 $^{210}\text{Pb}_{\text{ex}}$ activity profile, magnetic susceptibility, loss on ignition, charcoal counts with sediment depth

Examining the plot of sediment depth versus ^{210}Pb activity, it is evident that ^{210}Pb activity levels off at 24.5 cm (Figure 25). Therefore, ^{210}Pb activity below that depth is considered supported by radioactive decay of ^{226}Ra (half-life 1600 yrs) already present in the sediments (Figure 25). The unsupported ^{210}Pb activity from sedimentation of ^{222}Rn daughter product ($^{210}\text{Pb}_{\text{ex}}$) appears above 24.5 cm depth, and varies unpredictably with depth. The magnetic susceptibility, $\delta^{15}\text{N}_{\text{BOM}}$ values, and charcoal particles ($>150 \mu\text{m}$) count increase concordantly by ~ 10 SI units, $\sim 3.0\%$, and ~ 40 particles per cc., respectively, from 25 cm to 20 cm depth, while LOI values at 550 $^{\circ}\text{C}$ decrease by $\sim 1\%$ for the same interval.

Core description

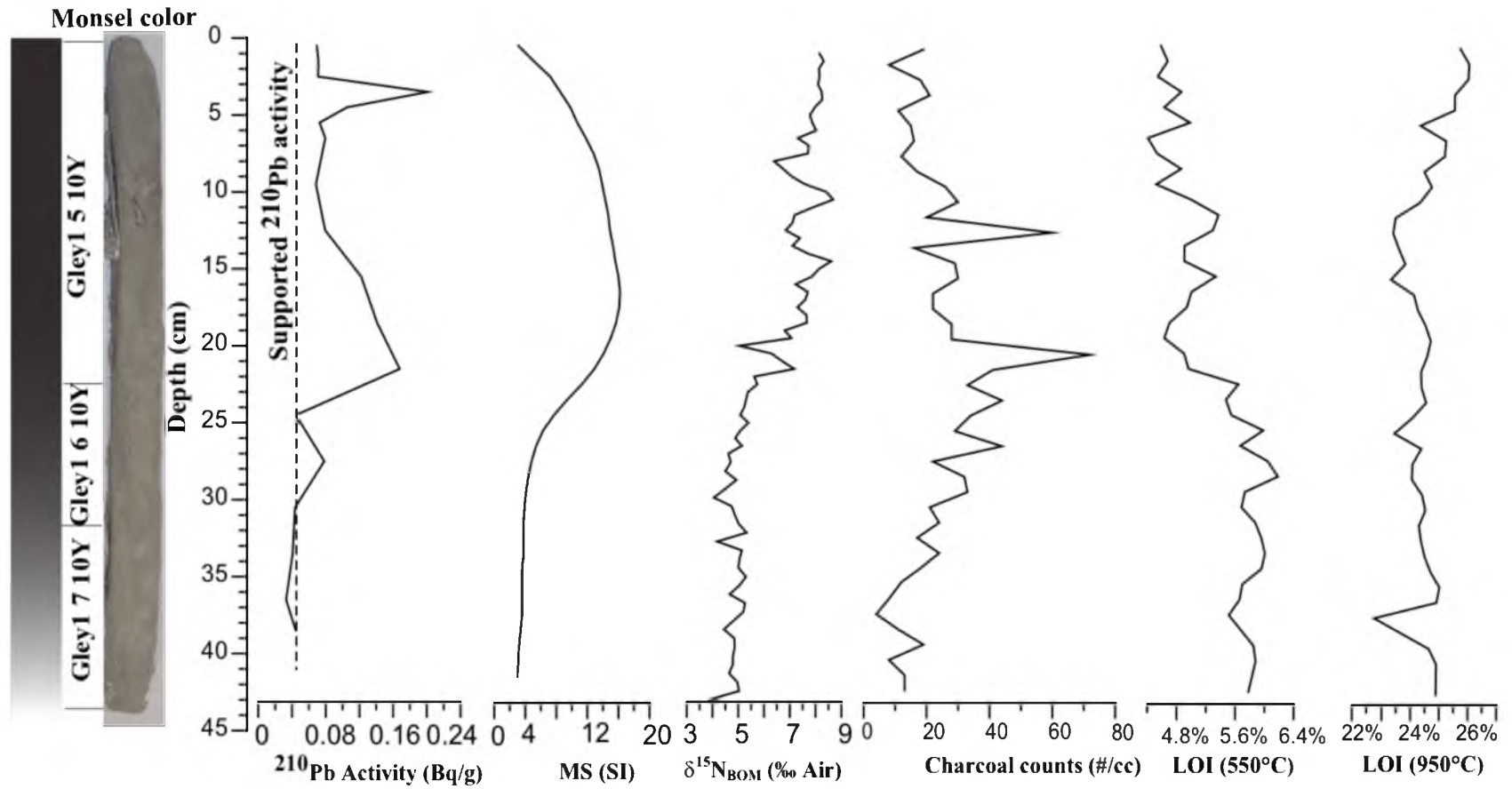


Figure 25. The $^{210}\text{Pb}_{\text{ex}}$ activity, magnetic susceptibility, $\delta^{15}\text{N}_{\text{SOM}}$ values, charcoal counts, LOI at 550 °C, and LOI at 950 °C of Utah Lake sediments with depth.

4.4.2 $\delta^{13}\text{C}_{\text{SOM}}$ and C:N ratios records with depth

C:N ratios below 28 cm vary between 9.5 and 10.5 (Figure 26). Above 28 cm depth, the C:N ratio decreases steadily from 9 to ~8 with the exception of two major excursions at 21 cm (C:N ratio ~12.5) and 14 cm (C:N ratio ~16). The variations in $\delta^{13}\text{C}_{\text{BOM}}$ values are modest, ranging from ~ -26.5‰ to -28‰. There, $\delta^{13}\text{C}_{\text{BOM}}$ values decrease steadily from ~- 26.5‰ at 28 cm to ~-28.0‰ at 17.5 cm and then increase steadily to ~-26.5‰ at 11 cm depth. The % C increase steadily from ~2% at 26 cm to ~3.5% at 11 cm depth.

4.4.3 Pollen records

The pollen abundance records of Utah Lake indicate that nonarboreal pollen dominates the vegetation around the lake (Figure 27). Other dominant taxa include members of the goosefoot/amaranth family (*Chenopodium/Amaranthus* labeled “Cheno/Ams”), sagebrush (*Artemisia*), and sedge family (Cyperaceae), which are the most abundant nonarboreal pollen in the lake while Juniper and Pinaceae dominate arboreal pollen. Results of cluster analysis of pollen record suggest four major zones: the pre-settlement zone (below 28 cm depth), transition (between 23 and 28 cm depth), settlement zone (between 16 and 23 cm depth), postsettlement (between 8 and 16 cm depth), and recent (above 8 cm depth). Change in the relative abundance of grass pollen is most significant in the postsettlement period.

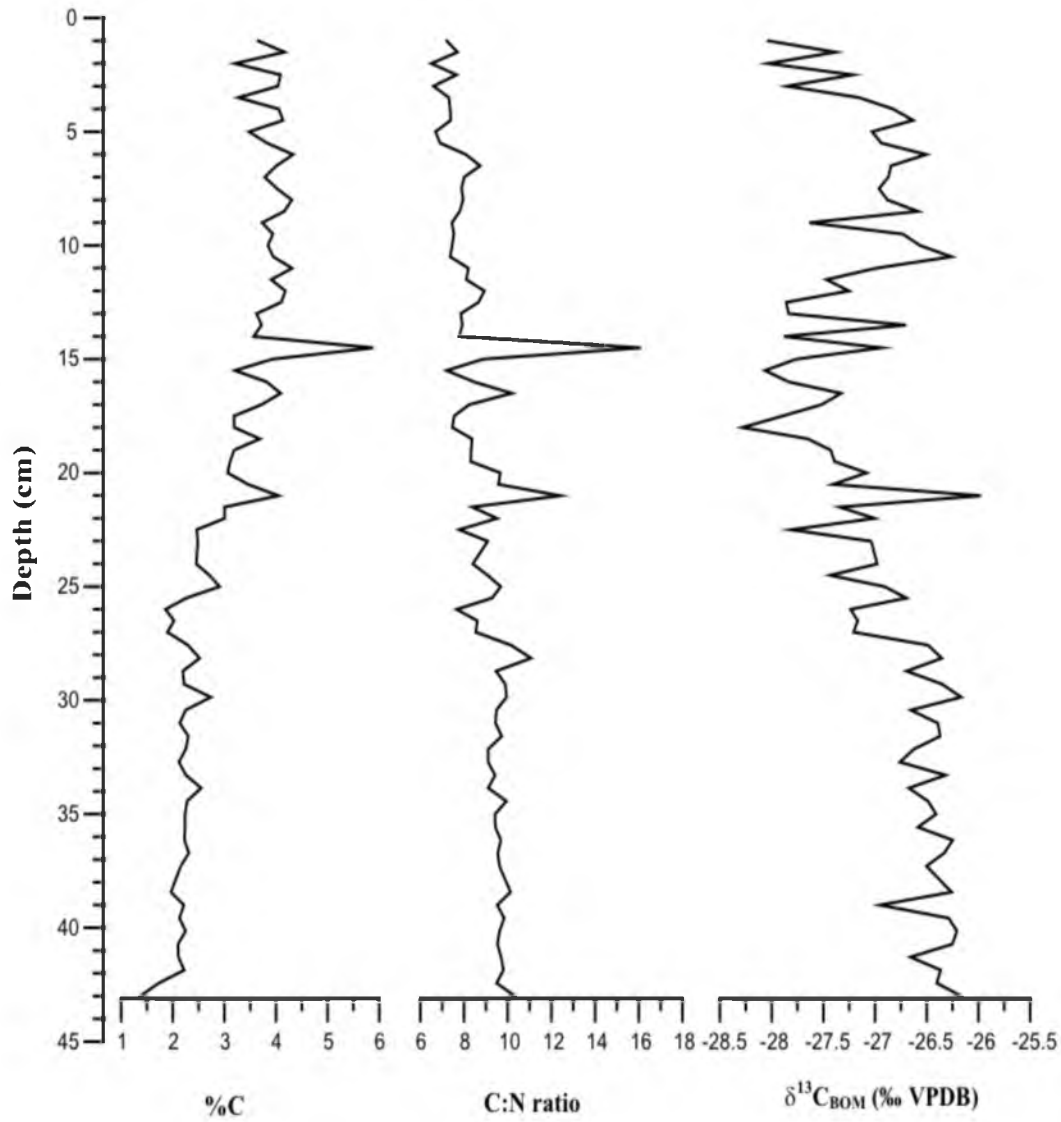


Figure 26. The %C, C:N ratios, and $\delta^{13}\text{C}_{\text{SOM}}$ values of Utah Lake sediments with depth.

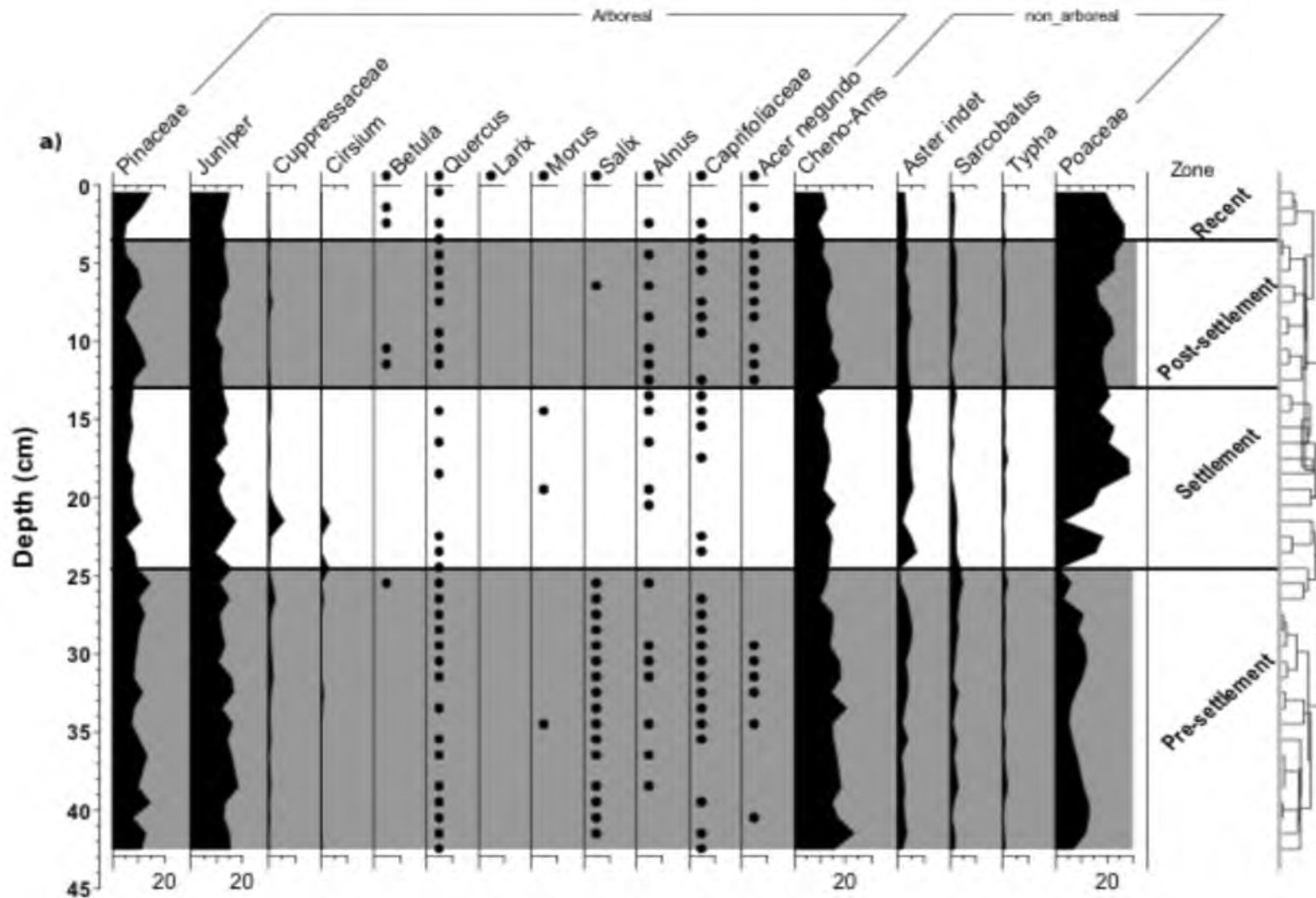


Figure 27. The relative abundance pollen record of Utah Lake. The label Cheno/Ams denotes members of *Chenopodium* and *Amaranthus* pollen. Poaceae, Cheno/Am, Juniper, and Cyperaceae are the most abundant pollen types in this lake.

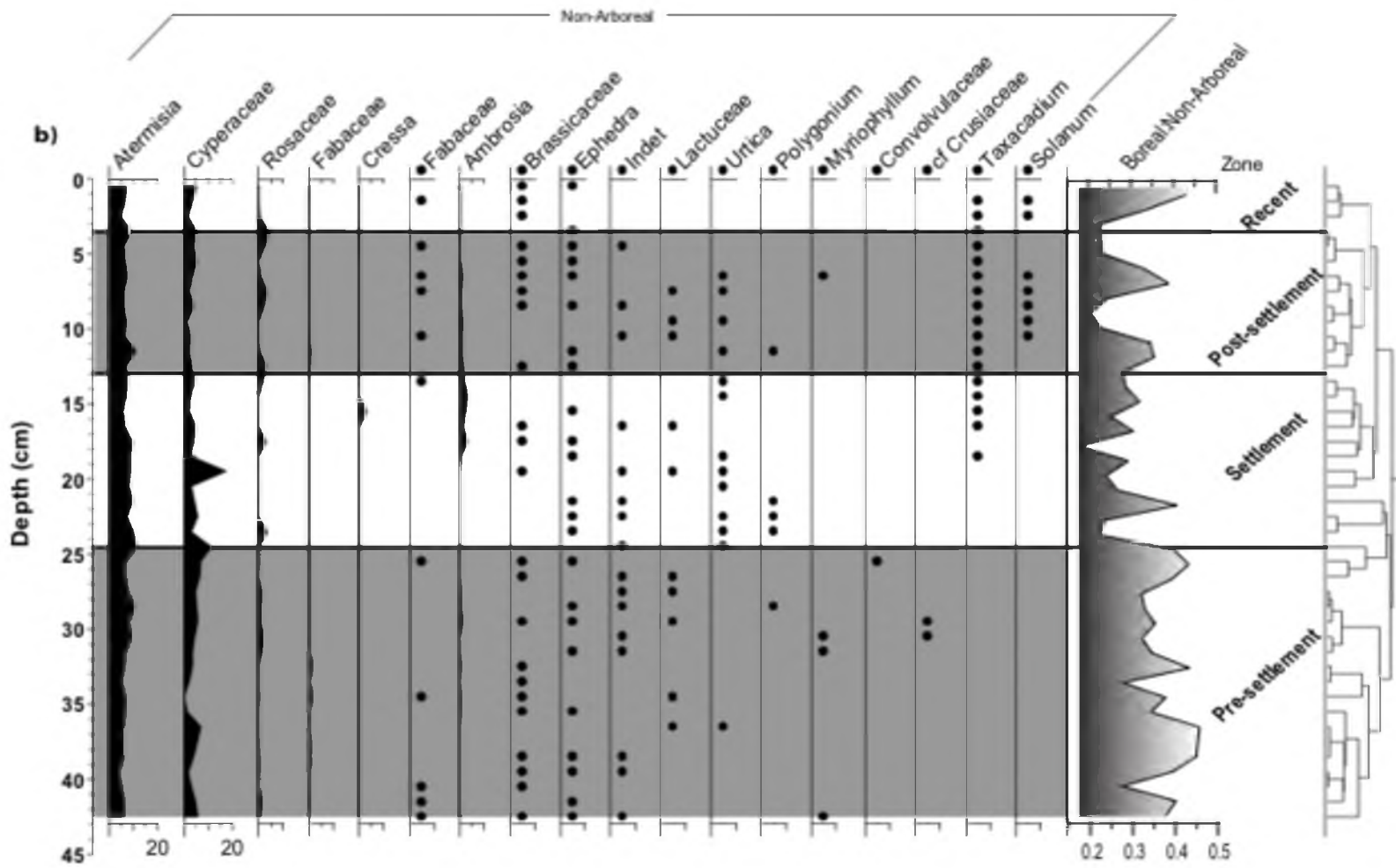


Figure 27. Continued

4.4.4 Stable isotope records

Bivariate scatterplots of $\delta^{15}\text{N}_{\text{BOM}}$ and nitrogen content (%N) show a strong positive correlation in Utah Lake ($R^2 \approx 0.8$) (Figure 28). The waters of Utah Lake are more enriched in deuterium (D) and ^{18}O than the source water (Figure 29). The $\delta^{13}\text{C}_{\text{CaCO}_3}$ values of Utah Lake range from -1 to -1.3‰. The $\delta^{18}\text{O}_{\text{CaCO}_3}$ values range from -10 to -9.5‰. Evaluation of the lake evaporation lines (LEL) against the global meteoric water line (GMWL) reveals that $\delta^{18}\text{O}_{\text{H}_2\text{O}}$ and $\delta\text{D}_{\text{H}_2\text{O}}$ values of source precipitation in Utah are -16.5‰ and -121‰, similar to those of Provo River. However, Jordan River, which originates from Utah Lake, has more depleted $\delta^{18}\text{O}_{\text{H}_2\text{O}}$ and $\delta\text{D}_{\text{H}_2\text{O}}$ values than Utah Lake.

4.5 Discussion

Pollen, charcoal, isotopic, and loss on ignition records reveal that historically, human disturbance has played a dominant role in geochemical transforming of Utah Lake, mainly through cultural eutrophication. The disturbance triggers an influx of nutrients, causing algal blooms that mask climatic signals in the sediments through changes in primary productivity. We discuss how cultural eutrophication manifests itself in sediments in reference to the sedimentation based on ^{210}Pb age model, changes in stable isotope compositions, pollen and charcoal influx, and loss on ignition data.

4.5.1 ^{210}Pb radiometric profile

Previous attempts to estimate the sedimentation rate in Utah Lake show varying results (e.g., 13.8 mm/year; Bushman, 1980, 1 mm/yr; Brimhall & Merritt, 1981; Wiggins & Assay, 2010). The ^{210}Pb activity still presents challenges while estimating the

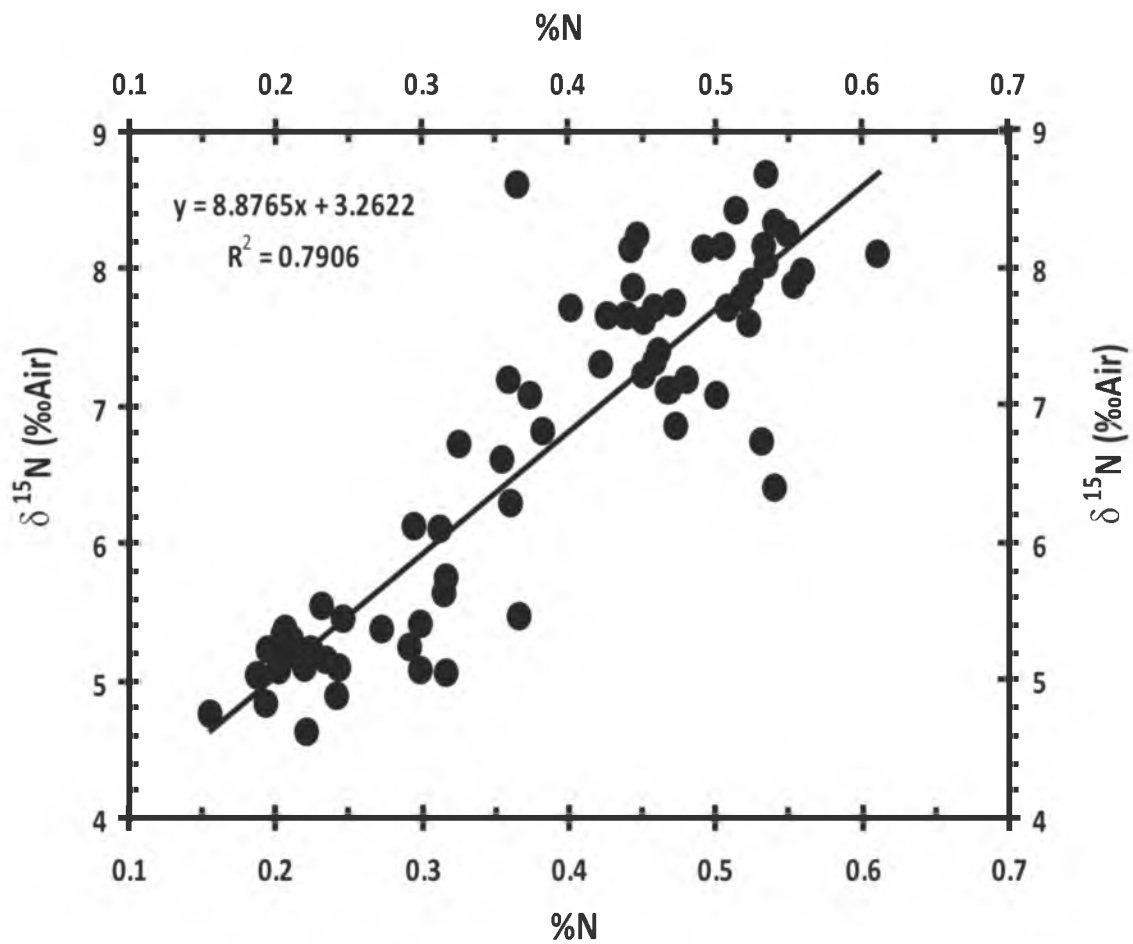


Figure 28. Utah Lake organic nitrogen exhibits a significant correlation between $\delta^{15}\text{N}_{\text{BOM}}$ and nitrogen content (%N). This trend indicates an influx of ¹⁵N-enriched nutrients into Utah Lake from allochthonous sources.

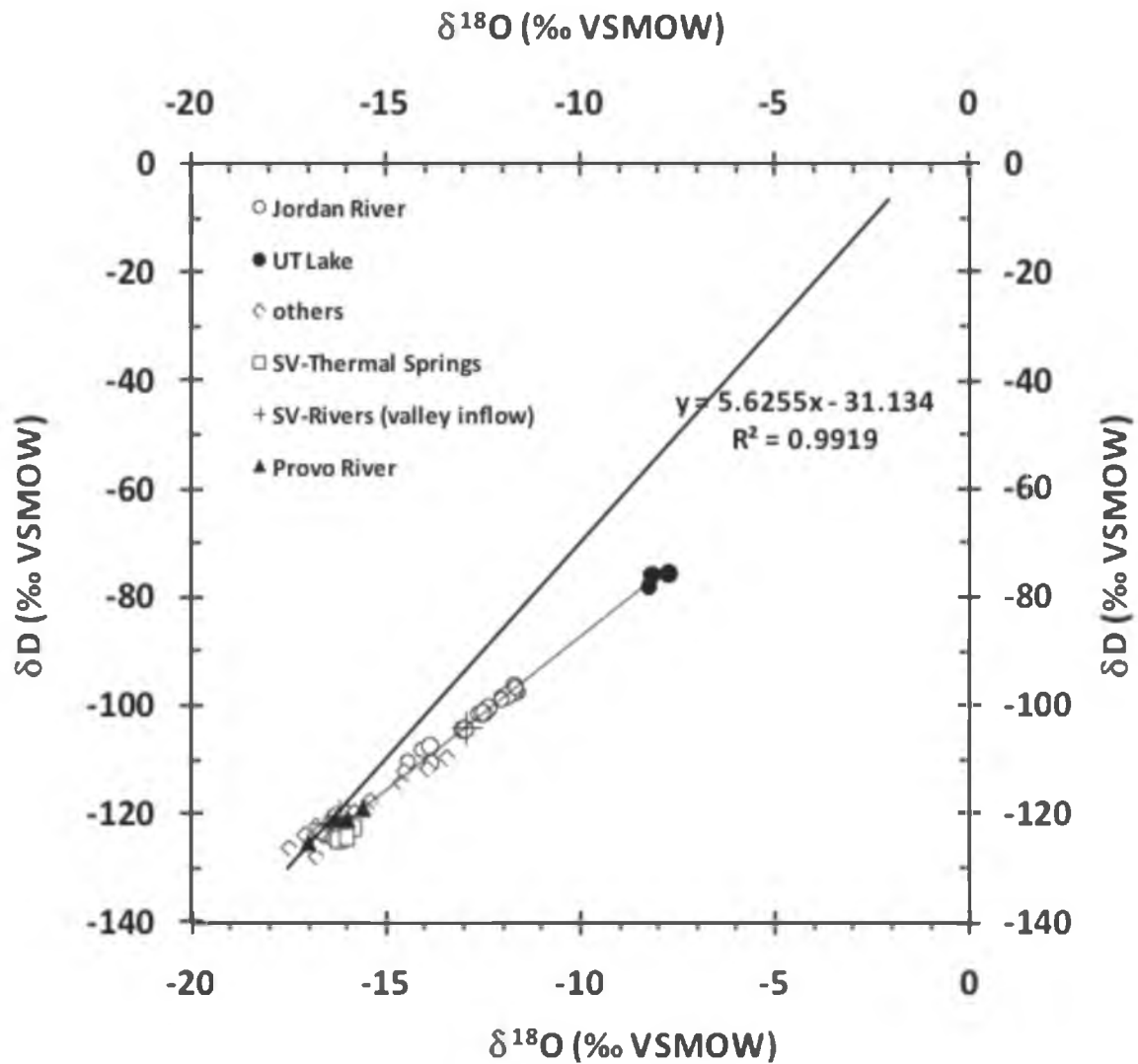


Figure 29. Scatter plot of $\delta^{18}\text{O}_{\text{H}_2\text{O}}$ versus δD values of Utah Lake. The intersection between the global meteoric water line (GMWL) and the local evaporation line (LEL) of water $\delta^{18}\text{O}_{\text{H}_2\text{O}}$ and δD indicates that the source of lake water is ~ -16.5 and -125 ‰ for $\delta^{18}\text{O}_{\text{H}_2\text{O}}$ and δD values, respectively. Water isotope data of Provo and Jordan rivers was obtained from published work of Carreon et al. (2003) and Kendall and Clopen (2001), respectively.

sedimentation rates in Utah Lake, judging by the unpredictable trend in ^{210}Pb activity (Figure 25). The ^{210}Pb activity is generally low and is typical of desert lakes that have very low atmospheric ^{210}Pb fallout (Appleby, 2008).

Considering the many factors, including the atmospheric flux, the rate of transport from the catchment, the water residence time, the fraction of the radionuclide attached to settling particles, the mean particle settling velocity, and postdepositional transport processes (Appleby, 2008), we discuss the unsupported ^{210}Pb activity ($^{210}\text{Pb}_{\text{ex}}$) profile in corroboration with other geochemical and palynomorphologic data.

It is expected that the unsupported $^{210}\text{Pb}_{\text{ex}}$ that has a half-life of 22.3 years would provide an age chronology based on the assumption that depth is connected to time, t by $x = vt$, where 'v' is the sediment accumulation rate (Equation 15–16; Carrol & Leche, 2003):

$$P(t) = P_0 \exp(-kx) \quad \text{Equation 17}$$

where kx is the least-square fitting of the data and k can be used to estimate the sediment accumulation rate v as:

$$v = \ln(2) (kT^{1/2}) \quad \text{Equation 18}$$

The constant rate of supply model (CRS), which assumes a constant rate of supply of fallout $^{210}\text{Pb}_{\text{ex}}$ (von Gunten et al., 2009) may not be an appropriate assumption for

determining the age chronology of Utah Lake sediment core in the postsettlement period. The concordant increase in $^{210}\text{Pb}_{\text{ex}}$, magnetic susceptibility, $\delta^{15}\text{N}_{\text{BOM}}$ values, and charcoal counts suggest that processes influencing the changes in magnetic susceptibility also alter $^{210}\text{Pb}_{\text{ex}}$ activity and imply that $^{210}\text{Pb}_{\text{ex}}$ is variable. The fallout of $^{210}\text{Pb}_{\text{ex}}$ occurs through dry and wet deposition onto soils, outcrop rocks, surface waters, and glaciers (Bierman et al., 1998). The changes in $^{210}\text{Pb}_{\text{ex}}$ influx may possibly arise from extent, stability, and erosion regime of the catchment soil cover (Bierman et al., 1998). If transport from the catchment is a significant source of $^{210}\text{Pb}_{\text{ex}}$ variability in sediments, then the $^{210}\text{Pb}_{\text{ex}}$ may reflect changes in lake hydrology in response to extreme weather events such as prolonged droughts and anomalous precipitation events, influencing the supply of $^{210}\text{Pb}_{\text{ex}}$ to Utah Lake. The large watershed area of the lake ($\sim 4,800 \text{ km}^2$) relative to the lake area ($\sim 500 \text{ km}^2$), and a shallow lake water depth ($< 4 \text{ m}$ at the deepest point) provides a large area where $^{210}\text{Pb}_{\text{ex}}$ may be sourced and washed into the lake during extreme weather and hence increase the $^{210}\text{Pb}_{\text{ex}}$ activity in Utah Lake sediments. Other processes within the lake that include resuspension of sediments through bioturbation, physical mixing, and scouring and sediment focusing by wave action may also result in changes in $^{210}\text{Pb}_{\text{ex}}$ activity in Utah Lake sediments.

Pending radiocarbon dates, we assign the arrival date for European settlement in Utah Valley (1847 A.D.) to correspond to 24.5 cm depth in sediments where the $^{210}\text{Pb}_{\text{ex}}$ activity levels off and magnetic susceptibility increases, as well as $\delta^{15}\text{N}_{\text{SOM}}$ values and charcoal influx. The decrease in organic matter from this time indicates an increase in sediment influx. The sediment influx associated with European settlement has implications on the bulk organic matter composition as elucidated by organic carbon

content (%C), $\delta^{13}\text{C}_{\text{SOM}}$ values, and C:N ratios in the lake sediments.

4.5.2 $\delta^{15}\text{N}_{\text{SOM}}$ evidence of agricultural and urban development

Previous studies in 16 watersheds of the eastern USA indicate that $\delta^{15}\text{N}$ values of nitrates for watersheds with limited land uses range from 3.5 to 5.5‰, whereas watersheds with greater than 15% agricultural or urban land use range from 6 to 9‰ (Mayer et al., 2002). The top (~25 cm) sediment $\delta^{15}\text{N}_{\text{BOM}}$ values are comparable to those reported by Mayer et al. (2002) for watersheds with greater than 15% agricultural or urban land use (i.e., 6 to 9‰). Estimates based on GAP analysis maps indicate that about 13% of the Utah Lake watershed is under agriculture and about 5.2% developed (roads and houses). Farming and grazing constitute the significant land use in the lake watershed (Squires & Rushforth, 1972).

The strong correlation between %N and $\delta^{15}\text{N}_{\text{BOM}}$ and ~ 3.0‰ enrichment in $\delta^{15}\text{N}_{\text{BOM}}$ values between the bottom (5.0‰) and the top (8.0‰) of the Utah Lake sediment core indicates that influx of ^{15}N -enriched nutrients increases the primary productivity within Utah Lake (Figure 25). The $\delta^{15}\text{N}_{\text{SOM}}$ values increase is likely due to the increasing input of isotopically heavy sewage carried into the lake. Based on Bushman (1980), effluents from sewage plants may be among the major sources of nutrients that could have caused ^{15}N -enrichment in Utah Lake. Associated with sewage influx into Utah Lake, phosphorus loading into Utah Lake is estimated to be ~ 297.6 tons per year, of which approximately 83.5 tons per year are exported to the Jordan River, the only surface water outlet of the lake (PSOMAS and SWCA, 2007).

4.5.3 Feedback mechanisms maintaining Utah Lake in eutrophic and turbid state

The transformation of Utah Lake from a clear to turbid state has been attributed to the resuspension of calcite in the water column by exotic benthivorous fish, including the German carp, combined with abrupt changes in dam-controlled lakes (e.g., Deer Creek Reservoir), and climate variability, including “the dust bowl” drought of the 1930s (Bushman, 1980).

Several factors in concert contribute to the maintenance of Utah Lake in a eutrophic state. Land use has allowed unimpeded influx of nutrients to the lake, increasing the nitrogen and phosphorus loadings over the historical period. These include effluents from farmlands and urban areas, sediment resuspension by the benthivorous fishes, including the German carp (*Cyprinus carpio*), and turbulent mixing from wind activity. Nutrient loading from resuspended sediments as well as from irrigation canals and storm drains constitute major feedback mechanisms that maintain the lake in a eutrophic state. Removal of nutrients, primarily nitrogen and phosphorus, from shallow lakes require unconventional remediation methods (Elliot & Brush, 2006).

4.5.4 $\delta^{13}\text{C}_{\text{SOM}}$ and C:N ratios as evidence of eutrophication

Algal bloom promoted by historical eutrophication is largely responsible for high calcite precipitation in the lake. The C and N isotopic changes are undoubtedly related with the development of the agroindustry and urban sprawl in the surrounding area of Utah Lake. The decrease in the C:N ratio from 10 ± 0.5 to $\sim 8.0 \pm 0.5$ between ~ 24.4 cm and the top of the sediments follows the period of land clearing and brush burning (Figure 25). Above ~ 14 cm depth, the bulk organic matter is maintained at constant C:N

ratio (~ 8) and the negative $\delta^{13}\text{C}_{\text{BOM}}$ values ($\sim -27\text{‰}$), indicating algal dominated organic matter (Figure 26). The period of gradual decreasing $\delta^{13}\text{C}_{\text{BOM}}$ values in the core between 27 cm and 17 cm depth most likely corresponds with the development of more eutrophic conditions promoted by effluents from agricultural fields and urban areas around Utah Lake. The causes of $\delta^{13}\text{C}_{\text{SOM}}$ variations are not yet clear, although previous studies indicate that dissolved phosphate concentrations enhanced ^{13}C fractionation between dissolved CO_2 and for algal biomass (Bidigare et al., 1997). The $\delta^{13}\text{C}_{\text{SOM}}$ values and C:N ratios indicate algal dominated sedimentary organic matter (Meyers & Lallier-Vergès, 1999) and corroborates previous findings that show rapid changes in diatom communities consistent with a rapid eutrophication in Utah Lake (Bolland, 1974; Grimes & Rushfold, 1982; Squires & Rushforth, 1986).

4.5.5 Pollen evidence of land use change in Utah Lake

The pollen relative abundances provide additional evidence of processes resulting in changes in the Utah Lake watershed. The changes in relative abundance of grass (Poaceae) pollen (Figure 27) are concordant with changes in $^{210}\text{Pb}_{\text{ex}}$, magnetic susceptibility, and $\delta^{15}\text{N}_{\text{SOM}}$ values (Figure 25). The increase in $^{210}\text{Pb}_{\text{ex}}$ activity at 3.5 cm and 24.5 cm, in concert with an increase in relative abundance of grass pollen and charcoal concentration, suggest an increase in erosive events around the lake that accompany brush burning in the Utah Lake watershed. At the time of European settlement in Utah Valley, irrigation channels were developed, water diverted from major rivers (e.g., American Fork), and farmlands and ranches established (Squires &

Rushforth, 1972). These developments constitute the major drivers of sedimentation, nutrient dynamics, and vegetation changes in Utah Valley.

Warm/dry taxa (*Artemisia*, Chenopodiaceae-Amaranthaceae, *Sarcobatus*, *Juniperus*) dominate the pollen record in Utah Lake (Figure 27). Pine pollen is also a significant part of the arboreal pollen (Figure 27) but represents regional pollen rain. Sagebrush (*Artemisia*) and juniper (*Juniperus*) constitute cold desert steppe species while Chenopodiaceae-Amaranthaceae, as well as Ambrosia-type Asteraceae and greasewood (*Sarcobatus*), constitute species inhabiting saline mud flats around Utah Lake and lake margins. Marsh species are dominated by reeds (*Phragmites*) while others such as willow (*Salix*), Mormon tea (*Ephedra*), and cattail (*Typha*) are rare. Cyperaceae, Pinaceae, Chenopodiaceae/Amaranthaceae, and *Juniperus* pollen dominate the presettlement (before 1847 A. D.) period but significant changes occurred in the postsettlement period (Figure 27).

The significant increase in abundance of grass (Poaceae) pollen above 24.5cm sediment depth (Figure 27) suggests that grassland expanded following European settlement in Utah Valley. Invasive grasses, including cheat grass (*Bromus tectorum* L.), constitute a major grassland around the lake (Lowry et al., 2007), and may have contributed to the observed increase in grass pollen in Utah Lake. A concomitant increase in grass pollen (Poaceae) and decrease in Cyperaceae and Chenopodiaceae/Amaranthaceae signifies clearing of the plant communities and intensification of agriculture from the time of settlement (after 1847 A. D.).

4.5.6 Carbonate accumulation as evidence of enhanced algal photosynthesis

The carbonates have relatively uniform isotopic composition across depth with mean $\delta^{18}\text{O}_{\text{CaCO}_3}$ and $\delta^{13}\text{C}_{\text{CaCO}_3}$ values of $-9.7 \pm 0.2\text{‰}$ and $-1.2 \pm 0.1\text{‰}$ (VPDB), respectively. Given that (1) the sedimentation rate in Utah Lake is very low (0.95–1.05 mm / year; Wiggins & Assay, 2010), (2), the lake is very shallow and holomictic (Max. depth ~4 m), and (3), the lake is algal rich (C:N ratios <10) and eutrophic, the shifts in $\delta^{18}\text{O}$ and $\delta^{13}\text{C}$ composition likely emanate from carbon concentration mechanisms (CCM) by algae during photosynthetic activity.

The increased carbonate content following European settlement in the Utah Valley indicates enhanced carbonates precipitating from an increase in algal biomass and photosynthesis from eutrophication. In addition, very high carbonate precipitation may also be attributed to differences in evaporation/freshwater input ratios and temperature (e.g., Winder et al., 2009).

4.5.7 $\delta^{18}\text{O}_{\text{CaCO}_3}$, δD and $\delta^{18}\text{O}_{\text{H}_2\text{O}}$ evidence of authigenic carbonate in Utah Lake

The δD and $\delta^{18}\text{O}_{\text{H}_2\text{O}}$ values of Utah Lake water ($8.0 \pm 0.3\text{‰}$ and $-76.5 \pm 0.3\text{‰}$ on VSMOW, respectively) indicate that the lake water is 8.5‰ and 48.5‰ more enriched than the source water (~ -16.5 and -125‰ for $\delta^{18}\text{O}_{\text{H}_2\text{O}}$ and δD on VSMOW scale, respectively) (Figure 30). These data also indicate that water in Utah Lake has a high residence time, allowing significant ^{18}O and D enrichment to occur via evaporation. Further, the calculated water temperature during carbonate precipitation ranges from 21 to 24 °C (Appendix D), and falls within the documented temperature range of carbonate

precipitation in Utah Lake (17– 25 °C; Psomas, 2007; Callister, 2008) and indicates that the carbonates are in equilibrium with lake water.

Reconstructing climate records within the postsettlement period is challenging since the influx of the materials (nutrients and particulate matter) may mask climate signals. High-resolution analysis of historical sedimentary records from Utah Lake is important for quantitatively assessing natural climate variability versus anthropogenic activities, and for evaluating the impacts of extreme events such as megadroughts on the water balance (e.g., Fawcett et al., 2011). Since recent geochemical changes in Utah Lake are likely driven by anthropogenic activities, pollutants emitted from industrial, agricultural, and urban settlements may be used to develop age models especially where radiometric methods (e.g., ^{210}Pb activity profile) are problematic (von Gunten et al., 2009). Industrial pollutants in sediments such as spheroidal carbonaceous particles (reflecting fossil fuel emissions), Cu from a local Cu mine (von Gunten et al., 2009), Pb from gasoline (e.g., lead alkyls) (Rizzo et al., 2009), and coliforms and faecal sterols associated with sewage (Vane et al., 2010) may also be used to evaluate the post-settlement impact on Utah Lake.

This study shows that anthropogenic modifications of the area surrounding Utah Lake for agriculture and urban settlement significantly impact the lake geochemistry, and complicate the interpretation of sediment records to help understand the impact of regional ecosystem drivers (e.g., precipitation events and drought episodes). The reconstruction of climate around Utah Lake during pre-European settlement period may be less problematic due to the low impact of anthropogenic disturbance in the watershed. In this regard, the influence of climate variability on Utah Lake water balance would

contribute to understanding presettlement changes in response to climate forcing.

According to previous studies, at least 38 spring areas within the lake contribute about 16% of its inflow (Brimhall et al., 1976; Bushman, 1980). Employing paleotemperature models to lake carbonates would help reconstruct the past temperature regimes in Utah lake (e.g., Nelson et al., 2005) and integration of a paleoaridity index based on plant biomarkers (e.g., Polissar & Freeman, 2010) would help disentangle the influence of aridity on vegetation cover around the watershed.

4.6 Conclusion

Disturbance at the time of establishment of agriculture and urban settlement around Utah Lake has altered nutrient and particulate matter fluxes into lakes traceable via ^{15}N enrichment, pollen, charcoal, and loss on ignition at 550 °C and 950 °C. The shifts in organic matter fluxes and productivity resulting from cultural eutrophication are manifested in C:N ratios, and recorded in charcoal and pollen.

4.7 Acknowledgements

This project was made possible through collaborative funding by Dr. Steve Nelson (Brigham Young University), Dr. Thure Cerling (University of Utah), and Dr. Mitch Power (University of Utah). We thank our colleagues (students and faculty of the Brigham Young University and University of Utah), as well as members of The Utah Lake Commission, June Sucker Restoration Program, USGS, and faculty members of Utah Valley University, Utah State University, and Webber State University for their

advice and support on this project. This study was partly funded by the grants from the Don Currey Foundation.

4.8 References

Anderson, T. F., & Arthur, M. A. (1983). Stable isotopes of oxygen and carbon and their application to sedimentological and palaeoenvironmental problems. In: Arthur, M. A. Anderson, T. F. Kaplan, I. R. Veizer, J., & Land, L. S., (Eds.), *Stable Isotopes in Sedimentary Geochemistry* (Vol. 10. pp. 1–151: *Society of Economic Palaeontologists and Mineralogists Short course*.

Appleby, P. G. & Oldfield, F. (1983). The assessment of ^{210}Pb data from site with varying sedimentation rates. *Hydrobiologia*, 103, 29–35.

Appleby, P.G. (2008). Three decades of dating recent sediments by fallout radionuclides: a review. *The Holocene*, 18(1), 83–93.

Bidigare, R. R., Fluegge, A., Freeman, K. H., Hanson, K. L., Hayes, J. M., Hollander, D., Jasper, J. P., King, L. L., Laws, E. A., Milder, J., Millero, F. J., Pancost, R., Popp, B. N., Steinberg, P. A., & Wakeham, S. G. (1997). Consistent fractionation of ^{13}C in nature and in the laboratory: Growth-rate effects in some haptophyte algae. *Global Biogeochemical Cycles*, 11(2), 279–292.

Bierman, P. R., Albrecht, A., Bothner M. H., Brown, E. T., Bullen, T. D., Gray, L. B., & Turpin, L. (1998). Erosion, weathering, and sedimentation (Edited by Kendall, C. & McDonnell, J. J.). *Isotope tracers in catchment hydrology*: Elsevier Science B. V.

Bolland, R. F. (1974). Paleocological interpretation of the diatom succession in recent sediments of Utah Lake, Utah. Ph.D. Thesis, University of Utah, Salt Lake City. 100 pp.

Brimhall, W. H. (1972). Recent history of Utah Lake as reflected in its sediments: a first report. *Brigham Young University Geological Studies*, 19, 121–126.

Brimhall, W. H., Basset, I. G., & Merritt, L. B. (1976). Reconstruction of deep water springs and strata of Utah Lake. Mountainlands Ass. Gov't Tech. Rep. Eyring Research Inst. Provo, Utah. 21 pp.

Bushman, J. R. (1980). The Rate of Sedimentation in Utah Lake and the use of Pollen as an indicator of Time in the Sediments. *Geology Studies, Brigham Young University*, 27(3), 35–43.

- Callister, E. V. (2008). A three dimensional, time dependent circulation model of Utah Lake. All Graduate Theses and Dissertation. Paper, 86.
<http://digitalcommons.usu.edu/etd/86>.
- Carreón-Diazconti, C., Nelson, S. T., Mayo, A. L., Tingey, D. G., & Smith, M. (2003). A mixed groundwater system at Midway, UT: discriminating super-imposed local and regional discharge. *Journal of Hydrology*, 273, 119–138.
- Carrol, J., & Lerche I. (2003). Sedimentary processes: Quantification of sedimentation rates using radionuclides. 272, pp. Eslevier, Amsterdam.
- Coplen, T. B. & Kendall, C. (2000). Stable hydrogen and oxygen isotope ratios for selected sites of the U.S. Geological Survey's NASQAN and benchmark surface-water networks. U.S. Geological Survey, Open-File Report 00–160: 409 pp.
- Craig, H. (1961). Isotopic variations in meteoric waters. *Science*, 133, 1702–1703.
- Craig, H. (1965). The measurement of oxygen isotope palaeotemperatures. In: Tongiorgi E. (ed.), *Stable Isotopes in Oceanographic Studies and Palaeotemperatures* (pp. 161–182). Pisa, Consiglio Nazionale delle Ricerche Laboratorio di Geologia Nucleare.
- Elliot, E. M., & Brush, G. S. (2006). Sedimented organic nitrogen isotopes in freshwater wetlands record long-term changes in watershed nitrogen source and land use. *Environmental Science & Technology*, 40, 2910–2916.
- Epstein, S., Buchsbaum, R., Lowenstam, H. A. & Urey, H. C. (1953). Revised carbonate water isotopic temperature scale. *Geological Society of America Bulletin*, 64, 1315–1326.
- Fawcett, P. J., Werne, J. P., Anderson, R. S., Heikoop, J. M., Brown, E. T., Berke, M. A., Smith, S. J., Goff, F., Donohoo-Hurley, L., Cisneros-Dozal, L. M., Schouten, S., Damste, J. S. S., Huang, Y. S., Toney, J., Fessenden, J., WoldeGabriel, G., Atudorei, V., Geissman, J. W., & Allen, C. D. (2011). Extended megadroughts in the southwestern United States during Pleistocene interglacials. *Nature*, 470, 518–521.
- Friedman, I., & O'Neil, J. R. (1977). Compilation of stable isotope fractionation factors of geochemical interest. U.S. Geological Survey Professional Paper 440-KK: 49 pp.
- Grimes, J. A., & Rushforth, S. R. (1982). Diatoms of recent bottom sediments of Utah Lake, U.S.A. *Bibliotheca Phycologia*, 55, 1–79.
- Kapenman, K. M., Webb, M. A. H., Cureton, E. S., Ilgen, J. 2010. Determination of upper temperature tolerance in June sucker larvae: is the transition to Utah Lake temperatures a recruitment bottleneck? *Transactions of the American Fisheries Society*, 139, 1386–1398, doi: 10.1577/T09-169.1.

- Leavitt, P. R., Fritz, S. C., Anderson, N. J., Baker, P. A., Blenckner, T., Bunting, L., Catalan, J., Conley, D. J., Hobbs, W. O., Jeppesen, E., Korhola, A., McGowan, S., Rühland, K., Rusak, J. A., Simpson, G. L., Solovieva, N., & Werne, J. (2009). Paleolimnological evidence of the effects on lakes of energy and mass transfer from climate and humans. *Limnology and Oceanography*, *54*(6, part 2), 2330–2348.
- Lowry, J., Ramsey, R. D., Thomas, K., Schrupp, D., Sajwaj, T., Kirby, J., Waller, E., Schrader, S., Falzarano, S., Langs, L., Manis, G., Wallace, C., Schulz, K., Comer, P., Pohn, K., Rieth, W., Velasquez, C., Wolk, B., Kepner, W., Boykin, K., O'Brien, L., Bradford, D., Thompson, B., & Prior-Magee, J. (2007). Mapping moderate-scale land-cover over very large geographic areas within a collaborative framework: A case study of the Southwest Regional Gap Analysis Project (SWReGAP). *Remote Sensing of Environment*, *108*, 59–73.
- Mayer, B., Boyer, E. W., Goodale, C., Jaworski, N. A., Van Breemen, N., Howarth, R. W., Seitzinger, S., Billen, G., Lajtha, L. J., Nosal, M., & Paustian, K. (2002). Sources of nitrate in rivers draining sixteen watersheds in the Northeastern U.S.: Isotopic constraints. *Biogeochemistry*, *57*, 171–197.
- Nelson, S. T., Wood, M. J., Mayo, A. L., Tingey, D. G., & Eggett, D. (2005). Shoreline tufa and tufaglomerate from Pleistocene Lake Bonneville, Utah, USA: stable isotopic and mineralogical records of lake conditions, processes, and climate. *Journal of Quaternary Science*, *20*(1), 3–19, doi: 10.1002/jqs.889.
- Polissar, P. J., & Freeman, K. H. (2010). Effects of aridity and vegetation on plant-wax δD in modern lake sediments. *Geochimica et Cosmochimica Acta*, *74*, 5785–5797.
- PSOMAS and SWCA (2007). Utah Lake TMDL: Pollutant Loading Assessment & Designated Beneficial Use Impairment Assessment. August.
- Rizzo, S., Basile, S., Caruso, A., Cosentino, C., Tranchina, L., & Bram, M. (2009). Dating of a sediment core by $^{210}Pb_{ex}$ method and Pb pollution chronology in Palermo Gulf (Italy). *Water, air, and soil pollution*, *202*, 109–120, doi 10.1007/s11270-008-9961-z.
- Rosén, P., Hall, R., Korsman, T., & Renberg, I. (2000). Diatom transfer-functions for quantifying past air temperature, pH and total organic carbon concentration from lakes in northern Sweden. *Journal of Paleolimnology*, *24*, 109–123.
- Squires, L.E., & Rushforth, S. R. (1986). Winter phytoplankton communities of Utah Lake, Utah, USA. *Hydrobiologia*, *131*, 235–248.
- Vane, C.H., Kim, A.W., McGowan, S., Leng, M.J., Heaton T.H.E., Kendrick, C.P., Coombs, P., Yang, H., & Swann, G.E.A. (2010) Sedimentary records of sewage pollution using faecal markers in contrasting peri-urban shallow lake. *Science of the Total Environment*, *409*, 345–356, doi:10.1016/j.scitotenv.2010.09.033.

von Gunten, L., Grosjean, M., Beer, J., Grob, P., Morales, A., & Urrutia, R. (2009). Age modeling of young non-varved lake sediments- methods and limits. Examples from two lakes in Central Chile. *Journal of Paleolimnology*, *42*, 401–412, doi 10.1007/s10933-008-9284-5.

Wiggins, S., & Asay, M. (2010). Determination of Sedimentation Rates in Utah Lake Using ^{210}Pb Analysis. *Geology*, *446*, Brigham Young University.

Winder, M., Reuter, J. E., & Schladow, S. G. (2009). Lake warming favours small-sized planktonic diatom species. *Proceedings of the Royal Society London, B*, *276*: 427–435.

CHAPTER 5

A SYNTHETIC REVIEW OF TERRESTRIAL AND LACUSTRINE INDICATORS OF CLIMATE AND DISTURBANCE FROM RECORDS IN UTAH LAKE, UT, FOY LAKE, MT, AND SOIL ORGANIC MATTER, EAST AFRICA

5.1 Introduction

Ecosystems are inherently complex, heterogeneous in time and space, and are comprised of many interacting components that involve the exchange of energy and materials (Leavitt et al., 2009). Studies of soils in East Africa and sediments in Utah and Foy Lake show that local and regional factors alter vegetation structure and change material fluxes into soils and lakes. Linking palaeoecological data such as fossil pollen and $\delta^{13}\text{C}$ values of organic matter in sediments and soils to environmental change requires an understanding of inherent variability in ecosystem properties across space and time in relation to ecosystem drivers such as fire, precipitation, and herbivory. For instance, the woody cover distribution patterns at any given scale are dependent on the interacting large-scale variables such as geology, topography, and precipitation, and small-scale variables such as plant to plant interaction, herbivory, and fires (Figure 30).

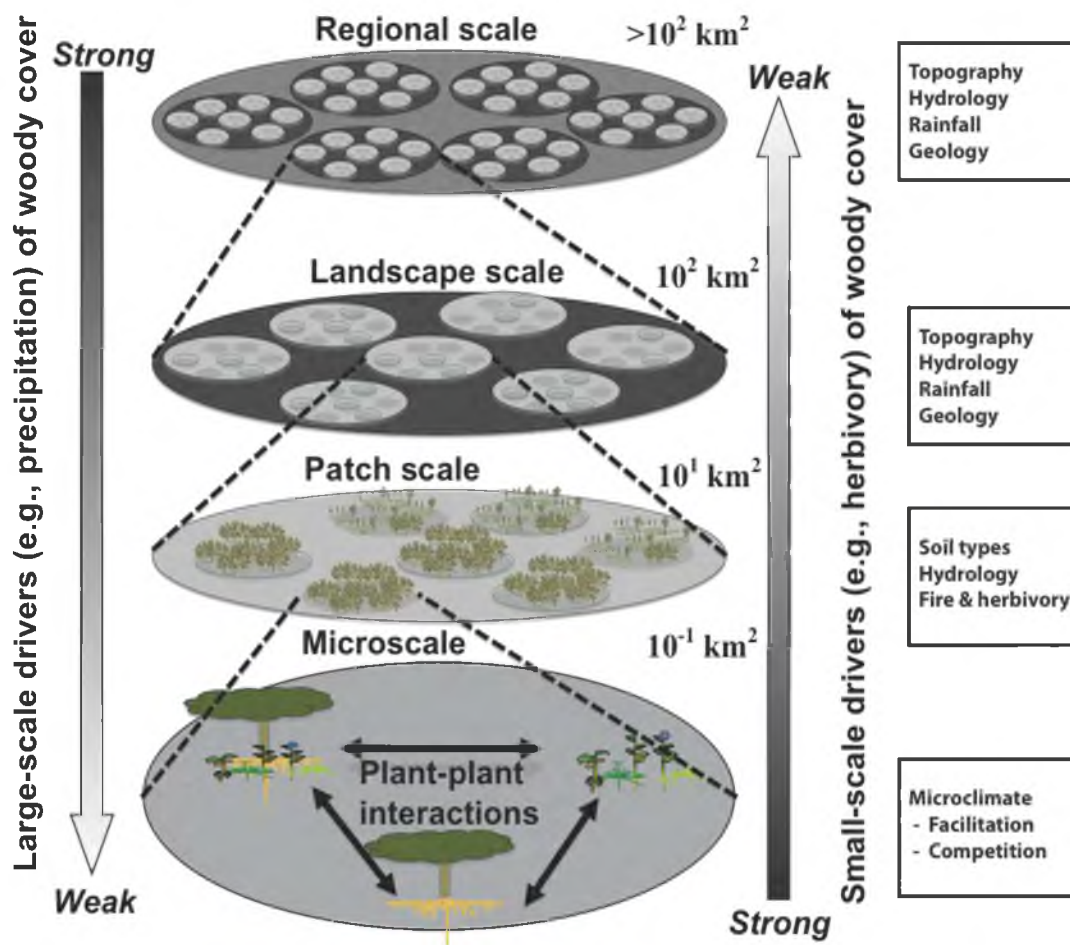


Figure 30. A hierarchical patch dynamics conceptual model accounting for woody cover dynamics at various spatial scales (modified after Gillson, 2004).

5.2 Woody cover patterns in watersheds

Scale-free reconstructions of environments that assume a temporal sequence of events that are spatially neutral are ambiguous (Gilson, 2004). At a given spatial or temporal scale, the impact of ecosystem drivers (e.g., herbivory, fire, precipitation) may vary in their intensity and extent, and can act independently or interactively to transform the woody cover in a patch or landscape. The Hierarchical Patch Dynamics Paradigm (e.g., Gilson, 2004) provides a conceptual framework to reconstruct woody cover from palaeoecological datasets (e.g., stable isotopes) while accounting for spatial and temporal variability (Figure 30).

At the lower spatial scales, plants interact with one another and these interactions may vary from patch to patch. At micro-scale, shading by woody plants creates conducive environments for C₃ herbaceous plants, while competition for resources (e.g., light, water, or nutrients) determines how successful seedling establishment is in the understorey. Consequently, the nature of plant-plant interaction may vary from competition where shading and chemoallelopathy may reduce the chances of certain plants from establishing (e.g., C₄ plants), or facilitation through hydraulic lifting and shading may increase the chances of certain plants (e.g., C₄ plants) to establish.

Patches are spatially and structurally discrete plants communities that differ from other surrounding patches, and are defined by species interactions and local ecosystem factors and processes such as fires, herbivory, soil types, and moisture availability. Therefore, individual patches may be at different succession stages from other surrounding patches. Several contiguous patches form vegetation assemblages that characterize landscape-scale and regional-scale vegetation patterns. At landscape- and

regional-scale, the variations in geology, topography, rainfall, and hydrology confer greater influence of woody cover distribution patterns.

The factors driving woody cover dynamics are numerous and poor understanding of the physiological and ecological mechanisms mediating climate-induced woody cover dynamics limits the ability to model or project woody cover changes through time (e.g., McDowell et al., 2008; McDowell & Sevanto, 2010). For instance, rainfall events are not randomly distributed in time but tend to occur in clusters (Schwinning & Sala, 2004). Moisture availability patterns set up by large-scale drivers of precipitation are offset by topography and orography (William & Ehleringer, 2000; Loik et al., 2004). Subsequently, other processes alter soil moisture patterns after a precipitation event, resulting in vertical and horizontal heterogeneity in soil water availability for uptake by plant roots (Loik et al., 2004). Factors causing such moisture heterogeneity within a site include soil depth, soil texture, petrocalcic layers, parent material, organic matter content, snow-pack depth, snow redistribution, vegetation type, leaf area index, and soil surface characteristics (Loik et al., 2004).

Moisture availability determines tree recruitments and mortality across spatial and temporal scales. For instance, plants that operate at narrow hydraulic safety margins like trembling aspen (*Populus tremuloides*) are predisposed to hydraulic failure and therefore susceptible to drought-induced mortality that may occur at landscape-scale and regional-scale (Anderegg et al., 2012). A hydraulically based carbon-starvation theory developed by McDowell et al. (2008) to account for woody cover dynamics considers carbon balance to be impaired by drought-induced hydraulic failure via stomatal closure,

resulting in carbon starvation and reduced resistance to biotic agents such as insect attacks like spruce beetles.

Ecosystem drivers such as fires and herbivory provide positive feedbacks that prevent the establishment of woody cover as may be potentially supported by the prevailing climate. Further, the interaction between temperature and soil moisture dynamics has been implicated in recent increase in fire activity in Western U. S. (Westerling et al., 2006). Above normal spring temperatures (McDowell et al., 2008) and recent increase in human-induced dust deposition (Neff et al., 2008) result in earlier snowmelt that results in a longer fire season while warmer summers result in lower soil moisture. Therefore, woody cover dynamics is a function of independent and interactive factors that occur at any given scale and need to be accounted for when reconstructing the past environments.

5.3 Woody cover reconstruction in East Africa

In relation to East Africa, the long-term changes in woody cover have been linked to tectonically driven aridification during the development of East African Rift System (EARS) in the Late Neogene (8–2 million years ago) (Sepulchre et al., 2006). On the eastern branch (in southern Ethiopia and the Turkana depression in northern Kenya), the uplift began during the Eocene-Oligocene times proceeding to reach the maximum uplift at the Plio-Pleistocene interval. On the western branch of the EARS, the uplift started in the central Tanganyika Basin at about 12 to 10 Ma, followed by later phases of major uplift between 5 and 2 Ma in the Tanganyika and Malawi rifts during the middle-late Miocene. These uplifts, mostly oriented north-south and bordered by crests that

culminate between 1500 and 5100 m, resulted in the reorganization of the circulation patterns in the region. The direction of low tropospheric winds that convey a lot of moisture responsible for precipitation in the region was altered by the continental topography, resulting in a stronger meridional flow rather than zonal moisture transport. These shifts in the direction resulted in clustered precipitation patterns in the region. The impact of tectonically driven changes in African topography on climate, especially the monsoon rainfall patterns, has therefore been a major determinant of vegetation patterns in East Africa. These patterns persist today as exemplified by the diversity of physiognomies in this region. Therefore, the reconstruction of woody cover in East Africa ought to account for geomorphological, hydrological, climatic, and geological factors at any specific spatial and temporal scale.

In East Africa, there is a lot of spatial variability in woody cover, where patches with interlocking canopies coexist with patches with open canopy woodland, and grasslands. The woody cover abundance among these patches defines the woody cover abundance at a landscape scale and regional scale. In East Africa, the variations in the abundance of C₃ and C₄ plants at various scales may be inferred from the calibration model based on the $\delta^{13}\text{C}$ of surface soil samples with reference to the spatial scale under consideration (Chapter 2). Concerted changes in the vegetation dynamics and nutrient cycling among many patches are likely to manifest at landscape-scale or regional-scale. The conceptual understanding of how ecosystem processes alter the ecosystem structure and function from small to large spatial and temporal scales is necessary for enhancing reconstruction of past environments. Therefore, moisture availability does not in itself

determine the woody cover, as is evident in the poor correlation between woody cover and water deficit in East Africa (Chapter 2).

Fire is an important driver of ecosystem structure and provides a positive feedback mechanism that maintains open canopies (Hirota et al., 2011; Staver et al., 2011; Keeley & Rundel, 2005) and results in discontinuous woody cover at intermediate rainfall (1000 to 2500 millimeters) in the tropics (Hirota et al., 2011; Staver et al., 2011). Reconstructing the changes in vegetation cover within watersheds in East African necessitates a multiproxy approach that includes pollen, charcoal, grass cuticles, grass phytoliths (Mohammed et al., 1996; Mworira-Maitima, 1997), and stable isotope records (Gillson, 2004).

5.4 The influence of woody cover on material fluxes in lakes

Geomorphology, disturbance, hydrology, and climate are the major factors that drive material fluxes and biogeochemical transformation that are reflected in stable isotope composition in lake sediments. Sediments in Foy Lake (Chapter 3) and Utah Lake (Chapter 4) exhibit variations in $\delta^{13}\text{C}$ values of bulk organic matter (hereafter $\delta^{13}\text{C}_{\text{BOM}}$) and C:N ratio with the contribution of terrigenous organic matter relative to autochthonous organic matter. In addition, the ratio of arboreal to nonarboreal pollen helps to account for the changes in woody cover in the watershed and therefore the contribution of terrigenous organic matter to lakes. These results indicate that watersheds with high fractional woody cover (FWC) are likely to experience a greater influx of organic matter derived from woody cover into lakes in the form of dissolved organic carbon (DOC), woody fragments, pollen, and charcoal than watersheds with low FWC.

Nutrient-poor environments produce small amounts of litter and conserve nutrients in long-lived and recalcitrant tissues, thus reinforcing the infertile environment. In general, plant species occupying environments of low nutrient supply exhibit a higher degree of sclerophylly and evergreenness and are characterized by lower plant growth rate and higher resource conservation than plants growing in environments with high nutrient supply (Ordoñez et al., 2009). The soil C:N is a good indicator of the quality of the soil organic matter.

5.5 The influence of topography, hydrology, and bathymetry on material and energy fluxes in lakes

The lake bathymetry, water depth, mode of water flow into the lake (surface or groundwater), and steepness of adjacent slopes all determine the rates of terrigenous material flux into the lake (Figure 31–32). In this study, the groundwater-fed Foy Lake is deep (~40 m deep) and surrounded by steep slopes (~45°) and therefore experiences a rapid influx of terrigenous materials as well as sediment focusing of materials derived from shallow sections of the lake (Chapter 3). In contrast, Utah Lake is shallow (~4 m at the deepest point), mainly surface water-fed, and is surrounded by gentle slopes (<10°) and therefore likely to experience low influx of terrigenous materials (Chapter 4). Moreover, lakes that are sufficiently deep to have well-defined benthic zones (e.g., Foy Lake; ~ 40 m deep) have high tendencies for sediment focusing as benthic environments are stirred up by disturbance (Chapter 3) or wind-driven sediment focusing arising from climate-associated changes in lake water level (Stone & Fritz, 2004) and redeposited in deeper sections of the lake, causing a shift in benthic to planktonic ratios (Chapter 3). These lines of evidence reveal that topography, bathymetry, and hydrology influence the

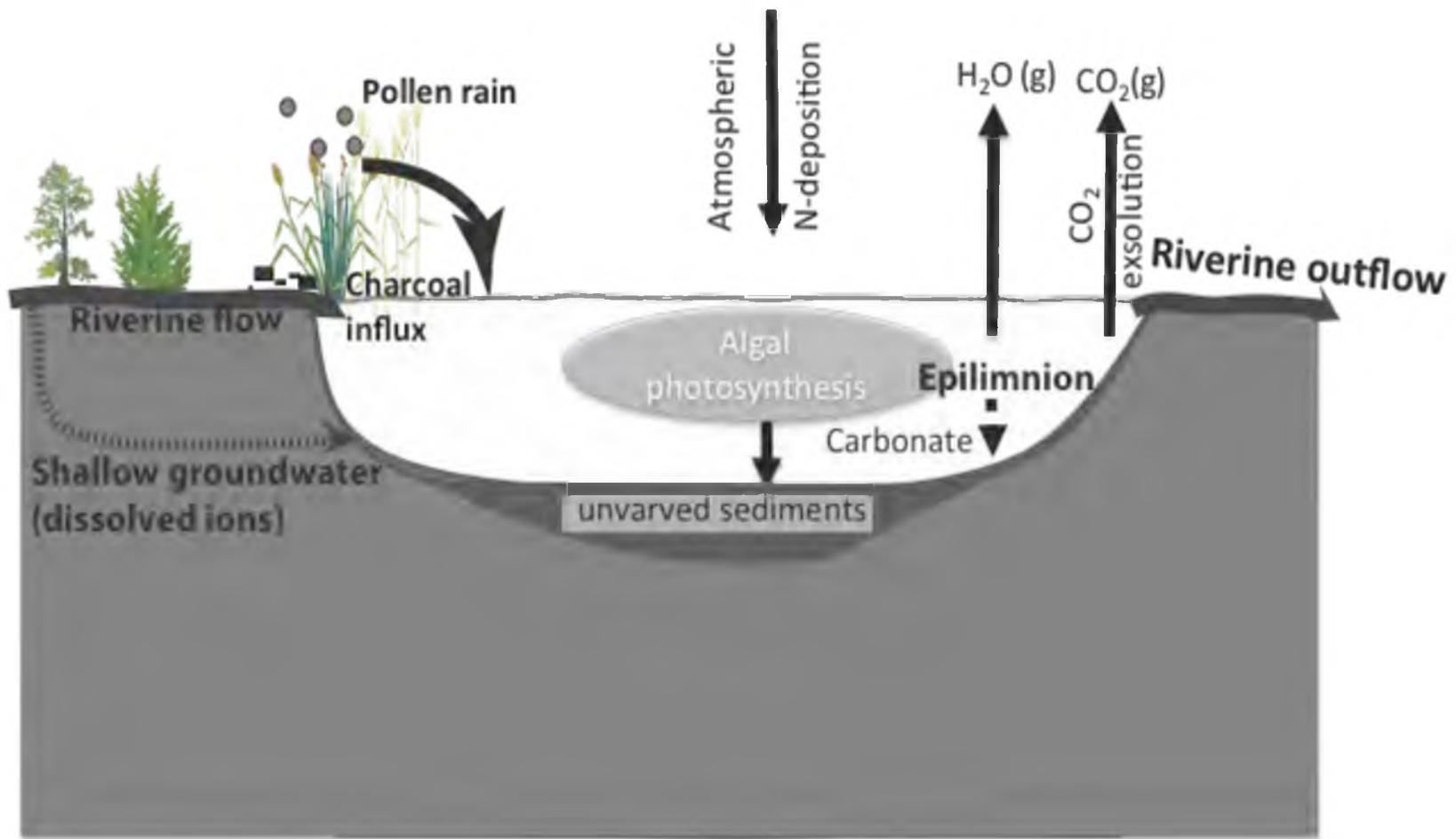


Figure 31. A conceptual model of material fluxes into and out of a lake. The pathways of material fluxes in a shallow lake having surface water inlets and outlets (e.g., Utah Lake) are shown.

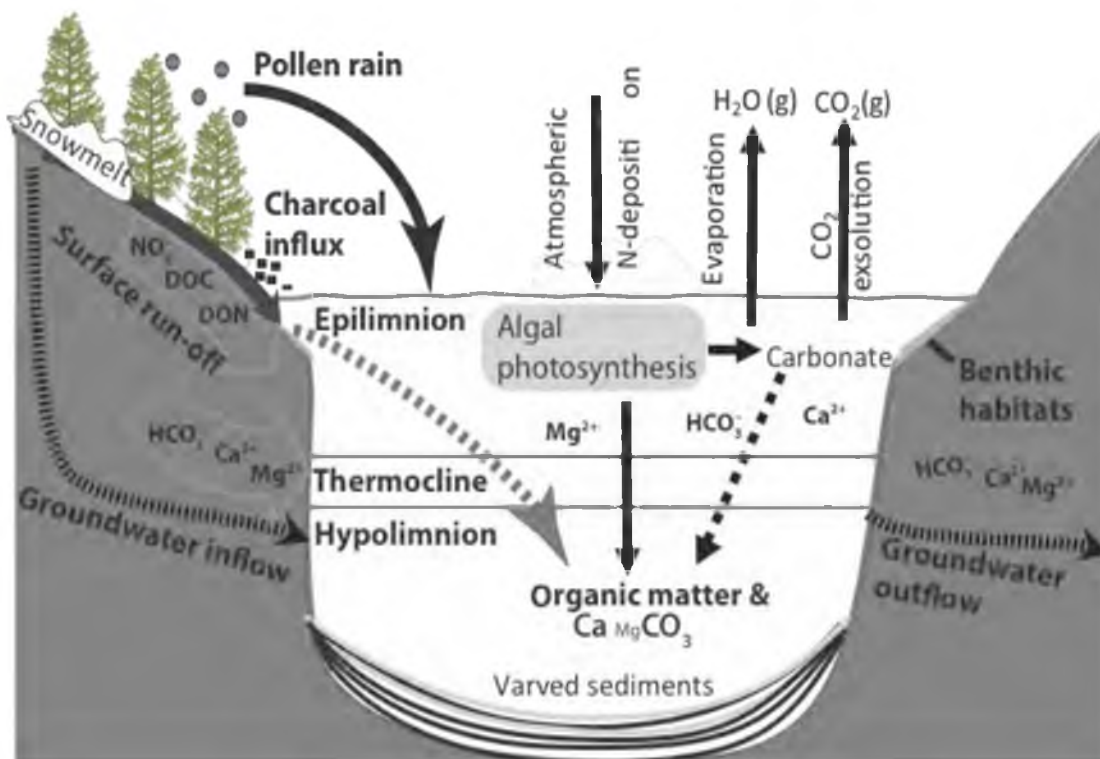


Figure 32. A conceptual model of material fluxes into and out of a lake. The pathways of material fluxes in a deep lake lacking inlets or outlets (e.g., Foy Lake) are shown.

rates of materials fluxes that may interact with ecosystem drivers such as climate variability and anthropogenic disturbance to alter material fluxes into lakes.

5.6 The role of fire on material fluxes in lakes

Plants occupying nutrient-poor environments exhibit lower plant growth rates, making them less productive and promoting conservation of nutrients in long-lived and recalcitrant tissues (Ordoñez et al., 2009). In contrast, plant species adapted to growing in nutrient replete habitats exhibit higher leaf nitrogen concentration per mass (mg g^{-1}), specific leaf area (SLA, $\text{m}^2 \text{kg}^{-1}$), leaf nitrogen concentration per mass (LNC_{mass} mg g^{-1}), leaf phosphorus concentration per mass (LPC_{mass} mg g^{-1}), and leaf N:P (Ordoñez et al., 2009). Leaf traits like SLA, LNC, and LPC are positively related to plant relative growth rates, leaf carbon assimilation rates, and energy supply and their leaf traits allow a fast use of nutrients and growth but for shorter time spans (Ordoñez et al., 2009). Consequently, the soil C:N ratio is a good indicator of the quality of the soil organic matter (Ordoñez et al., 2009). Temperature and precipitation primarily determine the rates of decomposition and mineralization, factors that control the forms and levels of nutrients available in the soil (e.g., Austin & Vitousek, 2000; Amundson et al., 2003).

5.7 $\delta^{15}\text{N}_{\text{BOM}}$ enrichments as indicator of nitrogen sources

The presettlement $\delta^{15}\text{N}_{\text{BOM}}$ values in Foy lake and Utah Lake were both low (generally $\leq 6\text{‰}$), which indicates nutrients derived from mineralization and nitrogen fixation (Mayer et al., 2002). These $\delta^{15}\text{N}_{\text{BOM}}$ values conform to climate-induced nitrogen mineralization whereby mean annual precipitation and mean annual temperature are the

main drivers of nitrogen cycling (e.g., Martinelli et al., 1999; Amundson et al., 2003; Bustamante et al., 2004; Codron et al., 2005; Craine et al., 2009). Understanding how nitrogen availability and gaseous nitrogen emissions within watershed affect soil and sediments $\delta^{15}\text{N}$ values is useful in reconstructing ecosystem changes from climate, land cover, and land use.

As evident from the studies of Utah Lake and Foy Lake sediments, anthropogenic disturbance and fire episodes in the watershed are major drivers of changes in nutrient cycling, sedimentation, and lake sediment biogeochemistry. The $\delta^{15}\text{N}$ values of bulk organic matter in sediments ($\delta^{15}\text{N}_{\text{BOM}}$) are reliable indicators of nutrient influx into lakes. For instance, a ^{15}N enrichment of $\sim 3\%$ in Utah Lake (Chapter 4) following European settlement to $\sim 8\%$ is consistent with an influx of nutrients derived from agriculture and urban sources (Mayer et al., 2002). Similarly, there was a significant ^{15}N enrichment of at least $\sim 2.5\%$ in Foy Lake (Chapter 2) following timber harvesting, which indicates rapid nutrient loadings in the lake from the watershed.

5.8 $\delta^{15}\text{N}_{\text{BOM}}$ enrichments as indicator of fire episodes

The transformation of organic nitrogen into inorganic nitrogen during fire is accompanied by an increase in soil $\delta^{15}\text{N}$ values due to kinetic fractionation associated with nitrogen volatilization (Grogan et al., 2000). In the pre-settlement period, the shifts in $\delta^{15}\text{N}_{\text{BOM}}$ values of Foy Lake were influenced by fire episodes (Chapter 3). The pre-settlement trends in $\delta^{15}\text{N}_{\text{BOM}}$ values of Foy Lake were less abrupt than during the pre- and post-settlement period. This trend is consistent with other observations that show that fire creates an initial pulse of available nitrogen that lasts a few months after burning,

whereupon net nitrogen mineralization determines the subsequent increase in available nitrogen (Monleon et al., 1997). Through combustion of organic materials, fire promotes the pyrolytic release of nitrogen into the soil, mainly as ammonium (NH_4^+) but also nitrate (NO_3^-) and nitrite (NO_2^-) (Grogan et al., 2000; Gumeno-Garcia et al., 2000; Wan et al., 2000). Increased soil repellency from surface accumulation of hydrophobic substances in ashes following a fire event (Gumeno-Garcia et al., 2000) enhances surface run-off. The nutrients, charcoal, and ashes arising from fire events flushed during snowmelt events constitute the major source of nutrient subsidies to lakes and rivers, as observed in the positive shifts in $\delta^{15}\text{N}_{\text{BOM}}$ values in Foy Lake following a fire episode (Chapter 3). Moreover, fire intensity, frequency, and duration determine the extent of nitrogen loss via volatilization (Gumeno-Garcia et al., 2000) and grasslands have significantly lower losses than forests (Wan et al., 2000). Studies indicate that nutrients accumulated in pre-melt waters in winter become flushed into rivers during spring snowmelt (Piatek et al., 2005) and constitute nutrient sources in spring snowmelt-fed lakes like Foy Lake.

5.9 Conclusion

This research established that (1) increases in woody cover is accompanied by more increased ^{13}C depletion of the $\delta^{13}\text{C}$ values of tropical soils from greater contribution of C_3 biomass to soil organic matter, but species interactions, geomorphology, hydrology, and edaphic factors cause spatial heterogeneity in woody cover while ecosystem drivers such as fire and precipitation cause woody cover to vary both spatially and temporally; (2) the $\delta^{13}\text{C}$ values and C:N ratios of organic matter of sediments of temperate lakes reflect the contribution of terrigenous relative to autochthonous organic matter in lake sediments,

where woody cover in the proximity of a lake is a major determinant of the contribution of terrigenous organic matter into lakes; (3) fires and anthropogenic modifications of watersheds through agriculture, urban development, and timber harvesting increase terrigenous material influx into lakes that complicate the reconstruction of climate records archived in lake sediments; and (4) hydrology and geomorphology of watersheds influences the rate of terrigenous material influx into lakes, while lake depth and bathymetry determines the degree of sediment focusing within lakes, and therefore the organic and inorganic matter composition of the lake sediments.

5.10 Acknowledgements

I thank my committee members, Dr. Mitchell Power, Dr. Francis Brown, Dr. Andrea Brunelle, Dr. Thure Cerling, and Dr. Phil Dennison, for their comments and constructive criticisms during the preparation of this manuscript.

5.11 References

- Amundson, R., Austin, A. T., Schuur, E. A. G., Yoo, K., Matzek, V., Kendall, C., Uebersax, A., Brenner, D., & Baisden, W. T. (2003). Global patterns of the isotopic composition of soil and plant nitrogen. *Global Biogeochemical Cycles*, *17*, 1031, doi:10.1029/2002GB001903.
- Anderegg, W. R. L., Berry, J. A., Smith, D. D., Sperry, J. S., Anderegg, L. D. L., & Field, C. B. (2012). The roles of hydraulic and carbon stress in a widespread climate-induced forest die-off. *PNAS*, *109*(1), 233–237, doi/10.1073/pnas.1107891109.
- Anderson, T. F., & Arthur, M. A. (1983). Stable isotopes of oxygen and carbon and their application to sedimentological and palaeoenvironmental problems. In: Arthur, M. A. Anderson, T. F. Kaplan, I. R. Veizer, J., Land, L. S., (Eds.). *Stable Isotopes in Sedimentary Geochemistry* (Vol. 10, pp. 1–151). Society of Economic Palaeontologists and Mineralogists Short course.

- Bond, W. J., Woodward, F. I., & Midgley, G. F. (2005). The global distribution of ecosystems in a world without fire. *New Phytologist*, *165*, 525–538.
- Callister, E. V. (2008). A three dimensional, time dependent circulation model of Utah Lake. All Graduate Theses and Dissertations. Paper, 86.
<http://digitalcommons.usu.edu/etd/86>.
- Campbell, D. H., Kendall, C., Chang, C. C. Y., Silva, S. R., & Tonnessen, K. A. (2002). Pathways for nitrate release from alpine watershed: Determination using $\delta^{15}\text{N}$ and $\delta^{18}\text{O}$. *Water Resources Research*, *38*(5), 1 – 9.
- Coplen, T. B., Kendall, C., & Hopple, J. (1983). Comparison of stable isotope reference samples. *Nature*, *302*, 236–238.
- Drummond, C. N., Patterson, W. P., & Walker, J. G. G. (1995). Climatic forcing of carbon-oxygen isotopic covariance in temperate-region marl lakes. *Geology*, *23*(11), 1031–1034, doi: 10.1130/0091-7613(1995)023<1031:CFOCOI>2.3.CO;2.
- Friedman, I., & O'Neil, J. R. (1977). Compilation of stable isotope fractionation factors of geochemical interest. In: Fleischer M. (ed.), *Data of Geochemistry. Sixth edition* (pp. 1–40). Geological Survey Professional Paper 440-KK, US Government Printing Office, Washington,.
- Harrison, J. E., Cressman, E. R., & Whiple, J. W. (1986). Geologic and structure maps of the Kalispell 1 degree x 2 degree quadrangle, Montana, and Alberta and British Columbia. Map I-226, sheet 1 of 2, scale 1:250,000. In: USGS Miscellaneous Investigations Series.
- Henderson, A. K., & Shuman, B. N. (2009). Hydrogen and oxygen isotopic compositions of lake water in the western United States. *Geological Society of America Bulletin*, *121*, 1179–1189, doi: 10.1130/B26441.1.
- Geider, R. J., & La Roche, J. (2002). Redfield revisited: Variability in the N:P ratio of phytoplankton and its biochemical basis. *European Journal of Phycology*, *37*, 1–17.
- Grossman, E. L. (1982). Stable Isotopes in Live Benthic Foraminifera from the Southern California Borderland. Ph.D. dissertation, University of Southern California, Los Angeles, 164 p
- Gardner, K. K., & McGlynn, B. L. (2009). Seasonality in spatial variability and influence of land use/land cover and watershed characteristics on stream water nitrate concentrations in a developing watershed in the Rocky Mountain West. *Water Resources Research*, *45*, W08411, doi:10.1029/2008WR007029

- Gillson, L. (2004). Evidence of Hierarchical Patch Dynamics in an East African Savanna? *Landscape Ecology*, *19*, 883–894.
- Grogan, P., Bruns, T. D., & Chapin, III F. S. (2000). Fire effects on ecosystem nitrogen cycling in a Californian bishop pine forest. *Oecologia*, *122*, 537–544.
- Gumeno-Garcia, E., Andreu, V., & Rubio J. L. (2000). Changes in nitrogen, phosphorus, and cations in soil as a result of fire and water erosion in a Mediterranean landscape. *European Journal of Soil Science*, *51*, 201–210.
- Hirota, M., Holmgren, M., Van Nes, E. H., & Scheffer, M. (2011). Global resilience of tropical forest and savanna to critical transitions. *Science*, *334*, 232–235, doi: 10.1126/science.1210657
- Keeley, J., & Rundel, P. (2005). Fire and the Miocene expansion of C₄ grasslands. *Ecological letters*, *8*, 683–690, doi: 10.1111/j.1461-0248.2005.00767.x
- Kim, S. T., & O'Neil, J. R. (1997). Equilibrium and nonequilibrium oxygen isotope effects in synthetic carbonates. *Geochimica et Cosmochimica Acta*, *61*, 3461–3475.
- Leng, M. J., & Marshall, J. D. (2004). Palaeoclimate interpretation of stable isotope data from lake sediment archives. *Quaternary Science Reviews*, *23*, 811–831.
- Leng, M. J., Jones, M. D., Frogley, M. R., Eastwood, W. J., Kendrick, C. P., & Roberts, C. N. (2010). Detrital carbonate influences on bulk oxygen and carbon isotope composition of lacustrine sediments from the Mediterranean. *Global and Planetary Change*, *71*, 175–182.
- Leavitt, P. R., Fritz, S. C., N. J., Baker, P. A., Blenckner, T., Bunting, L., Catalan, J., Conley, D. J., Hobbs, W. O., Jeppesen, E., Korhola, A., McGowan, S., Rühland, K., Rusak, J. A., Simpson, G. L., Solovieva, N., & Werne, J. (2009). Paleolimnological evidence of the effects on lakes of energy and mass transfer from climate and humans. *Limnology and Oceanography*, *54*(6, part 2): 2330–2348.
- Liu, W., Li, X., Zhang, L., An, Z., & Xu, L., (2009). Evaluation of oxygen isotopes in carbonate as an indicator of lake evolution in arid areas: The modern Qinghai Lake, Qinghai–Tibet Plateau. *Chemical Geology*, *268*, 126–136.
- Loik, M. E., Breshears, D. D., Lauenroth, W. K., & Belnap, J. (2004). Multiscale perspective of water pulses in dry-land ecosystems: Climatology and ecohydrology of the western USA. *Oecologia*, *141*, 269–281.
- Mast, M. A., & Clow, D. W. (2008). Effects of 2003 wildfires on stream chemistry in Glacier National Park, Montana. *Hydrological Processes*, *22*(26), 5013–5023, doi: 10.1002/hyp.7121.

- Mayer, B., Boyer, E. W., Goodale, C., Jaworski, N. A., Van Breemen, N., Howarth, R. W., Seitzinger, S., Billen, G., Lajtha, L. J., Nosal, M., & Paustian, K. (2002). Sources of nitrate in rivers draining sixteen watersheds in the Northeastern U.S.: *Isotopic constraints*. *Biogeochemistry*, *57*, 171–197.
- McDowell, N. G., Pockman, W., Allen, C., Breshears, D., Cobb, N., Kolb, T., Plaut, J., Sperry, J., West, A., Williams, D. G., & Yezzer, E. A. (2008). Mechanisms of plant survival and mortality during drought: why do some plants survive while others succumb? *New Phytologist*, *178*, 719–739.
- McDowell, N. G., & Sevanto, S. (2010). The mechanisms of carbon starvation: How, when, or does it even occur at all? *New Phytologist*, *186*, 264–266.
- Meyers, P. A. & Lallier-Verges, E. (1999). Lacustrine sedimentary organic matter records of Late Quaternary paleoclimates. *Journal of Paleolimnology*, *21*, 345–372.
- Mohammed M.U., Bonnefille R., & Johnson T.C. (1996). Pollen and isotopic records in Late Holocene sediments from Lake Turkana, Kenya. *Palaeogeography, Palaeoclimatology, Palaeoecology*, *119(3–4)*, 371–383.
- Monleon, V. J., Cromack, Jr. K., & Landsbergs, J. D. (1997). Short-term and long-term effects of prescribed under-burning on nitrogen availability in a ponderosa pine stands in Central Oregon. *Canadian Journal of Forest Research*, *27*, 369–378.
- Mworia-Maitima, J. (1997). Prehistoric fires and land-cover change in western Kenya: evidences from pollen, charcoal, grass cuticles and grass phytoliths. *The Holocene*, *7*, 409–417, doi: 10.1177/095968369700700404.
- Nanus, L., Campbell, D. H., Ingersoll, G. P., Clow, D. W., & Mast, M. A. (2003). Atmospheric deposition maps for the Rocky Mountains. *Atmospheric Environment*, *37*, 4881–4892.
- Neff, J. C., Ballantyne, A. E., Farmer, G. L., Mahowald, N. M., Conroy, J. L., Landry, C. C., Overpeck, J. T., Painter, T. H., Lawrence, C. R., & Reynolds, R. L. (2008). Increasing eolian dust deposition in the western United States linked to human activity. *Nature Geoscience*, doi:10.1038/ngeo133.
- Ordoñez, J. C., van Bodegom, P. M., Jan-Philip M. Witte, J. M., Wright, I. J., Reich, P. B., & Aerts, R. (2009). A global study of relationships between leaf traits, climate and soil measures of nutrient fertility. *Global Ecology and Biogeography*, *18*, 137–149, doi: 10.1111/j.1466-8238.2008.00441.x

- Piatek, K. B., Mitchell, M. J., Silva, S. R., & Kendall, C. (2005). Sources of nitrate in snowmelt discharge: Evidence from water chemistry and stable isotopes of nitrate. *Water, Air, and Soil Pollution*, *165*, 13–35.
- Shapley, M. D., Ito, E., & Forester, R. M. (2010). Negative correlations between Mg:Ca and total dissolved solids in lakes: False aridity signals and decoupling mechanism for paleohydrologic proxies. *Geology*, *38*(5), 427–430, doi: 10.1130/G30718.1; 5.
- Schwinning, S., & Sala, O. E. (2004). Hierarchy of responses to resource pulses in arid and semi-arid ecosystems. *Oecologia*, *141*, 211–220.
- Sepulchre, P., Ramstein, G., Fluteau, F., Schuster, M., Tiercelin, J., & Brunet, M. (2006). Tectonic uplift and Eastern Africa aridification. *Science*, *313*, 1419–1423, doi: 10.1126/science.1129158.
- Staver, A.C., Archibald, S., & Levin, S.A. (2011). The global extent and determinants of savanna and forest as alternative biome states. *Science*, *334*, 230–232, doi: 10.1126/science.1210465.
- Stone, J. R., & Fritz, S. C. (2004). Three-dimensional modeling of lacustrine diatom habitat areas: Improving paleolimnological interpretation of planktic:benthic ratios. *Limnology & Oceanography*, *49*, 1540–1548.
- Turk, J. T., Taylor, H. E., Ingersoll, G. P., Tonnessen, K. A., Clow, D. W., Mast, M. A., Campbell, D. H., & Melack, J. M. (2001). Major-ion chemistry of the Rocky Mountain snowpack, USA. *Atmospheric Environment*, *35*, 3957–3966.
- Wan, S., Hui, D., & Luo, Y. (2000). Fire effects on nitrogen pools and dynamics in terrestrial ecosystems: A meta-analysis. *Ecological Applications*, *11*(5): 1349–1365.
- Westerling, A. L., Hidalgo, H. G., Cayan, D. R., & Swetnam, T. W. (2006). Warming and earlier spring increase Western U.S. forest wildfire. *Science*, doi: 10.1126/science.1128834 , 940.
- William, D. G., & Ehleringer, J. R. (2000). Intra- and interspecific variation for summer precipitation use in pinyon juniper woodlands. *Ecological Monographs*, *70*, 517–537.

APPENDIX A

SUPPLEMENTAL INFORMATION FOR CHAPTER 1

Table 4. A summary of equations used to model that past water temperature from $\delta^{18}\text{O}_{\text{H}_2\text{O}}$, $\delta\text{D}_{\text{H}_2\text{O}}$, and $\delta^{18}\text{O}_{\text{CaCO}_3}$ values.

Equation no.	Temperature (°C)	Reference	Material
1	$16.5 - 4.3 * ((1.01025 * (10^3 + \delta^{18}\text{O}_{\text{calcite}}) - 10^3) - (1.0412 * (10^3 + (0.97002 * \text{TM}^{18}\text{O}_{\text{water}} - 29.98)) - 10^3)) + 0.14 * ((1.01025 * (10^3 + \delta^{18}\text{O}_{\text{calcite}}) - 10^3) - (1.0412 * (10^3 + (0.97002 * \text{TM}^{18}\text{O}_{\text{water}} - 29.98)) - 10^3))^2$	Epstein <i>et al.</i> 1953	Calcite
2	$16.9 - 4.2 * ((1.01025 * (1000 + \delta^{18}\text{O}_{\text{calcite}}) - 10^3) - (1.0412 * (10^3 + (0.97002 * \delta^{18}\text{O}_{\text{water}} - 29.98)) - 10^3)) + 0.13 * ((1.01025 * (10^3 + \delta^{18}\text{O}_{\text{calcite}}) - 10^3) - (1.0412 * (10^3 + (0.97002 * \delta^{18}\text{O}_{\text{water}} - 29.98)) - 10^3))^2$	Craig 1965	Calcite
3	$16 - 4.14 * (\delta^{18}\text{O}_{\text{CaCO}_3} - \delta^{18}\text{O}_{\text{H}_2\text{O}} + 0.13 * (\delta^{18}\text{O}_{\text{calcite}} + \delta^{18}\text{O}_{\text{H}_2\text{O}}))^2$	Anderson & Arthur 1983	Calcite
4	$((10^6 * 2.78) / (10^3 * \ln((10^3 + \delta^{18}\text{O}_{\text{CaCO}_3} / (10^3 + \delta^{18}\text{O}_{\text{H}_2\text{O}})) + 2.89))^{0.5} - 273.15$	Kim & O'Neil 1997	Calcite
5	$(18.03 * 10^3) / (10^3 * \ln((10^3 + \delta^{18}\text{O}_{\text{CaCO}_3} / (10^3 + \delta^{18}\text{O}_{\text{H}_2\text{O}})) + 32.17) - 273.15$	Kim & O'Neil 1997	Calcite
6	$21.8 - 4.69 * (\delta^{18}\text{O}_{\text{CaCO}_3} - (\delta^{18}\text{O}_{\text{H}_2\text{O}} - 0.2))$	Grossman & Ku (1986)	Aragonite
7	$20.6 - 4.34 * (\delta^{18}\text{O}_{\text{CaCO}_3} - (\delta^{18}\text{O}_{\text{H}_2\text{O}} - 0.2))$	Grossman & Ku (1986)	Aragonite
8	$20 - 4.42 * (\delta^{18}\text{O}_{\text{CaCO}_3} - \delta^{18}\text{O}_{\text{H}_2\text{O}})$	Bohm <i>et al.</i> (2000)	Aragonite
9	$(17.88 * 1000) / (1000 * \text{LN}((1000 + [1.03091 * \delta^{18}\text{O}_{\text{CaCO}_3} + 30.91]) / (1000 + \delta^{18}\text{O}_{\text{H}_2\text{O}})) + 30.85) - 273.15$	Kim <i>et al.</i> (2007)	Aragonite
10	$(18.56 * 1000) / (1000 * \text{LN}((1000 + [1.03091 * \delta^{18}\text{O}_{\text{CaCO}_3} + 30.91]) / (1000 + \delta^{18}\text{O}_{\text{H}_2\text{O}})) + 33.49) - 273.15$	Patterson <i>et al.</i> (1993)	Aragonite
11	$(18.56 * 1000) / (1000 * \text{LN}((1000 + [1.03091 * \delta^{18}\text{O}_{\text{CaCO}_3} + 30.91]) / (1000 + \delta^{18}\text{O}_{\text{H}_2\text{O}})) + 32.54) - 273.15$	Thorrold <i>et al.</i> (1997)	Aragonite
12	$(16.74 * 1000) / (1000 * \text{LN}((1000 + [1.03091 * \delta^{18}\text{O}_{\text{CaCO}_3} + 30.91]) / (1000 + \delta^{18}\text{O}_{\text{H}_2\text{O}})) + 26.39) - 273.15$	White <i>et al.</i> (1999)	Aragonite
13	$(20.44 * 1000) / (1000 * \text{LN}((1000 + [1.03091 * \delta^{18}\text{O}_{\text{CaCO}_3} + 30.91]) / (1000 + \delta^{18}\text{O}_{\text{H}_2\text{O}})) + 41.48) - 273.15$	Zhou & Zheng (2003)	Aragonite

APPENDIX B

SUPPLEMENTAL INFORMATION FOR CHAPTER 2

Table 5. A summary of the average $\delta^{13}\text{C}$ values of soil samples for canopy gaps, forests, and combined (forests and gaps) of the sites, and woody cover (%WC) values. The corresponding standard deviations are indicated.

Location	Veg. class	Lat.	Long.	Elev. (m)	$\delta^{13}\text{C}_{\text{Gap}}$ ($\% \pm \text{stdev}$)	$\delta^{13}\text{C}_{\text{Forest}}$ ($\% \pm \text{stdev}$)	$\delta^{13}\text{C}_{\text{average}}$ ($\% \pm \text{stdev}$)	%WC ($\pm \text{stdev}$)
Awash	G	11.069	40.536	516	-18.2 \pm 1.1	-21.5 \pm 4.1	-18.6 \pm 1.8	0.13 \pm 0.06
Awash	F	11.067	40.539	515	-22.9 \pm 2.1	-23.6 \pm 1.3	-23.4 \pm 1.5	0.77 \pm 0.12
Ileret	F	4.317	36.261	391	-23.6 \pm 0.6	-25.8 \pm 1.2	-25.0 \pm 1.0	0.63 \pm 0.05
Ileret	G	4.277	36.221	364	-17.4 \pm 0.8	-18.5 \pm 2.0	-17.4 \pm 0.8	0.01 \pm 0
Ileret	B	4.287	36.260	435	-21.7 \pm 1.1	-22.6 \pm 0.8	-22.2 \pm 0.9	0.6 \pm 0.05
Kakamega †	F	0.356	34.861	1628	NV	-25.6 \pm 1.2	-25.6 \pm 1.2	0.91 \pm 0.06
Kakamega †	G	0.348	34.869	1571	-14.7 \pm 0.7	-21.3 \pm 0.2	-15.1 \pm 0.6	0.06 \pm 0.05
Meru †	B	-0.070	38.413	342	-20.2 \pm 0.6	-25.4 \pm 0.6	-23.6 \pm 0.6	0.66 \pm 0.04
Meru *	F	-0.072	38.419	330	-25.2 \pm 0.1	-26.0 \pm 1.2	-25.8 \pm 1.0	0.71 \pm 0.2
Meru *	G	0.180	38.227	590	-15.9 \pm 1.3	-18.6 \pm 1.9	-16.2 \pm 1.4	0.11 \pm 0.01
Mzima Springs	F	-4.337	38.022	690	-21.1 \pm 3.9	-24.9 \pm 1.0	-23.7 \pm 2.3	0.69 \pm 0.02
Nakuru *	B	-0.466	36.103	1798	-14.7 \pm 2.0	-17.4 \pm 1.3	-15.8 \pm 1.8	0.4 \pm 0.06
Nakuru *	F	-0.418	36.125	1783	-21.8 \pm 1.8	-22.1 \pm 1.9	-22.0 \pm 1.9	0.74 \pm 0.13
Nakuru *	G	-0.417	36.126	1779	-14.0 \pm 1.4	-13.6 \pm 0	-14.0 \pm 1.4	0.02 \pm 0.01
Nakuru *	G	-0.358	36.059	1799	-14.9 \pm 1.1	NV	-14.9 \pm 1.1	0.02 \pm 0.01
Nairobi *	F	-1.348	36.767	1792	-23.4 \pm 1.4	-24.2 \pm 1.5	-24.0 \pm 1.5	0.8 \pm 0.07
Nairobi *	G	-1.352	36.796	1689	-14.6 \pm 0.5	-18.2 \pm 2.0	-14.7 \pm 0.6	0.02 \pm 0
Samburu †	F	0.567	37.528	872	-27.1 \pm 0	-27.6 \pm 0	-27.5 \pm 0	0.82 \pm 0.13
Samburu †	G	0.582	37.537	884	-19.9 \pm 1.5	-22.9 \pm 1.6	-20.6 \pm 1.6	0.22 \pm 0.02
Shimba Hill †	F	-4.235	39.418	405	NV	-27.7 \pm 0.5	-27.7 \pm 0.5	0.77 \pm 0.04
Shimba Hill †	G	-4.234	39.419	395	-18.1 \pm 1.6	No data	-18.0 \pm 1.6	0.02 \pm 0.01
Arobuke Sokoke †	F	-3.322	39.925	30	-25.2 \pm 1.1	-26.2 \pm 0.8	-26.0 \pm 0.9	0.78 \pm 0.07
Arobuke Sokoke †	F	-3.321	39.887	60	NV	-26.6 \pm 0.8	-26.6 \pm 0.8	0.97 \pm 0.02
Arobuke Sokoke †	F	-3.322	39.932	26	-27.5 \pm 1.2	-27.7 \pm 0.8	-27.7 \pm 0.8	0.97 \pm 0.02
Turkwell	B	3.140	35.868	449	-23.7 \pm 1.2	-25.4 \pm 1.3	-24.4 \pm 1.3	0.41 \pm 0
Tana River †	F	-1.877	40.140	44	-26.4 \pm 2.4	-28.1 \pm 0.3	-27.8 \pm 1.0	0.84 \pm 0.14
Tsavo East*	B	-3.362	38.645	505	-18.0 \pm 0.9	-23.5 \pm 2.8	-20.2 \pm 1.9	0.4 \pm 0.01
Tsavo West *	B	-2.747	38.129	884	-18.7 \pm 1.1	-21.5 \pm 0.9	-19.8 \pm 1.1	0.39 \pm 0.03

† symbolizes a national reserve
 * symbolizes a national park
 G symbolizes a grassland
 F symbolizes a forest
 B Symbolizes a bushland
 WG symbolizes a wooded grassland

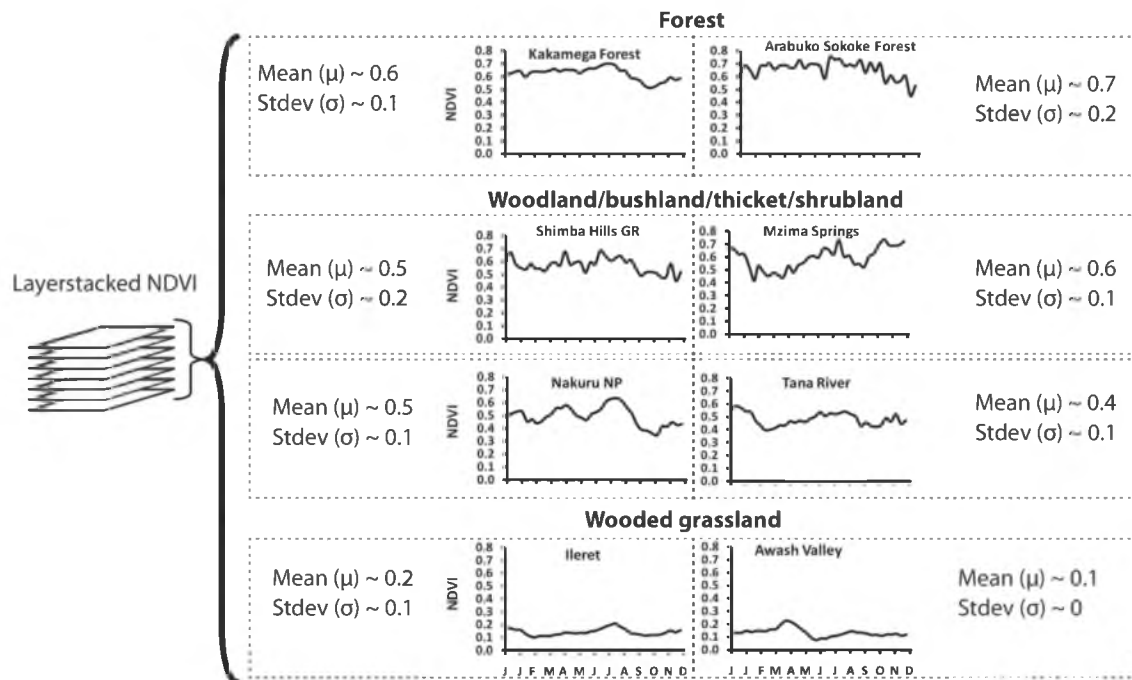
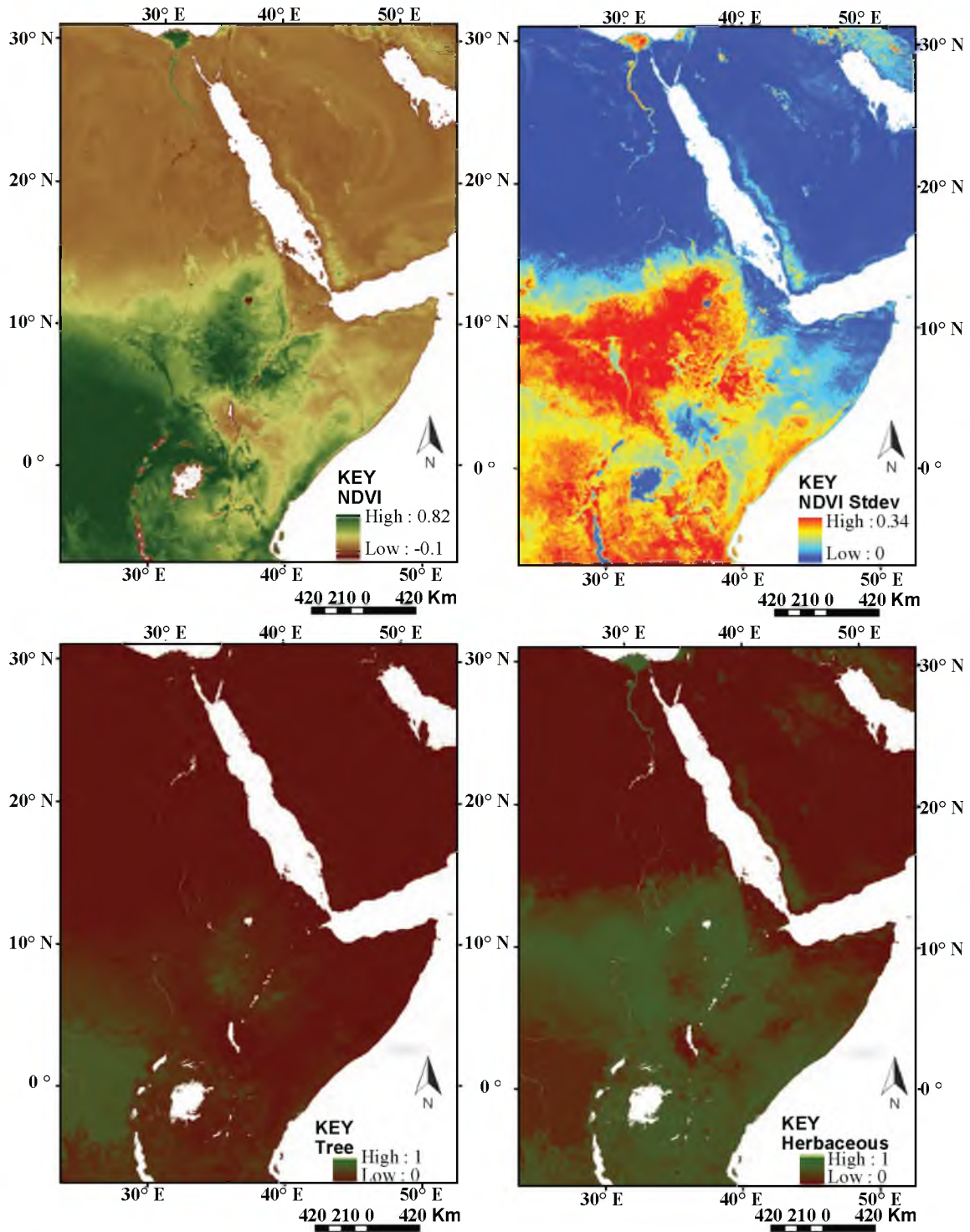


Figure 33. The seasonal AG-NPP response patterns as observed in Spot NDVI values for some of the sites in Eastern Africa covered in this study. The sites with high woody cover (e.g., Arabuko Sokoke and Kakamega forests) have high NDVI values while areas with low woody cover (e.g., Ileret and Awash) have low NDVI values. The areas between these extremes consist of a combination of physiognomies ranging from woodland, bushland, thicket, shrubland, and grassland. The temporal NDVI variations coincide with the abundance of herbaceous vegetation that are dominated by C_4 vegetation.

Figure 34. Comparison between a 12-year average and standard deviation (Stdev) of SPOT S10 NDVI series data (top panel) to MODIS Vegetation Continuous Fields (VCF) estimates of tree and herbaceous woody cover (bottom panel) for Eastern Africa. The areas with stronger variation in AG-NPP (high NDVI Stdev) have a greater proportion of herbaceous plants than areas with higher woody cover. These trends illustrate that herbaceous plants that are dominated by C₄ grasses account for significant variation of AG-NPP in the East African region in open grasslands and wooded environments.



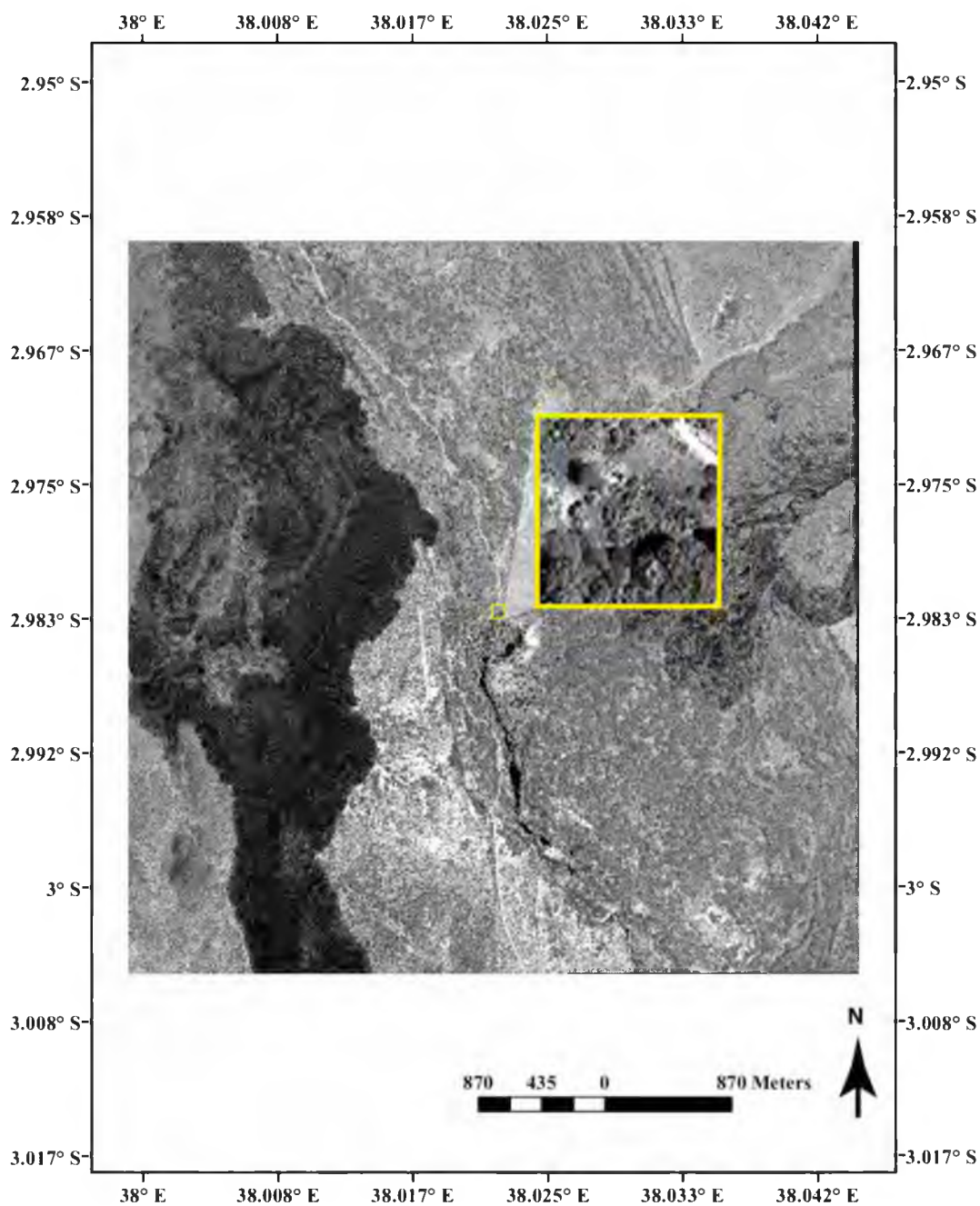


Figure 35. Mzima Springs WV01 orthoimagery acquired on 30-Jan-2010, showing the study area used in the woody cover regression analysis.

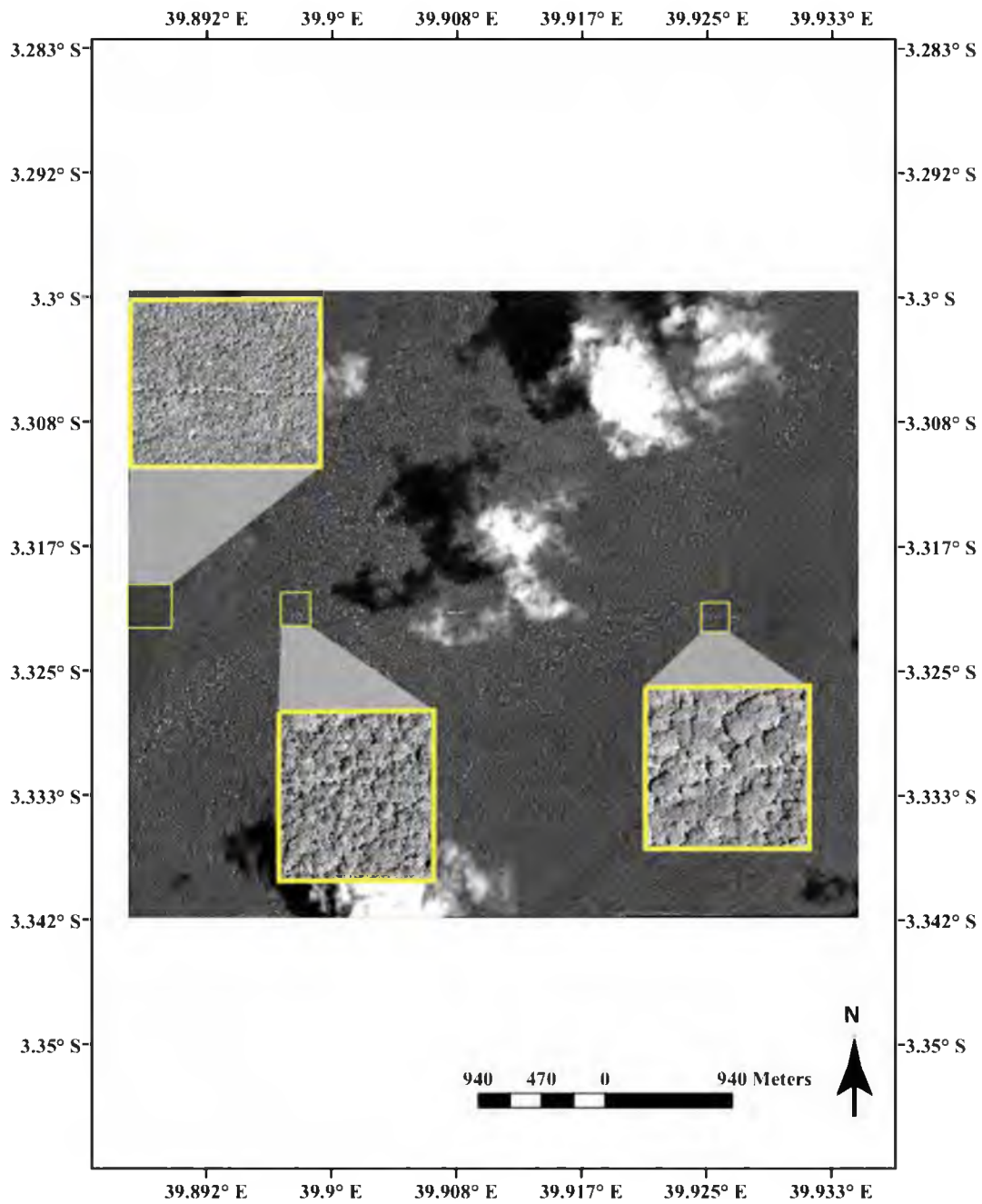


Figure 36. Arabuko Sokoke WV01 orthoimagery acquired on 14-Jan-2008, showing from left to right *Cynometra* forest, mixed forest, and *Brachystegia* forest study sites used in the woody cover regression analysis.

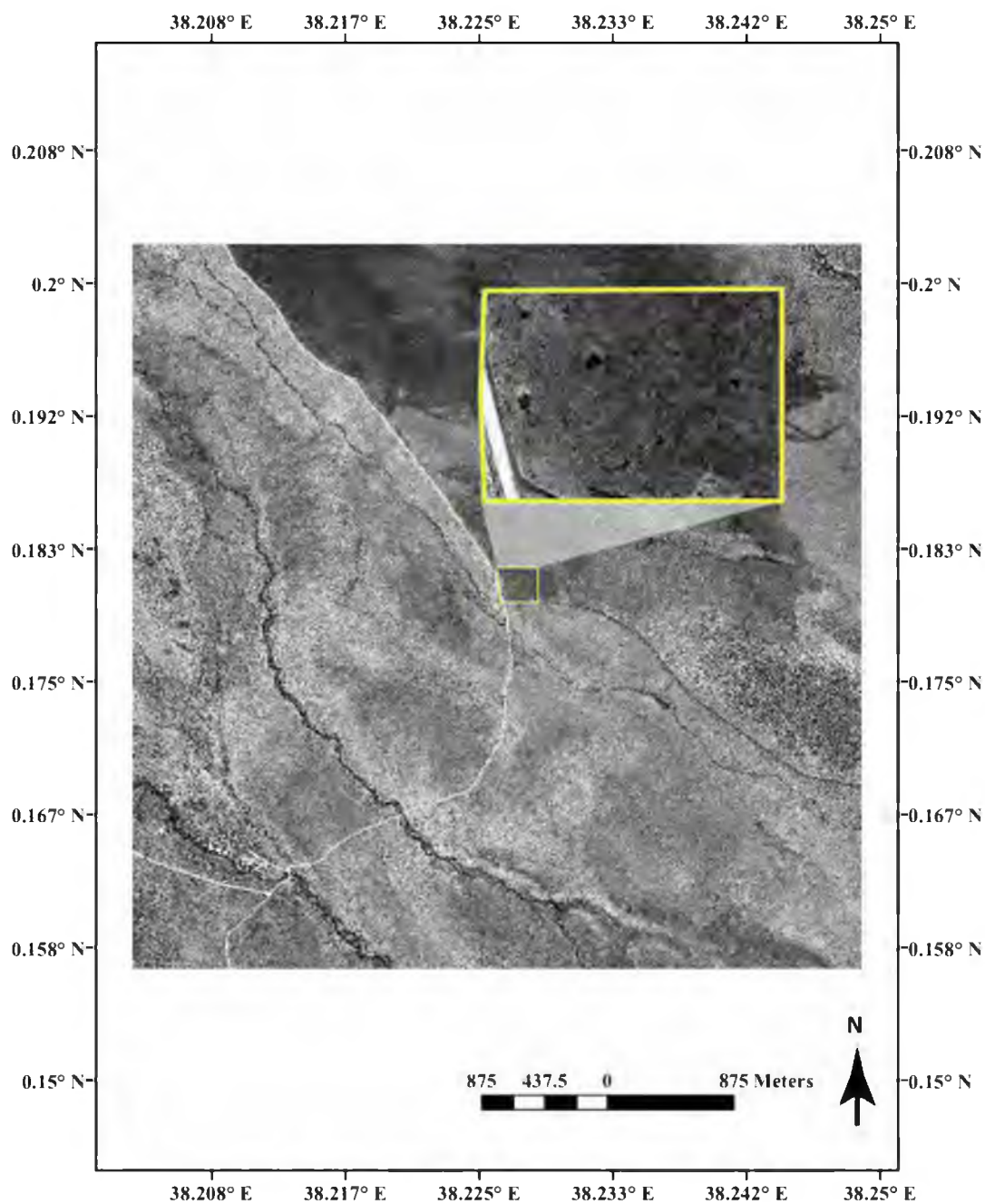


Figure 37. Meru WV01 orthoimagery acquired on 2-Oct-2008, showing the open grassland study area used in the woody cover regression analysis.

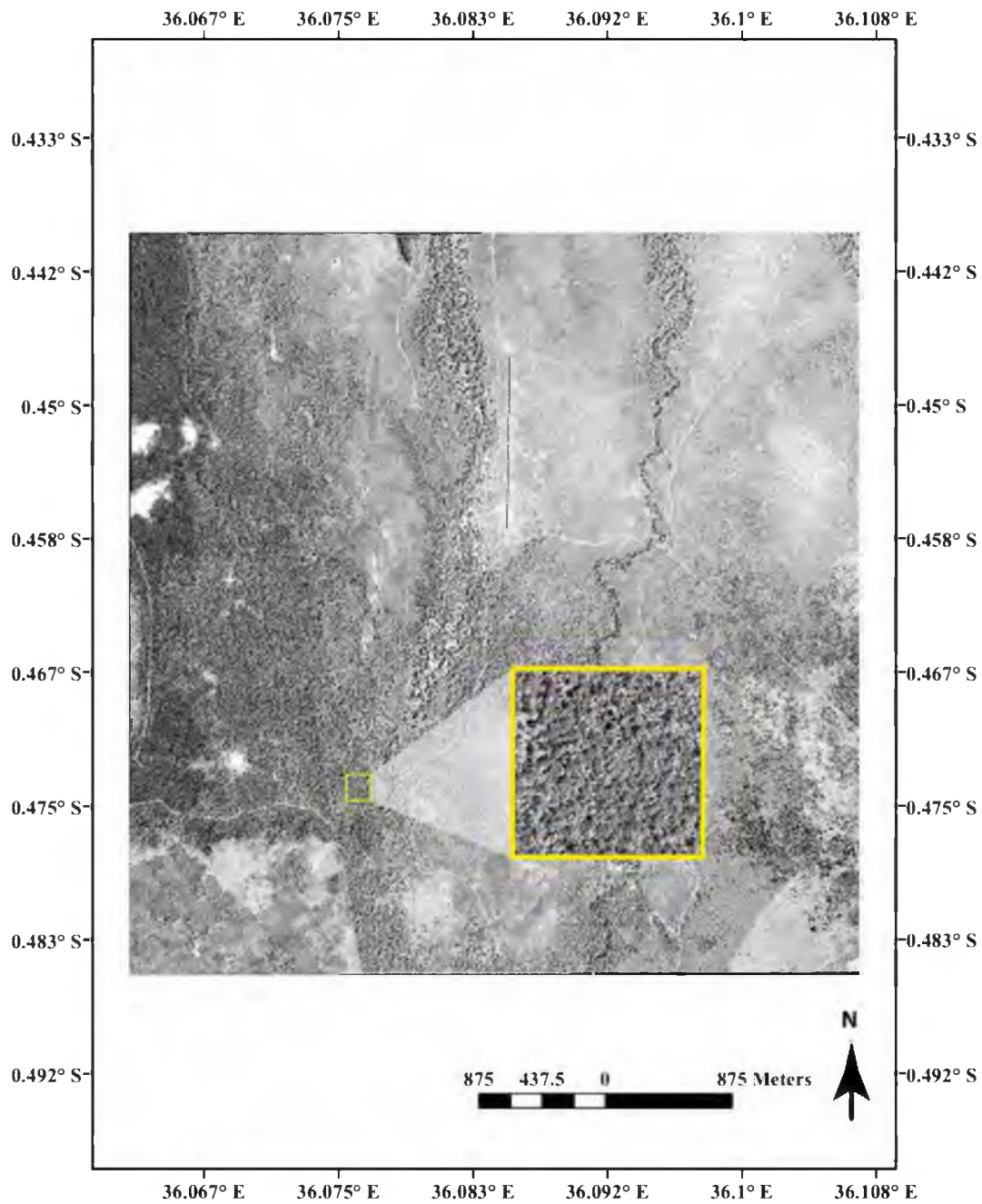


Figure 38. Nakuru WV01 orthoimagery acquired on 30-Nov-2008, showing the dense forest study area used in the woody cover regression analysis.

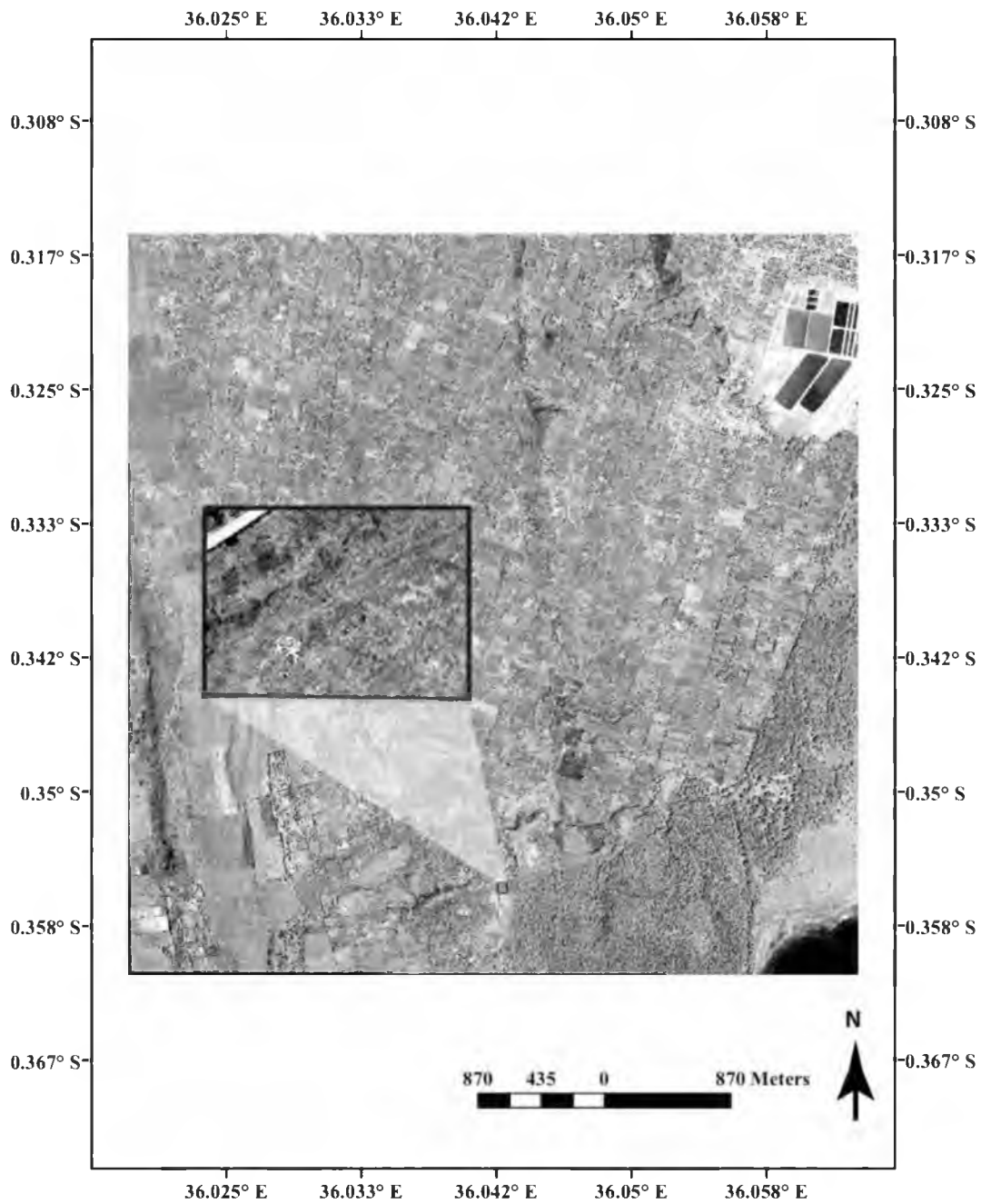


Figure 39. Nakuru WV01 orthoimagery acquired on 30-Nov-2008, showing the grassland study area used in the woody cover regression analysis.

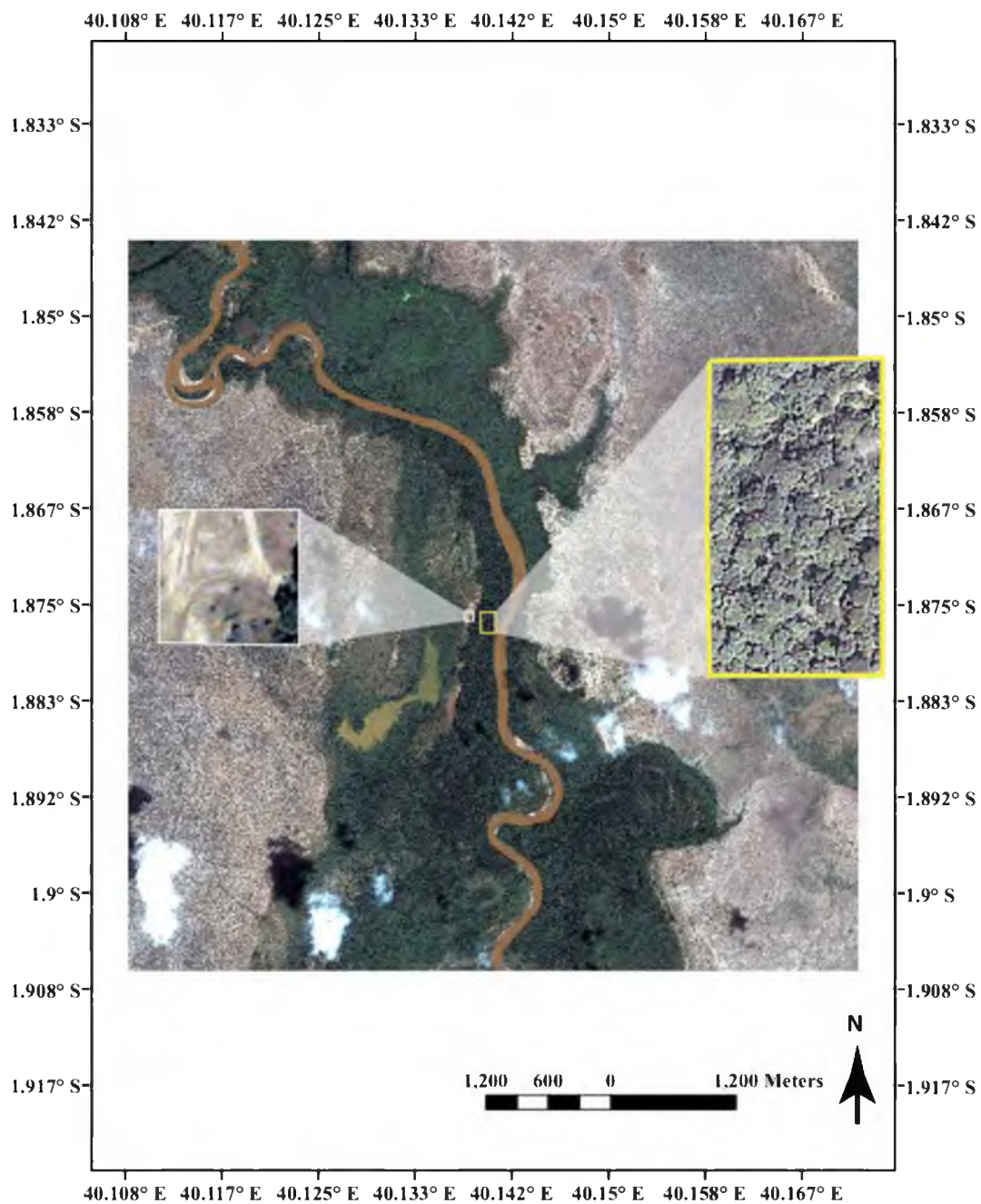


Figure 40. Tana River IKONOS-2 orthoimagery acquired on 15-Feb-2007, showing the grassland and riparian forest study areas used in the woody cover regression analysis.

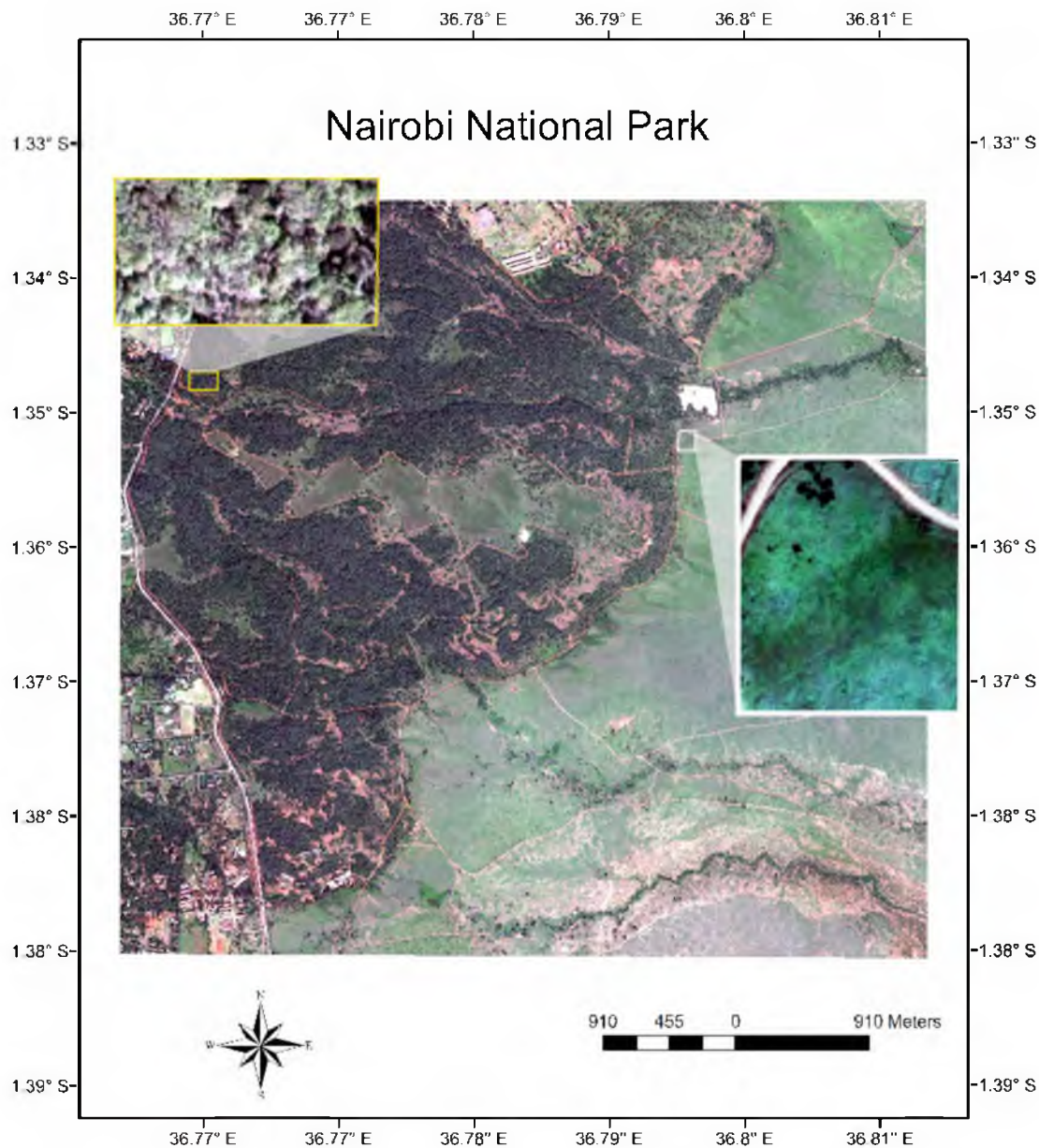


Figure 41. Nairobi National Park IKONOS-2 orthoimagery acquired on 15-Feb-2007, showing the grassland and riparian forest study areas used in the woody cover regression analysis.

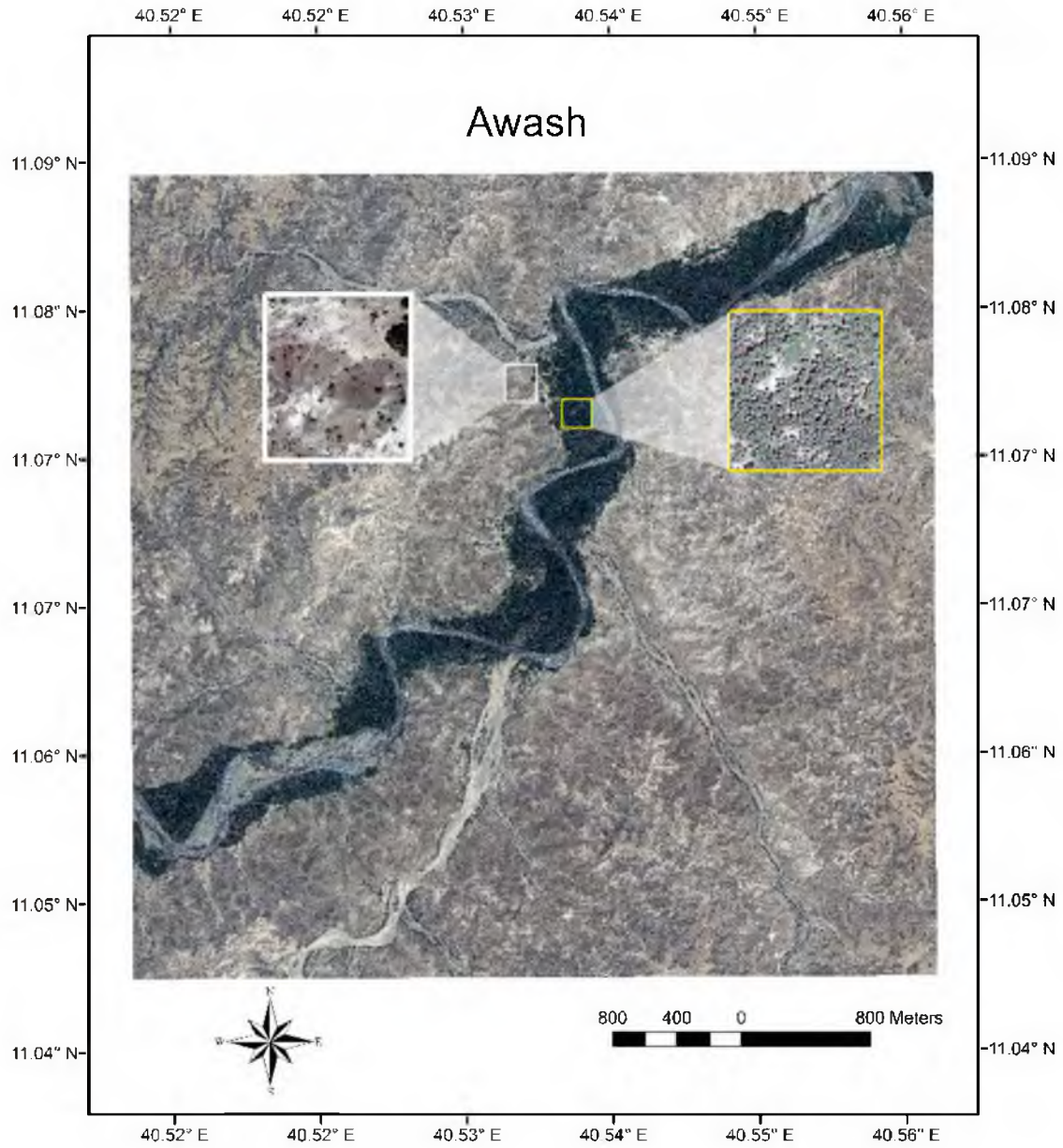


Figure 42. Awash QB02 orthoimagery acquired on 23-Sep-2008, showing the grassland and riparian forest study areas used in the woody cover regression analysis.

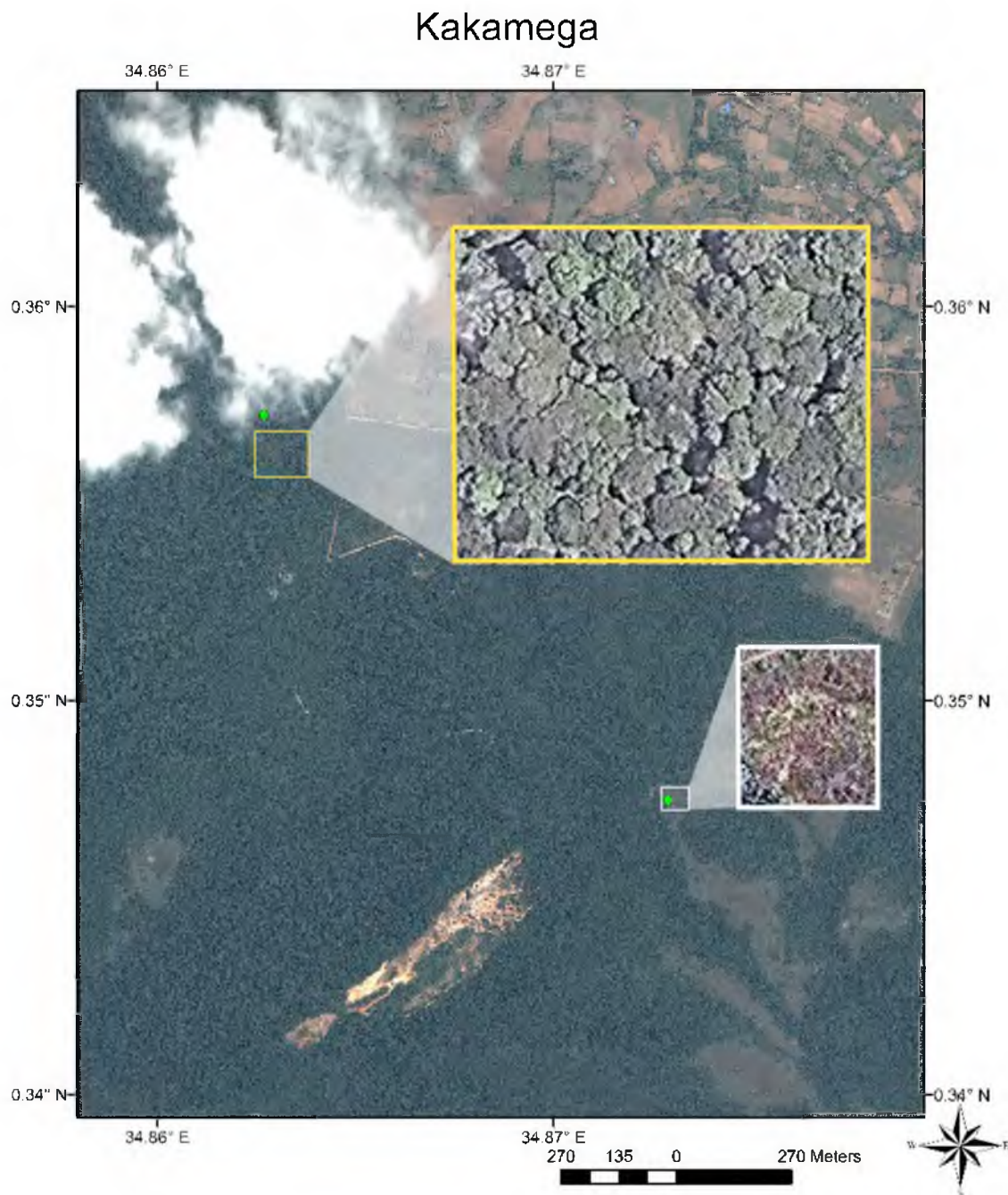


Figure 43. Kakamega Forest QB02 orthoimagery acquired on 25-Aug-2004, showing the grassland and forest study areas used in the woody cover regression analysis.

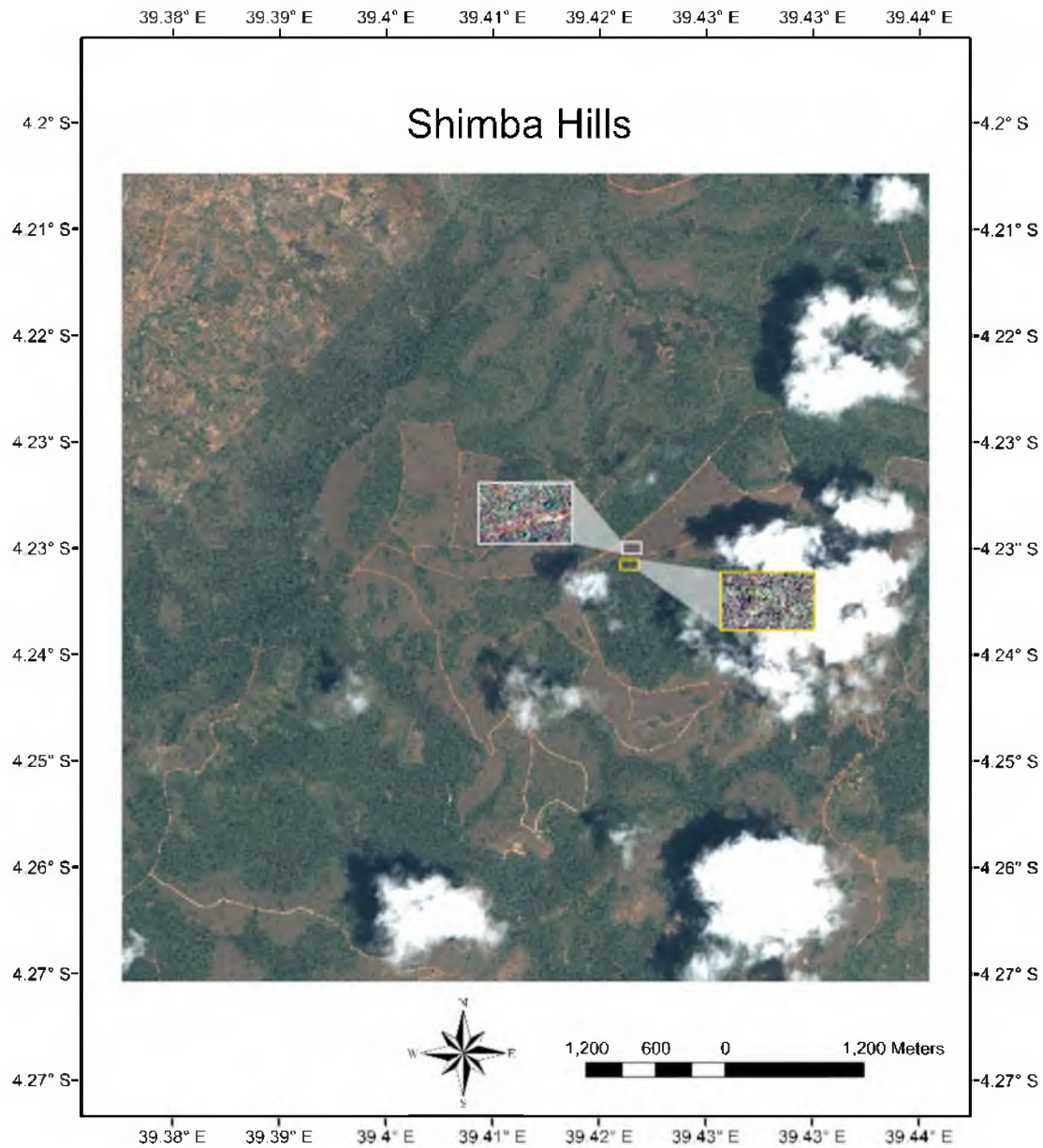


Figure 44. Shimba Hills IKONOS-2 orthoimagery acquired on 13-Jan-2008, showing the grassland and forest study areas used in the woody cover regression analysis.

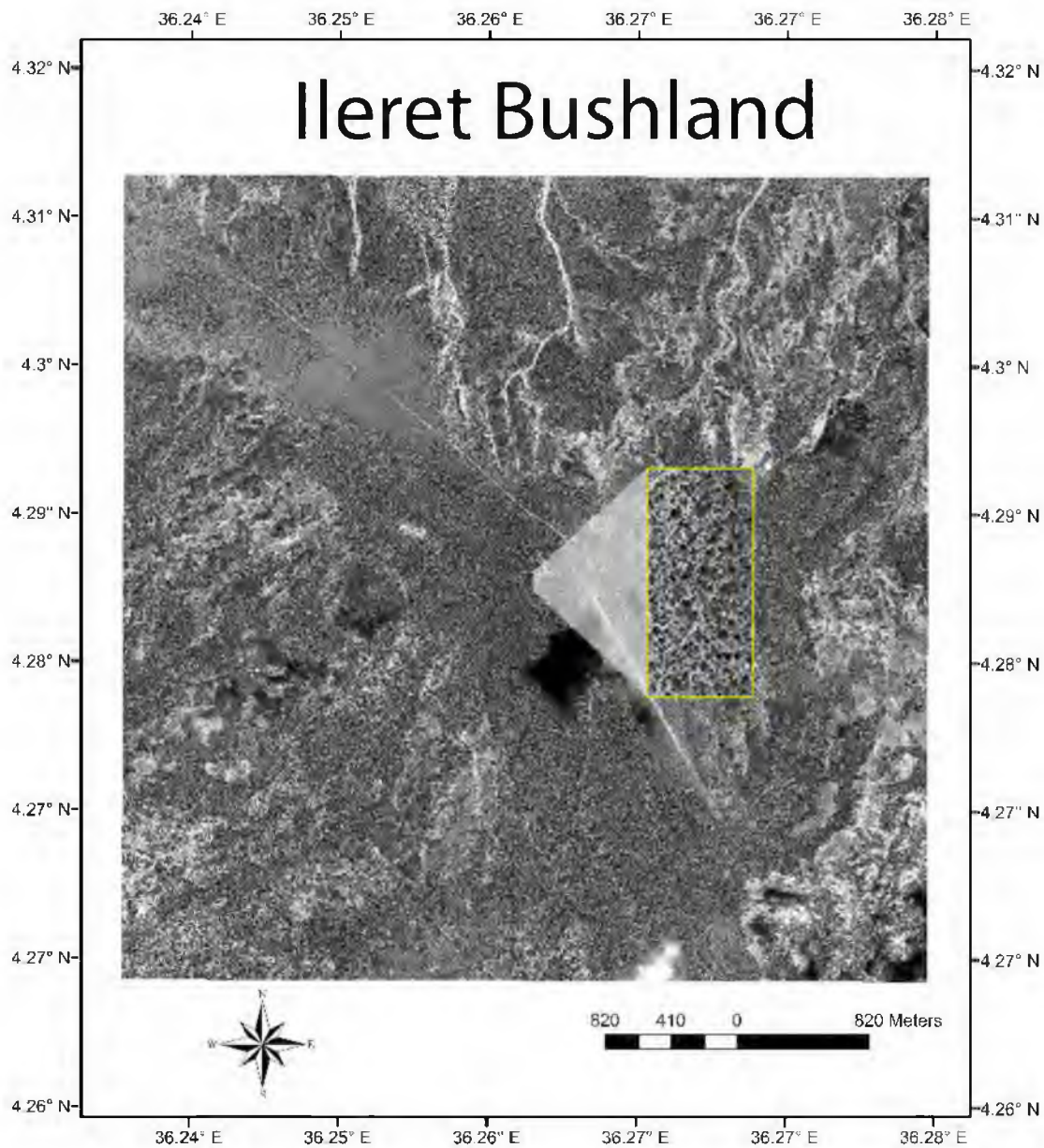


Figure 45. Ileret WV01 orthoimagery acquired on 26-Nov-2008, showing the bushland study area used in the woody cover regression analysis.

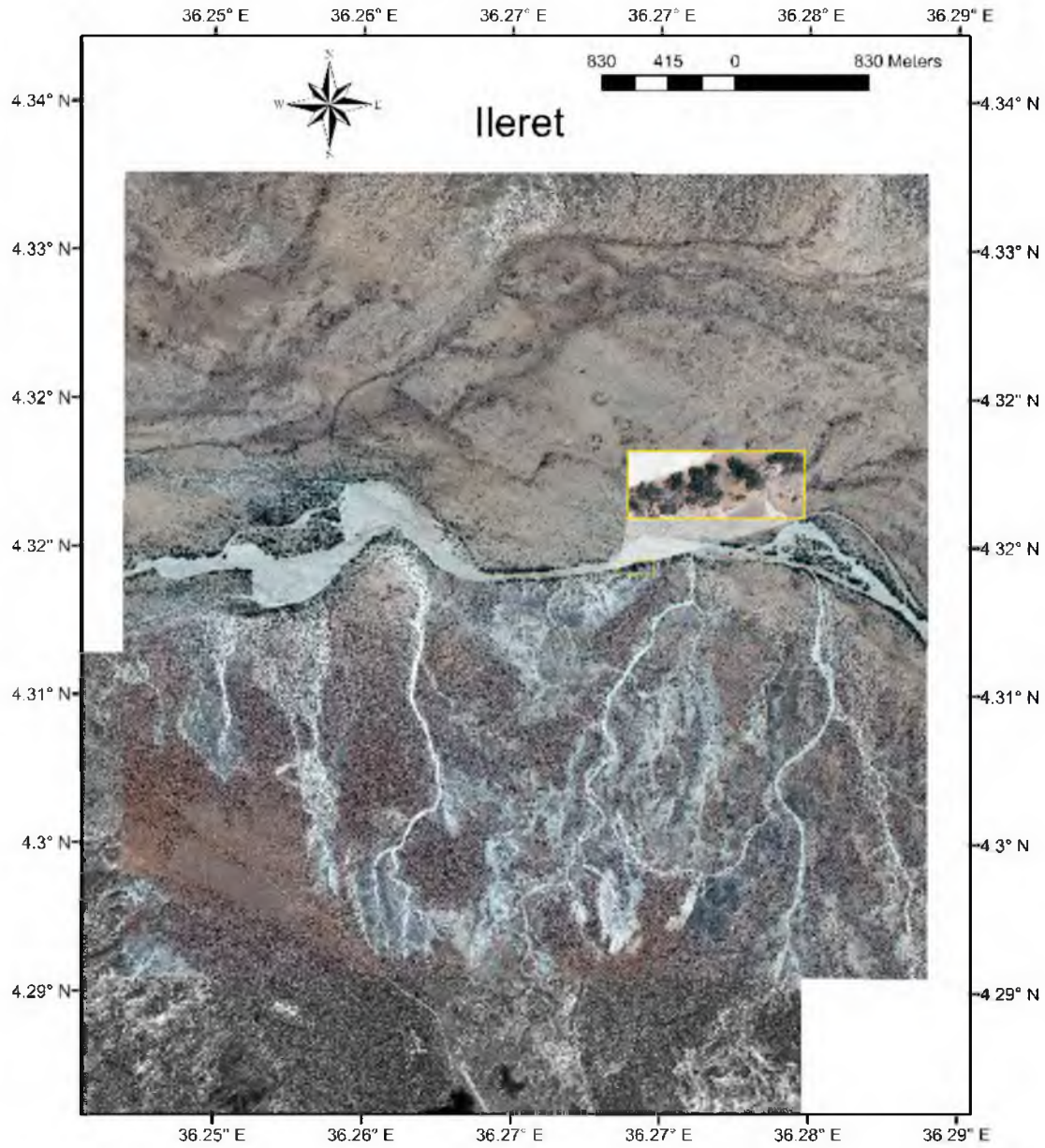


Figure 46. Ileret QB02 orthoimagery acquired on 23-Sep-2008, showing the riparian forest study area used in the woody cover regression analysis.

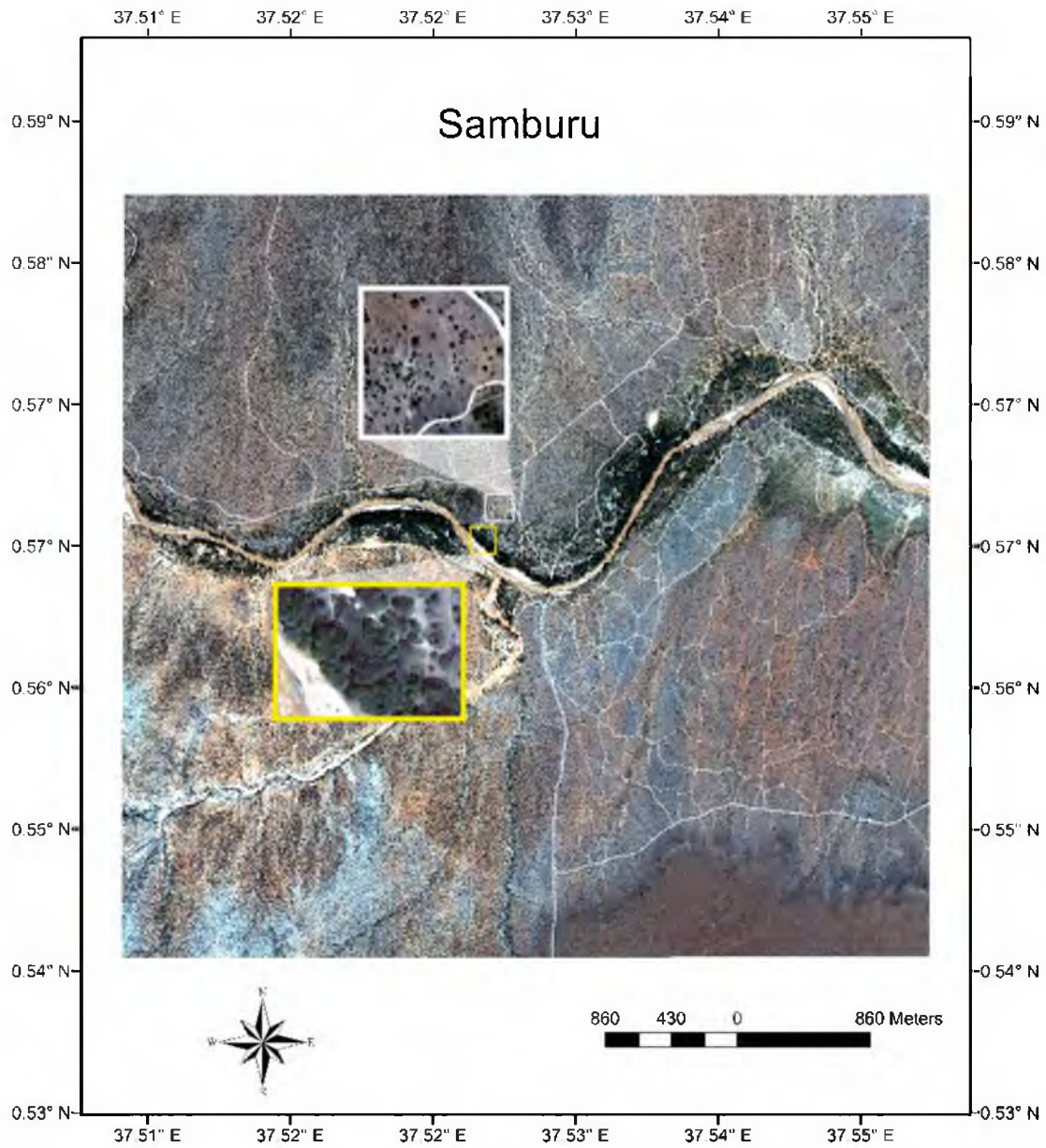


Figure 47. QB02 orthoimagery acquired on 7-Jan-2008, showing the wooded grassland and riparian woodland study areas used in the woody cover regression analysis.

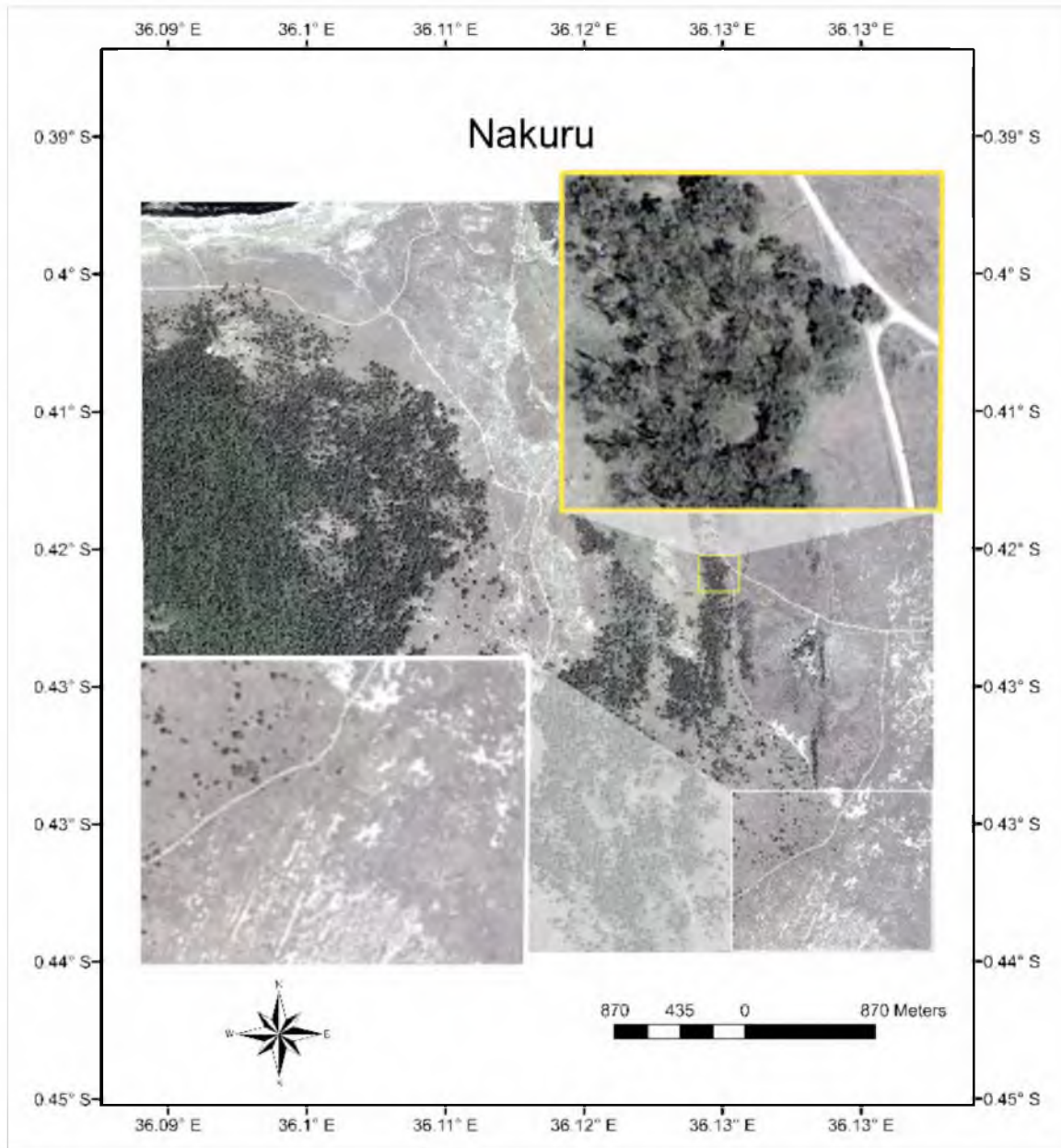


Figure 48. QB02 orthoimagery acquired on 22-Jan-2004, showing the wooded grassland and riparian woodland study areas used in the woody cover regression analysis.

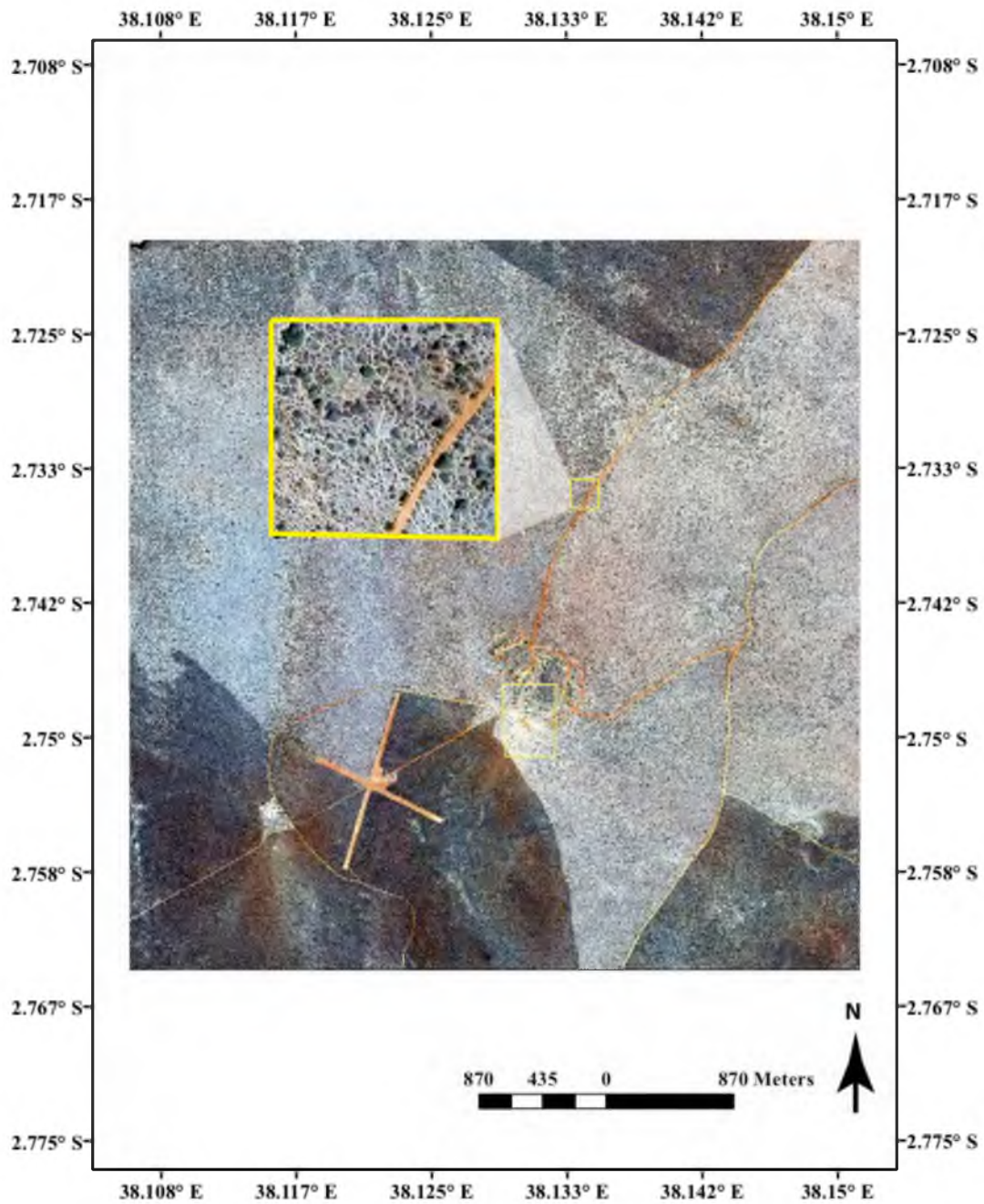


Figure 49. WV02 orthoimagery acquired on 27-Jan-2010, showing the wooded Acacia bushland study area used in the woody cover regression analysis.

APPENDIX C

SUPPLEMENTAL INFORMATION FOR CHAPTER 3

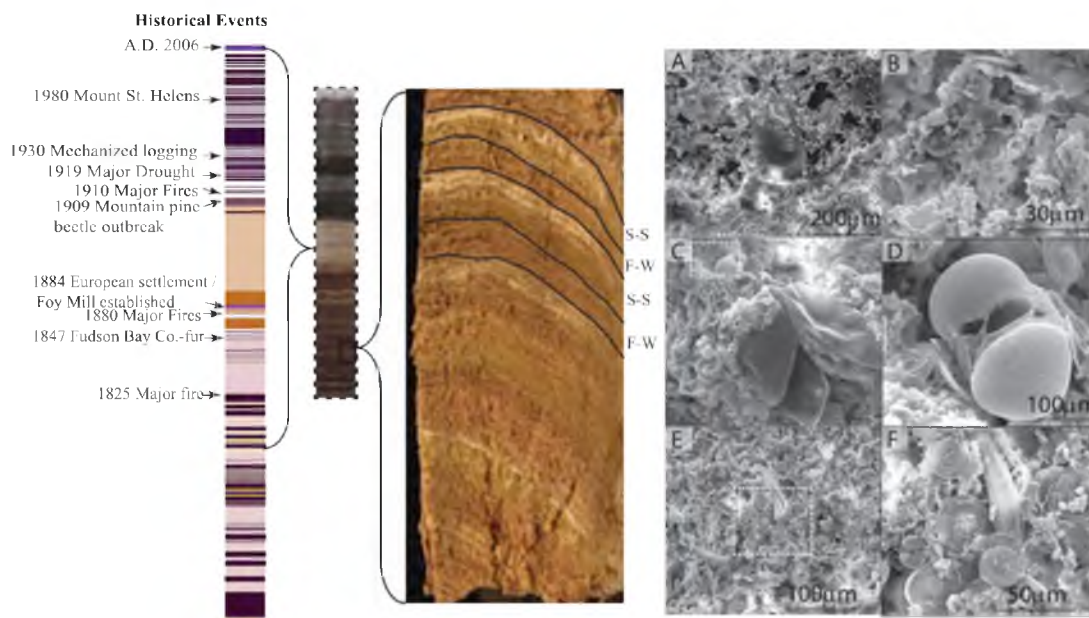


Figure 50. A description of Foy Lake freeze core. Historical events and the corresponding varves in which they are recorded are indicated. The annual couplets, SS (Spring-Summer) and FW (Fall-Winter), are recognized from color change on a section of the sediment core. The dark-brown to olive-green color corresponds to FW while olive-green to white corresponds to the SS part of the couplet. The Scanning Electron Microscope (SEM) images of samples obtained from the brown, green, and white sections of the core reveal the materials responsible for the color change. During the summer, carbonates accumulate, resulting in dissolution of diatom frustules but favoring ostracods (A-B) and hence white color. At the start of spring, there is an influx of plants pollen (*Pinus* sp.) and growth of algae as well as diatoms (C-D) and hence the olive-green color. At the transition from fall to winter, the centrate and pennate diatoms dominate as populations of algae disappear and hence the brown color. However, there are large variations in color throughout that result from various events and processes incorporated in sediments.

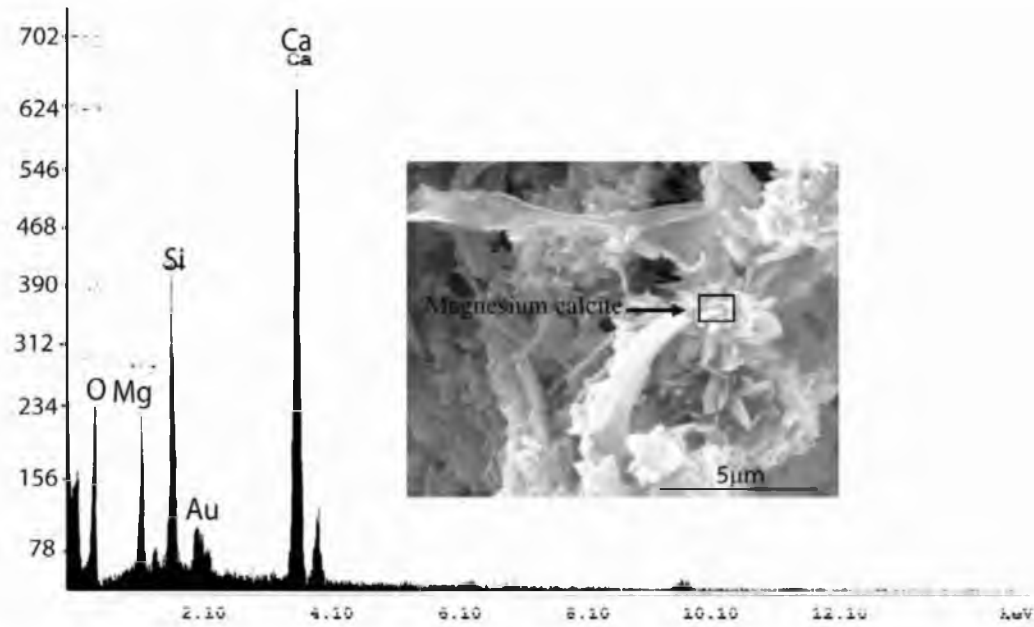


Figure 51. EDX analysis of the rosette-like crystals within the white section of the bottom varves of Foy Lake freeze core described in Figure 1 that reveal the mineral as high magnesium calcite.

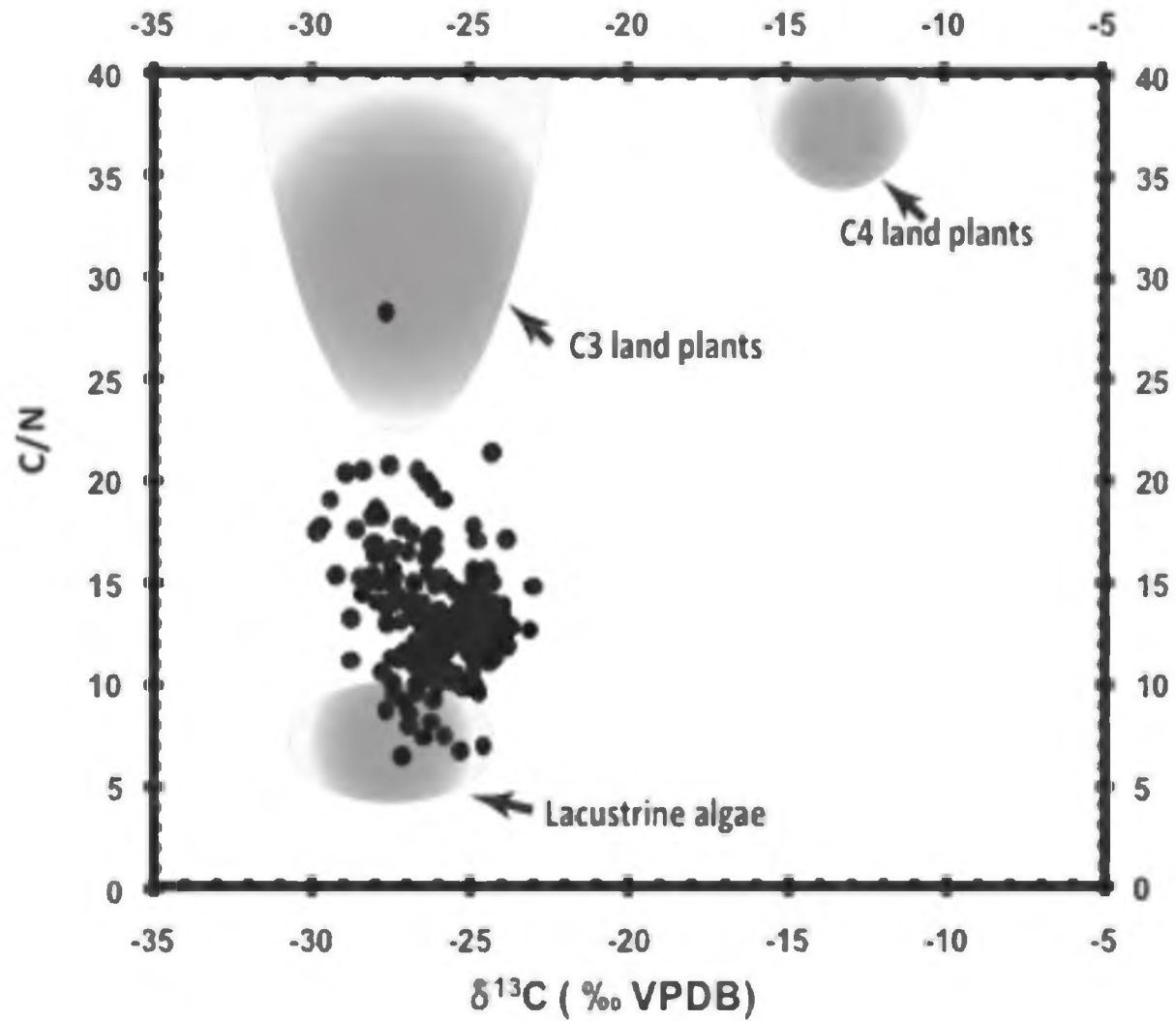


Figure 52. Foy Lake $\delta^{13}\text{C}_{\text{BOM}}$ versus C:N ratio scatterplot indicating the expected values (gray polygon) for lacustrine algae, C₃, and C₄ derived organic matter (modified after Meyers & Lallier-Verges, 1999). Foy Lake organic matter is derived from C₃ plants and lacustrine algae.

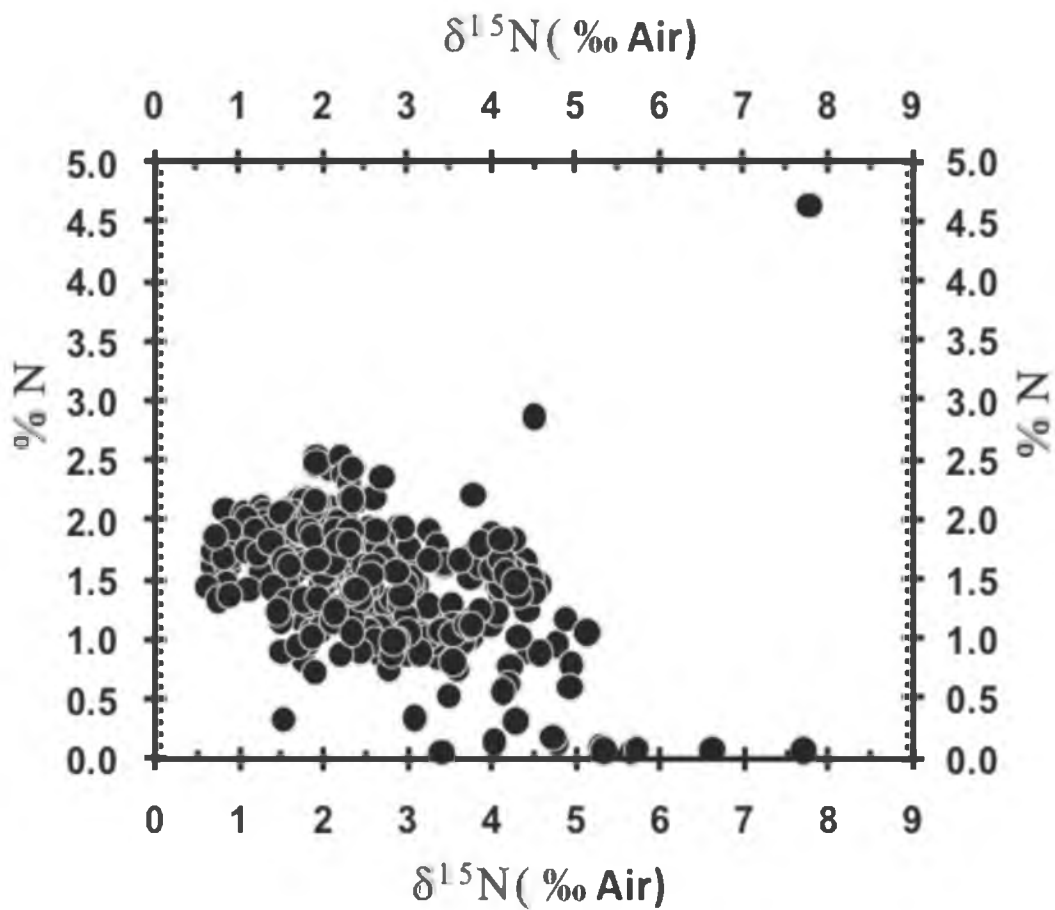


Figure 53. Foy Lake $\delta^{15}\text{N}_{\text{BOM}}$ versus %N ratio scatterplot. There is no correlation between $\delta^{15}\text{N}_{\text{BOM}}$ and % N. However, there is a wide range in % N and $\delta^{15}\text{N}_{\text{BOM}}$ values range from almost 0.1 to 4.6%, and 0.5 to 7.8‰, respectively.

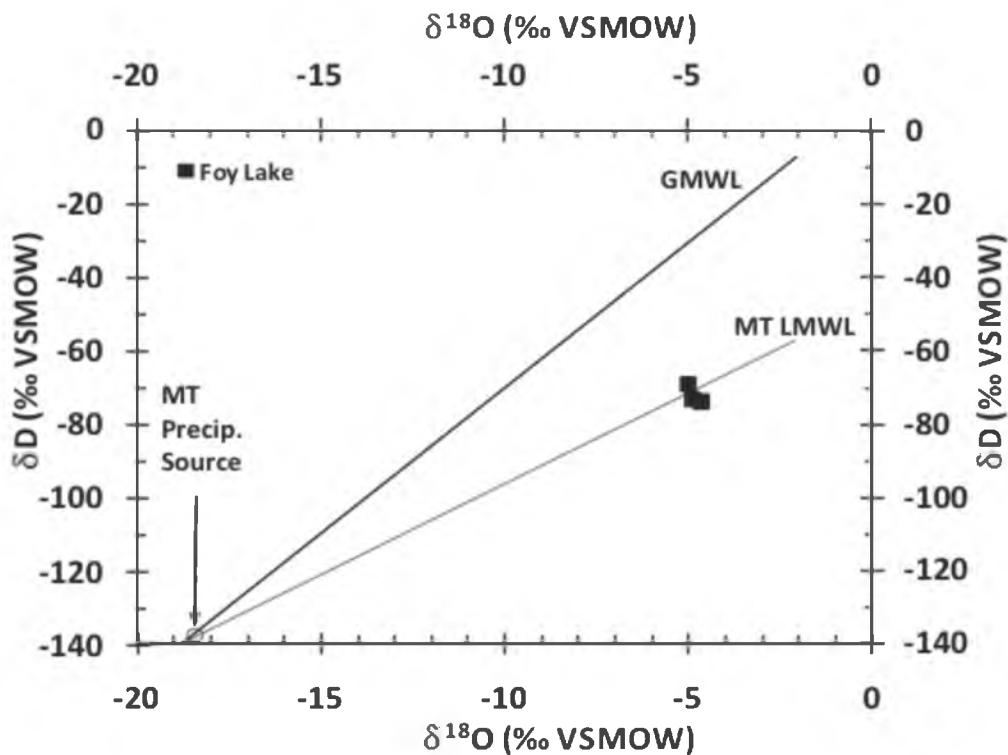


Figure 54. The scatter plot of $\delta^{18}\text{O}_{\text{H}_2\text{O}}$ and $\delta^{13}\text{D}_{\text{H}_2\text{O}}$ of Foy Lake water. The plot shows the Foy Lake water as significantly enriched relative to the source water, as inferred from the intersection of the local meteoric water line of Montana (MTLMWL) as modeled from Kendall and Clopen (2000) data and Global Meteoric Waterline (GMWL) using Craig's equation (Craig, 1961).

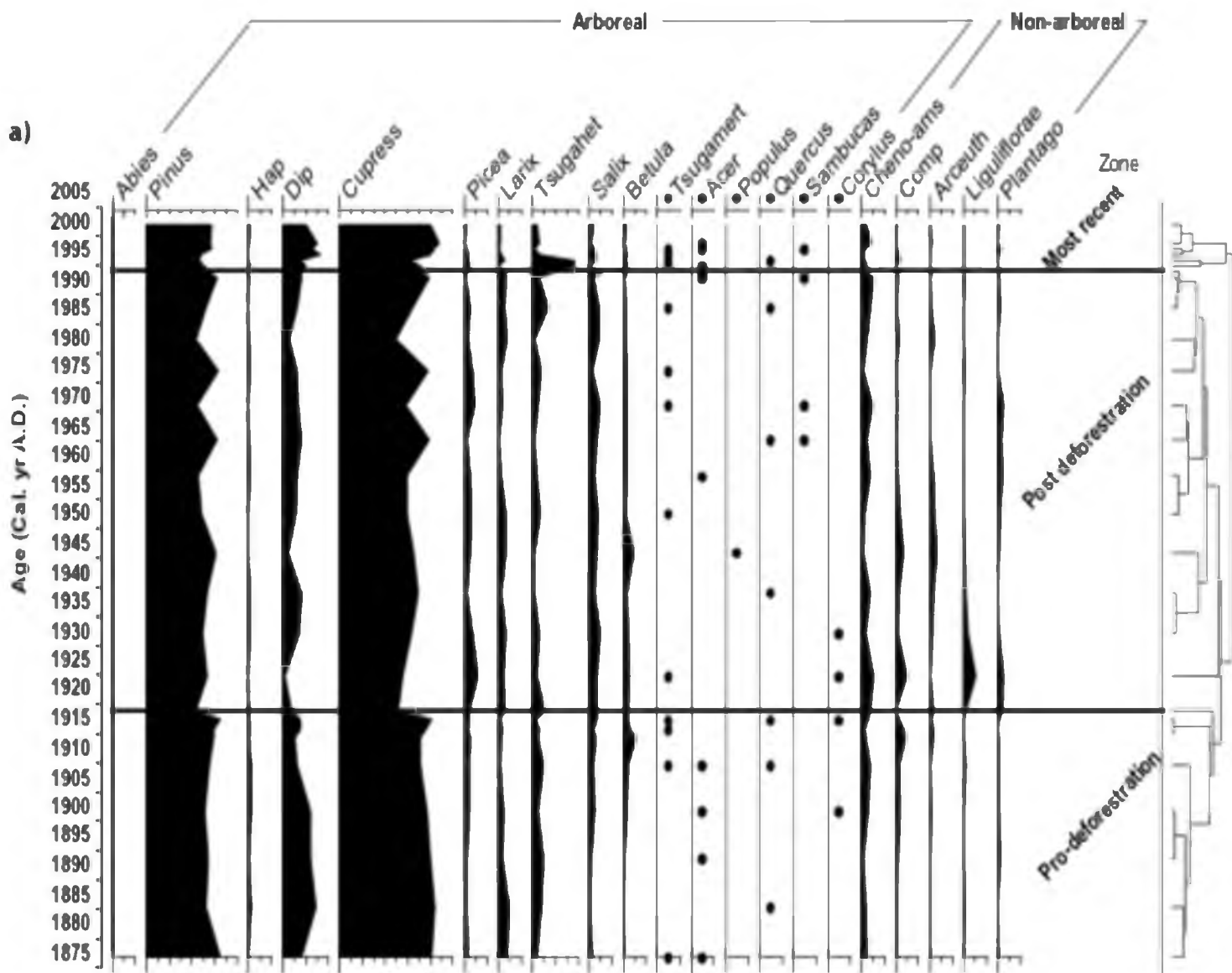


Figure 55. The pollen abundance record of Foy Lake. The arboreal pollen record shows conifer dominated woodland in Foy Lake watershed. *Pinus* and Cupressaceae are the most dominant woody cover taxa.

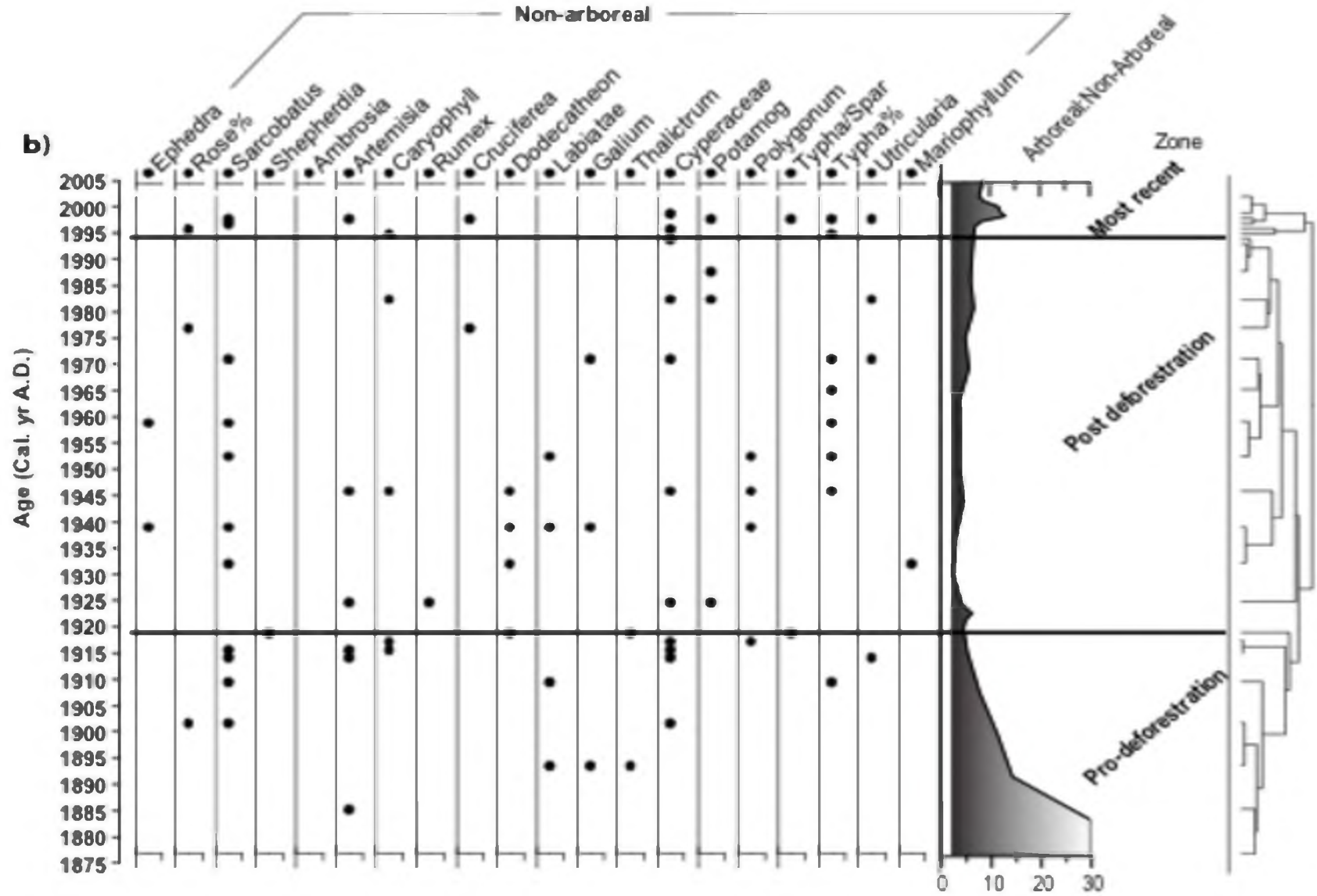


Figure 55 Continued

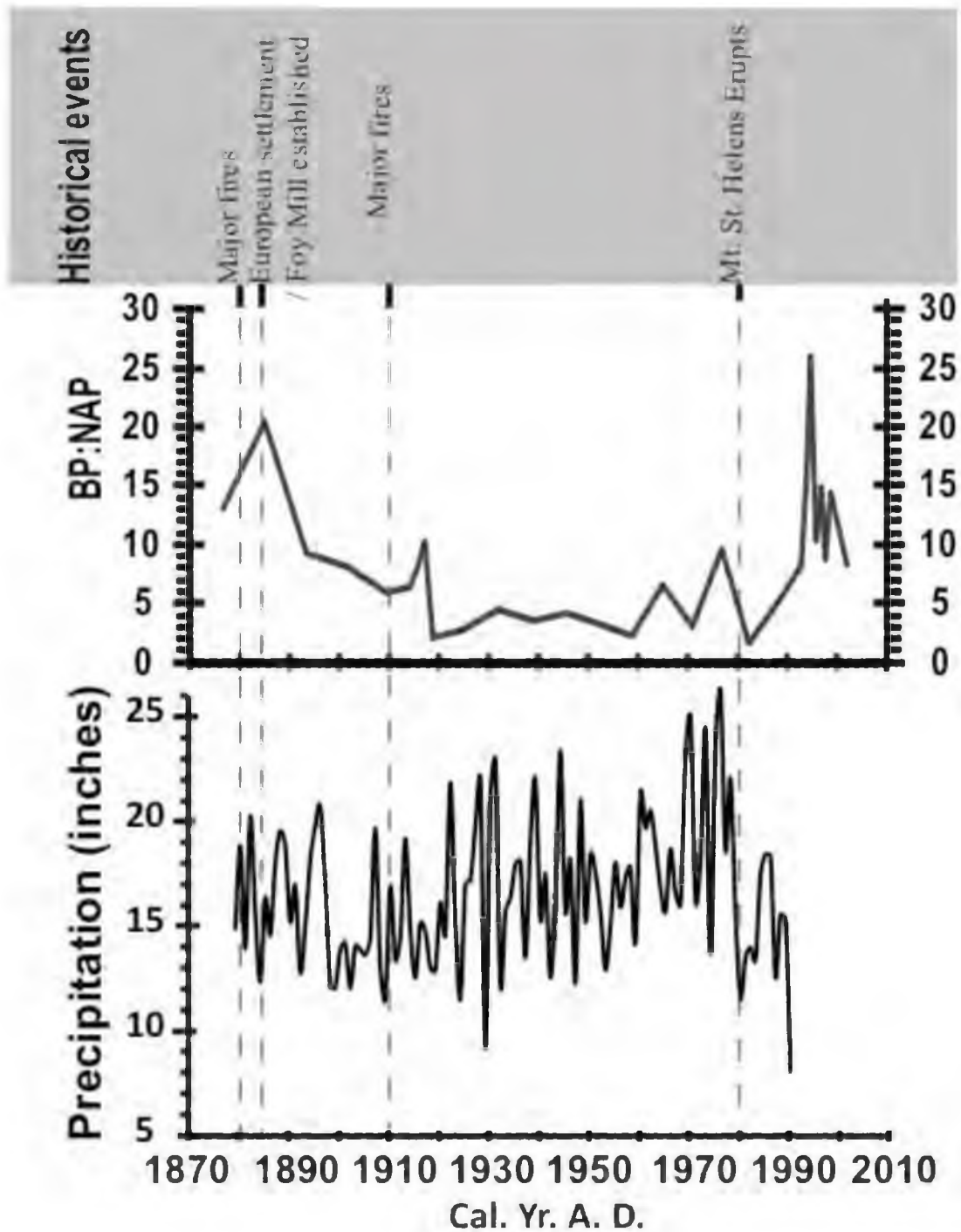


Figure 56. A timeline of historical events and precipitation records around Foy Lake relative to the ratio of pollen counts for boreal to nonarboreal plant species (BP:NAP). The precipitation records are based on Western Regional Climate Center (<http://www.wrcc@dri.edu>) data for Kalispell, MT.

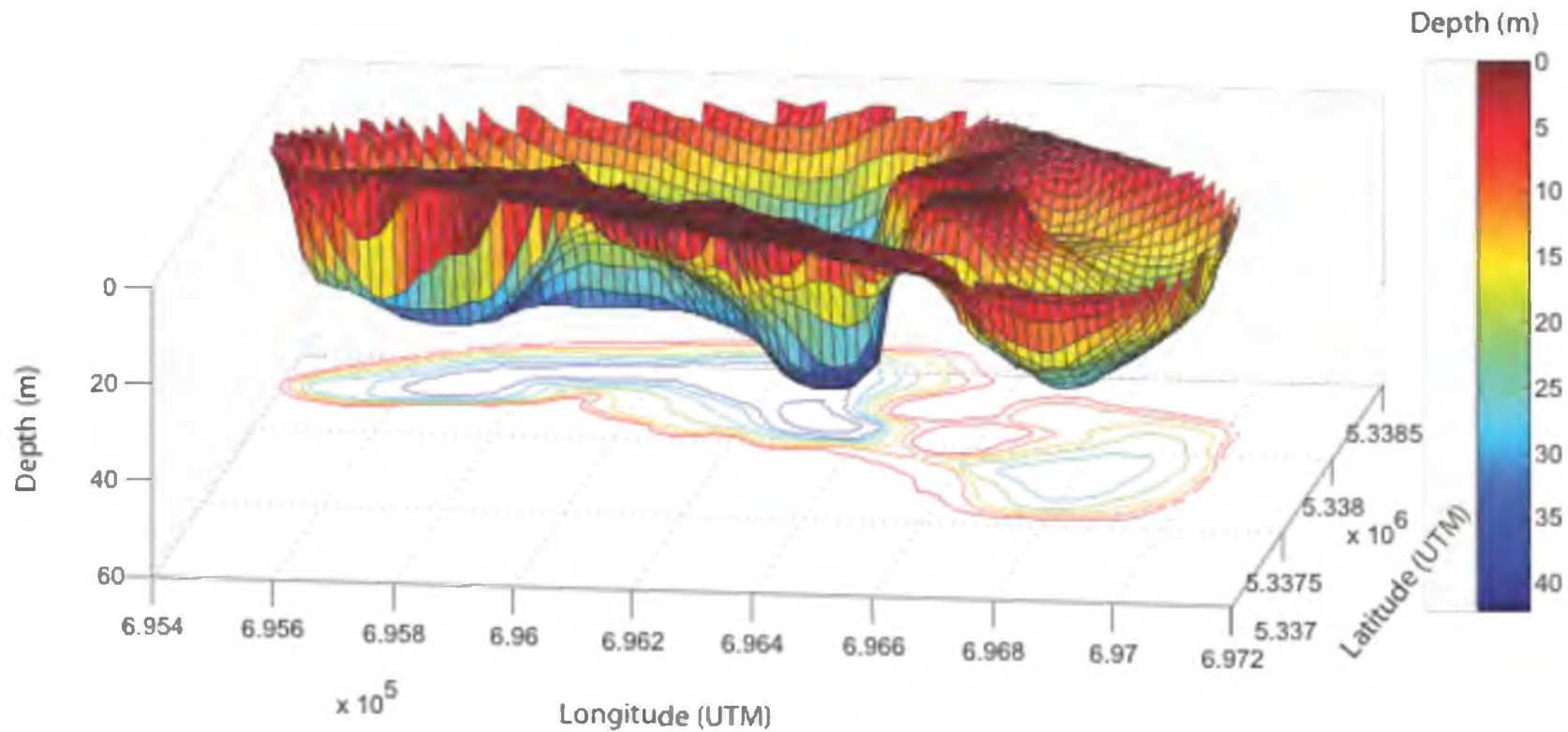


Figure 57. The conceptual model of material fluxes in Foy Lake (modified after Fritz & Stone, 2004). The lake receives particulate matter (dust, charcoal, and pollen) either via aeolian or melt water, and dissolved materials via precipitation, melt water, and groundwater pathways. Decrease in lake water level causes materials from shallow sections of the lake (including benthic areas) to be eroded and redeposited into deeper sections of the lake (sediment focusing). The influx of these materials causes changes in C:N ratios, $\delta^{15}\text{N}_{\text{BOM}}$, $\delta^{13}\text{C}_{\text{BOM}}$ of organic matter, and $\delta^{18}\text{O}_{\text{H}_2\text{O}}$ and $\delta^{13}\text{C}_{\text{CaCO}_3}$ of carbonates.

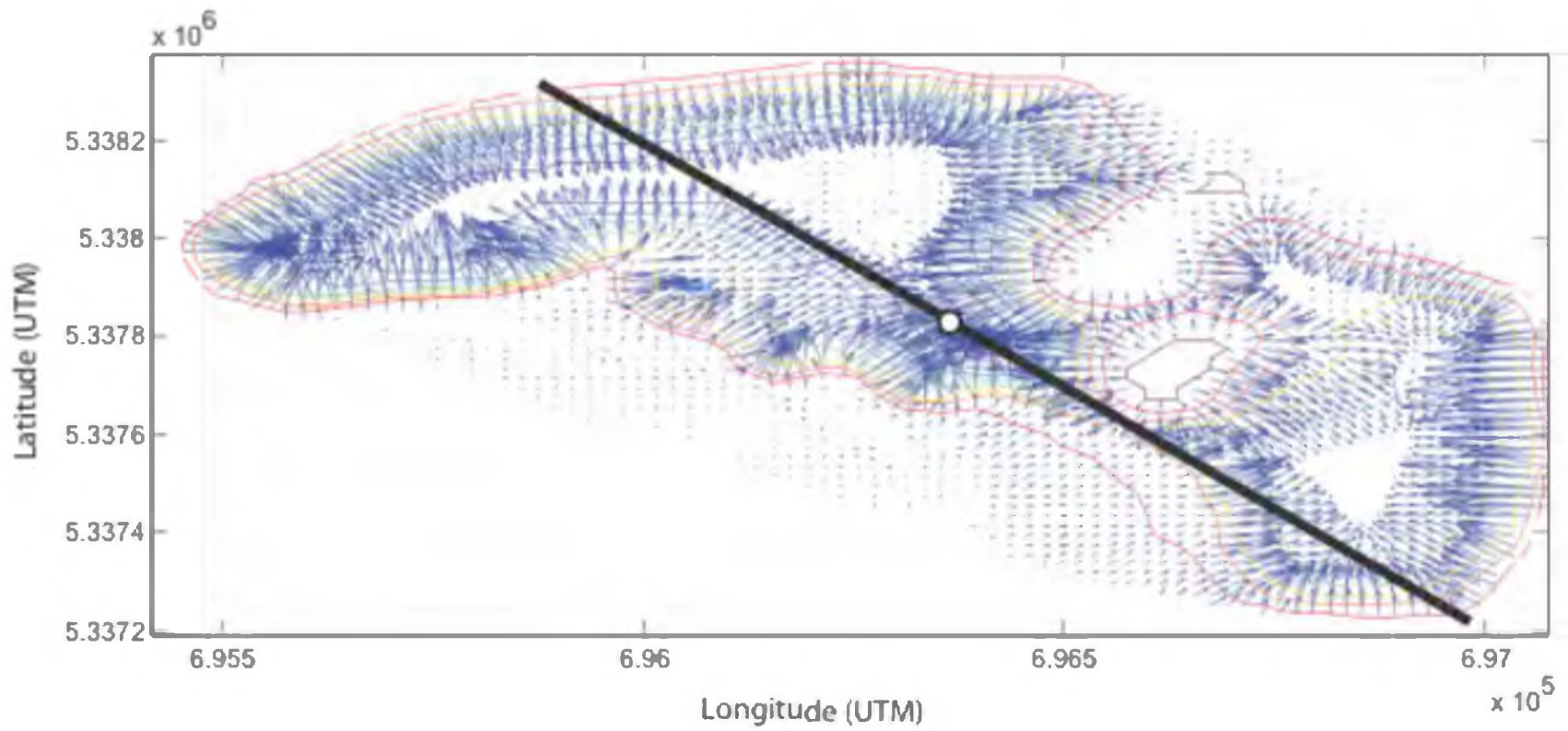


Figure 57 continued.

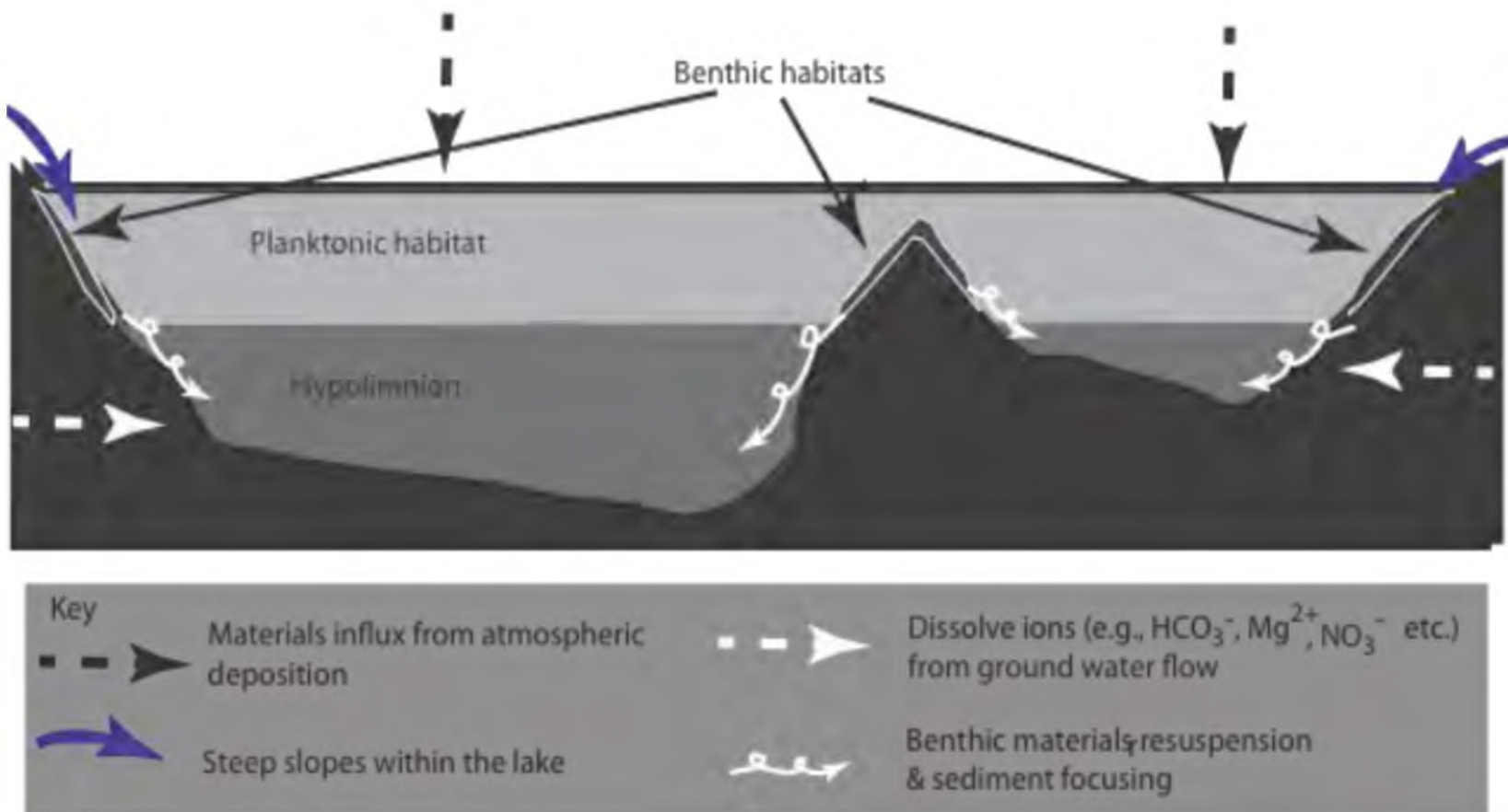


Figure 57 continued.

APPENDIX D

SUPPLEMENTAL INFORMATION FOR CHAPTER 4

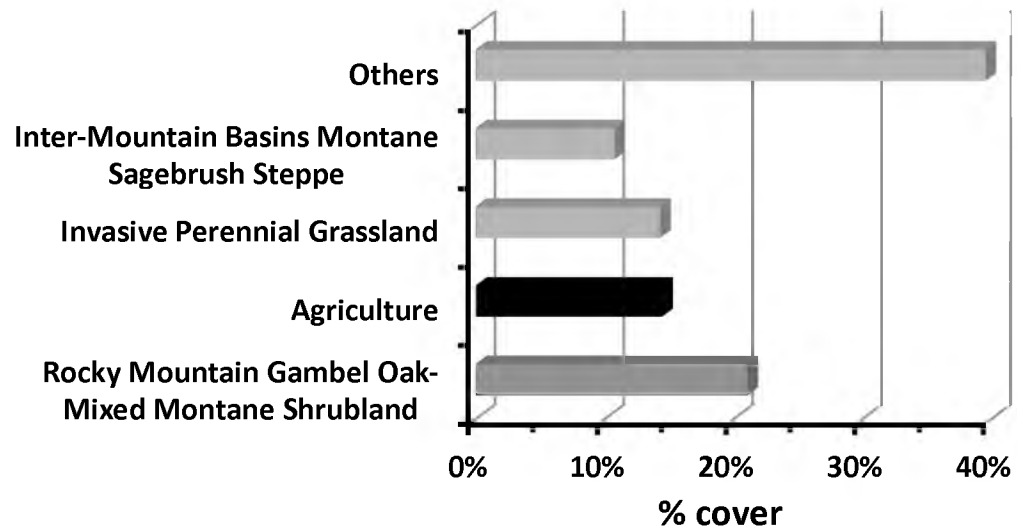


Figure 58. GAP Analysis land cover and land use map of Utah Lake surroundings. The proportions of different land cover / land use classes of Utah Lake and indicate a larger area is under agriculture.

Table 6. Temperature reconstruction of Utah Lake from $\delta^{18}\text{O}_{\text{calcite}}$ (‰) VPDB and $\delta^{18}\text{O}_{\text{water}}$ (‰) VSMOW

$\delta^{18}\text{O}_{\text{calcite}}$ (‰) VPDB	$\delta^{18}\text{O}_{\text{water}}$ (‰) VSMOW	T (°C); Epstein et al. (1953)	T (°C); Craig (1965)	T (°C); Anderson & Arthur (1983)	T (°C) Friedman & O'Neil (1977)	T (°C) Kim & O'Neil (1997)
-9.5	-8.2	21.2	21.5	21.6	21.7	21.0
-10	-8.2	23.5	23.7	23.9	24.1	23.4

The sedimentary $\delta^{18}\text{O}_{\text{CaCO}_3}$ values range from 9.3‰ to 10 ‰ in VPDB scale while the lake water $\delta^{18}\text{O}_{\text{H}_2\text{O}}$ and δD values are water $8.0 \pm 0.3\text{‰}$ and $-76.5 \pm 0.3\text{‰}$ on VSMOW scale respectively. Based on these observations, the modeled temperature of Utah Lake that range from 20 to 25 °C and is comparable to the documented temperature range for carbonates precipitation in Utah Lake (17– 25 °C; Psomas 2007; Callister 2008) and indicates that the carbonates are well-equilibrated with lake water.

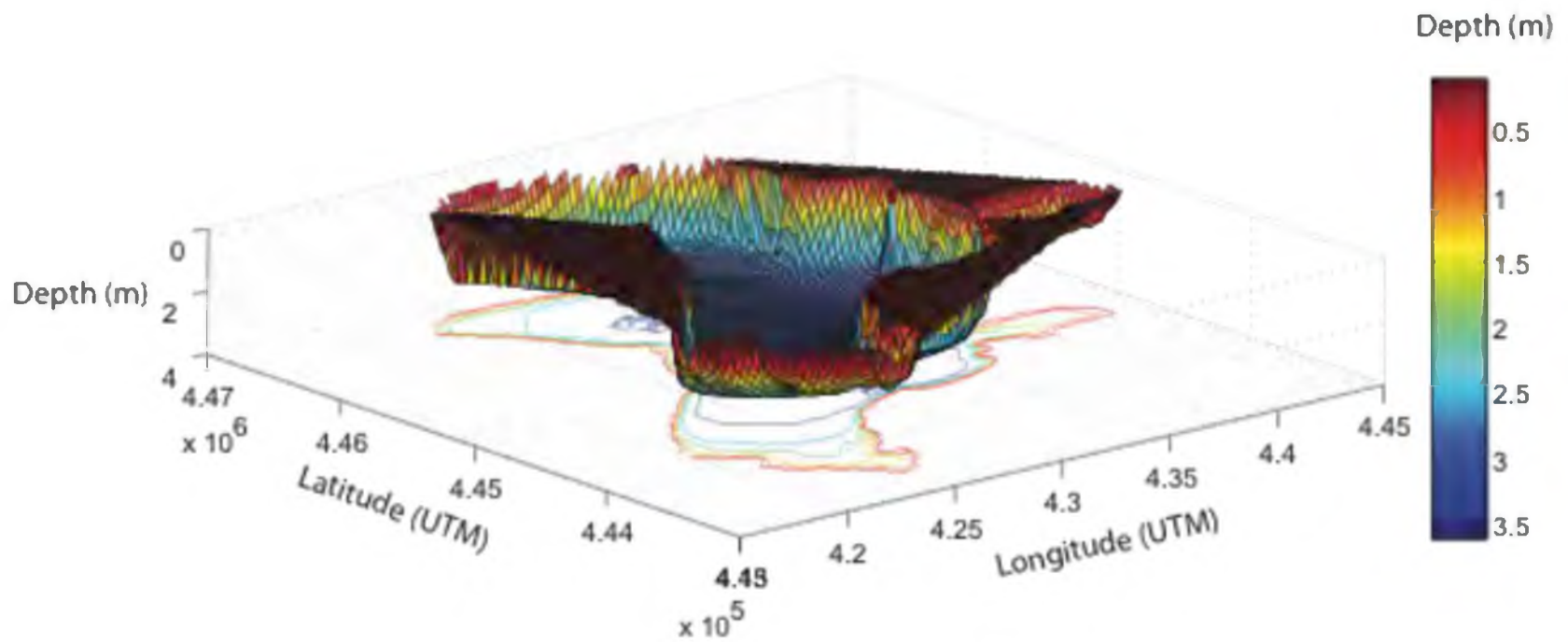


Figure 59. Utah Lake materials flux model as influenced by the lake bathymetry.

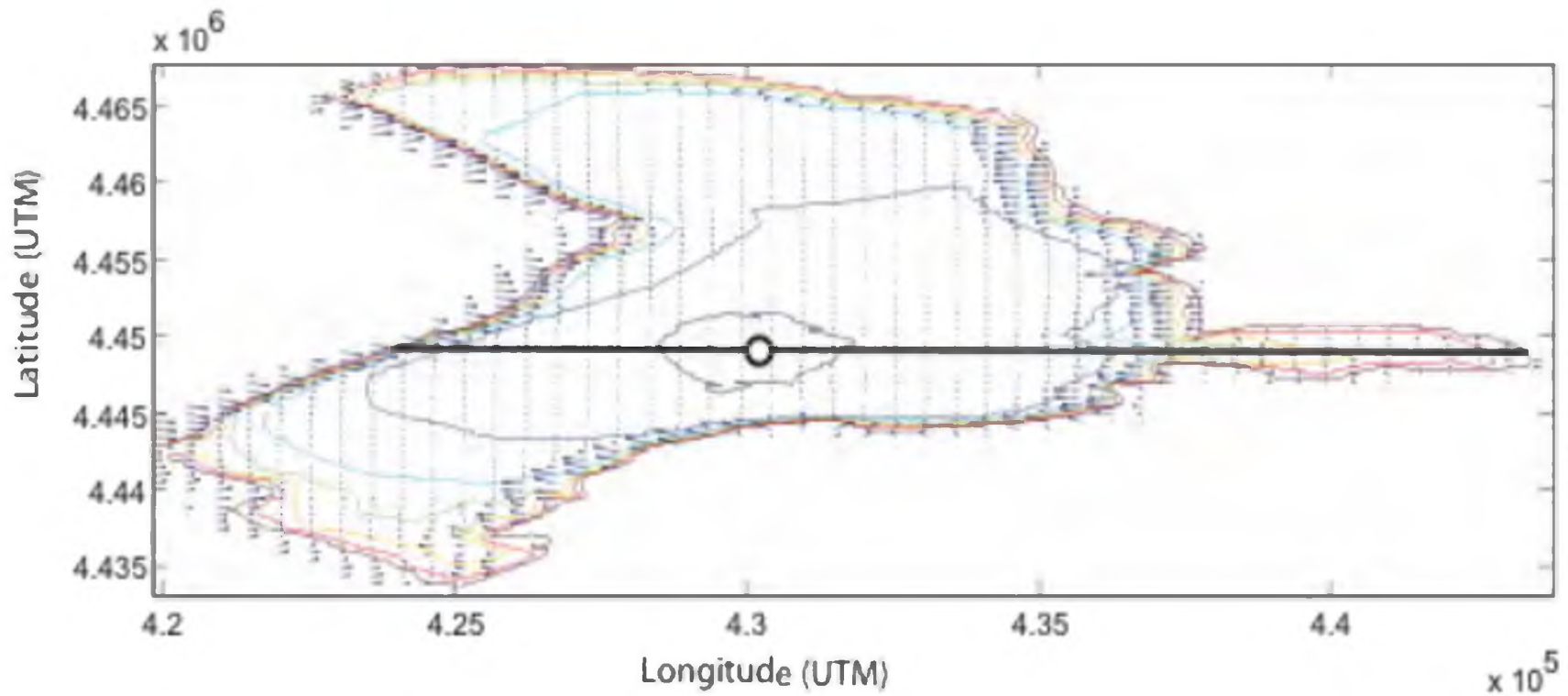


Figure 59 continued.

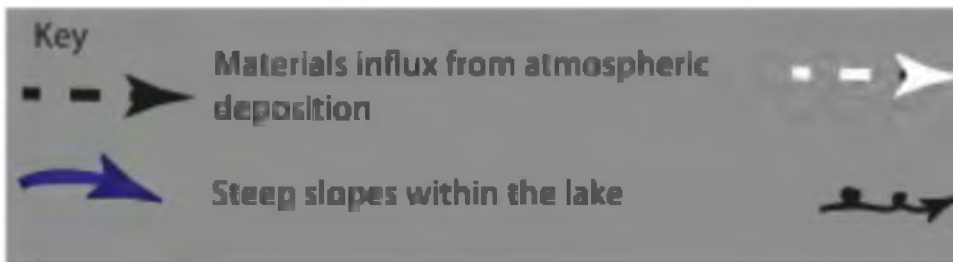


Figure 59 continued.



Dissolve ions (e.g., HCO_3^- , Mg^{2+} , NO_3^- etc.)
from ground water flow

Materials resuspension
& sediment focusing